MESOPOROUS ORGANOSILICAS FOR CO_2 CAPTURE AND UTILIZATION:

REACTION INSIGHT AND MATERIAL DEVELOPMENT

by

Joel Motaka Kolle

Thesis submitted to the University of Ottawa

in partial Fulfillment of the requirements for the degree of

Doctorate in Philosophy in Chemistry

Department of Chemical and Biomolecular Sciences

Faculty of Science

University of Ottawa

DECLARATION AND STATEMENT OF CONTRIBUTIONS OF COLLABORATORS

I hereby declare that this thesis is my original work and has been written by me in its entirety. I performed experimental design/implementation and associated data analysis.

My supervisor, Prof. Abdelhamid Sayari provided valuable guidance throughout this work and made editorial comments and corrections to my written work.

Prof. Tangour's group at the University of Tunis – Tunisia provided theoretical data to elucidate a unified CO_2-amine interaction. This data was complemented by experimental evidence which I collected. Accordingly, members of the Tangour and Sayari labs are co-authors of the manuscript provided in Chapter 3.

This thesis is void of any material that infringes copyright and I have acknowledged all sources of information which have been used.

Ottawa, May 04, 2020

Joel Motaka Kolle

Dedication

To my family.

ABSTRACT

As mankind attempts to halt climate change and global warming, large-scale carbon dioxide (CO_2) capture, utilization and storage (CCUS) technologies are viewed as an indispensable approach to curb CO_2 emission. This thesis focused on better understanding CO_2-amine interactions during adsorption, while developing in parallel covalently immobilized polyethylenimine (PEI) adsorbents for CO_2 adsorption. In addition, catalyst reusability issues reported in the synthesis of cyclic carbonates (CCs) from CO_2 and epoxides using metal-free supported immobilized quaternary ammonium salts are addressed, while developing new organosilicas for the synthesis of CCs.

The reaction between CO_2 and amine was investigated at the gas-solid interface in an attempt to provide a unified CO_2-amine interaction both in adsorption and absorption. A combination of density functional theory calculations and experimental data (FTIR and ^{13}C NMR) showed that the formation of the zwitterion intermediate often reported in the literature is highly unlikely, instead a six-atom centered zwitterion mechanism involving the "assisting" effect of water, amine or other functional groups was found to be more feasible due to its lower activation energy. Moreover, evidence was provided to suggest that under humid conditions, bicarbonate and carbonate are formed from the reaction between water and CO2, and not the widely reported carbamate hydrolysis.

With a goal of minimizing the leaching of amines on PEI-impregnated adsorbents, PEI was covalently immobilized on mesoporous aluminosilica using 3-glycidoxypropyltrimethoxysilane or 3-triethoxysilylpropyl isocyanate as linkers. The resultant materials were found to be more resistant to leaching (in ethanol) and degradation (air at 100 ^oC) compared to their impregnated counterparts. Further enhancement in oxidation stability was achieved by covalently grafting epoxide-functionalized PEI onto mesoporous aluminosilica.

CO_2 uptake over amine-containing adsorbents is widely reported to be enhanced in the presence of moisture. However, the same cannot be said for other adsorbents, such as, carbonaceous and zeolite-based materials, and most MOFs. In a soon to be submitted review manuscript, a comprehensive analysis on the role of water on CO_2 uptake (equilibrium and kinetics), material structure and regeneration over a wide range of adsorbents is presented.

As for CO_2-epoxides fixation to cyclic carbonates, a quaternary ammonium salt supported on SBA-15 was used to investigate the observed literature trend between product yield and substrate type with catalyst reuse. Under mild reaction conditions (1.0 MPa CO_2, 100 ^oC and 4 h), 1,2-butylene carbonate was obtained in high yields (> 95%) over 5 cycles as the substrate is easy to activate and the product can be completely removed from the catalyst surface due to its low boiling point. Nonetheless, using styrene oxide led to decrease in yield over reuse cycles, mainly because styrene carbonate crystals were trapped on the catalysts surface (^{13}C MAS NMR and TGA data), thereby blocking access to active sites. By extensively washing all spent catalysts in acetone and using chromatographic grade SiO_2 as support material, styrene carbonate was obtained in very good yield (> 93%) over five cycles.

Finally, novel quaternary ammonium iodide-based organosilicas, grouped into disordered, ordered and periodic mesoporous organosilicas, were prepared and tested for the cycloaddition of CO_2 to epoxide to yield cyclic carbonates. Under mild reaction conditions (0.5 MPa CO_2, 50 ^oC and 10 – 15 h) catalysts with the ordered mesoporous organosilicas structure were found to be more active owing to their larger surface area and pore volume, enhancing the accessibility of active sites by epoxides.

ACKNOWLEDGMENT

I would like to express my deepest gratitude to my supervisor Prof Abdelhamid Sayari for accepting me into his research group, thereby giving me the opportunity to fulfil this academic milestone. I will equally like to thank him for his invaluable advice and guidance, unwavering patience, constant inspiration and encouragement throughout these years. Research-wise, I have improved a lot under his supervision.

I present my sincere gratitude to all members of the Sayari group for their ideas and valued discussions that helped improved the quality of my research.

My sincere gratitude goes to my partner, our kids, families and friends for their unstinted support and endless encouragement during these years.

Finally, I would like to thank God Almighty for giving me the strength and health to pursue my endeavors.

TABLE OF CONTENTS

LIST OF ABBREVIATIONS AND SYMBOLS

1,2-BC	1,2-Butylene Carbonate
1,2-EB	1,2-Epoxybutane
4-CDO	4-(Chloromethyl)-1,3-Dioxolan-2-One
4-PDO	4-((3-(Trimethoxysilyl)Propoxy)Methyl)-1,3-Dioxolan-2-One
ACAs	Amine-Containing Adsorbents
ACs	Activated Carbon
API	Active Pharmaceutical Ingredients
APTES	3-Aminopropyltriethoxysilane
ATR-IR	Attenuated Total Reflection (*ATR*) - Infra-Red Spectroscopy
BET	Brunauer-Emmett-Teller
BHBPD	*N,N*'-Bis(2-Hydroxyethyl)-*N,N*'-Bis(Trimethoxysilylpropyl)Ethylenediamine
C_{60}	Fullerene
CCs	Cyclic Carbonates
CCUS	Carbon Capture, Utilization and Storage
CHO	Cyclohexene Oxide
CNTs	Carbon Nanotubes
CO_2	Carbon Dioxide
COPs	Coordination Organic Polymers
CP-MAS	Cross Polarization Magic Angle Spinning
DAC	Direct Air Capture
DFT	Density Functional Theory
DMO	Disordered Mesoporous Silica
D_p	Pore Diameter
EDTA	Ethylenediaminetetraacetic Acid
EDX	Energy Dispersive X-Ray Analysis
EOR	Enhanced Oil Recovery
EPH	Epichlorohydrin
FID	Flame Ionization Detector
FTIR	Fourier-Transform Infrared Spectroscopy
GHG	Greenhouse Gas
GPS	3-Glycidoxypropyltrimethoxysilane
HDO	Hexahydrobenzo[*D*][1,3]Dioxol-2-One
HKUST	Hong Kong University of Science and Technology
HMS	Hexagonal Mesoporous Silica
HOMO	Highest Occupied Molecular Orbital
IPCC	Intergovernmental Panel on Climate Change
IRC	Intrinsic Reaction Coordinate
LDH	Layered Double Hydroxides
LUMO	Lowest Occupied Molecular Orbital

MCM-41	Mobil Composition of Matter No. 41
MCM-48	Mobil Composition of Matter No. 48
MCT	Mercury Cadmium Telluride
MEA	Monoethanolamine
MOFs	Metal Organic Frameworks
NMR	Nuclear Magnetic Resonance
OMO	Ordered Mesoporous Silica
P	Adsorbate gas pressure (bar)
P0	Adsorbate gas pressure (bar)
P123	$HO[CH_2CH_2O]_2O[CH_2CH(CH_3)O]_{70}[CH_2CH_2O]_2OH$.
PE-$AlSiO_2$	Pore-Expanded Aluminosilica
PEI	Polyethylenimine
PEO	Polyethylene Oxide
PES	Potential Energy Surface
PHS	Porous Hybrid Solid
PMO	Periodic Mesoporous Silica
PO	Propylene Oxide
PSA	Pressure Swing Adsorption
PVA	Polyvinyl Alcohol
RD&D	Research and Development and Demonstration
RIRC	Reactive Internal Reaction Coordinates
S_A	Surface Area
SBA-15	Santa Barbara Amorphous-15
SC	Styrene Carbonate
SiO_2	Silica
SO	Styrene Oxide
TEA	Triethylamine
TEOS	Tetraethyl Orthosilicate
TGA	Thermogravimetric Analysis
TMOS	Tetramethyl Orthosilicate
TPS	3-Triethoxysilylpropyl Isocyanate
TSA	Temperature Swing Adsorption
V_p	Pore Volume
VSA	Vacuum Swing Adsorption
WHO	World Health Organization

LIST OF FIGURES

LIST OF TABLES

Chapter 1 INTRODUCTION TO THESIS

1.1. Introduction to carbon dioxide capture, utilization and storage (CCUS)

The current debate on detrimental effects of greenhouse gas (GHG) emissions on global warming and climate change is overwhelmingly supported by scientific evidence. Numerous reports by the Intergovernmental Panel on Climate Change (IPCC)[1], World Metrological Organization (WMO),[2] and other international organizations[3,4], point to our long-standing dependence on fossil fuel (oil, coal and natural gas) and increasing deforestation as the main reasons for the continuous increase of GHG emissions, notably carbon dioxide (CO_2), while equally emphasizing the urgency to mitigate these emissions. Although not the most potent GHG, the sheer volume of CO_2 emissions (ca. 60% of GHG) has drawn close attention as a synonym for GHG, and the main anthropogenic contributor to global warming and climate change.[3] A recent report showed that the CO_2 emissions of every country showed a general increase over the years.[5] Accordingly, cutting down on CO_2 emissions has been the focus of many governments and environmental agencies, as is reflected in the number of international treaties on climate change, with the 2015 Paris Agreement (COPS21) ratified by more countries than any previous treaty.[6] With the demand for electricity, cement, steel and base chemicals expected to stay high to support a growing and increasingly urbanised global population, the future production of these materials and others must be more energy efficient, emitting less CO_2. Different technologies and approaches are needed to address the decarbonisation challenge while supporting sustainable and competitive industries. Three general courses of action are proposed to curb CO_2 emissions; (i) substitution of fossil fuels with renewable energy sources, (ii) reduction in energy consumption by improving the efficiency of existing processes and buildings, (iii) CO_2 capture, utilization and

sequestration/storage (CCUS); with the first being the most significant and effective, notably in the long term[7]. Nonetheless, CCUS technologies are required in the short and long term to mitigate CO_2 emissions. Although strides have been made in CCUS technologies, these developments face both technological and non-technical challenges. Available CO_2 capture and storage techniques are still energy intensive, while limited storage capacity exists for CO_2. Moreover, environmental risks of storing CO_2 in underground reservoirs (e.g. potential for CO_2 leakage, impacts on drinking water, and induced seismicity), to establishing an adequate legal and regulatory framework to fully support such technologies are limiting their large-scale application around the globe.[8]

With high capital cost and energy demand and environmental issues associated with CO_2 capture based on mature aqueous amine solution technologies, CO_2 capture using solid adsorbents has been considered as a more viable option. Of the different materials used for CO_2 adsorption, the use of amine-containing adsorbents for large-scale CO_2 capture is attracting commercial interest.[9,10] As for CO_2 utilization, urea production and enhanced oil recovery (EOR) are the two large-scale processes that reuse CO_2. Large scale conversion of CO_2 to fuels and chemicals is largely in the early stages of development. CO_2 conversion to polymers for instance has the advantage of holding up CO_2 in these materials for years to come.[11] Accordingly, polymerization reactions than utilize CO_2 as a reagent have the potential to provide both economic and climate benefits. Cyclic carbonates (CCs), produced from the cycloaddition of CO_2 to epoxides, are used as monomers for the synthesis of polycarbonates.[12] CCs are equally used as green (biodegradable) solvents in the production of lithium ion batteries and other applications.[13]

1.2. Thesis structure

This thesis addresses specific aspects on reaction insight and material development vis-a-vis CO_2 capture and utilization; with the first part devoted to CO_2 capture via adsorption, and the second to CO_2 conversion to chemicals (with a focus on cyclic carbonates). The thesis is organized as follows:

Chapter 1: Introduction to thesis. This chapter provides a general introduction to CO_2 capture, utilization and storage (CUSS) and the structure of the thesis.

Chapter 2: Mesoporous Organosilicas for CO_2 Capture: Reaction Insight and Material Development. This section introduces CO_2 capture including opportunities, technologies, industrial-scale operations and challenges.

Chapter 3: CO_2 – Amine Reaction Mechanisms: A Unified Approach. This Chapter addresses some questionable issues, notably zwitterion formation and carbamate hydrolysis during CO_2-amine reaction with and without moisture. The augments provided are supported by both experimental and theoretical data.

Chapter 4: Covalently Immobilized Polyethylenimine (PEI) for CO_2 Adsorption. In this section grafting PEI on mesoporous aluminosilica using 3-glycidoxypropyltrimethoxysilane or 3-triethoxysilylpropyl isocyanate as linkers is presented as a method that significantly reduces leaching of PEI from the support in PEI-impregnated adsorbents. This method was further extended to graft epoxide-functionalized PEI on mesoporous aluminosilica, with the obtained material demonstrating superior oxidation stability compared to both the PEI-impregnated and epoxide-functionalized PEI-impregnated materials.

Chapter 5: Understanding the Effect of Water Vapor on CO_2 Adsorption – A Review. This section summarises a review manuscript in progress devoted to understanding the role played by water during CO_2 adsorption over different types of adsorbents. The effect of water on the CO_2 uptake (equilibrium uptake and kinetics), and on the structural stability of and regenerability of adsorbents is discussed.

Chapter 6: Mesoporous Organosilicas for CO_2 Fixation to Cyclic Carbonates: Reaction Insight and Material Development. This section provides an introduction to CO_2 utilization, including opportunities, challenges and current commercial processes for CO_2 reuse.

Chapter 7: Substrate Dependence on the Fixation of CO_2 to Cyclic Carbonates over Reusable Porous Hybrid Solids. In this chapter, data from TGA, ^{13}C MAS NMR and textural properties were used to delineate the observed literature trend showing decreasing yield with catalyst reuse when styrene oxide (as opposed to propylene or butylene oxides) was used as a substrate in the cycloaddition of CO_2 to epoxides to yield CCs over immobilized quaternary ammonium salts. *N,N,N*-tributyl-*N*-propylammonium iodide immobilized on silicas was used as catalyst, with the apparent density and catalyst recovery steps proving to be key parameters affecting the reusability of this catalyst.

Chapter 8: Novel Porous Organocatalysts for Cycloaddition of CO_2 and Epoxides. In this chapter, organosilicas with the same chemical composition but belonging to three different classes, i.e. disordered, ordered and periodic mesoporous organosilicas, were prepared and their catalytic activity compared using the cycloaddition of CO_2 and epoxide as a model reaction. Due to their larger surface area and pore volume, ordered mesoporous organosilicas (OMOs) were found to

be the most active organosilicas over a wide range of substrates (epoxides) and showed very good stability and yield of 1,2-butylene carbonate (≥ 93%) reusability over 5 cycles.

Chapter 9: Conclusion and Recommendation for Future Works. This section highlights the main findings and contributions of chapters 3, 4, 7 and 8; while suggesting future research areas to complement these findings.

References

(1) IPCC. *Global Warming of 1.5°C. An IPCC Special Report: Summary for Policymakers*; Masson-Delmotte, V., Zhai, P., Pörtner, H. O., Roberts, D., J. Skea, P. R., Shukla, Pirani, A., Moufouma-Okia, W., Péan, C., Pidcock, R., et al., Eds.; Geneva, 2018.

(2) WMO. WMO Statement on the Status of the Global Climate in 2017 http://www.wmo.int/pages/mediacentre/press_releases/documents/WMO_1108_EN_web_000.pdf (accessed Dec 11, 2019).

(3) Ritchie, H.; Roser, M. CO_2 and Greenhouse Gas Emissions https://ourworldindata.org/co2-and-other-greenhouse-gas-emissions (accessed Dec 11, 2019).

(4) Committee on Climate Change. Net Zero Technical Report. https://www.theccc.org.uk/wp-content/uploads/2019/05/Net-Zero-Technical-report-CCC.pdf (accessed Dec 11, 2019).

(5) Muntean, M.; Guizzardi, D.; Schaaf, E.; Crippa, M.; Solazzo, E.; Olivier, J.; Vignati, E. *Fossil CO2 Emissions of All World Countries - 2018 Report*; Luxembourg, 2018.

(6) UNFCCC. 2015 Paris Agreement (COP21) https://unfccc.int/files/essential_background/convention/application/pdf/english_paris_agreement.pdf (accessed Dec 11, 2019).

(7) *Advances in Renewable Energies and Power Technologies. Volume 1: Solar and Wind Energies*, 1st ed.; Yahyaoui, I., Ed.; Elsevier, 2018.

(8) Rahman, F. A.; Aziz, M. M. A.; Saidur, R.; Bakar, W. A. W. A.; Hainin, M. R.; Putrajaya, R.; Hassan, N. A. Pollution to Solution: Capture and Sequestration of Carbon Dioxide (CO2) and Its Utilization as a Renewable Energy Source for a Sustainable Future. *Renew. Sustain. Energy Rev.* **2017**, *71*, 112–126. https://doi.org/http://dx.doi.org/10.1016/j.rser.2017.01.011.

(9) Pardakhti, M.; Jafari, T.; Tobin, Z.; Dutta, B.; Moharreri, E.; Shemshaki, N. S.; Suib, S.; Srivastava, R. Trends in Solid Adsorbent Materials Development for CO2 Capture. *ACS Appl. Mater. Interfaces* **2019**, *11* (38), 34533–34559. https://doi.org/10.1021/acsami.9b08487.

(10) Chaffee, A. L.; Knowles, G. P.; Liang, Z.; Zhang, J.; Xiao, P.; Webley, P. A. CO2 Capture by Adsorption: Materials and Process Development. *Int. J. Greenh. Gas Control* **2007**, *1* (1), 11–18. https://doi.org/https://doi.org/10.1016/S1750-5836(07)00031-X.

(11) International Energy Agency. Putting CO2 to Use: Creating value from emissions

https://www.iea.org/topics/carbon-capture-and-storage/policiesandinvestment/ (accessed Dec 21, 2019).
(12) Ariga, T.; Takata, T.; Endo, T. Cationic Ring-Opening Polymerization of Cyclic Carbonates with Alkyl Halides To Yield Polycarbonate without the Ether Unit by Suppression of Elimination of Carbon Dioxide. *Macromolecules* **1997**, *30* (4), 737–744. https://doi.org/10.1021/ma9607325.
(13) Pyo, S.-H.; Park, J. H.; Chang, T.-S.; Hatti-Kaul, R. Dimethyl Carbonate as a Green Chemical. *Curr. Opin. Green Sustain. Chem.* **2017**, *5*, 61–66. https://doi.org/https://doi.org/10.1016/j.cogsc.2017.03.01

PART ONE

CHAPTER 2 MESOPOROUS ORGANOSILICAS FOR CO_2 CAPTURE: REACTION INSIGHT AND MATERIAL DEVELOPMENT

2.0. Introduction to CO_2 capture

Over the next 10 to 20 years, capturing CO_2—a powerful greenhouse gas emitted from sources such as fossil-fuel-burning power plants, natural-gas processing plants and cement plants—could become a significant method for mitigating climate change. On May 11 2019, carbon dioxide levels in our atmosphere reached 415 parts per million for the first time in human history.[1] The last time CO_2 levels were this high was probably 2.5 to 5 million years ago, when temperatures were 2 to 3˚C higher than today.[2] The Intergovernmental Panel on Climate Change (IPCC) has warned that we need to limit global warming to 1.5˚C to avert the most catastrophic effects of climate change. CO_2 capture has the potential to achieve up to 14% global GHG reductions by 2050 and is viewed as the leading practical option to decarbonize the industrial sector. Besides capturing carbon from fossil fuel plants directly,[3,4] there are a variety of ways to remove CO_2 from the atmosphere.[5,6] Four general methods are employed for CO2 capture (Figure 2-1), including, *(1)* industrial processes - CO_2 removal to purify other industrial gases, such as hydrogen and natural gas; *(2)* post-combustion CO_2 capture - CO_2 from fossil fuel combustion units; *(3)* Pre-combustion CO_2 capture - fuel is transformed to CO and H_2 and CO_2 via steam reforming and water gas shift reactions, followed by hydrogen separation; and *(4)* oxyfuel CO_2 capture - fossil fuel combustion in pure oxygen to generate a CO_2-rich exhaust gas.[7–9] The

captured CO_2 is then compressed and mainly used directly in enhanced oil recovery (EOR) or stored (sequestration).

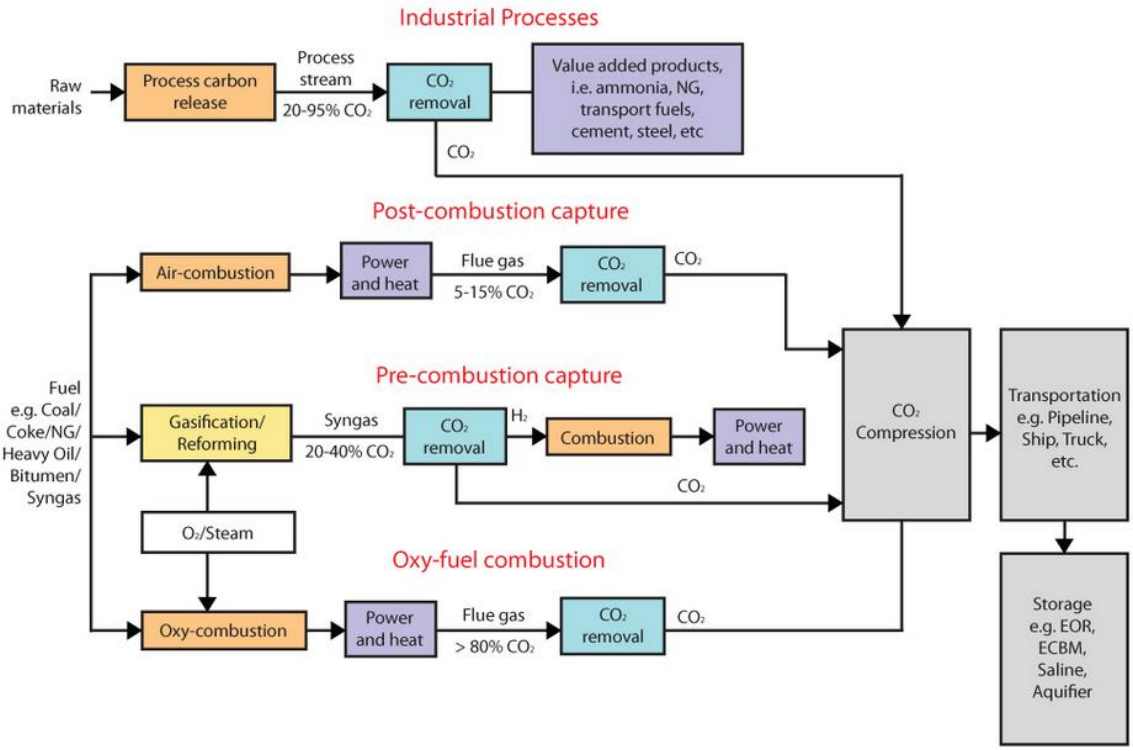

Figure 2-1. Generalized CO_2 Capture Pathways.[8] Reproduced with the permission of the Department of Natural Resources Canada (2020).

As of 2017, over 21 commercial-scale carbon capture projects (Table 2-1) are operating in six countries around the world (i.e. USA, Canada, Norway, Saudi Arabia, Brazil and United Arab Emirates),[10] with over 20 more in development (demonstration plants).[11] Large-scale carbon capture is commercial operational in the following sectors; ethanol production, fertilizer production, natural gas processing, refinery hydrogen production and coal-fired power generation.[10] Over 90% of industrial facilities are thought to consist of post-combustion systems, making post-combustion CO_2 capture an important method for CO_2 capture.

Table 2-1. Large-scale carbon capture projects in operation and under construction.[12] Copyright (2016) Global Carbon Institute.

Country	Project name	Location	Lifecycle Stage				Operation date	Capture capacity (Mt/y)
			Early development	Advanced development	Construction	Operation		
USA	Terrell Natural Gas Processing Plant	Texas				×	1972	0.4–0.5
	Enid Fertilizer	Oklahoma				×	1982	0.7
	Shute Creek Gas Processing Plant	Wyoming				×	1986	7.0
	Century Plant	Texas				×	2010	8.4
	Air Products Steam Methane Reformer	Texas				×	2013	1.0
	Coffeyville Gasification Plant	Kansas				×	2013	1.0
	Lost Cabin Gas Plant	Wyoming				×	2013	0.9
	Petra Nova Carbon Capture	Texas				×	2017	1.4
	Illinois Industrial Carbon Capture and Storage	Illinois				×	2017	1.0
	Lake Charles Methanol	Louisiana		×			2021	4.2
	Texas Clean Energy Project	Texas		×			2021	1.5–2.0
Canada	Great Plains Synfuel Plant and Weyburn-Midale	Saskatchewan				×	2000	3.0
	Boundary Dam Carbon Capture and Storage	Saskatchewan				×	2014	1.0
	Quest	Alberta				×	2015	Approx. 1.0
	Alberta Carbon Trunk Line with Agrium CO_2 Stream	Alberta		×			2018	0.3–0.6
China	Yanchang Integrated Carbon Capture and Storage	Shaanxi			×		2018	0.4
	Sinopec Qilu Petrochemical CCS	Shandong		×			2019	0.5
	Sinopec Eastern China CCS	Jiangsu	×				2020	0.5
China	Sinopec Shengli Power Plant CCS	Shandong		×			2020	1.0
	China Resources Power (Haifeng) Integrated CCS	Guangdong	×				2020	1.0
	Huaneng GreenGen IGCC Project (Phase 3)	Tianjin	×				2020	2.0
	Shanxi International Energy Group CCUS	Shanxi		×			2020	2.0
	Shenhua Ningxia CTL	Ningxia		×			2020	2.0
	CNPC Jilin Oil Field CO_2 EOR	Jilin			×		2017	0.5
Australia	Gorgon Carbon Dioxide Injection	Western Australia			×		2017	3.4–4.0
	CarbonNet	Victoria		×			2020	1.0–5.0
	South West Hub	Western Australia	×				2025	2.5
Korea	Korea-CCS 1	Either Gangwon Province or Chungnam	×				2020	1.0
	Korea-CCS 2	Unknown	×				2020	1.0
Norway	Sleipner CO_2 Storage	North Sea				×	1996	1.0
	Snøhvit CO_2 Storage	Barents Sea				×	2008	0.7
	Norway Full Chain CCS	Southern Norway		×			2022	1.2
UK	Teesside Collective	Tees Valley	×				2020	0.8
	Caledonia Clean Energy	Scotland	×				2022	3.8
Saudi Arabia	Uthmaniyah CO2-EOR Demonstration	Eastern Province				×	2015	0.8
United Arab Emirates	Abu Dhabi CCS Project (Phase 1)	Abu Dhabi				×	2016	0.8

As seen in Figure 2-2, technologies for post-combustion capture of CO_2 include; absorption,[13] adsorption,[14] membrane-based methods,[15] and cryogenics.[16] The high cost of operating most of these strategies is driving the need for more efficient materials and processes for large scale CO_2 capture. Moreover, finding new commercial uses for the captured CO_2 is key to lowering the costs of these technologies and scaling them up. Besides cost, the absence of policy incentives, lack of confidence in CO_2 storage and public acceptance are holding up progress in large-scale CO_2 capture and storage implementation.[16] This has been the case in Germany, where CO_2 capture and storage technologies have met strong opposition from the public.[17]

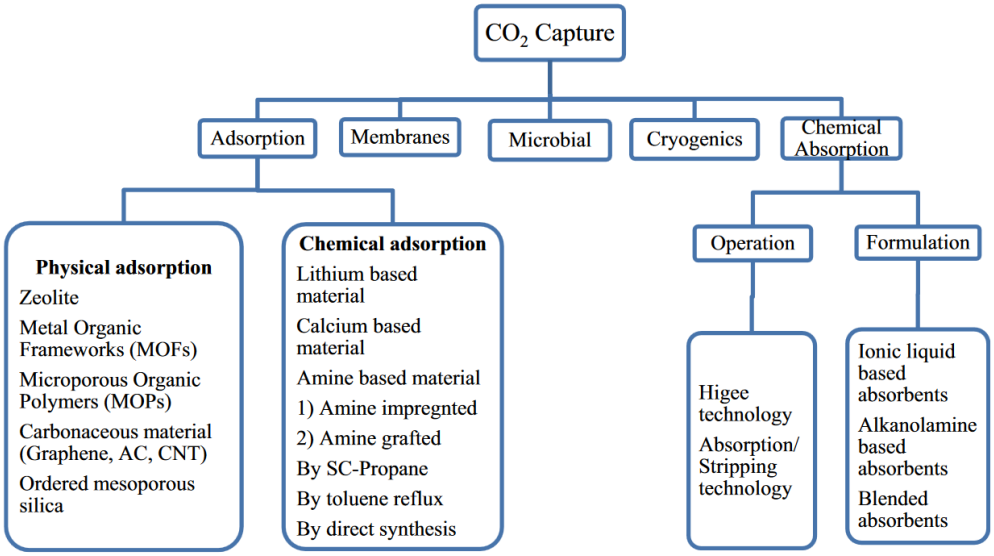

Figure 2-2. Classification of post-combustion CO_2 capture technologies.[18] Copyright (2016) Springer Nature

While post-combustion CO_2 capture based on amine solution has been practiced for decades, high energy for solvent regeneration, health and environmental concerns, and capital cost means this method is not sustainable.[19–22] Adsorption is considered as a more viable technology for CO_2 capture from large point sources.[23] Accordingly, several materials were developed as solid adsorbents, including metal-organic frameworks (MOFs),[24–26] coordination

organic polymers (COPs),[27] clays,[28,29] carbons,[30] basic oxides[31,32] and amine-containing porous materials.[33] The latter materials were found to be attractive for post-combustion, low temperature CO_2 capture due to their excellent adsorptive properties, including high capacity and selectivity as well as favorable adsorption and desorption kinetics.[34–36] Amine-containing adsorbents are prepared using different methodologies[37], including impregnation of amines or polyamines on porous supports, particularly silicas,[38–40] and less frequently activated carbons,[41,42] zeolites[43] and MOFs,[44,45] or grafting of amine-containing silanes via coupling with surface silanol groups.[46–48] Despite significant progress in fundamental understanding of CO_2 – amine interactions under a variety of adsorption conditions,[49,50] some aspects are still debatable or not well understood.

While structural variation of amines offers different basicity, it is the steric hindrance effect that impact their reactivity with CO_2. It is generally reported that aliphatic primary or secondary amines form a zwitterion upon reacting with CO_2 (eq 2.1), which then proceeds to the formation of a fairly stable carbamate complex with another amine (eq 2.2) [35,51] or carbamic acid by intramolecular hydrogen transfer.[52] In the presence of water, this carbamate complex hydrolyses to form a bicarbonate ion and a free amine (eq 2.3). In the presence of water, tertiary amines react with CO_2 to form bicarbonate and alkylammonium ion (eq 2.4).

$$RR^1NH + CO_2 \longleftrightarrow RR^1NH^+COO^- \quad (2.1)$$

$$RR^1NH^+COO^- + RR^1NH \longleftrightarrow RR^1NCOO^- + RR^1NH_2^+ \quad (2.2)$$

$$RR^1NCOO^- + H_2O \longleftrightarrow RR^1NH + HCO_3^- \quad (2.3)$$

$$RR^1R^2N + CO_2 + H_2O \longleftrightarrow RR^1R^2NH^+ + HCO_3^- \quad (2.4)$$

Similar to aqueous amine, CO_2 adsorption over supported amines under dry conditions led to the formation of mainly alkylammonium carbamate, while under humid conditions, carbamate and bicarbonate were found to be the dominant species. Although introduced in the 1960s,[53] a zwitterion species, presumed to be formed through a four-centered mechanism, has never been detected experimentally, calling into question its existence. Moreover, the origin of bicarbonate or carbonate species detected during CO_2 uptake in the presence of moisture is equally debatable. In **Chapter 3**, experimental and theoretical data are combined to provide answers to the following questions; (1) how likely is it that carbamic acid or ammonium carbamate form through the intermediacy of the much reported zwitterion?, (2) does the formation of ammonium bicarbonate/carbonate involve the hydrolysis of carbamate species or reaction between water and CO_2? And (3) is there a possible unified mechanism for the interactions of CO_2 with amines and water (or other species), whether in solution or at the solid-gas interface?

Although significant progress has been achieved regarding this type of solid adsorbents, efforts to improve their performance (kinetics and capacity) and stability (chemical, thermal, hydrothermal and reusability) are continuing. Impregnated amines, e.g. tetraethylenepentamine (TEPA), PEI etc., are attractive adsorbents due to their high amine density which translates to high CO_2 capacity. [54,55] However, such materials are susceptible to active-site leaching,[56] evaporation[57,58] and oxidative degradation.[59,60] In **chapter 4**, an attempt to address these setbacks through covalent immobilization of epoxide-functionalized PEI on aluminosilica is presented. The effects of two linking agents, i.e. 3-glycidoxypropyltrimethoxysilane or 3-triethoxysilylpropyl isocyanate, and epoxidation are discussed.

References

(1) Mauna Loa Observatory. Carbon dioxide levels hit record peak in May https://research.noaa.gov/article/ArtMID/587/ArticleID/2461/Carbon-dioxide-levels-hit-record-peak-in-May (accessed Dec 25, 2019).

(2) IPCC. *Global Warming of 1.5°C. An IPCC Special Report: Summary for Policymakers*; Masson-Delmotte, V., Zhai, P., Pörtner, H. O., Roberts, D., J. Skea, P. R., Shukla, Pirani, A., Moufouma-Okia, W., Péan, C., Pidcock, R., et al., Eds.; Geneva, 2018.

(3) Wang, Y.; Zhao, L.; Otto, A.; Robinius, M.; Stolten, D. A Review of Post-Combustion CO2 Capture Technologies from Coal-Fired Power Plants. *Energy Procedia* **2017**, *114*, 650–665. https://doi.org/10.1016/j.egypro.2017.03.1209.

(4) Bhattacharyya, D.; Miller, D. C. Post-Combustion CO2 Capture Technologies — a Review of Processes for Solvent-Based and Sorbent-Based CO2 Capture. *Curr. Opin. Chem. Eng.* **2017**, *17*, 78–92. https://doi.org/10.1016/j.coche.2017.06.005.

(5) Fasihi, M.; Efimova, O.; Breyer, C. Techno-Economic Assessment of CO2 Direct Air Capture Plants. *J. Clean. Prod.* **2019**, *224*, 957–980. https://doi.org/10.1016/j.jclepro.2019.03.086.

(6) Sanz-Pérez, E. S.; Murdock, C. R.; Didas, S. A.; Jones, C. W. Direct Capture of CO2 from Ambient Air. *Chem. Rev.* **2016**, *116* (19), 11840–11876. https://doi.org/10.1021/acs.chemrev.6b00173.

(7) The Carbon Capture and Information Source. CO2 Capture Methods http://ccs101.ca/ccs_pro/what__how_of_ccs/co2_capture_methods (accessed Dec 25, 2019).

(8) Natural Resources Canada. CO2 Capture Pathways https://www.nrcan.gc.ca/energy/energy-sources-distribution/coal-and-co2-capture-storage/carbon-capture-storage/co2-capture-pathways/4289 (accessed Dec 25, 2019).

(9) IPCC. *Carbon Dioxide Capture and Storage - Summary for Policymakers*; Metz, B., Davidson, O., Coninck, H. de, Loos, M., Meyer, L., Eds.; IPCC, 2005.

(10) Centre for Climate and Energy Solutions. Technology solutions: Carbon Capture https://www.c2es.org/content/carbon-capture/ (accessed Dec 23, 2019).

(11) Lee, S. Y.; Park, S. J. A Review on Solid Adsorbents for Carbon Dioxide Capture. *J. Ind. Eng. Chem.* **2015**, *23*, 1–11. https://doi.org/10.1016/j.jiec.2014.09.001.

(12) Li, H.; Jiang, H. D.; Yang, B.; Liao, H. An Analysis of Research Hotspots and Modeling Techniques on Carbon Capture and Storage. Sci. Total Environ. 2019, 687 (June), 687–701. https://doi.org/10.1016/j.scitotenv.2019.06.013.

(13) Dutcher, B.; Fan, M.; Russell, A. G. Amine-Based CO2 Capture Technology Development from the Beginning of 2013-A Review. *ACS Appl. Mater. Interfaces* **2015**, *7* (4), 2137–2148. https://doi.org/10.1021/am507465f.

(14) Lu, X.; Xiao, H. A Review on CO2 Sorbents. *Rev. Adv. Mater. Sci.* **2015**, *42* (1), 50–57.

(15) Zhao, S.; Feron, P. H. M.; Deng, L.; Favre, E.; Chabanon, E.; Yan, S.; Hou, J.; Chen, V.; Qi, H. Status and Progress of Membrane Contactors in Post-Combustion Carbon Capture: A State-of-the-Art Review of New Developments. *J. Memb. Sci.* **2016**, *511*, 180–206. https://doi.org/10.1016/j.memsci.2016.03.051.

(16) Song, C.; Liu, Q.; Deng, S.; Li, H.; Kitamura, Y. Cryogenic-Based CO2 Capture Technologies:

State-of-the-Art Developments and Current Challenges. *Renew. Sustain. Energy Rev.* **2019**, *101* (November 2018), 265–278. https://doi.org/10.1016/j.rser.2018.11.018.
(17) Vögele, S.; Rübbelke, D.; Mayer, P.; Kuckshinrichs, W. Germany's "No" to Carbon Capture and Storage: Just a Question of Lacking Acceptance? *Appl. Energy* **2018**, *214* (January), 205–218. https://doi.org/10.1016/j.apenergy.2018.01.077.
(18) Younas, M.; Sohail, M.; Kong, L. L.; Bashir, M. J. K.; Sethupathi, S. Feasibility of CO2 Adsorption by Solid Adsorbents: A Review on Low-Temperature Systems. *Int. J. Environ. Sci. Technol.* **2016**, *13* (7), 1839–1860. https://doi.org/10.1007/s13762-016-1008-1.
(19) Gjernes, E.; Helgesen, L. I.; Maree, Y. Health and Environmental Impact of Amine Based Post Combustion CO 2 Capture. *Energy Procedia* **2013**, *37* (1876), 735–742. https://doi.org/10.1016/j.egypro.2013.05.162.
(20) Liang, Z.; Fu, K.; Idem, R.; Tontiwachwuthikul, P. Review on Current Advances, Future Challenges and Consideration Issues for Post-Combustion CO2 Capture Using Amine-Based Absorbents. *Chinese J. Chem. Eng.* **2016**, *24* (2), 278–288. https://doi.org/https://doi.org/10.1016/j.cjche.2015.06.013.
(21) Rao, A. B.; Rubin, E. S.; Keith, D. W.; Morgan, M. G. Evaluation of Potential Cost Reductions from Improved Amine-Based CO2 Capture Systems. *Energy Policy* **2006**, *34* (18), 3765–3772. https://doi.org/https://doi.org/10.1016/j.enpol.2005.08.004.
(22) Rao, A. B.; Rubin, E. S.; Keith, D. W.; Granger Morgan, M. Evaluation of Potential Cost Reductions from Improved Amine-Based CO2 Capture Systems. *Energy Policy* **2006**, *34* (18), 3765–3772. https://doi.org/10.1016/j.enpol.2005.08.004.
(23) Sjostrom, S.; Krutka, H. Evaluation of Solid Sorbents as a Retrofit Technology for CO2 Capture. *Fuel* **2010**, *89* (6), 1298–1306. https://doi.org/10.1016/j.fuel.2009.11.019.
(24) Trickett, C. A.; Helal, A.; Al-Maythalony, B. A.; Yamani, Z. H.; Cordova, K. E.; Yaghi, O. M. The Chemistry of Metal–Organic Frameworks for CO2 Capture, Regeneration and Conversion. *Nat. Rev. Mater.* **2017**, *2* (17045), 1–16.
(25) Shalini, S.; Nandi, S.; Justin, A.; Maity, R.; Vaidhyanathan, R. Potential of Ultramicroporous Metal-Organic Frameworks in CO2 Clean-Up. *Chem. Commun.* **2018**, *54* (96), 13472–13490. https://doi.org/10.1039/c8cc03233e.
(26) Andirova, D.; Cogswell, C. F.; Lei, Y.; Choi, S. Effect of the Structural Constituents of Metal Organic Frameworks on Carbon Dioxide Capture. *Microporous Mesoporous Mater.* **2016**, *219*, 276–305. https://doi.org/10.1016/j.micromeso.2015.07.029.
(27) Zou, L.; Sun, Y.; Che, S.; Yang, X.; Wang, X.; Bosch, M.; Wang, Q.; Li, H.; Smith, M.; Yuan, S.; et al. Porous Organic Polymers for Post-Combustion Carbon Capture. *Adv. Mater.* **2017**, *29* (37), 1–35. https://doi.org/10.1002/adma.201700229.
(28) Aschenbrenner, O.; McGuire, P.; Alsamaq, S.; Wang, J.; Supasitmongkol, S.; Al-Duri, B.; Styring, P.; Wood, J. Adsorption of Carbon Dioxide on Hydrotalcite-Like Compounds of Different Compositions. *Chem. Eng. Res. Des.* **2011**, *89* (9), 1711–1721. https://doi.org/10.1016/j.cherd.2010.09.019.
(29) Elkhalifah, A. E. I.; Maitra, S.; Bustam, M. A.; Murugesan, T. Effects of Exchanged Ammonium Cations on Structure Characteristics and CO2 Adsorption Capacities of Bentonite Clay. *Appl. Clay Sci.* **2013**, *83–84*, 391–398. https://doi.org/10.1016/j.clay.2013.07.016.
(30) Creamer, A. E.; Gao, B. Carbon-Based Adsorbents for Postcombustion CO2 Capture: A

Critical Review. *Environ. Sci. Technol.* **2016**, *50* (14), 7276–7289. https://doi.org/10.1021/acs.est.6b00627.
(31) Radfarnia, H. R.; Sayari, A. A Highly Efficient CaO-Based CO2 Sorbent Prepared by a Citrate-Assisted Sol-Gel Technique. *Chem. Eng. J.* **2015**, *262*, 913–920. https://doi.org/10.1016/j.cej.2014.09.074.
(32) Hu, Y.; Guo, Y.; Sun, J.; Li, H.; Liu, W. Progress in MgO Sorbents for Cyclic CO2 Capture: A Comprehensive Review. *Journal of Materials Chemistry A*. Royal Society of Chemistry 2019, pp 20103–20120. https://doi.org/10.1039/c9ta06930e.
(33) Ünveren, E. E.; Monkul, B. Ö.; Sarıoğlan, Ş.; Karademir, N.; Alper, E. Solid Amine Sorbents for CO2 Capture by Chemical Adsorption: A Review. *Petroleum* **2017**, *3* (1), 37–50. https://doi.org/10.1016/j.petlm.2016.11.001.
(34) Darunte, L. A.; Walton, K. S.; Sholl, D. S.; Jones, C. W. CO2 Capture via Adsorption in Amine-Functionalized Sorbents. *Curr. Opin. Chem. Eng.* **2016**, *12*, 82–90. https://doi.org/10.1016/j.coche.2016.03.002.
(35) Choi, S.; Drese, J. H.; Jones, C. W. Adsorbent Materials for Carbon Dioxide Capture from Large Anthropogenic Point Sources. *ChemSusChem* **2009**, *2* (9), 796–854. https://doi.org/10.1002/cssc.200900036.
(36) Sayari, A.; Belmabkhout, Y.; Serna-Guerrero, R. Flue Gas Treatment via CO2adsorption. *Chem. Eng. J.* **2011**, *171* (3), 760–774. https://doi.org/10.1016/j.cej.2011.02.007.
(37) Jahandar Lashaki, M.; Khiavi, S.; Sayari, A. Stability of Amine-Functionalized CO2 Adsorbents: A Multifaceted Puzzle. *Chem. Soc. Rev.* **2019**, *48*, 3320–3405. https://doi.org/10.1039/C8CS00877A.
(38) Xu, X.; Song, C.; Miller, B. G.; Scaroni, A. W. Influence of Moisture on CO2 Separation from Gas Mixture by a Nanoporous Adsorbent Based on Polyethylenimine-Modified Molecular Sieve MCM-41. *Ind. Eng. Chem. Res.* **2005**, *44* (21), 8113–8119. https://doi.org/10.1021/ie050382n.
(39) Kodasma, R.; Fermoso, J.; Sanna, A. Li-LSX-Zeolite Evaluation for Post-Combustion CO2 Capture. *Chem. Eng. J.* **2019**, *358* (May 2018), 1351–1362. https://doi.org/10.1016/j.cej.2018.10.063.
(40) Choi, W.; Min, K.; Kim, C.; Ko, Y. S.; Jeon, J. W.; Seo, H.; Park, Y. K.; Choi, M. Epoxide-Functionalization of Polyethyleneimine for Synthesis of Stable Carbon Dioxide Adsorbent in Temperature Swing Adsorption. *Nat. Commun.* **2016**, *7*, 1–8. https://doi.org/10.1038/ncomms12640.
(41) Gadipelli, S.; Patel, H. A.; Guo, Z. An Ultrahigh Pore Volume Drives Up the Amine Stability and Cyclic CO2 Capacity of a Solid-Amine@Carbon Sorbent. *Adv. Mater.* **2015**, *27* (33), 4903–4909. https://doi.org/10.1002/adma.201502047.
(42) Gibson, J. A. A.; Gromov, A. V.; Brandani, S.; Campbell, E. E. B. The Effect of Pore Structure on the CO2 Adsorption Efficiency of Polyamine Impregnated Porous Carbons. *Microporous Mesoporous Mater.* **2015**, *208*, 129–139. https://doi.org/10.1016/j.micromeso.2015.01.044.
(43) Song, G.; Zhu, X.; Chen, R.; Liao, Q.; Ding, Y. D.; Chen, L. An Investigation of CO2 Adsorption Kinetics on Porous Magnesium Oxide. *Chem. Eng. J.* **2016**, *283*, 175–183. https://doi.org/10.1016/j.cej.2015.07.055.
(44) Martinez, J.; Castro-Osma, J. A.; Alonso-Moreno, C.; Rodriguez-Dieguez, A.; North, M.;

Otero, A.; Lara-Sanchez, A. One-Component Aluminum(Heteroscorpionate) Catalysts for the Formation of Cyclic Carbonates from Epoxides and Carbon Dioxide. *ChemSusChem* **2017**, *10* (6), 1175–1185. https://doi.org/10.1002/cssc.201601370.

(45) Su, X.; Bromberg, L.; Martis, V.; Simeon, F.; Huq, A.; Hatton, T. A. Postsynthetic Functionalization of Mg-MOF-74 with Tetraethylenepentamine: Structural Characterization and Enhanced CO2 Adsorption. *ACS Appl. Mater. Interfaces* **2017**, *9* (12), 11299–11306. https://doi.org/10.1021/acsami.7b02471.

(46) Heydari-Gorji, A.; Belmabkhout, Y.; Sayari, A. Degradation of Amine-Supported CO2 Adsorbents in the Presence of Oxygen-Containing Gases. *Microporous Mesoporous Mater.* **2011**, *145* (1–3), 146–149. https://doi.org/10.1016/j.micromeso.2011.05.010.

(47) Jahandar Lashaki, M.; Sayari, A. CO2 Capture Using Triamine-Grafted SBA-15: The Impact of the Support Pore Structure. *Chem. Eng. J.* **2018**, *334* (October 2017), 1260–1269. https://doi.org/10.1016/j.cej.2017.10.103.

(48) Foo, G. S.; Lee, J. J.; Chen, C. H.; Hayes, S. E.; Sievers, C.; Jones, C. W. Elucidation of Surface Species through in Situ FTIR Spectroscopy of Carbon Dioxide Adsorption on Amine-Grafted SBA-15. *ChemSusChem* **2017**, *10* (1), 266–276. https://doi.org/10.1002/cssc.201600809.

(49) Sayari, A.; Belmabkhout, Y.; Serna-Guerrero, R. Flue Gas Treatment via CO2 Adsorption. *Chem. Eng. J.* **2011**, *171* (3), 760–774. https://doi.org/10.1016/j.cej.2011.02.007.

(50) Gelles, T.; Lawson, S.; Rownaghi, A. A.; Rezaei, F. *Recent Advances in Development of Amine Functionalized Adsorbents for CO2 Capture*; 2020. https://doi.org/10.1007/s10450-019-00151-0.

(51) Sayari, A.; Belmabkhout, Y. Stabilization of Amine-Containing CO2 Adsorbents: Dramatic Effect of Water Vapor. *J. Am. Chem. Soc.* **2010**, *132* (18), 6312–6314. https://doi.org/10.1021/ja1013773.

(52) Kortunov, P. V.; Siskin, M.; Baugh, L. S.; Calabro, D. C. In Situ Nuclear Magnetic Resonance Mechanistic Studies of Carbon Dioxide Reactions with Liquid Amines in Non-Aqueous Systems: Evidence for the Formation of Carbamic Acids and Zwitterionic Species. *Energy and Fuels* **2015**, *29* (9), 5940–5966. https://doi.org/10.1021/acs.energyfuels.5b00985.

(53) Caplow, M. Kinetics of Carbamate Formation and Breakdown. *J. Am. Chem. Soc.* **1968**, *90* (24), 6795–6803. https://doi.org/10.1021/ja01026a041.

(54) Heydari-Gorji, A.; Yang, Y.; Sayari, A. Effect of the Pore Length on CO2 Adsorption over Amine-Modified Mesoporous Silicas. *Energy & Fuels* **2011**, *25* (9), 4206–4210. https://doi.org/10.1021/ef200765f.

(55) Shen, X.; Du, H.; Mullins, R. H.; Kommalapati, R. R. Polyethylenimine Applications in Carbon Dioxide Capture and Separation: From Theoretical Study to Experimental Work. *Energy Technol.* **2017**, *5* (6), 822–833. https://doi.org/10.1002/ente.201600694.

(56) Lawson, S.; Griffin, C.; Rapp, K.; Rownaghi, A. A.; Rezaei, F. Amine-Functionalized MIL-101 Monoliths for CO2 Removal from Enclosed Environments. *Energy and Fuels* **2019**, *33* (3), 2399–2407. https://doi.org/10.1021/acs.energyfuels.8b04508.

(57) Jeon, S.; Jung, H.; Jo, D. H.; Kim, S. H. Development of Crosslinked PEI Solid Adsorbents for CO2 Capture. *Energy Procedia* **2017**, *114* (November 2016), 2287–2293. https://doi.org/10.1016/j.egypro.2017.03.1373.

(58) Zhang, H.; Goeppert, A.; Czaun, M.; Prakash, G. K. S.; Olah, G. A. CO2 Capture on Easily Regenerable Hybrid Adsorbents Based on Polyamines and Mesocellular Silica Foam. Effect of Pore Volume of the Support and Polyamine Molecular Weight. *RSC Adv.* **2014**, *4* (37), 19403–19417. https://doi.org/10.1039/c4ra02145b.
(59) Ahmadalinezhad, A.; Sayari, A. Oxidative Degradation of Silica-Supported Polyethylenimine for CO2adsorption: Insights into the Nature of Deactivated Species. *Phys. Chem. Chem. Phys.* **2014**, *16* (4), 1529–1535. https://doi.org/10.1039/c3cp53928h.
(60) Heydari-Gorji, A.; Sayari, A. Thermal, Oxidative, and CO2-Induced Degradation of Supported Polyethylenimine Adsorbents. *Ind. Eng. Chem. Res.* **2012**, *51* (19), 6887–6894. https://doi.org/10.1021/ie3003446.

CHAPTER 3 CO_2 – AMINE REACTION MECHANISMS: A UNIFIED APPROACH

3.0. Overview

A unified CO_2-amine reaction mechanism applicable to absorption in aqueous or non-aqueous solutions and to adsorption on immobilized amines in the presence of both dry or humid conditions is proposed. Key findings supported by theoretical calculations and experimental evidence are as follows. (1) The formation of 1,3-zwitterion, RH_2N^+-COO^- is highly unlikely, because not only the associated 4-centered mechanism has a high energy barrier, but it is not consistent with the orbital symmetry requirements for chemical reactions. (2) The nucleophilic attack of CO_2 by amine requires the catalytic assistance of a Brønsted base through a 6-centered mechanism to achieve proton transfer/exchange. An important consequence of this concerted mechanism is that the N and H atoms added to the C=O double bond do not originate from a single amine group. Using ethylenediamine for illustration, detailed description of the reaction pathway is reported using the Reactive Internal Reaction Coordinate (RIRC) as a new tool to visualize the reaction path. (3) In the presence of protic amines, the formation of ammonium bicarbonate/carbonate does not take place through the widely accepted hydration of carbamate/carbamic acid. Instead, water behaves as a nucleophile that attacks CO_2 with catalytic assistance by amine groups, and carbamate/carbamic acid decomposes back to amine and CO_2. (4) Generalization of the catalytic assistance concept to any Bronsted base established through theoretical calculations, was supported by infrared measurements. A unified six-centered mechanism was proposed to describe all possible interactions of CO_2 with amines and water, each playing the role of nucleophile and/or Brønsted base, depending on the actual conditions.

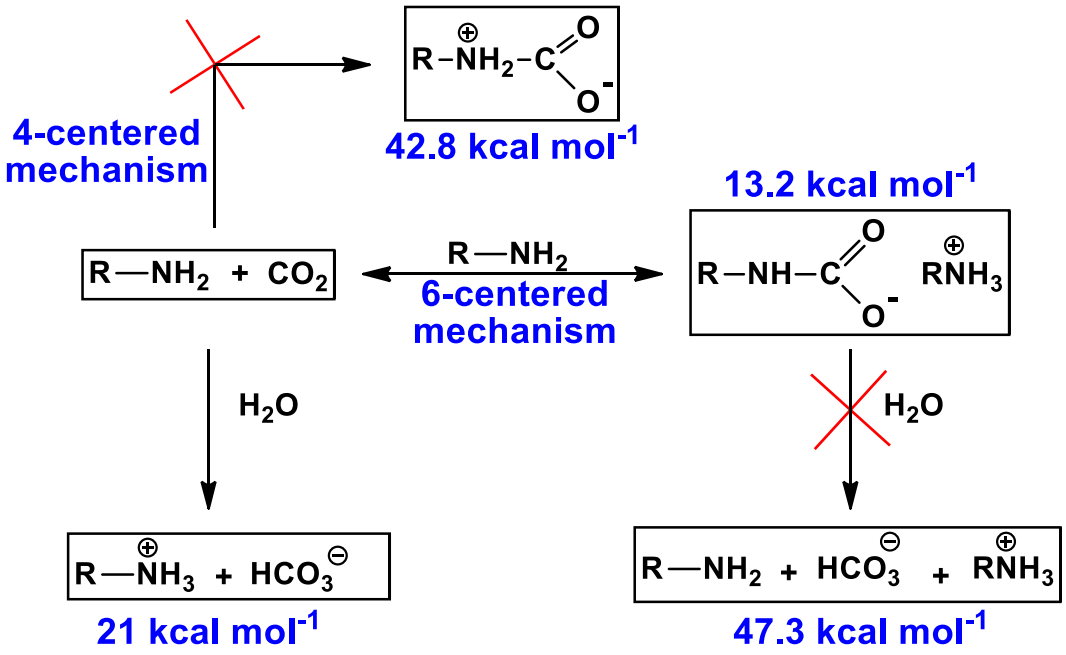
4-centered mechanism
R–NH2–C(=O)–O-
42.8 kcal mol-1
13.2 kcal mol-1
R—NH2 + CO2
R—NH2
6-centered mechanism
R–NH–C(=O)–O- RNH3
H2O
H2O
R—NH3 + HCO3
21 kcal mol-1
R—NH2 + HCO3 + RNH3
47.3 kcal mol-1

3.1. Introduction

The increasingly rapid development of amine-based adsorbents for the removal of CO_2 from large point sources or via direct air capture to mitigate the greenhouse gas effect is currently close to commercial-scale implementation. Although many practical issues are yet to be fully addressed such as oxidative degradation and other deactivation processes,[1] there has been significant progress in fundamental understanding of CO_2 - amine interactions under a variety of adsorption conditions.[2,3] Similar effort is being deployed for the development of viable amine absorption technologies for CO_2 capture.[4]

The main species actually detected upon interaction of CO_2 with supported amines or amine solutions are strikingly similar. In a series of reports, Kortunov *et al.*[5–8]. applied in situ ^{1}H and ^{13}C NMR to systematically investigate the chemistry of CO_2 absorption in a wide range of conditions, including different temperatures and pressures. They studied a variety of amines and promoters, in both aqueous and non-aqueous solvents. Depending on the prevailing conditions, the following species were detected in different proportions: ammonium carbamate, carbamic acid and carbonate/bicarbonate. Only ionic species occurred in aqueous solutions, whereas carbamic acid was detected in particular in polar non-aqueous solvents.[8] Likewise, CO_2 adsorption over supported amines generates carbamic acid and alkylammonium carbamate and/or bicarbonate, depending on the amine loading and the adsorption conditions.[9] Such species were characterized mostly by FTIR[10–16] and ^{13}C solid state NMR,[17–20] and to a lesser extent ^{15}N NMR[21,22] and X-ray diffraction.[23] They are typically

stabilized through hydrogen bonding with other species, including amines, water and hydroxyl groups.[18–20,23–25] Furthermore, the nature of the chemical species formed as well as the amine efficiency, i.e. CO_2/N ratio, were found to depend on the surface density of amine groups.[16,19,24,26] Although the formation of alkylammonium carbamate is often dominating under dry condition, Cendak *et al.*[19] found that at low surface density, supported amines give rise mainly to carbamic acid, whereas at high density, the formation of alkylammonium carbamate prevails. Carbamic acid was also demonstrated to occur in the absence of moisture, on primary amine-bearing metal-organic framework,[21] or other hydrophobic media.[23] In contrast, under humid condition, carbamate and bicarbonate were found to be the dominating species.[21,24]

With regard to the reaction mechanism, based on the nature of the products and their evolution, Kortunov *et al*.[5] surmised that the first step is a nucleophilic attack of CO_2 carbon by amine (Lewis base), leading to zwitterion RH_2N^+-COO^-, which will be referred to as 1,3-zwitterion, where 1 and 3 indicate the positive and negative centers, respectively. Depending on the actual conditions, the 1,3-zwitterion may undergo an intermolecular proton transfer with another amine (Brønsted base) to form ammonium carbamate [5], or an intramolecular hydrogen transfer to afford carbamic acid.[8] As for water, it may also behave as a nucleophile, reacting with CO_2 to afford carbonic acid, which in turn reacts with amine to generate carbonate/bicarbonate.[5,6] It may also hydrate the carbamate anion to form carbonate/bicarbonate, releasing one amine molecule for further reaction with CO_2.[5,7] As in amine solution, the formation of 1,3-

zwitterion during CO_2 adsorption over supported amines was often mentioned, but never observed.[13,15,27]

Parallel to experimental work, theoretical studies were conducted to unravel the nature of adsorbed species and elucidate the CO_2 capture mechanism by supported amines in the presence and absence of moisture[10,13,14,27–31]. Didas *et al.*[10] and others[14,27,30,31] demonstrated that the energy barrier for the formation of carbamic acid using two amine molecules per CO_2 (ca. 16 kcal mol^{-1}) was much lower than the one-to-one reaction (ca. 40-50 kcal mol^{-1}). Presumably, one amine acting as a nucleophile (Lewis base), attacks the CO_2 carbon, whereas the other (Brønsted base) facilitates the proton transfer/exchange. There is evidence that surface hydroxyl groups[28,29] and water molecules[29,32] are also capable of assisting the proton transfer process.

Nonetheless, despite the apparently simple species involved and decades of effort, the mechanisms of CO_2 interaction with amines, whether immobilized or in solution, are still a matter of debate. For example, 1,3-zwitterions introduced since the 1960s,[33,34] were mentioned repeatedly in the literature, but never detected, and their involvement in CO_2 - amine interactions has been controversial. Numerous kinetic and computational arguments were put forward both in favor,[34,35] and against,[27,36,37] the formation of 1,3-zwitterions in aqueous amines. Alternatively, other investigations pointed out that the nucleophilic attack of CO_2 carbon by amine is *assisted* or *catalyzed* by another species such as amine, water or OH groups, playing the role of a Brønsted base to achieve the proton transfer/exchange required for the formation of ions pairs, such as ammonium carbamate,[5,10,27–29] obviating the intermediacy of 1,3-zwitterion.

This termolecular mechanism is strongly supported by kinetic[36,37] and theoretical[27,28,38] data.

The main questions to be addressed in this chapter are as follows. How likely that carbamic acid or ammonium carbamate form through the intermediacy of a 1,3-zwitterion? Does the formation of ammonium bicarbonate/carbonate involve reaction of water with CO_2 or the hydrolysis of carbamate species? Is there a unified mechanism for the interactions of CO_2 with amines and water, whether in solution or at the solid-gas interface? Accordingly, the objectives of the current work are threefold: (i) provide theoretical and experimental evidence that the mechanisms of CO_2 reactions with protic amines under different conditions, including adsorption in dry or humid conditions, and absorption in aqueous or organic solvents, takes place through a 6-centered mechanism, without the intermediacy of the widely reported 1,3-zwitterion. (ii) demonstrate based on theoretical and experimental data that the formation of bicarbonate/carbonate occurs via amine-assisted nucleophilic attack of CO_2 by water, instead of the highly popular carbamate hydrolysis. (iii) establish a unified mechanism for all CO_2 interactions with amines and water, each playing the role of nucleophile and/or Brønsted base, depending on the actual conditions.

Our calculations dealt primarily with CO_2-amine-water interactions in the gas state to uncover the intrinsic reactivity of these species. Solvent effects were also discussed using water and CCl_4 as representative polar and non-polar solvents. The most salient theoretical findings were further supported by specifically designed FTIR and NMR experiments.

3.2. Experimental

3.2.1. Modelling Methods

Density functional theory (DFT) calculations were carried out using the Gaussian 09 software package[39] associated to the B3LYP[40], M06-2X[41] and PW6B95[42] functionals. All the obtained data are listed in Tables 1 and S1. As seen, all three methods gave consistent results with no systematic departure from each other. As shown in Table 3-1, Post HF calculations MP2 and CCSD(T) for amine - CO_2 reaction fitted better with the B3LYP results. Hence, the discussion will be based primarily on data of the latter functional. Optimization of geometrical structures of the reactants, transition states, and products was performed using the 6-311++G(d,p) basis set.[43] This included polarization and diffuse functions, which are required for investigating dipolar species. All stationary points of the potential energy surface (PES) corresponded to local minima, all with real vibrational frequencies or to transition states characterized by only one imaginary frequency. Energy, force and internal coordinate profiles were obtained from the intrinsic reaction coordinate (IRC) analysis.[44–46]

Table 3-1: Activation energy Ea and Gibbs activation energy Δ_rG^* in kcal mol^{-1} calculated in the gas phase and in the presence of CCl_4 and water solvents by DFT/ 6-311++G(d,p) with the three functionals M06-2X, PW6B95 et B3LYP

			CH_3NH_2	$H_2NCH_2CH_2NH_2$	CH_3NH_2/ CH_3NH_2[a]	CH_3NH_2/ H_2O[a]	CA[b] + H_2O	H_2O/ CH_3NH_2[a]
Ea	Gas	B3LYP	42.8	26.5	13.2	16.5	47.3	21.0
		M062X	40.3	19.8	15.5	20.0	53.8	16.4
		PW6B95	41.4	27.4	18.8	24.1	54.3	21.7
Δ_rG^*	Gas	B3LYP	44.8	32.6	25.9	27.7	55.4	18.5
		M062X	42.2	27.8	20.7	22.2	55.1	19.1
		PW6B95	43.1	30.0	22.5	27.7	55.1	23
	CCl_4	B3LYP	41.8	23.4	16.7	24.7	54.9	20.5
		M062X	36.9	18.3	9.3	19.1	50.4	16.3
		PW6B95	39.6	20.9	15.8	25.1	53.4	18.4
	H_2O	B3LYP	31.3	5.2	2.4	15.1	53.1	9.4
		M062X	30.2	8.3	1.6	13.1	51.7	6.5
		PW6B95	36.4	10.9	1.9	15.8	52.5	13.0

[a] The first compound is the reactant and the second is the assisting species. [b] CA designates carbamic acid.

To include solvent effects, if any, additional calculations were carried out using water and CCl_4 as representative polar and non-polar solvents. The PCM model[47] was used with the three above-mentioned functionals B3LYP, M06-2X and pw6b95. To discuss solvent effects, we used the free Gibbs activation energy, which stems from statistical thermodynamics, rather than the activation energy, which is more appropriate to discuss molecular properties.

3.2.2. Preparation of Adsorbent

Propylamine-grafted silica was prepared as described elsewhere.[48] 1 g of pre-dried Q-10 CARiACT silica (Fuji Silysia, Japan) support was dispersed in 40 mL of toluene in a 100 mL two-neck round bottom flask immersed in an oil bath. After 30 min stirring at room temperature, 0.3 mL of distilled water was added while stirring continued for 30 min. The temperature of the mixture was then raised to 100 ^{o}C. After 30 min, 2 mL of (3-aminopropyl) trimethoxysilane was added and the mixture kept under reflux for 2 h. The flask was cooled down to room temperature and the material was filtered, washed with toluene and ethanol, and dried under vacuum at 60 ^{o}C for 5 h. The amine content was determined by decomposition using a thermogravimetric analyzer. The material was first heated in N_2 up to 800 ^{o}C at 10 ^{o}C/min, then in air at 800 ^{o}C for 10 min. The amine content based on the weight loss beyond 200 ^{o}C was 4.4 mmol/g.

3.2.3. FT-IR spectroscopy

In situ FT-IR experiments were specifically designed to demonstrate that CO_2 adsorption on immobilized amine in humid conditions takes place through a six-centered mechanism assisted by water (here D_2O). Measurements were carried out on a Nicolet 6700 spectrometer equipped with a mercury cadmium telluride (MCT) detector, using ambient air as background. Self-supported translucent wafers of about 5 mg and 1 cm diameter were placed inside a stainless-steel IR cell equipped with CaF_2 windows. The sample was thermally pre-treated in N_2 at 120 ^{o}C for 2 h to remove any adsorbed species. Then, the cell was allowed to cool down to room temperature, and a spectrum was recorded through 128 scans under nitrogen. The material was exposed

for 15 min to N_2 saturated in D_2O at 20 °C, then regenerated at 120 °C, and a spectrum was recorded. A similar experiment was carried out replacing N_2 by 15% CO_2/N_2.

3.3. Results and Discussion

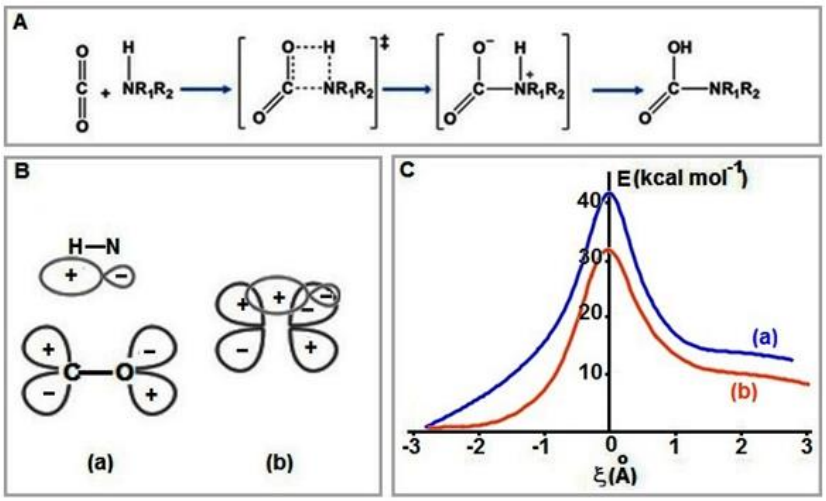

Figure 3-1. Formation of 1,3-zwitterion and carbamic acid. (A) Four-centered mechanism, (B) Frontier orbitals involved in four-centered mechanism: (a) HOMO and LUMO of N-H and C=O, (b) symmetry-forbidden orbital recovery. (C) Corresponding energy profile: (a) in gas state, (b) in the presence of water as solvent.

3.3.1. Reaction mechanism for carbamate/carbamic acid formation

3.3.1.1. Four-centered mechanism.

Fig. 3-1A shows the reaction mechanism of a primary or secondary amine with CO_2 involving 1,3-zwitterion as a reaction intermediate. Calculations in the gas state showed that carbamic acid, the ultimate product of the reaction, is obtained by a concerted elementary reaction through a single transition state with synchronous formation of C-N and O-H bonds. The energy barrier (Gibbs activation energy resp.) Ea (Δ_rG^* resp.) for the 4-centered mechanism outlined in Fig. 3-1A, was found to be 42.8

(44.8 resp.) and 40.0 (41.0 resp.) kcal mol^{-1}, for primary and secondary amines (Table A3-1), respectively. Several authors reported high activation energy barriers of the order of 40-50 kcal mol^{-1} for 1:1 reaction between CO_2 and amines,[10,14,27,30,31] indicating that this mechanism is unlikely to occur. Moreover, regardless of the energy barrier, this mechanism is not consistent with the symmetry requirements according to Wigner's orbital symmetry conservation rule.[49,50] Accordingly, for any symmetry-allowed reaction, the nuclear coordinates must belong to the same point group along the whole pathway from reagents to transition state and products. Transfer of electrons takes place from HOMO of the nucleophile to LUMO of the electrophile (Fig. 3-1B(a)) to achieve positive orbital overlap. As illustrated in Fig. 3-1B(b), four-centered reactions are symmetry forbidden, because the LUMO-HOMO orbitals exhibit opposite signs in the overlap area.

We also investigated the effect of CCl_4 and H_2O solvent on the reaction of CO_2 and methylamine. In both cases, the activation energy was lower than in the gas state (Table 3-2), the lowest being in the presence of water (Fig. 3-1C). As shown in Table 3-2, the activation free energy for the four-centered mechanism of CO_2-methylamine reaction involving 1,3-zwitterion, remained high in the presence of not only CCl_4 (41.8 versus 44.8 kcal mol^{-1} in the gas state), but even in water (31.3 kcal mol^{-1}).

Table 3-2. Activation energy Ea* and free Gibbs energy ΔrG* in kcal mol-1 for the reaction involving CO_2 and several amines in dry and wet conditions in gas state and in the presence of Cl_4 and H_2O solvents

		CH_3NH_2	$H_2N(CH_2)_2NH_2$	CH_3NH_2/ CH_3NH_2[a]	CH_3NH_2/ H_2O[a]	CA[b] + H_2O	H_2O/ CH_3NH_2[a]
Ea	Gas	42.8	26.5	13.2	16.5	47.3	21.0
ΔrG*	Gas	44.8	32.6	25.9	27.7	55.4	18.5
	CCl4	41.8	23.4	16.7	24.7	54.9	20.5
	H2O	31.3	5.2	2.4	15.1	53.1	9.4

The first compound is the nucleophile (Lewis base), and the second compound is the assisting species (Brønsted base). [b] CA designates carbamic acid formed by addition of methylamine and CO_2.

Catalytic assistance by a Brønsted base involving a six-centered mechanism may significantly lower the energy barrier.[10,27,31] Interestingly, this mechanism indicates that the hydrogen atom that binds to the oxygen does not originate from the same amine group whose nitrogen attaches to CO_2. This is demonstrated below in three representative instances, based on theoretical and experimental arguments.

3.3.1.2. Self-assistance in CO_2 adsorption over diamines.

The reaction of CO_2 with ethylenediamine in the gas state shows that the catalytic assistance of a Brønsted base is a *requirement* rather than a convenient procedure to generate a low energy transition state. Fig. 3-2A depicts the optimized structures of the transition state TS, the 1,6-zwitterion, the transition state TS', and carbamic acid, corresponding to CO_2 reaction with H_2N-$(CH_2)_2$-NH_2. Fig. 3-2B(a) shows the energy profile in the gas state of the carbamic acid formation obtained by the IRC option of Gaussian 09. The calculated activation barrier was 26.5 kcal mol^{-1} (Table 3-2), and the two ends in this curve corresponded to the reactants and the expected

carbamic acid product. The transition state TS is the outcome of the N1 atom approaching the CO_2 carbon atom C, and the hydrogen H1 leaving. Interestingly, this hydrogen does not approach the nearby O1 oxygen of CO_2, but it moves toward the other nitrogen atom N2, leading to the formation of an ammonium group. Notice that the transition state forms a six-membered ring as shown in Fig. 3-2A(a) and corresponds to an imaginary frequency of i926 cm^{-1}. In TS, the H1 to N1 and N2 distances were 1.46 Å and 1.17 Å, respectively, while the H2-O1 distance was 2.09 Å. Moreover, the N1-C distance of 1.53 Å was close to the final bond length in carbamic acid, estimated to be 1.48 Å. Notice that similar calculations using diamines with up to 5 carbon chain spacers gave similar activation energies and mechanisms.

After completion, this process leads to a 1,6-zwitterion (Fig. 3-2A(b)). Unless the zwitterion is stabilized by polar species such as the solvent or surface OH groups, one hydrogen atom of the ammonium group, H2, is detached and binds asynchronously to the negatively charged oxygen (Fig. 3-2A(c)), giving rise to carbamic acid (Fig. 3-2A(d)). In the corresponding transition state TS' (Fig. 3-2A(c)), H2 was located at 1.16 Å and 1.39 Å from O1 and N2, respectively. It is clear that the 6-centered mechanism stems directly from the CO_2 interactions with the two amine groups, without any external artifact. Therefore, the nitrogen and hydrogen atoms that add to the carbonyl of CO_2 originate from two different amine groups. Using propylenediamine, Heldebrant *et al*.[51] provided spectroscopic evidence for the occurrence of 1,7-zwitterionic carbamate, consistent with the proposed self-assistance mechanism.

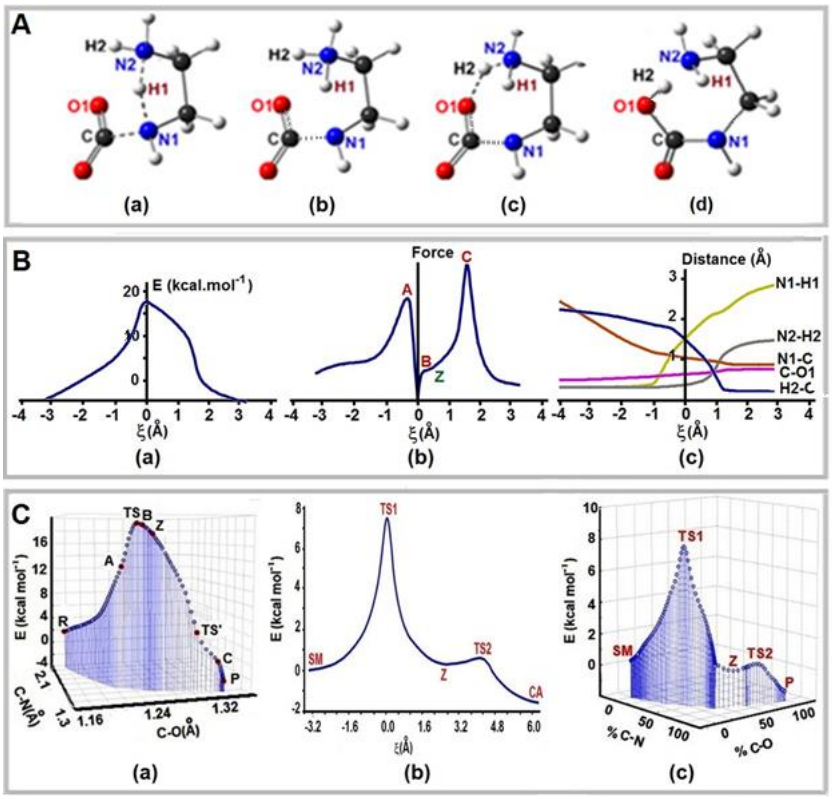

Figure 3-2. CO_2 reaction with ethylenediamine. (A) Calculated structures: (a) TS, (b) 1,6-zwitterion, (c) TS', and (d) carbamic acid. (B) (a) Energy profile of carbamic acid formation in the gas state, (b) the corresponding force profile, and (c) variation of selected internuclear distances versus reaction coordinate in gas state. (C) (a) RIRC versus N1-C and C-O1 internuclear distances in the gas state. (b) Energy profile of carbamic acid formation in water, and (c) RIRC versus N1-C and C-O1 internuclear distances in water as percentages of final distances in carbamic acid. R and P = reactants and product, Z = 1,6-zwitterion, TS and TS' = transition states, A and B = limits of TS zone of influence, C = preparation of the product.

To elucidate the reaction mechanism, it is customary to consider the energy profile (Fig. 3-2B(a)), the force profile obtained as RMS gradient norm (Fig. 3-2B(b)) and the variations of selected internal coordinates (Fig. 3-2B(c)) as a function of the intrinsic reaction coordinate. Considering the variations of pertinent internuclear bond distances such as N1-H1, N2-H2 and C-O1 (the C=O bond length is assumed to be fixed),

the reaction progress can be described as depicted in Fig. 3-2B(b). At the onset of the reaction, the energy starts to increase at coordinate ca. -1.59 Å, whereas the transition state TS zone of influence lies between the two maxima A and B located at coordinates -0.37 and 0.11 Å of the force profile. The species Z (Fig. 3-2B(b)) associated with the asymptotic behavior of the energy profile section corresponding to the transition state TS is located at coordinate 0.58 Å and has a 1,6-zwitterion structure (Fig. 3-2A(b)) as further confirmed by NBO calculations.[52] The N1-C distance of 1.50 Å in the 1,6-zwitterion represents the typical length of a single bond. The C-O1 increased from its original length of 1.22 Å in CO_2 to 1.26 Å in the 1,6-zwitterion. The third maximum C located at coordinate 1.59 Å (Fig. 3-2B(b)) corresponds to the transition state TS' (Fig. 3-2A(c)) controlling the transfer of proton H2 from N2 to O1, leading to carbamic acid (Fig. 3-2A(d)). Analysis of Fig. 3-2B(c), which represents the evolution of the internuclear distances of active bonds, i.e. those that break or form, shows clearly that the formation of carbamic acid involves two asynchronous processes. The 1,6-zwitterion formation stage ends with the N1-H1 bond almost broken (equal to 1.8 Å) and N1-C bond almost established (equal to 1.49 Å), just after the occurrence of the transition state TS. Furthermore, the N2-H2 bond begins to break up at coordinate 1.59 Å, while H2 approaches O1 to establish the O-H bond.

Our work shows that for ethylenediamine-CO_2 reaction, the 1,6-zwitterion forms first as a long-lived active transitory species acting as an intermediate species in the formation of carbamic acid via an asynchronous process. Being a transient species, the 1,6-zwitterion does not correspond to a local minimum, i.e. to a metastable state, but

its presence is associated with a flat region of the potential surface. Therefore, it is difficult to gain further insights into such species with the conventional quantum chemistry tools such as the energy profile or contour plot. To address this shortcoming, we developed an alternative methodology enabling the visualization of the reaction path versus two internal coordinates referred to as Reactive Internal Reaction Coordinates (RIRC).[46] Such coordinates often represent the distances associated with bonds that form or break. The RIRC is a 3D representation of the reaction path (Fig. 3-2C(a)) independently from the PES. It provides a visual representation of the energy as a function of the internal coordinates, not the reaction coordinate. This representation is highly informative because internal coordinates are easier to apprehend than the reaction coordinate.

Table 3-3. Activation energy Ea* and free Gibbs energy ΔrG* in kcal mol-1 for the reaction involving CO_2 and several amines in dry and wet conditions in gas state and in the presence of Cl_4 and H_2O solvents

		CH_3NH_2	$H_2N(CH_2)_2NH_2$	CH_3NH_2/ CH_3NH_2[(a)]	CH_3NH_2/ H_2O[(a)]	CA[(b)] + H_2O	H_2O/ CH_3NH_2[(a)]
Ea	Gas	42.8	26.5	13.2	16.5	47.3	21.0
ΔrG*	Gas	44.8	32.6	25.9	27.7	55.4	18.5
	CCl4	41.8	23.4	16.7	24.7	54.9	20.5
	H2O	31.3	5.2	2.4	15.1	53.1	9.4

[(a)] The first compound is the nucleophile (Lewis base), and the second compound is the assisting species (Brønsted base). [(b)] CA designates carbamic acid formed by addition of methylamine and CO_2.

As in the case of monoamine, the non-polar aprotic solvent CCl_4 did not affect the proposed mechanism for diamines. Its role was limited to decreasing the energy barrier (Table 3-2). However, in the presence of water as solvent, the energy profile (Fig. 3-2C(b)) no longer reflects an asynchronous concerted mechanism with a single transition state,

but becomes characteristic of a two-step reaction with two transition states, each corresponding to the transfer of a single hydrogen atom. Hence, the 1,6-zwitterion becomes an actual reaction intermediate that evolves instantaneously into carbamic acid, because the second transition state is associated with an extremely low energy barrier.

The structure of 1,6-zwitterion together with the NBO analysis show that the C-N bond was completely established (Tables A3-2 and A3-3), the N2 nitrogen had three N-H bonds, consistent with an ammonium group, and O1 was negatively charged since it had three lone pairs, although partially conjugated with the C=O2 pi electrons. Consistently, the bond indices for C-N, C-O1 and C-O2 as indicated by the corresponding Wiberg indices were 1.1, 1.3 and 1.5, respectively.

Fig. 3-2C(c) clearly shows the two reaction steps and their evolution as x and y axes in the RIRC representation correspond to the percent formation of the N-C bond and the percent cleavage of the pi C=O bond, respectively. It is seen that at the 1,6-zwitterion stage, the C-N bond was ca. 80% established, whereas the C-O1 bond was only 20% shorter than its final length in carbamic acid.

3.3.1.3. Amine-CO_2 reaction assisted by another amine.

The foregoing discussion of six-centered mechanism of CO_2 interaction with a diamine was extended to single primary or secondary amines. Fig. 3-3 shows the optimized structures of TS, ammonium carbamate, and the TS' that transforms directly into carbamic acid, using methylamine for illustration. This is the same mechanism as for the diamine, shown in Fig. 3-2A. The calculated activation barrier of 13.2 kcal mol^{-1} (Table 3-2) is consistent with literature data.[10,53]

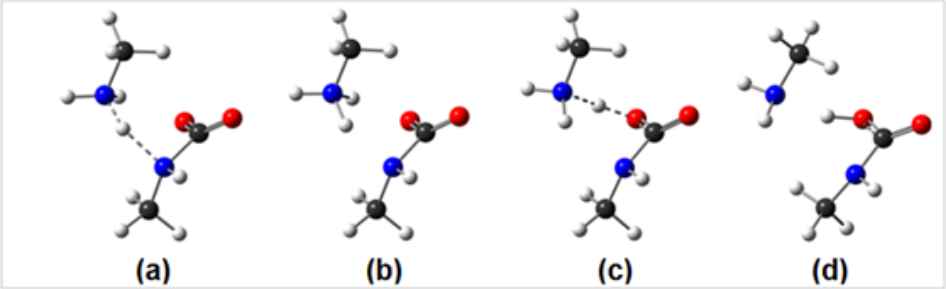

Figure 3-3. CO_2 reaction with a primary amine. (A) Amine-assisted reaction: (a) transition state TS, (b) ammonium carbamate, (c) transition state TS', and (d) carbamic acid.

In all amine-containing media, the actual species detected by spectroscopic techniques such as NMR and FTIR, depend on the environment, particularly on the occurrence of stabilizing species. As for CO_2 absorption in amine solutions, it is expected that dipolar species such as 1,6-zwitterions or ionic species such as alkylammonium carbamate will be stabilized by polar solvent molecules, e.g. water,[5] whereas neutral species such as carbamic acid occur particularly in polar organic solvents that promote hydrogen bonding.[8] As for amine-functionalized silica, occurrence of ammonium carbamate versus carbamic acid is strongly dependent on the amine surface density.[19,24] At high density, the nucleophilic attack of CO_2, is typically assisted by a nearby amine, leading to ammonium carbamate, often stabilized by hydrogen bonding,[13,14,18,19] whereas hydrogen bonded carbamic acid is favored at low amine loading.[14,19,24]

3.3.1.4. Water-assisted formation of carbamic acid.

Another important question arises when CO_2 adsorption takes place in the presence of moisture or in aqueous solvent is whether water assists the CO_2 – amine reaction? It is worth noting that the base ionization equilibrium, $R\text{-}NH_2 + H_2O \leftrightarrow R\text{-}NH^- +$

H_3O^+, shifts almost completely to the right in the presence of CO_2, given that what counts in CO_2-amine reactions is the nucleophilicity of the base, with R-NH_2 being more nucleophilic than R-NH^-; although R-NH^- is a stronger base. Our calculations indicated that similar to amine, water may assist the formation of carbamic acid (Fig. 3-4). This is an elementary stage with simultaneous proton exchange between water and amine through a 6-centered mechanism. The barrier was found to be 16.5 kcal mol^{-1} (Table 3-2), indicating that from a kinetics point of view, the water-assisted pathway is less competitive than the amine-assisted formation of carbamic acid. Notice that in the presence of non-hindered protic amine aqueous solutions, the carbamate anion and ammonium cation form in equal amounts until amine depletion,[5,54,55] indicating that, because such amines are stronger nucleophiles and stronger Brønsted bases than water, they play both roles.

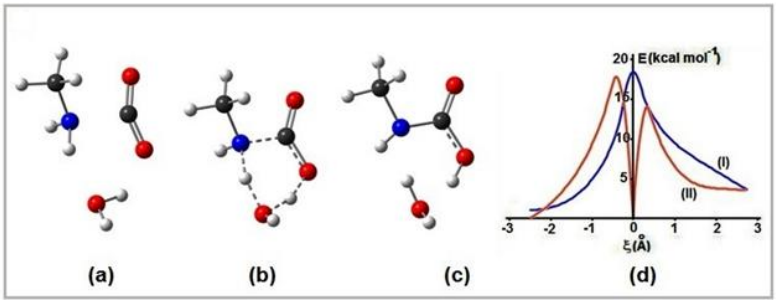

Figure 3-4. Water-assisted reaction: Calculated structures of (a) reactants, (b) transition state TS, (c) product P, (d-I) corresponding energy profile and (d-II) force profile.

As for solid-supported amines, because of the limited mobility of amine groups, it is surmised that water catalytic assistance becomes prominent for low amine surface density, leading to carbamic acid or hydronium carbamate (CO_2/N = 1), often stabilized by hydrogen bonding.[15,19,24,29] Notice that hydroxyl groups may play the same assisting role

as water vapor.[28] This is consistent with experimental evidence as the enhancement of amine efficiency in humid condition was found to be most pronounced for low amine surface coverage.[24]

3.3.1.5. Experimental evidence of six-centered mechanism.

Catalytic assistance of a Brønsted base toward the formation of carbamic acid/carbamate was substantiated experimentally using D_2O as an assisting species. Fig. 3-5a shows the FTIR spectrum of propylamine grafted silica after the initial thermal treatment. It exhibits bands at 3357-3159 cm^{-1} and 1595 cm^{-1}, attributable to NH_2 stretching and deformation, respectively. Difference spectra after exposure to CO_2/D_2O mixture and D_2O vapor are shown in Figs. 3-5b and c, respectively.

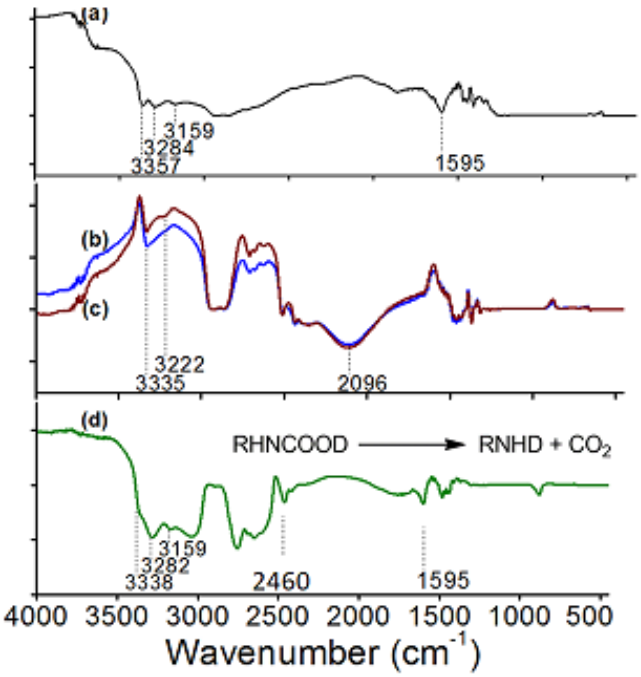

Figure 3-5. FT-IR data in support of CO_2-amine reaction assisted by D_2O. (Spectrum a): thermally treated adsorbent, (Spectrum b): difference between the spectrum of adsorbent exposed to D_2O and Spectrum a, (Spectrum c): difference between the spectrum of adsorbent exposed to D_2O/CO_2 mixture and Spectrum a, (Spectrum d): difference between Spectrum b and c.

In both cases, the band at 1595 cm^{-1} characteristic of δ(NH_2) deformation disappeared, and two bands at 3335 and 2096 cm^{-1} attributed to νN-H and νN-D stretching in –NHD, developed. This indicates that H/D exchange took place in both cases, but not to the same extent, since the difference spectra are not strictly identical. Interestingly, as shown in Fig. 3-5d, subtracting spectrum 3-5b from 3-5c led to qualitatively the same spectrum as the starting material shown in Fig. 3-5a. This is clear evidence that the H/D isotopic exchange due to D_2O is partial (eq 3-1), because spectrum 1c contains the characteristic bands of both NH_2 and NHD, whereas upon regeneration of the material after exposure to CO_2/D_2O (eq. 3-2), the deuteration was quantitative. This provides direct evidence that a D atom from D_2O was added to CO_2 to form the carbamic acid/carbamate (eq. 3-2), which becomes bonded to the amine N-atom upon regeneration (eq. 3-3), leading to the observed ν(N-D) vibrations.

$$RNH_2 + D_2O \longrightarrow RNHD + HOD \qquad (3.1)$$

$$RNH_2 + CO_2 + D_2O \longrightarrow RHNCOOD + HOD \qquad (3.2)$$

$$RHNCOOD \longrightarrow RNHD + CO_2 \qquad (3.3)$$

In Fig. 3.5d, note the presence of symmetric and asymmetric νC-H stretching of at 2750 and 2645 cm^{-1} respectively, νC-H bending at 1475 cm^{-1} of propyl chain (–CH_2–), and the –NH stretching of primary amine (–NH_2) at 1590 cm^{-1} suggests that H/D exchange is only partial. This may indicate that not all immobilized amines are involved with D_2O assistance.

3.3.2. Carbonate and bicarbonate formation

3.3.2.1. Carbamate hydrolysis.

Numerous literature reports indicated the formation of ammonium bicarbonate/carbonate during CO_2 capture by supported amines under humid conditions, mostly by inference since the amine efficiency increases in the presence of moisture,[48] but in some cases, experimental[11,20] or theoretical[13] evidence was provided. Likewise, carbamate and ammonium bicarbonate were found to apparently occur stepwise in amine aqueous solutions.[5,54,55] It is widely believed that in the presence of primary and secondary amines, bicarbonate/carbonate originate from carbamate hydrolysis both in CO_2 absorption or adsorption, mostly because bicarbonate/carbonate are observed[5] or presumed to occur[56] after the formation of ammonium carbamate. Hence, we investigated this process by optimizing the structures of the compounds involved and the transition state. As shown in Fig. 3-6, the formation of carbonic acid from carbamic acid (or bicarbonate from carbamate) follows a concerted one-step mechanism. The transition state is characterized by the simultaneous breakage of O-H bond, elongation of the carbamic acid C-N bond, and nucleophilic attack of the CO_2 carbon by water oxygen. Notice that the formation of carbonic acid is concerted but asynchronous, i.e. the proton from H_2O attaches to the nitrogen before oxygen binds to the CO_2 carbon. However, the calculated barrier of 47.3 kcal mol^{-1} is very high. Even when assisted by another water molecule (Fig. 3-7), the energy barrier associated with the six-centered mechanism remains as high as 38 kcal mol^{-1}. In line with our data, Matsuzaki *et al*.[57] reported

activation energies of 41 and 37 kcal mol^{-1} for non-assisted and water-assisted hydrolysis of monoethanolamine carbamate.

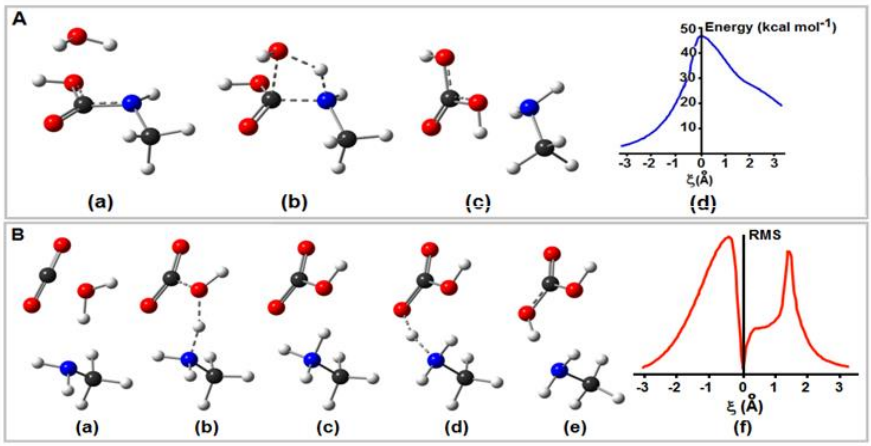

Figure 3-6. Carbonate/bicarbonate formation. (A) Calculated structures associated with hydrolysis of carbamic acid: (a) reactants, (b) transition state TS, and (c) product P, (d) corresponding energy profile. (B) Calculated structures associated with amine-assisted CO_2 reaction with water: (a) reactants, (b) transition state TS, (c) 1,6-zwitterion Z, (d) transition state TS' and (e) product, (f) corresponding force profile.

The high energy barriers indicate that the formation of carbonic acid/bicarbonate by this route is highly unlikely. Moreover, based on literature reports,[5,54,55] it is clear that in the presence of aqueous solutions of protic unhindered amines (strong Lewis bases), the formation of bicarbonate/carbonate starts only after quantitative formation of ammonium carbamate. It is thus intriguing that as long as ammonium carbamate is accumulating at the expense of amine, no bicarbonate/carbonate formed.

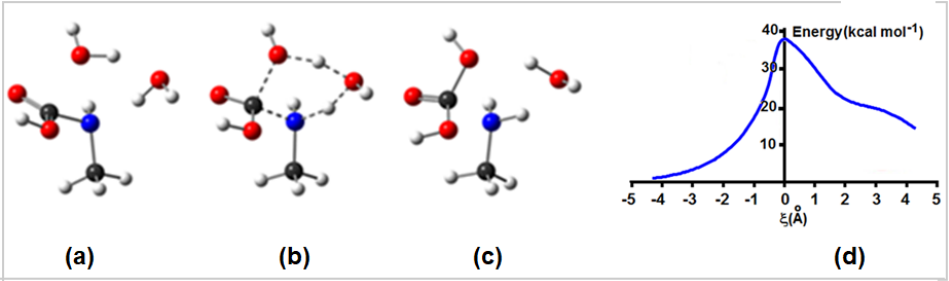

Figure 3-7. Hydrolysis of carbamic acid assisted by another water molecule. Calculated structures of (a) supermolecule, (b) transition state, and (c) product, (d) corresponding energy profile.

To gain further insights into the potential carbamate hydrolysis or the lack thereof, we exposed aqueous monoethanolamine to flowing CO_2, and took samples before and after complete depletion of amine. ^{13}C NMR analysis showed (Fig. 3-8) that none of the species evolved over several days even though the sample solutions contained ammonium carbamate and water, indicating that the formation of bicarbonate/carbonate requires CO_2, but in the absence of significant amounts of protic amines. It is thus clear, that the occurrence of bicarbonate/carbonate is not the direct result of carbamate hydrolysis. A similar argument can be made for CO_2 adsorption over immobilized amines.[56]

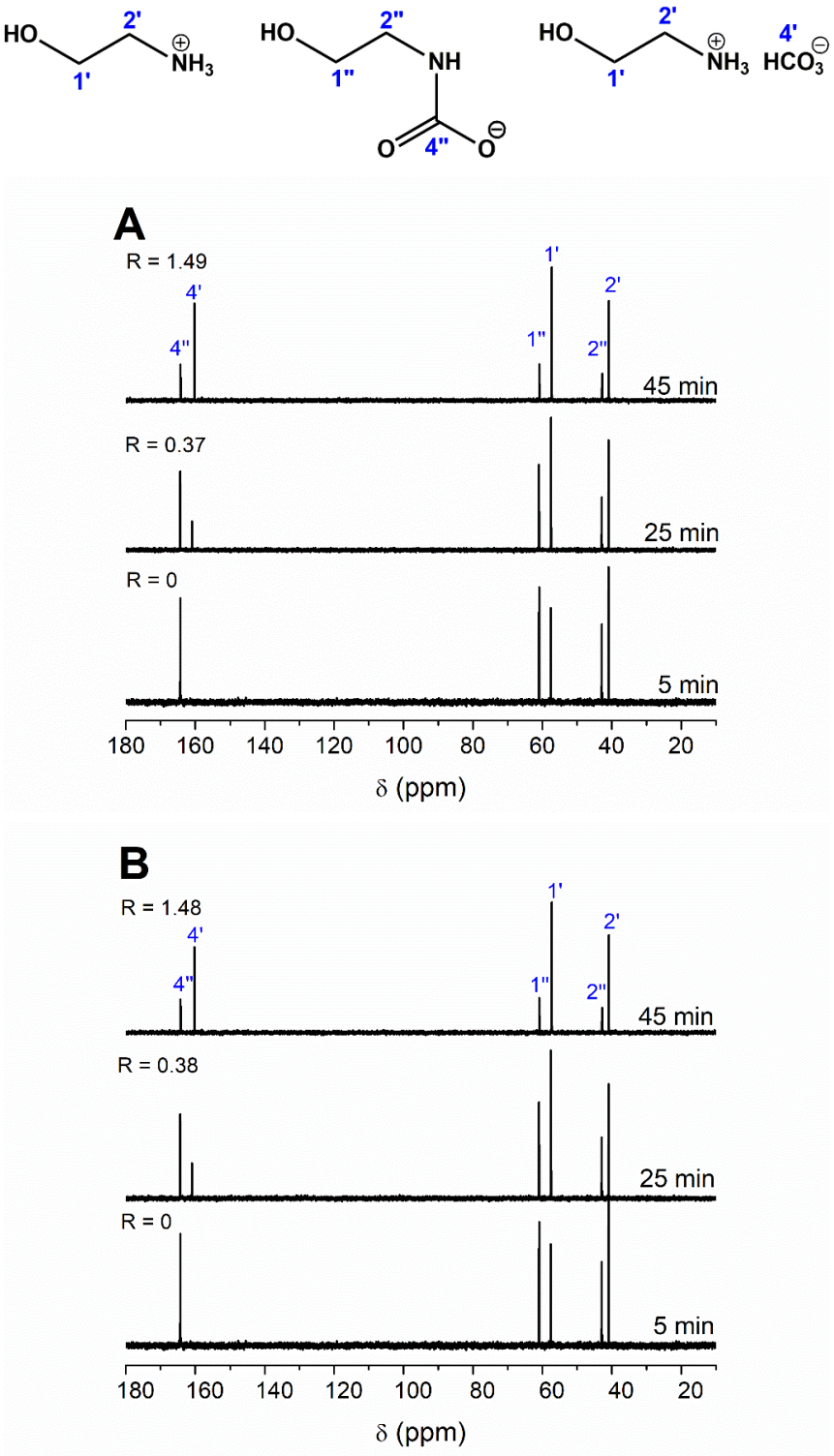

Figure 3-8. ^{13}C NMR Spectra of; (A) Ethanolamine (18 wt%) after bubbling CO_2 for different periods of time at room temperature as indicated, (B) for the samples shown in Fig A3-3(A) after 5 days (without additional exposure to CO_2). R is the ratio of the area of peak 4' to 4"

3.3.2.2. Amine-assisted formation of ammonium bicarbonate.

The formation of ammonium bicarbonate and carbonic acid by nucleophilic attack of CO_2 by a water molecule assisted by an amine group (Fig. 3-6B) was investigated. The energy profile has a force profile (Fig. 3-6B(f)) comparable to the already discussed CO_2 reaction with diamine (Fig. 3-2B(b)). Furthermore, the activation barrier was found to be about 21.0 kcal mol^{-1} (Table 3-2). It is proposed here that in the presence of aqueous amines, the main route to bicarbonate/carbonate is the reaction of CO_2 and water.

In the presence of unhindered primary and secondary amines, CO_2 reaction generates primarily ammonium carbamate (eq 3-4) since such amines are more basic and more nucleophilic than water. However, provided that the CO_2 pressure is maintained, when the amine is almost depleted, ammonium bicarbonate/carbonate starts forming according to eq 3-5. This in turn leads to the gradual decomposition of ammonium carbamate (opposite eq 3-4). Notice that addition of eq 3-5 and opposite eq 3-4 represents the apparent hydrolysis of ammonium carbamate (eq 3-6).

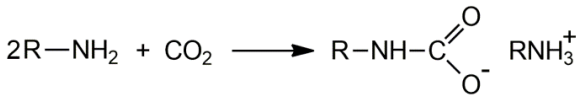

(3.4)

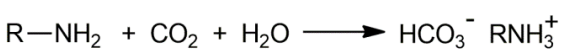

(3.5)

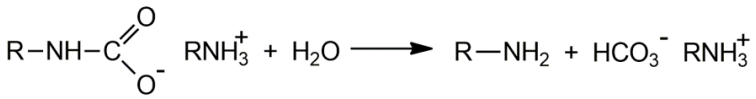

(3.6)

In the presence of tertiary amines [5] or weak amine nucleophiles such as sterically hindered amines,[7,58] water becomes a competitive nucleophile, attacking the electrophilic CO_2 and generating ammonium bicarbonate/carbonate concurrently with, or at the exclusion of, ammonium carbamate, depending on the severity of the steric hindrance.

This mechanism is actually not limited to water. It was shown for example that in non-aqueous solvent, hindered aminoalcohol such as N-*t*But-ethanolamine reacts with CO_2, exclusively through the hydroxyl group with assistance of the amine group, leading to 1,6-zwitterionic carbonate species.[59]

It is clear that, conceptually, CO_2 capture by amines, whether in solution or in solid adsorbents under dry or humid conditions follows similar reaction mechanisms, depending on the nature of the nucleophile (Lewis base), the assisting species (Bronsted base) and other stabilizing components. Fig. 3-9 captures the mechanisms of all possible reactions of CO_2 with amines and water, depending on the actual conditions. As for CO_2 adsorption by supported non-hindered primary or secondary amines, the mechanism depends on the amine surface density and on whether the feed gas is dry or humid. At high amine loading under dry condition, the nucleophilic attack of CO_2 by amine is primarily assisted by a neighboring amine (X = N, Y = N), leading to a 1,n-zwitterion (n > 3) or to alkylammonium carbamate, depending on whether the two amines involved are linked or separate. At low amine loading, the nucleophilic attack of CO_2 by isolated amines may be assisted by hydroxyl groups (X = N, Y = O), leading to carbamic acid or hydronium carbamate. Under humid conditions, water may also assist the nucleophilic attack of CO_2 by amine (X = N, Y = O) to form hydronium carbamate or play the role of nucleophile assisted by amine to form ammonium bicarbonate (X = O, Y = N) at the expense of carbamate. The latter mechanism applies also for tertiary and hindered amines, regardless of their surface density.[20,60]

The most common CO_2 absorption processes use non-hindered protic amines, where the amine plays both the role of nucleophile and Brønsted base (X = N, Y = N),[5] leading to ammonium carbamate or carbamic acid, depending on existing stabilizing species. The assisting species could also be a non-nucleophile strong Brønsted base, such as guanidines.[6,8] In aqueous solutions, when the amine is almost depleted, water acts as a Lewis base attacking CO_2 with the catalytic assistance of trace amine (X = O, Y = N), leading to the formation of ammonium bicarbonate and the decomposition of carbamate, until equilibrium is reached. Such equilibrium was found to depend on the nature of the amine and the absorption conditions.[5–7] However, in the presence of increasingly hindered amines (i.e., weaker Lewis bases) or tertiary amines, water becomes a more and more competitive Lewis base, giving rise to increased formation of ammonium bicarbonate (X = O, Y = N) in comparison to carbamate [7].

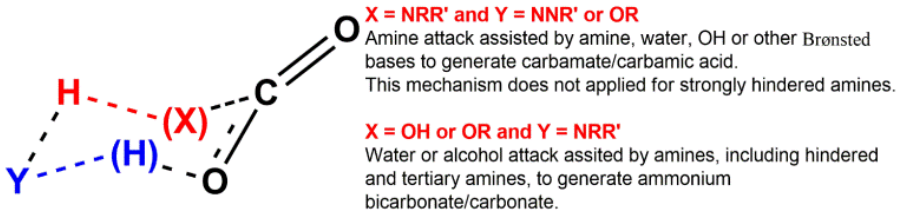

Figure 3-9. Unified schematic mechanism for CO_2-amine-water interactions.

Conclusion

In summary, the 4-centered mechanism leading to 1,3-zwitterion often reported in the literature was found to be systematically associated with high activation barriers, greater than 30 kcal mol^{-1}. More importantly, such mechanisms are unlikely to occur because they violate Wigner's orbital symmetry conservation rule. Instead, a unified 6-centered mechanism involving nucleophilic attack of CO_2 by a Lewis base assisted by a

Brønsted base for hydrogen transfer/exchange, is proposed. Depending on the conditions, different Lewis bases such as amine, water or alcohol and different Brønsted bases such as amine, water, guanidine or OH groups may compete, leading to a variety of end-products. The role of non-polar aprotic solvents such as CCl_4 was limited to slightly decreasing the reactions energy barriers, but without any change in the reaction mechanisms, whether synchronous or asynchronous. However, in the presence of water as solvent, the shape of the energy profiles associated with synchronous mechanisms remain unchanged, whereas for asynchronous mechanisms, the energy profiles indicate that they are no longer concerted with a single transition state, but become characteristic of two-step reactions.

References

(1) Jahandar Lashaki, M.; Khiavi, S.; Sayari, A. Stability of Amine-Functionalized CO2 Adsorbents: A Multifaceted Puzzle. *Chem. Soc. Rev.* **2019**, *48*, 3320–3405. https://doi.org/10.1039/C8CS00877A.

(2) Sayari, A.; Belmabkhout, Y.; Serna-Guerrero, R. Flue Gas Treatment via CO2 Adsorption. *Chem. Eng. J.* **2011**, *171* (3), 760–774. https://doi.org/10.1016/j.cej.2011.02.007.

(3) Gelles, T.; Lawson, S.; Rownaghi, A. A.; Rezaei, F. Recent Advances in Development of Amine Functionalized Adsorbents for CO2 Capture. *Adsorption* **2020**, *26* (1), 5–50. https://doi.org/10.1007/s10450-019-00151-0.

(4) Bui, M.; Adjiman, C. S.; Bardow, A.; Anthony, E. J.; Boston, A.; Brown, S.; Fennell, P. S.; Fuss, S.; Galindo, A.; Hackett, L. A.; et al. Carbon Capture and Storage (CCS): The Way Forward. *Energy Environ. Sci.* **2018**, *11* (5), 1062–1176. https://doi.org/10.1039/c7ee02342a.

(5) Kortunov, P. V.; Siskin, M.; Baugh, L. S.; Calabro, D. C. In Situ Nuclear Magnetic Resonance Mechanistic Studies of Carbon Dioxide Reactions with Liquid Amines in Aqueous Systems: New Insights on Carbon Capture Reaction Pathways. *Energy and Fuels* **2015**, *29* (9), 5919–5939. https://doi.org/10.1021/acs.energyfuels.5b00850.

(6) Kortunov, P. V.; Baugh, L. S.; Siskin, M.; Calabro, D. C. In Situ Nuclear Magnetic Resonance Mechanistic Studies of Carbon Dioxide Reactions with Liquid Amines in Mixed Base Systems: The Interplay of Lewis and Brønsted Basicities. *Energy and Fuels* **2015**, *29* (9), 5967–5989. https://doi.org/10.1021/acs.energyfuels.5b00988.

(7) Kortunov, P. V.; Siskin, M.; Paccagnini, M.; Thomann, H. CO2 Reaction Mechanisms with

Hindered Alkanolamines: Control and Promotion of Reaction Pathways. *Energy and Fuels* **2016**, *30* (2), 1223–1236. https://doi.org/10.1021/acs.energyfuels.5b02582.

(8) Kortunov, P. V.; Siskin, M.; Baugh, L. S.; Calabro, D. C. In Situ Nuclear Magnetic Resonance Mechanistic Studies of Carbon Dioxide Reactions with Liquid Amines in Non-Aqueous Systems: Evidence for the Formation of Carbamic Acids and Zwitterionic Species. *Energy and Fuels* **2015**, *29* (9), 5940–5966. https://doi.org/10.1021/acs.energyfuels.5b00985.

(9) Afonso, R.; Sardo, M.; Mafra, L.; Gomes, J. R. B. Unravelling the Structure of Chemisorbed CO2 Species in Mesoporous Aminosilicas: A Critical Survey. *Environ. Sci. Technol.* **2019**, *53* (5), 2758–2767. https://doi.org/10.1021/acs.est.8b05978.

(10) Didas, S. A.; Zhu, R.; Brunelli, N. A.; Sholl, D. S.; Jones, C. W. Thermal, Oxidative and CO2 Induced Degradation of Primary Amines Used for CO2 Capture: Effect of Alkyl Linker on Stability. *J. Phys. Chem. C* **2014**, *118* (23), 12302–12311. https://doi.org/10.1021/jp5025137.

(11) Foo, G. S.; Lee, J. J.; Chen, C. H.; Hayes, S. E.; Sievers, C.; Jones, C. W. Elucidation of Surface Species through in Situ FTIR Spectroscopy of Carbon Dioxide Adsorption on Amine-Grafted SBA-15. *ChemSusChem* **2017**, *10* (1), 266–276. https://doi.org/10.1002/cssc.201600809.

(12) Sayari, A.; Heydari-Gorji, A.; Yang, Y. CO2-Induced Degradation of Amine-Containing Adsorbents: Reaction Products and Pathways. *J. Am. Chem. Soc.* **2012**, *134* (33), 13834–13842. https://doi.org/10.1021/ja304888a.

(13) Hahn, M. W.; Steib, M.; Jentys, A.; Lercher, J. A. Mechanism and Kinetics of CO2 Adsorption on Surface Bonded Amines. *J. Phys. Chem. C* **2015**, *119* (8), 4126–4135. https://doi.org/10.1021/jp512001t.

(14) Hahn, M. W.; Jelic, J.; Berger, E.; Reuter, K.; Jentys, A.; Lercher, J. A. Role of Amine Functionality for CO2 Chemisorption on Silica. *J. Phys. Chem. B* **2016**, *120* (8), 1988–1995. https://doi.org/10.1021/acs.jpcb.5b10012.

(15) Wilfong, W. C.; Srikanth, C. S.; Chuang, S. S. C. In Situ ATR and DRIFTS Studies of the Nature of Adsorbed CO2on Tetraethylenepentamine Films. *ACS Appl. Mater. Interfaces* **2014**, *6* (16), 13617–13626. https://doi.org/10.1021/am5031006.

(16) Danon, A.; Stair, P. C.; Weitz, E. FTIR Study of CO2 Adsorption on Amine-Grafted SBA-15: Elucidation of Adsorbed Species. *J. Phys. Chem. C* **2011**, *115* (23), 11540–11549. https://doi.org/10.1021/jp200914v.

(17) Sayari, A.; Belmabkhout, Y. Stabilization of Amine-Containing CO2 Adsorbents: Dramatic Effect of Water Vapor. *J. Am. Chem. Soc.* **2010**, *132* (18), 6312–6314. https://doi.org/10.1021/ja1013773.

(18) Mafra, L.; Čendak, T.; Schneider, S.; Wiper, P. V.; Pires, J.; Gomes, J. R. B.; Pinto, M. L. Structure of Chemisorbed CO2 Species in Amine-Functionalized Mesoporous Silicas Studied by Solid-State NMR and Computer Modeling. *J. Am. Chem. Soc.* **2017**, *139* (1), 389–408. https://doi.org/10.1021/jacs.6b11081.

(19) Čendak, T.; Sequeira, L.; Sardo, M.; Valente, A.; Pinto, M. L.; Mafra, L. Detecting Proton Transfer in CO2 Species Chemisorbed on Amine-Modified Mesoporous Silicas by Using 13C NMR Chemical Shift Anisotropy and Smart Control of Amine Surface Density. *Chem. - A Eur. J.* **2018**, *24* (40), 10136–10145. https://doi.org/10.1002/chem.201800930.

(20) Chen, C. H.; Shimon, D.; Lee, J. J.; Mentink-Vigier, F.; Hung, I.; Sievers, C.; Jones, C. W.; Hayes, S. E. The “Missing” Bicarbonate in CO2 Chemisorption Reactions on Solid Amine Sorbents. *J. Am. Chem. Soc.* **2018**, *140* (28), 8648–8651. https://doi.org/10.1021/jacs.8b04520.
(21) Flaig, R. W.; Osborn Popp, T. M.; Fracaroli, A. M.; Kapustin, E. A.; Kalmutzki, M. J.; Altamimi, R. M.; Fathieh, F.; Reimer, J. A.; Yaghi, O. M. The Chemistry of CO2 Capture in an Amine-Functionalized Metal-Organic Framework under Dry and Humid Conditions. *J. Am. Chem. Soc.* **2017**, *139* (35), 12125–12128. https://doi.org/10.1021/jacs.7b06382.
(22) Moschetta, E. G.; Sakwa-Novak, M. A.; Greenfield, J. L.; Jones, C. W. Post-Grafting Amination of Alkyl Halide-Functionalized Silica for Applications in Catalysis, Adsorption, and 15N NMR Spectroscopy. *Langmuir* **2015**, *31* (7), 2218–2227. https://doi.org/10.1021/la5046817.
(23) Inagaki, F.; Matsumoto, C.; Iwata, T.; Mukai, C. CO2-Selective Absorbents in Air: Reverse Lipid Bilayer Structure Forming Neutral Carbamic Acid in Water without Hydration. *J. Am. Chem. Soc.* **2017**, *139* (13), 4639–4642. https://doi.org/10.1021/jacs.7b01049.
(24) Didas, S. A.; Sakwa-Novak, M. A.; Foo, G. S.; Sievers, C.; Jones, C. W. Effect of Amine Surface Coverage on the Co-Adsorption of CO2 and Water: Spectral Deconvolution of Adsorbed Species. *J. Phys. Chem. Lett.* **2014**, *5* (23), 4194–4200. https://doi.org/10.1021/jz502032c.
(25) Li, K.; Kress, J. D.; Mebane, D. S. The Mechanism of CO2 Adsorption under Dry and Humid Conditions in Mesoporous Silica-Supported Amine Sorbents. *J. Phys. Chem. C* **2016**, *120* (41), 23683–23691. https://doi.org/10.1021/acs.jpcc.6b08808.
(26) Sayari, A.; Belmabkhout, Y.; Da’na, E. CO2 Deactivation of Supported Amines: Does the Nature of Amine Matter? *Langmuir* **2012**, *28* (9), 4241–4247. https://doi.org/10.1021/la204667v.
(27) Arstad, B.; Blom, R.; Swang, O. CO2 Absorption in Aqueous Solutions of Alkanolamines: Mechanistic Insight from Quantum Chemical Calculations. *J. Phys. Chem. A* **2007**, *111* (7), 1222–1228. https://doi.org/10.1021/jp065301v.
(28) Cho, M.; Park, J.; Yavuz, C. T.; Jung, Y. A Catalytic Role of Surface Silanol Groups in CO2 Capture on the Amine-Anchored Silica Support. *Phys. Chem. Chem. Phys.* **2018**, *20* (17), 12149–12156. https://doi.org/10.1039/c7cp07973g.
(29) Li, K.; Kress, J. D.; Mebane, D. S. The Mechanism of CO2 Adsorption under Dry and Humid Conditions in Mesoporous Silica-Supported Amine Sorbents. *J. Phys. Chem. C* **2016**, *120* (41), 23683–23691. https://doi.org/10.1021/acs.jpcc.6b08808.
(30) Mebane, D. S.; Kress, J. D.; Storlie, C. B.; Fauth, D. J.; Gray, M. L.; Li, K. Transport, Zwitterions, and the Role of Water for CO2 Adsorption in Mesoporous Silica-Supported Amine Sorbents. *J. Phys. Chem. C* **2013**, *117* (50), 26617–26627. https://doi.org/10.1021/jp4076417.
(31) Buijs, W.; De Flart, S. Direct Air Capture of CO2 with an Amine Resin: A Molecular Modeling Study of the CO2 Capturing Process. *Ind. Eng. Chem. Res.* **2017**, *56* (43), 12297–12304. https://doi.org/10.1021/acs.iecr.7b02613.
(32) Yu, J.; Chuang, S. S. C. The Role of Water in CO2 Capture by Amine. *Ind. Eng. Chem. Res.* **2017**, *56* (21), 6337–6347. https://doi.org/10.1021/acs.iecr.7b00715.
(33) Caplow, M. Kinetics of Carbamate Formation and Breakdown. *J. Am. Chem. Soc.* **1968**, *90*

(24), 6795–6803. https://doi.org/10.1021/ja01026a041.
(34) Danckwerts, P. V. The Reaction of CO2 with Ethanolamines. *Chem. Eng. Sci.* **1979**, *34* (4), 443–446. https://doi.org/10.1016/0009-2509(79)85087-3.
(35) Xie, H. Bin; Zhou, Y.; Zhang, Y.; Johnson, J. K. Reaction Mechanism of Monoethanolamine with CO 2 in Aqueous Solution from Molecular Modeling. *J. Phys. Chem. A* **2010**, *114* (43), 11844–11852. https://doi.org/10.1021/jp107516k.
(36) Ramachandran, N.; Aboudheir, A.; Idem, R.; Tontiwachwuthikul, P. Kinetics of the Absorption of CO2 into Mixed Aqueous Loaded Solutions of Monoethanolamine and Methyldiethanolamine. *Ind. Eng. Chem. Res.* **2006**, *45* (8), 2608–2616. https://doi.org/10.1021/ie0505716.
(37) Crooks, J. E.; Donnellan, J. P. Kinetics and Mechanism of the Reaction between Carbon Dioxide and Amines in Aqueous Solution. *J. Chem. Soc. Perkin Trans. 2* **1989**, 331–333. https://doi.org/10.1039/p29890000331.
(38) da Silva, E. F.; Svendsen, H. F. Ab Initio Study of the Reaction of Carbamate Formation from CO 2 and Alkanolamines . *Ind. Eng. Chem. Res.* **2004**, *43* (13), 3413–3418. https://doi.org/10.1021/ie030619k.
(39) Frisch, M. J. Gaussian 09, Revision A.02, Gaussian, Inc., Wallingford CT. 2016.
(40) Becke, A. D. A New Dynamical Correlation Functional and Implications for Exact-Exchange Mixing. *J. Chem. Phys.* **1996**, *104*, 1040–1046.
(41) Zhao, Y.; Truhlar, D. G. The M06 Suite of Density Functionals for Main Group Thermochemistry, Thermochemical Kinetics, Noncovalent Interactions, Excited States, and Transition Elements: Two New Functionals and Systematic Testing of Four M06-Class Functionals and 12 Other Function. *Theor. Chem. Acc.* **2008**, *120* (1–3), 215–241. https://doi.org/10.1007/s00214-007-0310-x.
(42) Zhao, Y.; Truhlar, D. G. Design of Density Functionals That Are Broadly Accurate for Thermochemistry, Thermochemical Kinetics, and Nonbonded Interactions. *J. Phys. Chem. A* **2005**, *109*, 5656–5667. https://doi.org/10.1021/jp050536c.
(43) McLean, A. D.; Chandler, G. S. Contracted Gaussian Basis Sets for Molecular Calculations. I. Second Row Atoms, Z=11-18. *J. Chem. Phys.* **1980**, *72* (10), 5639–5648. https://doi.org/10.1063/1.438980.
(44) Hratchian, H. P.; Schlegel, H. B. Accurate Reaction Paths Using a Hessian Based Predictor-Corrector Integrator. *J. Chem. Phys.* **2004**, *120* (21), 9918–9924. https://doi.org/10.1063/1.1724823.
(45) Fukui, K. The Path of Chemical Reactions - The IRC Approach. *Acc. Chem. Res.* **1981**, *14* (12), 363–368. https://doi.org/10.1021/ar00072a001.
(46) Smaoui, A.; Essalah, K.; Boubaker, T.; Assfeld, X.; Picaud, F.; Tangour, B. First-Principles Study of the Reaction Mechanism Governing the SNAr of the Dimethylamine on 2-Methoxy-5-Nitrothiophenes. *Theor. Chem. Acc.* **2020**, *139*, 2004. https://doi.org/10.1007/s00214-019-2519-x.
(47) Scalmani, G.; Frisch, M. J. Continuous Surface Charge Polarizable Continuum Models of Solvation. I. General Formalism. *J. Chem. Phys.* **2010**, *132* (11), 114110. https://doi.org/10.1063/1.3359469.
(48) Harlick, P. J. E.; Sayari, A. Applications of Pore-Expanded Mesoporous Silica . 5. Triamine Grafted Material with Exceptional CO2 Dynamic and Equilibrium Adsorption

Performance. *Ind. Eng. Chem. Res.* **2007**, *46* (2), 446–458. https://doi.org/10.1021/ie060774+.
(49) Pearson, R. G. Orbital Symmetry Rules and the Mechanisms of Inorganic Reactions. *Pure Appl. Chem.* **1971**, *27*, 145–160. https://doi.org/https://doi.org/10.1351/pac197127010145.
(50) Pearson, R. G. Symmetry Rules for Chemical Reactions. *Comput. Math.* **1986**, *12B* (1–2), 229–236. https://doi.org/10.1038/294114a0.
(51) Heldebrant, D. J.; Koech, P. K.; Ang, M. T. C.; Liang, C.; Rainbolt, J. E.; Yonker, C. R.; Jessop, P. G. Reversible Zwitterionic Liquids, the Reaction of Alkanol Guanidines, Alkanol Amidines, and Diamines with CO2. *Green Chem.* **2010**, *12* (4), 713–721. https://doi.org/10.1039/b924790d.
(52) Weinhold, F.; Landis, C. R. Natural Bond Orbitals and Extensions of Localized Bonding Concepts. *Chem. Educ. Res. Pr.* **2001**, *2* (2), 91–104. https://doi.org/10.1039/b1rp90011k.
(53) Blauwhoff, P. M. M.; Versteeg, G. F.; Swaaij, W. P. M. Van. A Study on the Reaction between CO2 and Alkanolamines in Aqueous Solutions. *Chem. Eng. Sci.* **1984**, *39* (2), 207–225.
(54) Balaji, S. P.; Gangarapu, S.; Ramdin, M.; Torres-Knoop, A.; Zuilhof, H.; Goetheer, E. L. V.; Dubbeldam, D.; Vlugt, T. J. H. Simulating the Reactions of CO2 in Aqueous Monoethanolamine Solution by Reaction Ensemble Monte Carlo Using the Continuous Fractional Component Method. *J. Chem. Theory Comput.* **2015**, *11* (6), 2661–2669. https://doi.org/10.1021/acs.jctc.5b00160.
(55) Böttinger, W.; Maiwald, M.; Hasse, H. Online NMR Spectroscopic Study of Species Distribution in MEA-H2O-CO2 and DEA-H2O-CO2. *Fluid Phase Equilib.* **2008**, *263* (2), 131–143. https://doi.org/10.1016/j.fluid.2007.09.017.
(56) Xu, X.; Song, C.; Miller, B. G.; Scaroni, A. W. Influence of Moisture on CO2 Separation from Gas Mixture by a Nanoporous Adsorbent Based on Polyethylenimine-Modified Molecular Sieve MCM-41. *Ind. Eng. Chem. Res.* **2005**, *44* (21), 8113–8119. https://doi.org/10.1021/ie050382n.
(57) Matsuzaki, Y.; Yamada, H.; Chowdhury, F. A.; Higashii, T.; Onoda, M. Ab Initio Study of CO2 Capture Mechanisms in Aqueous Monoethanolamine: Reaction Pathways for the Direct Interconversion of Carbamate and Bicarbonate. *J. Phys. Chem. A* **2013**, *117* (38), 9274–9281. https://doi.org/10.1021/jp406636a.
(58) Matsuzaki, Y.; Yamada, H.; Chowdhury, F. A.; Yamamoto, S.; Goto, K. Ab Initio Study of CO 2 Capture Mechanisms in Aqueous 2-Amino-2-Methyl-1-Propanol: Electronic and Steric Effects of Methyl Substituents on the Stability of Carbamate. *Ind. Eng. Chem. Res.* **2019**, *58* (8), 3549–3554. https://doi.org/10.1021/acs.iecr.8b06229.
(59) Im, J.; Hong, S. Y.; Cheon, Y.; Lee, J.; Lee, J. S.; Kim, H. S.; Cheong, M.; Park, H. Steric Hindrance-Induced Zwitterionic Carbonates from Alkanolamines and CO 2: Highly Efficient CO 2 Absorbents. *Energy Environ. Sci.* **2011**, *4* (10), 4284–4289. https://doi.org/10.1039/c1ee01801a.
(60) Lee, J. J.; Yoo, C. J.; Chen, C. H.; Hayes, S. E.; Sievers, C.; Jones, C. W. Silica-Supported Sterically Hindered Amines for CO2 Capture. *Langmuir* **2018**, *34* (41), 12279–12292. https://doi.org/10.1021/acs.langmuir.8b02472.

Appendix A3 – Supplementary Information for Chapter 3

Table A3- 1. Activation energy Ea and Gibbs activation energy Δ_rG^* in kcal mol^{-1}calculated in the gas phase by the DFT/ 6-311++G (d, p) method with the three functionals M06-2X, PW6B95 et B3LYP and by post HF techniques MP2 and CCSD(T)

	CH_3NH_2					CH_3-NH-CH_3				
	M062X	B3LYP	PW6B95	MP2	CCSD(T)	M062X	B3LYP	PW6B95	MP2	CCSD(T)
Ea	40.3	42.8	41.4	44.3	44.1	36.7	40.0	38.5	39.6	39.7
Δ_rG^*	42.2	44.8	43.1	46.3		37.9	41.0	39.4	41.7	

Table A3- 2. Table A3-3. Selected bond lengths of the 1,6-zwitterion obtained by addition de CO_2 on ethylenediamine $H_2N(CH_2)_2NH_2$.

Bond	Gas	Water
C-N1	1.51	1.40
CO1	1.26	1.29
CO2	1.22	1.25
H1-N2	1.05	1.11
H2-O1	1.85	1.44

Table A3- 3. Table A3-4. Zwitterion cartesian coordinates of addition de CO_2 on ethylenediamine.

	Gas			Water		
	x	y	z	x	y	z
N	1.539445	-0.952416	-0.616101	-1.78599	-1.03859	-0.06228
C	2.094221	0.146258	0.231525	-1.86809	0.43840	-0.32180
H	2.916511	0.608812	-0.316511	-2.84741	0.79650	-0.00497
H	2.468738	-0.27075	1.164196	-1.76399	0.59102	-1.39526
C	0.901971	1.133915	0.456715	-0.75388	1.16881	0.42776
H	0.561107	1.043414	1.489355	-0.98212	2.23452	0.39033
H	1.249287	2.155240	0.291650	-0.77306	0.87533	1.48574
N	-0.178421	0.818055	-0.480988	0.57472	0.99308	-0.15564
C	-1.252341	-0.106866	0.052270	1.35359	-0.16298	-0.00907
O	-2.388349	0.173423	-0.303494	2.58321	-0.06456	-0.19169
O	-0.773913	-1.045983	0.749174	0.72903	-1.25268	0.27283
H	0.861173	-0.422860	-1.234146	1.12731	1.83398	-0.22959
H	-0.613451	1.633764	-0.892798	-2.20284	-1.58456	-0.81408
H	0.847832	-1.490362	-0.029834	-2.26738	-1.28912	0.80049
H	2.221914	-1.512589	-1.118946	-0.69931	-1.26663	0.06234

CHAPTER 4 COVALENTLY IMMOBILIZED POLYETHYLENIMINE FOR CO_2 ADSORPTION

4.0. Overview

Covalent immobilization of PEI on PE-$AlSiO_2$ using 3-glycidoxypropyltrimethoxysilane (GPS) or 3-triethoxysilylpropyl isocyanate (TPI) as a grafting agent, and Et_3N or NaOH as catalyst was investigated. Compared to traditional PEI-impregnation, covalently immobilized PEI using TPI and NaOH retained the most CO_2 following oxidative degradation at 100 ^oC for up to 40 h and leaching in EtOH for 2 h. Further modification of PEI with 1,2-epoxybutane led to further enhancement in oxidation stability.

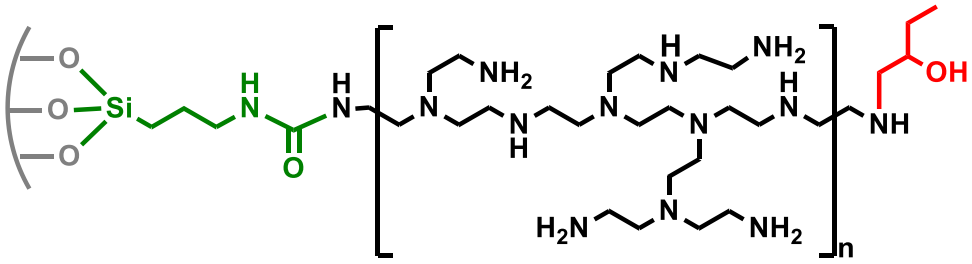

Material with enhanced leaching and oxidation stability vs. impregnated PEI

4.1. Introduction

Recent reports by the Intergovernmental Panel on Climate Change (IPCC)[1] and the U.N. World Metrological Organization (WMO)[2] dealing with the deleterious effect of greenhouse gas (GHG) on the environment and the economy, called for urgent steps toward mitigating the effect of such emissions. Although not the most harmful GHG, because of its exceeding large emissions, CO_2 is the largest contributor to global warming.[3] CO_2 capture and sequestration/utilization at least from large point sources, is recognized as one of the most promising strategies to mitigate its environmental impact. Adsorption using amine-based materials has gained prominence as a viable technology for CO_2 capture from CO_2-rich gas streams[4–7] as well as from air [8–11]. In particular, polyethylenimine (PEI) impregnated on porous supports is an attractive material owing to its high CO_2 capacity. [6,7,12–15]

Specifically, this class of adsorbent show good to excellent CO_2 uptake over a wide range of dry conditions, e.g., 3.7 mmol/g (carbon spheres, 15% CO_2/N_2 at 75 ^oC)[16], 2.26 mmol/g (HP20 resin, 400 ppm CO_2 at 25 ^oC)[17] and 4.73 mmol/g (multilamellar silica vesicle, pure CO_2 at 75 ^oC).[18] Significant progress was achieved to improve the CO_2 capacity of PEI-containing adsorbents, particularly through the use of; (1) support materials with larger surface areas, larger pore and pore volume, and higher pore connectivity,[7,15,19–21] (2) additives such as surfactants, polymers and hydroxyl group containing molecules,[8,22,23] and (3) as-synthesized mesoporous materials with occluded structure-directing agents.[7,8,24] Nonetheless, despite their excellent adsorption attributes, these materials are prone to amine leaching,[25] evaporation[26,27] and oxidative degradation.[28,29]

Covalent immobilization of PEI on support materials was introduced as a strategy to minimize leaching and improve thermal oxidation stability.[30–36] Kassab *et al.*[31] linked PEI onto a mesoporous silica using 3-glycidoxypropyltrimethoxysilane (GPS) as a grafting agent; but the CO_2 capacity was quite low (< 1 mmol/g at 30 °C, 25 wt% PEI). Similar low CO_2 capacity at 70 °C was obtained in the presence of PEI immobilized on carbon nanotubes through acyl chloride functional groups (16 wt% PEI, pure CO_2).[32] Higher CO_2 capacity was reported for porous organic polymers containing glycidyl methacrylate grafted PEI (2.1 mmol/g at 0 °C, 33 wt%, pure CO_2).[33] Even higher CO_2 capacities were obtained using covalently grafted hydroxylated graphene/PEI composite (4.1 mmol/g at 25°C, 50 wt% PEI, 10% CO_2/N_2).[34] Furthermore, using acrylamide to graft PEI on polypropylene fiber, a CO_2 capacity of 5.91 mmol/g (25 °C, 85wt% PEI, 10% CO_2/N_2) was reported by Wu *et al.*[35] In another study, Zhu *et al*.[36] used HKUST/porous polymer composite with grafted PEI via epoxy−amine reaction, and obtained an adsorption capacity of 4.17 and 4.31 mmol/g at 25 and 50 °C, respectively (30 wt% PEI, 15% CO_2/N_2). While good CO_2 working capacities were obtained from PEI covalently linked on large surface area supports, e.g. graphene, fibers and MOFs, there is a need to improve the performance of PEI grafted on less expensive supports, such as mesoporous silicas.

In addition, the limited thermal stability of PEI-containing adsorbents in an inert or oxidizing environment is a major factor that limits their application. TGA data acquired under N_2 at a heating rate of 2 °C/min up to 800 °C showed that for up to 60% PEI/SiO_2 adsorbent, evaporation of PEI occurred between 100 and 160 °C (ca. 6.5 wt% loss), while PEI decomposition began thereafter, contributing to most of the weight loss.[26] Using a heating rate of 0.25 °C/min up to 200 °C, Drage *et al*.[21] reported that for 40 wt% PEI/SiO_2 adsorbent, weight loss due to

evaporation and/or thermal degradation occurred from 135 ^{o}C (ca. 2 wt%). Introduction of specific additives was also reported to improve the thermal and oxidation stability of PEI-containing adsorbents. Enhanced thermal stability was reported for PEI impregnated onto as-synthesized KIT-6, which the authors attributed to the resultant Pluronic P123/PEI composite.[37] Moreover, PEI/PVA/SiO_2 adsorbents were reported to be more stable than their PEI/SIO_2 counterpart to cyclic CO_2 capture and oxidative degradation environment,[38] presumably because of multiple interactions between the −OH and amine groups. Nonetheless, lower amine capacity and efficiency were reported for the PEI/PVA/SiO_2 system due to polymer chain entanglement facilitated by H-bonding. However, in a related study, enhancement in CO_2 efficiency was reported for a PEG200/PEI adsorbent.[39] Furthermore, Choi *et al.*[40] reported three benefits of epoxide functionalization of PEI for CO_2 uptake under moist conditions; (1) increased resistance to oxidative degradation, (2) suppressed formation of urea during regeneration with 100% CO_2 at 120 ^{o}C, and (3) energy efficient CO_2 desorption due to weakened CO_2-amine interactions.[41] Based on current literature, there is a need to develop covalently immobilized PEI-based CO_2 adsorbents with improved thermal and oxidative stability, while maintaining high CO_2 capacity and efficiency. To achieve this goal the properties of the support material, as well as the mole ratio of PEI-grafting agents, and PEI-oxidation stability enhancing agents needs to be optimized. In this chapter, a simple, green and cost-effective methodology of covalently bonding PEI on mesoporous aluminosilica, with high CO_2 capacity/efficiency and improved thermal/oxidation stability, is presented. 3-(triethoxysilyl)propyl isocyanate (TPI) and GPS were used as a SiO_2-PEI linker, while 1,2-epoxybutane (1,2-EB) was used to enhance oxidation resistance, with Et_3N and 10% NaOH solution as catalysts for the hydrolysis and condensation of TPI and GPS onto SiO_2.

4.2. Methodology

4.2.1 Experimental

PEI (M_w 600), tetraethyl orthosilicate (TEOS, 98%), 3-triethoxysilylpropyl isocyanate (TPI, 97%), fumed silica (Cab-O-Sil, M5), tetramethylammonium hydroxide (TMAOH, 25wt% solution), cetyltrimethylammonium bromide (CTAB, 98%), *N,N*-dimethyldodecylamine (DMDA, 97%), triethylamine (Et_3N, 99%) and 1,2-EB (99%) were obtained from Sigma Aldrich. GPS (99%) was purchased from Sigma Aldrich. Sodium aluminate ($NaAlO_2$, 92%) was purchased from Strem Chemicals. Methanol (99 %), ethanol (99%), pentane (99%) and ammonia solution (28 wt%) were obtained from Fisher. All chemicals were used as obtained with no further purification. Ultra-high purity (99.999%) nitrogen and 15% CO_2 in nitrogen gas cylinders were purchased from Linde Canada.

4.2.2 Preparation of materials

Our previously reported method for the synthesis of pore-expanded MCM-41 was used for the synthesis of pore-expanded aluminosilica (PE-$AlSiO_2$) with some modifications.[42,43] In a typical synthesis, 4 g of TMAOH was diluted with water (38.5 g) in a 700 mL Teflon-lined container before adding 5.7 g CTAB under vigorous stirring. After 15 min, 0.2 g of $NaAlO_2$ was added and stirring continued for 30 min, after which 2.1 g Cab-O-Sil was added. The composition of the synthesis mixture was 1.0 SiO_2:0.317 TMAOH:0.45 CTAB:0.035 Al_2O_3:67 H_2O, with a nominal Si/Al ratio of ca. 15. The mixture was then sealed in an autoclave and placed in an oven preheated at 80 ^oC for 40 h. The obtained material was filtered, washed extensively with water and dried under ambient conditions to afford as-synthesized aluminosilica. Partial surfactant (CTAB) extraction was carried out in EtOH (10 mL EtOH/g solid) and room temperature for 1h. Pore expansion was

carried out through hydrothermal treatment of the resultant dried powder in the presence of DMDA. To a mixture of DMDA (1 g) and water (30 g) at RT, 0.8 g of the as-synthesized sample was added. After stirring for an hour, the mixture was heated at 120 ^{o}C for 2 days under autogenous pressure. The solid material was collected by filtration, dried at ambient temperature and calcined in flowing N_2 at 550 ^{o}C by raising the temperature at 1 ^{o}C/min. The gas was then switched to air at 550 ^{o}C and kept for 5 h to remove any remaining carbonaceous material, to afford PE-$AlSiO_2$.

Grafting of GPS and TPI on PE-$AlSiO_2$ in toluene was carried out using an established procedure.[44] In a typical preparation, 1.0 g of pre-dried PE-$AlSiO_2$ was dispersed in 30 mL of anhydrous toluene in a 100 mL two-neck round bottom flask immersed in an oil bath. After stirring for 30 min at room temperature, the temperature of the mixture was then raised to 85 ^{o}C. After 30 min, 0.5 mL (ca. 2 mmol) of GPS or TPI was added and the mixture kept under reflux for 16 h. The flask was allowed to cool down to room temperature and the grafted material was filtered, washed with toluene, ethanol and pentane, and dried under vacuum at 60 ^{o}C for 3 h, to afford GPS@PE-$AlSiO_2$ and TPI@PE-$AlSiO_2$, respectively.

Three methods were used to prepare 50 wt% PEI-containing adsorbents; mechanical mixing, impregnation and covalent immobilization. 0.5 g each of PE-AlSiO2 and PEI was mixed using a ceramic mortar and pestle for 15 min. In a typical procedure for impregnation, 0.5 g of PEI was dissolved in 30 mL of MeOH at RT for 30 min, followed by addition of 0.5 g of PE-$AlSiO_2$. Where applicable, the mixture was stirred for 2 h and 0.2 mL Et_3N or 10% NaOH solution was added. The mixture was then stirred to dryness. The preparation of covalently immobilized PEI was as follows; 0.22 mL (ca. 1 mmol) of GPS or TPI was added to a mixture of 0.5 g PEI/30 mL

MeOH, and where applicable, 0.1 mL of 1,2-EB was added after 2 h of stirring. Thereafter, 0.5 g PE-$AlSiO_2$ was added and stirring continued for another 2 h. Then, 0.2 mL of 10% NaOH solution or Et_3N was added and the mixture was stirred to dryness.

4.2.3. Material characterization

The specific surface area, pore volume and mean pore diameter of the supports and amine-grafted materials were determined by nitrogen adsorption measurements at −196 °C on a Micromeritics 2020 instrument, using a previously reported method.[45] Samples were degassed for 4 h at 100 or 150 ^oC prior to analysis. Specific surface areas were calculated using the BET method at relative pressures of 0.06 to 0.2. The total pore volume (Vp) was calculated using the amount of nitrogen adsorbed at $p/p_o = 0.99$ to exclude possible interparticle pores. The average pore size (Dp) was determined using the density functional theory; a molecular modeling method used to describe properties of fluid systems as a function of the fluid density.[46] As the gas pressure is increased during nitrogen adsorption measurements, nitrogen condenses, filling the pores. The pore size of the material is then determined from the density of the condensed fluid.

The thermal stability of selected adsorbents was determined using thermogravimetric analysis (TGA) on a TA Q500 instrument. Approximately 20 mg of material was heated to 100 ^oC at 5 $^oC\ min^{-1}$ under flowing nitrogen and held for 60 min to remove residual species (e.g. CO_2, water and solvent). The sample was further heated to 700 °C at 2 $^oC\ min^{-1}$ under flowing nitrogen, then air at 700 ^oC for 30 min, to remove any residual carbonaceous material. The PEI loading was calculated as the weight loss beyond 100 ^oC.

The ^{13}C solid-state NMR spectra of PEI-containing solid adsorbents are usually not well resolved, consisting of a broad signal between 30 and 65 ppm. In order to determine the identity

of the covalently immobilized species, from the reaction between GPS or TPI, 1,2-EB and PEI, 0.25 g of adsorbent was stirred in 1 mL 10% NaOH solution (prepared with D_2O). After filtration, the supernatant solution was diluted with D_2O and analyzed by NMR. ^{27}Al MAS NMR was used to investigate the state of aluminum sites in the PE-$AlSiO_2$ support. An AVIII 400 Bruker NMR spectrometer and a previously reported method were used.[47]

4.2.4. CO_2 adsorption measurements

CO_2 adsorption measurements were carried out using a thermogravimetric analyzer (Q500 TGA, TA Instruments) as previously reported.[48] In a typical procedure, about 30 mg of a powder material was preheated at 100 ^oC in N_2 for 60 min to remove residual species. The sample was cooled to 75 ^oC, then adsorption began by switching the purge gas to a mixture of 15% CO_2 in N_2. Adsorption capacity was determined based on weight gain after exposure of the dry material to 15% CO_2/N_2 mixture for 30 min.

4.2.5 Ethanol leaching test and oxidation stability

To determine the resistance of the materials to leaching, 0.5 g of powder material was stirred in 50 mL of EtOH for 2 h at room temperature. The solid was recovered by filtration, washed with MeOH and dried under low vacuum at 50 ^oC for 3 h, and the CO_2 uptake at 75 ^oC and PEI loading was determined

The effect of grafting agents and 1,2-EB on the oxidation stability of immobilized PEI was investigated as follows: a ceramic crucible (10 mL) containing 0.1 g of adsorbent was placed in a pre-heated oven at 100 ^oC. Samples were collected after 16, 24 and 40 h and their CO_2 capacity at 75 ^oC was determined by TGA.

4.3. Results and Discussion

4.3.1. Material characterization

As shown in Figure 4-1 the nitrogen adsorption–desorption isotherms of PE-$AlSiO_2$ and PEI-containing adsorbents were of Type IV with H1 hysteresis loop characteristic of mesoporous solids.[49] The corresponding textural properties of the pristine support (entry 1) and adsorbents prepared by mechanical mixing (entry 2), impregnation (entries 3 and 4) and covalent immobilization (entries 5 – 11) are presented in Table 4-1. It is worth mentioning that higher values were obtained for the surface area (850 m^2/g), pore volume (1.91 mL/g) and pore diameter (10.8 nm) when the support was degassed at 150 ^oC. All adsorbents had significantly lower BET surface areas and pore volumes than their corresponding supports. These observations provide strong evidence that the organic moieties were immobilized mostly on the internal surface. Introduction of NaOH during impregnation did not significantly alter the textural properties of the material (Table 4-1, entry 3 vs. 4).

^{27}Al MAS NMR spectra of PE-$AlSiO_2$ support showed two signals centered at 55 and 0 ppm with relative intensity of 80 and 20 %; corresponding to framework tetrahedral (Al^{IV}, AlO_4) and extra-framework octahedral (Al^{VI}, AlO_6) Al-sites, respectively (Figure 4-2). Earlier work showed that the latter species occurred by dealumination during calcination.[47]

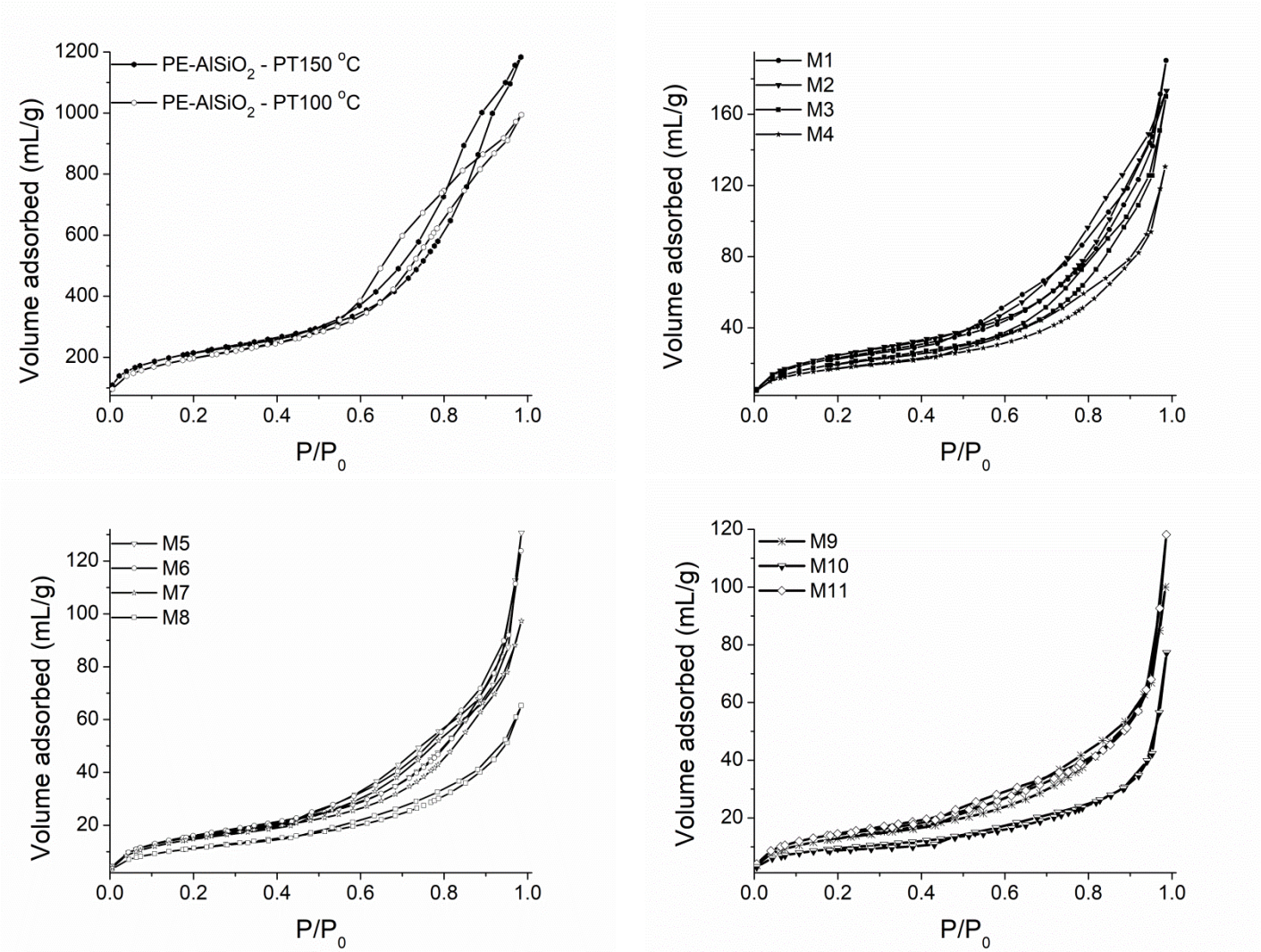

Figure 4-1. Nitrogen adsorption–desorption isotherms of pristine support and functionalized materials.

Table 4-1. Properties of PEI-containing CO_2 adsorbents

Entry	Material[a]	PEI (g)	GPS (mmol)	TPI (mmol)	1,2-EB (mmol)	BET (m^2/g)	Vp (mL/g)	Dp (nm)	organic content (wt%)
1	M0					716	1.56	9.0	-
2	M1	0.5	-	-	-	90	0.29	12.2	47.18
3	M2	0.5	-	-	-	96	0.27	10.4	52.32
4	M3[b]	0.5	-	-	-	77	0.26	12.6	47.31
5	M4	0.5	1	-	-	66	0.20	11.8	49.78
6	M5	0.5	-	1	-	66	0.20	13.0	49.78
7	M6[c]	0.5	1	-	-	62	0.19	12.2	51.20
8	M7[b]	0.5	1	-	-	57	0.15	10.5	51.58
9	M8[b]	0.5	-	1	-	43	0.10	9.5	53.44
10	M9[b]	0.5	1		1	50	0.16	12.2	49.15
11	M10[b]	0.5	-	1	1	35	0.12	14.2	50.12

PEI = Polyethyleneimine, GPS = 3-glycidyloxypropyltrimethoxysilane, TPI = 3-(triethoxysilyl)propyl isocyanate ,1,2-EB = 1,2-epoxybutane, M0 = PE-$AlSiO_2$, [a] = 0.5 g PE-$AlSiO_2$ used in material preparation, all samples degassed at 100 °C for 4 h, [b] = 0.2 mL 10% NaOH, [c] = 0.2 mL Et_3N. All materials were degassed at 100 °C for 4 h prior to BET analysis.

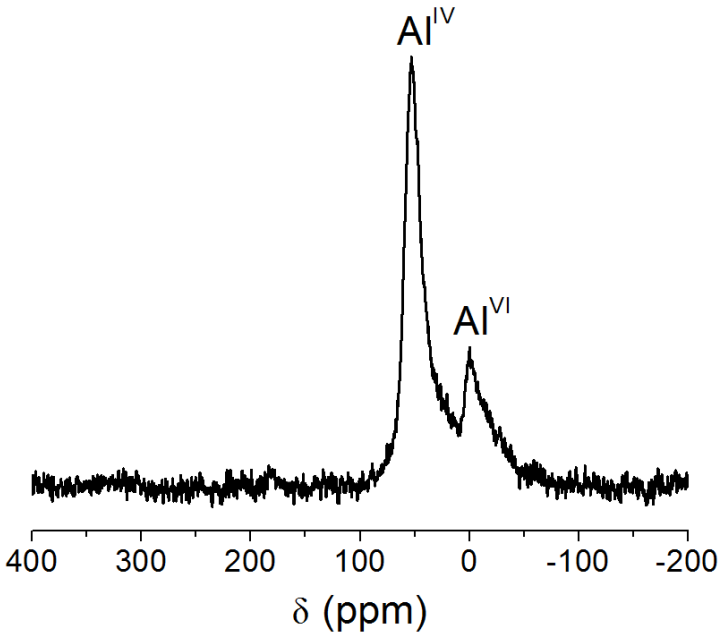

Figure 4-2. ^{27}Al NMR spectrum of PE-$AlSiO_2$

Given the high nitrogen content in PEI (ca. 11 mmol N for 0.5 g PEI) and limited grafting agent (1 mmol), the formation of PEI-grafting species is likely to proceed quantitatively. This was confirmed by calculations based on the weight loss of the sample before (i.e. only grafted GPS or TPI) and after PEI tethering as measured by TGA. The ^{13}C NMR (Figure 4-3) of grafted epoxide-modified PEI showed peaks which were assigned to the carbon nuclei as indicated in Scheme 1. Compared to pure PEI in D_2O (Figure A4- 1), all ^{13}C NMR spectra were characterized by low signal-to-noise ratios due to the high molar ratio between PEI-grafting agent and PEI-epoxide, and the highly basic medium. Separate experiments were carried out with four-time higher ratios to clarify the assigned carbon nuclei (Figure A4- 2). Signals at 77 ppm (*α*) and 79 ppm (*α'*) respectively arose from the fact that either the primary or secondary amine of PEI can react with the grafting agents.[40] All samples exhibited resonances attributed to the corresponding ammonium carbamate (*x* = 164.6 ppm) and carbamic acid (*y* = 168.3 ppm) respectively (Figure 4-3); stemming from interaction with atmospheric CO_2 and CO_2/H_2O, respectively.[50] Note that for each established bond between PEI and TPI, a 2° amine is formed, providing an additional site for CO_2 adsorption.

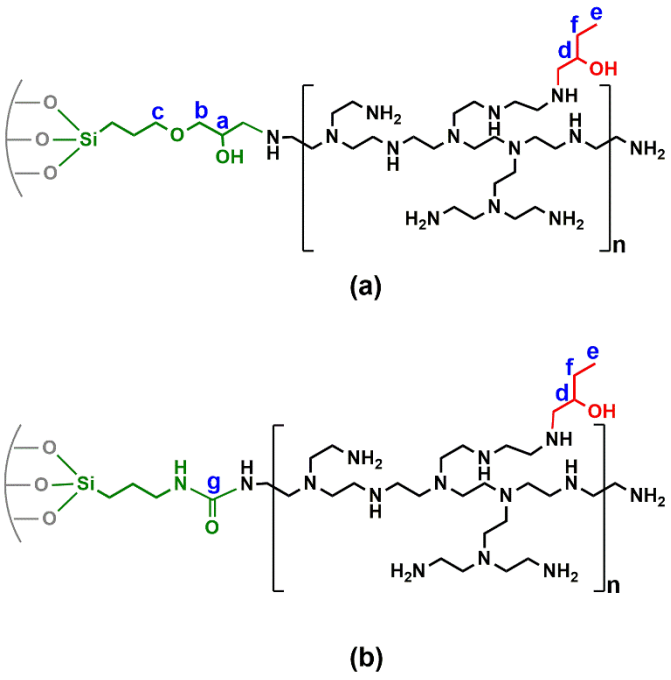

Scheme 4-1. Representative structures of immobilized epoxide-modified PEI using; (a) GPS – material M and (b) TPI as grafting agent

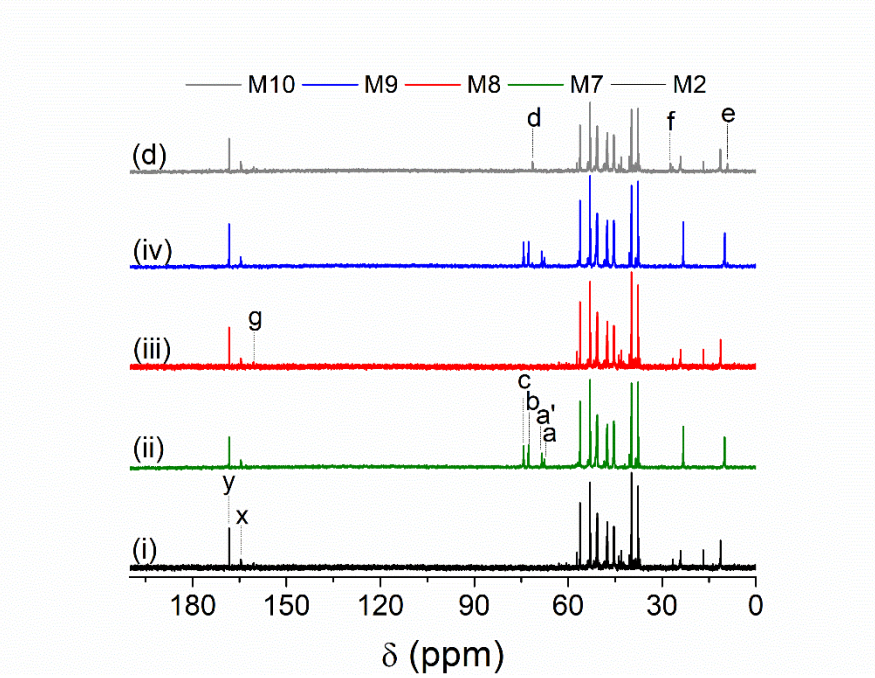

Figure 4-3. ^{13}C NMR of solid materials dissolved in 10% NaOH in D_2O.

It is worth mentioning that attempts to graft GPS and TPI onto PE-$AlSiO_2$ followed by PEI immobilization were not successful. Epoxide and isocyanate groups reacted with trace amount of water to form diol and urea (Scheme 4-2), respectively; which cannot further react with PEI. This reaction is reflected in the ^{13}C MAS NMR spectra of PE-$AlSiO_2$@GPS and PE-$AlSiO_2$@TPI (Figure 4-4). Hence, the covalent immobilization of PEI was not achieved via this route. Note that due to the higher nucleophilicity of $1^o/2^o$ amine compared to water, GPS and TPI will preferentially react with PEI rather than water.

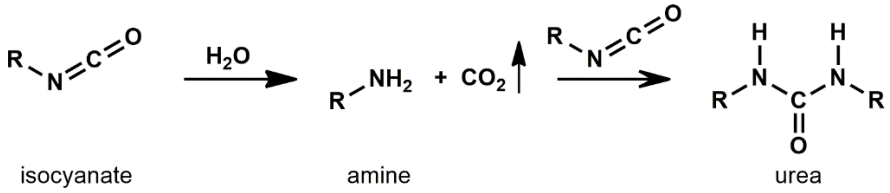

(a)

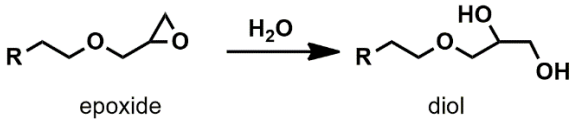

(b)

Scheme 4-2. Reaction of (a) isocyanate and (b) 2-(propoxymethyl)oxirane with water to form urea and diol, respectively

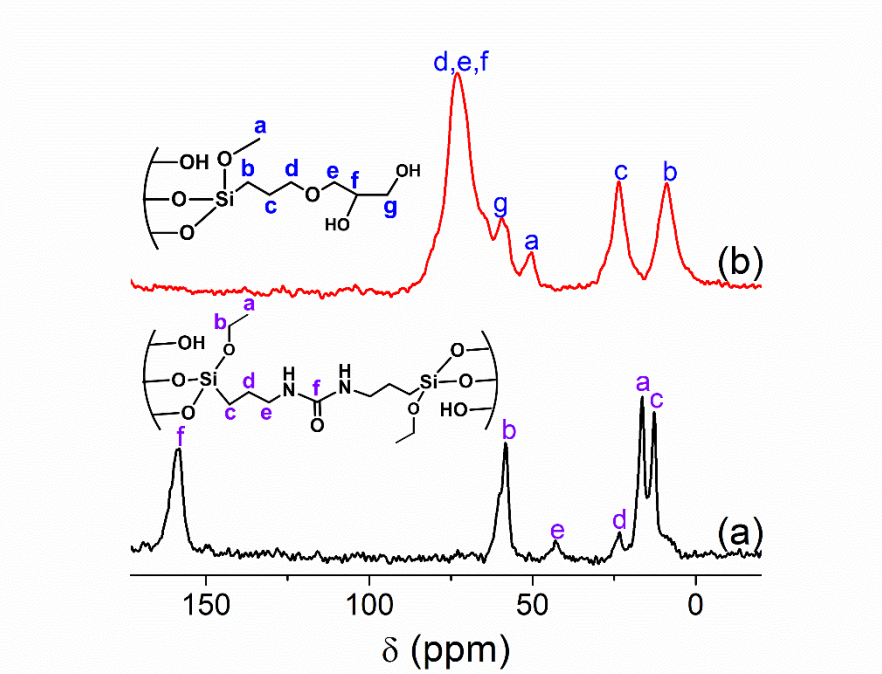

Figure 4-4. ^{13}C CP-MAS NMR spectra of GPS (top) and TPI (botton) immobilized on PE-$AlSiO_2$ in anhydrous toluene

Thermal decomposition of PEI-containing adsorbents showed similar stability for materials derived by mechanical mixing and impregnation up to 250 °C (Figure 4-5, M1 vs. M2), beyond which the impregnation-derived material was slightly more stable. In these materials, PEI interacts with the support through relatively weak hydrogen bonding between surface silanols and amine groups.[20] Materials with improved stability were obtained by covalently linking PEI to PE-$AlSiO_2$ via grafting agents, with loss of PEI at 300 °C up to 21 wt% lower compared to the impregnated material (Figure 4-5, M2 vs. M7/M8). GPS-linked PEI, with 14 wt% PEI loss at 300 °C, showed superior stability compared to TPI-linked PEI, with 19 wt% PEI loss at the same temperature (Figure 4-5, M7 vs. M8): this could be attributed to the –OH groups in the structure of M7. The -Si-O-Si-C- linkages at the interface of the silica surface and grafted PEI is thought to be responsible for improved thermal stability. Nonetheless, materials of similar stabilities were

obtained following epoxide-modification of PEI (Figure 4-5, M9 vs. M10). Similar decrease in thermal degradation was observed for low density polyethylene (LLDPE) following grafting on montmorillonite via vinyltrimethoxysilane during reactive extrusion, which the authors attributed to the formation of cross-linked structures during thermal oxidation.[38]

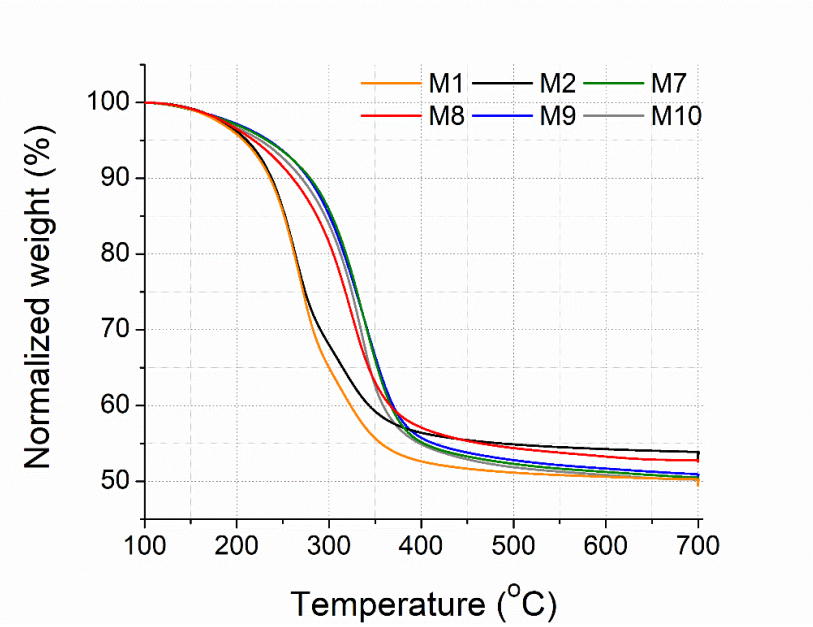

Figure 4-5. Thermal decomposition of PEI-containing adsorbents (rate = 2 °C/min under N_2)

To further verify the observed decrease in volatility or enhancement in thermal stability with grafting and epoxide-modification, samples were subjected to thermal decomposition experiments in N_2 at 150 °C for 4 h. As shown in Figure 4-6, similar weight losses (ca. 3.5 wt%) were observed for PEI-containing adsorbents derived by mechanical mixing (M1) and impregnation (M2), confirming the similar stability or PEI-volatility of these materials as mentioned earlier. Reduction in PEI evaporation and/or degradation was evident following grafting with GPS (M7) and TPI (M8). Although no noticeable change in thermal stability was observed by combining TPI grafting and epoxide-modification (M8 vs. M10), even smaller weight loss was observed for M9 (ca. 2.2 wt%), suggesting a combination of grafting with GPS and

epoxide-modification of PEI is effective to reduce PEI evaporation and decomposition. These findings suggest that while grafting PEI on PE-$AlSiO_2$ improved thermal stability, further enhancement in stability can be achieved by a combination of grafting and epoxide-modification of PEI.

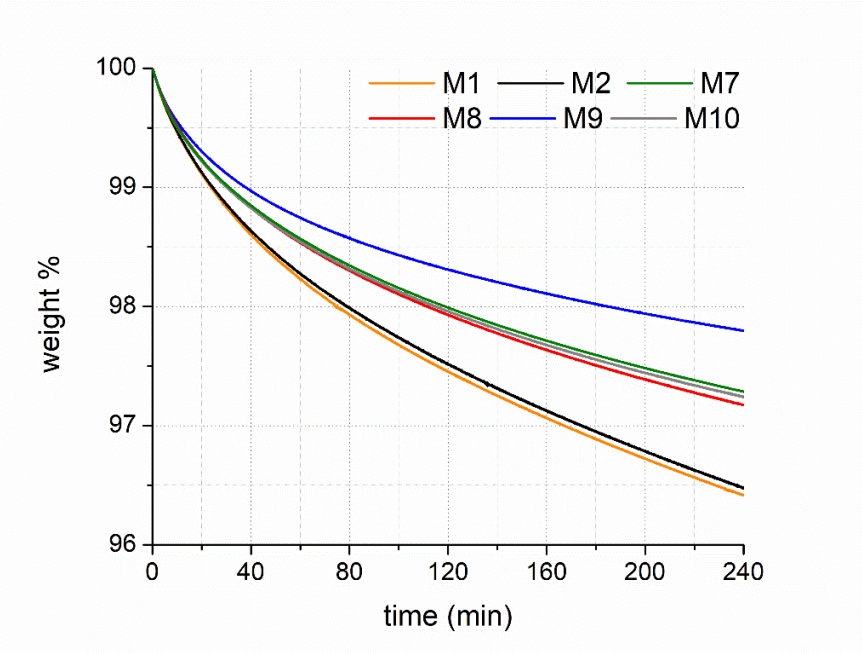

Figure 4-6. Thermal stability of PEI-containing adsorbents under isothermal conditions (150 $^oC/N_2$).

4.3.2. CO_2 capacity and the effect of ethanol leaching test

Owing to their high 1^o and 2^o amine content, materials derived by PEI impregnation (fresh M2, Figure 4-7) and mechanical mixing (Table A4- 1, fresh M1, , entry 2) adsorbed 2.76 mmol CO_2/g. A slightly higher uptake, 2.89 mmol/g, was obtained for PEI-impregnated material in the presence of NaOH solution (fresh M3;Table A4- 1, entry 2), suggesting that introduction of NaOH solution might have a positive impact on CO_2 uptake. Lower CO_2 capacities (ca. 2.30 mmol/g) were obtained for materials derived by reacting PEI and GPS or TPI, followed by impregnation

(fresh M4 and M5, Figure 4-7). This expected outcome was attributed to decrease in contents in 1° and 2° amines, as a result of PEI-GPS or PEI-TPI reactions.

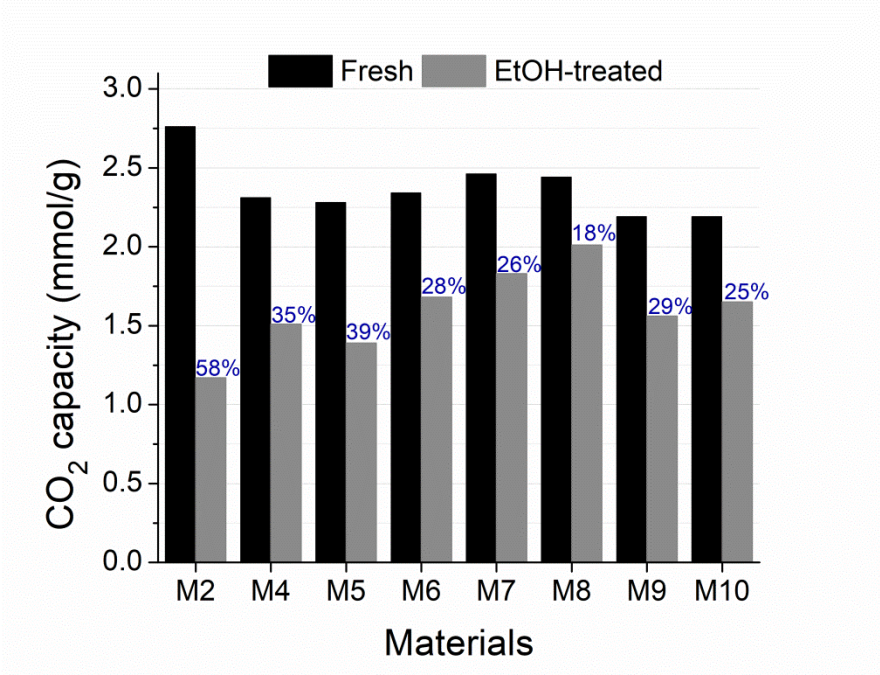

Figure 4-7. Decrease in CO_2 capacity of materials following leaching in EtOH. Percentage losses are indicated.

As with PEI impregnation in the presence of NaOH, higher CO_2 capacities were obtained for impregnated PEI-GPS in the presence of Et_3N and NaOH (fresh M6 and M7, respectively – Figure 4-7), compared to the material prepared without a base (fresh M4 – Figure 4-7). A 5% higher CO_2 capacity was recorded for M7 compared to M6, indicating a plausible beneficial effect of NaOH over Et_3N. Hence, NaOH solution was further used as catalyst to chemically immobilize PEI on PE-$AlSiO_2$. Impregnation of the PEI-TPI reaction mixture yielded an adsorbent (fresh M8 – Figure 4-7) with a similar capacity as that from the PEI-GPS reaction (fresh M7 – Figure 4-7), suggesting the longer GPS species compared to TPI did not affect CO_2 uptake. A combination of PEI grafting and epoxide-modification led to further reduction in CO_2 uptake (2.19 mmol/g – fresh

M9 and M10 - Figure 4-7), as more 1° and 2° amine of PEI were used up during these reactions. Hence, immobilized PEI with the highest CO_2 capacity was obtained by reacting 0.5 g PEI (11 mmol of N) with 1 mmol of TPI, followed by impregnation in MeOH, using 10% NaOH solution as catalyst. The capacity of this material (M8) was only 11 % less than that for conventional PEI-impregnated adsorbent, M2 (2.76 mmol/g).

Leaching of PEI from support material is of notable concern when the adsorbent comes in contact with steam[51] or other solvents. Nonetheless, this aspect has received less attention in the literature.[25] The percent loss in CO_2 capacity following exposure of selected materials to ethanol is shown in Figure 4-7, while complete data including percent losses in PEI can be found in Table A4- 1. A 58 % decrease in CO_2 uptake and 42% PEI loss were measured following M2 treatment with EtOH (Figure 4-7 and Table A4- 1 – entry 2). Even higher losses were obtained for materials derived by mechanical mixing (M1, Table A4- 1, entry 1); 83 and 50 % decrease in CO_2 uptake and organic content, respectively. Surface grafting of PEI-GPS (or TPI) decreased the losses in CO_2 uptake and PEI loading by 20% or more (Figure 4-7, M2 vs. M4/M5). Using NaOH or Et_3N as catalyst to enhance the hydrolysis of GPS on PE-$AlSiO_2$ further improved the materials resistance to leaching (Figure 4-7, M4 vs. M6/M7), with the PEI-TPI/NaOH system delivering the best result (M8 vs. M6/M7 – Figure 4-7). Being a stronger base, NaOH is thought to enhance the grafting of GPS- or TPI-linked PEI on PE-$AlSiO_2$, while the 2° amine formed during TPI-PEI reaction (Scheme 1b) could be attributed to the smaller loss in CO_2 capacity of M8 (18%) compared to M7 (26%). A combination of PEI grafting and epoxide-modification appeared to increase the leaching resistance of the final materials (Figure 4-7, M7 vs. M9 and M8 vs. M10). We think further reduction in leaching can be achieved by increasing the grafting agent-PEI molar ratio, although

this result in lower CO_2 capacity, with a less severe decrease with TPI as it provides an additional 2^o amine during grafting. The amine efficiency was estimated to be between 0.24 – 0.28 for the PEI impregnated adsorbents and 0.20 – 0.22 for the covalently grafted PEI materials. The observed decrease in efficiency was attributed to the loss of active amine during PEI and TPI (or GPS) reaction. The efficiency was calculated based on all amine groups, including tertiary amines.

Table 4-2 shows the CO_2 uptake of different covalently immobilized PEI materials reported in the literature alongside the corresponding PEI loading, with different PEI loadings and test conditions. Although a fair comparison is difficult under these varying conditions, the material presented in this work (Table 4-2, entries 7 and 8) had a decent CO_2 capacity at 50 and 75 ^{o}C.

Table 4-2. CO_2 capture performance of covalently anchored PEI

Entry	Support	Linking agent	PEI loading (wt%)	CO_2 uptake		Refs
				Test conditions	Capacity (mmol/g)	
1	SiO_2	GPS	25	30 ^{o}C, pure CO_2	< 1	[31]
2	Carbon nanotube	acyl chloride	16	70 ^{o}C, pure CO_2	≈1	[32]
3	Porous organic polymer	glycidyl methacrylate	33	0 ^{o}C, pure CO_2	2.1	[33]
4	Hydroxylated graphene	Hydroxyl groups of graphene	50	25^{o}C, 10% CO_2/N_2	4.1	[34]
5	Polypropylene fiber	acrylamide	85	25 ^{o}C, 10% CO_2/N_2	5.91	[35]
6	HKUST/porous polymer	epoxy	30	50 ^{o}C, 15% CO_2/N_2	4.31	[36]
7	AlSiO2	TPI	50	50 ^{o}C, 15% CO_2/N_2	2.51	This work
8	AlSiO2	TPI	50	75 ^{o}C, 15% CO_2/N_2	2.34	This work

4.3.3. Oxidation stability

The lack of stability of amine-containing adsorbents in oxygen-containing environment could be a major setback to their application, for example, if the feed is oxygen-rich, or if air is used to cool the material after regeneration in a temperature-swing adsorption (TSA) process. As shown in Figure 4-8 and Table A4- 2, a decrease in CO_2 capacity was observed when selected materials were exposed to air at 100 ^oC for up to 40 h, which was attributed to the oxidative degradation of the materials.

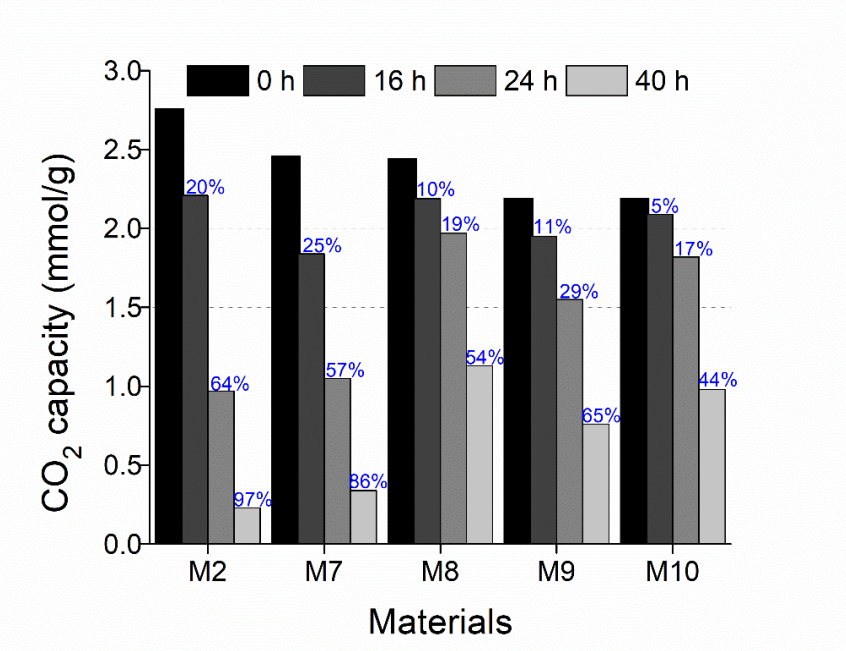

Figure 4-8. Variations in CO_2 uptake of materials after oxidation in air at 100 ^oC in an oven. Percentage losses are indicated.

Similar percent losses in CO_2 capacities were measured for the PEI-impregnated (M2) and grafted PEI-GPS (M7) materials after air exposure for 16, 24 and 40 h, suggesting that any enhancement in oxidation stability was minimal. Lower percent losses were obtained for TPI-linked PEI (M8) materials compared to M2; suggesting chemical immobilization of PEI on PE-$AlSiO_2$ using TPI led

to improved thermal stability. A combination of PEI grafting and epoxide-modification led to significantly lower percent losses in CO_2 uptake (Figure 4-8: M9 vs. M7 and M10 vs. M8), with the least decrease measured for M10. This result shows that while grafting PEI on PE-$AlSiO_2$ can improve the oxidation stability of the resultant material, further enhancement in stability was achieved by a combination of PEI grafting and epoxide-modification, which is consistent with the thermal stability data. Following exposure to 50 TSA cycles under humid conditions and desorption with 100% CO_2 at 120 ^oC, Choi *et al*.[40] reported that 1,2-EB/PEI ratio of 0.37 was optimal for enhancing oxidation stability and maintaining a steady CO_2 working capacity of 2.2 mmol/g, of silica impregnated with epoxide-modified PEI compared to unmodified PEI/SiO_2 (2.9 and 1.1 mmol/g in the 1^{st} and 50^{th} cycles, respectively). Although the current study involved lower 1,2-EB/PEI molar ratio (ca. 0.1) and CO_2 measurement under dry CO_2, we think the -Si-O-Si-C- linkage between TPI and PE-$AlSiO_2$ and urea connection between TPI-PEI, alongside the –OH groups introduced by epoxide-PEI reactions, are thought to be responsible for the improvement in oxidative stability.

Conclusion

Materials derived by traditional PEI-impregnation, mechanical mixing and the chemical immobilization of PEI on PE-$AlSiO_2$ using GPS and TPI as grafting agents, and Et_3N and 10% NaOH solution as catalyst for silane hydrolysis were prepared and characterized by TGA, nitrogen adsorption-desorption isotherm and solution and solid-state NMR. The application of these materials in CO_2 adsorption was investigated before and after EtOH leaching test, while their oxidation stability was also studied. TGA data showed that immobilized PEI had better thermal degradation properties, with up to 20% less weight lost at 300 ^oC/under N_2 compare to PEI-

impregnated material. Moreover, materials derived from PEI-grafting were more resistant to the EtOH leaching test, while optimum oxidation stability was achieved by a combination of PEI grafting and epoxide-modification with TPI and grafting agent.

References

(1) IPCC. *Global Warming of 1.5°C. An IPCC Special Report: Summary for Policymakers*; Masson-Delmotte, V., Zhai, P., Pörtner, H. O., Roberts, D., J. Skea, P. R., Shukla, Pirani, A., Moufouma-Okia, W., Péan, C., Pidcock, R., et al., Eds.; Geneva, 2018.

(2) WMO. WMO Statement on the Status of the Global Climate in 2017 http://www.wmo.int/pages/mediacentre/press_releases/documents/WMO_1108_EN_web_000.pdf (accessed Dec 11, 2019).

(3) Ritchie, H.; Roser, M. CO2 and other Greenhouse Gas Emissions https://ourworldindata.org/co2-and-other-greenhouse-gas-emissions (accessed Nov 26, 2018).

(4) Sayari, A.; Belmabkhout, Y.; Serna-Guerrero, R. Flue Gas Treatment via CO2 Adsorption. *Chem. Eng. J.* **2011**, *171* (3), 760–774. https://doi.org/10.1016/j.cej.2011.02.007.

(5) Choi, S.; Drese, J. H.; Jones, C. W. Adsorbent Materials for Carbon Dioxide Capture from Large Anthropogenic Point Sources. *ChemSusChem* **2009**, *2* (9), 796–854. https://doi.org/10.1002/cssc.200900036.

(6) Heydari-Gorji, A.; Yang, Y.; Sayari, A. Effect of the Pore Length on CO2 Adsorption over Amine-Modified Mesoporous Silicas. *Energy & Fuels* **2011**, *25* (9), 4206–4210. https://doi.org/10.1021/ef200765f.

(7) Heydari-Gorji, A.; Belmabkhout, Y.; Sayari, A. Polyethylenimine-Impregnated Mesoporous Silica: Effect of Amine Loading and Surface Alkyl Chains on CO2 Adsorption. *Langmuir* **2011**, *27* (20), 12411–12416. https://doi.org/10.1021/la202972t.

(8) Sayari, A.; Liu, Q.; Mishra, P. Enhanced Adsorption Efficiency Through Materials Design for Direct Air Capture Over Supported Polyethylenimine. *ChemSusChem* **2016**, *9* (19), 2796–2803. https://doi.org/10.1002/cssc.201600834.

(9) Sanz-Pérez, E. S.; Murdock, C. R.; Didas, S. A.; Jones, C. W. Direct Capture of CO2 from Ambient Air. *Chem. Rev.* **2016**, *116* (19), 11840–11876. https://doi.org/10.1021/acs.chemrev.6b00173.

(10) Gebald, C.; Meier, W.; Repond, N.; Ruesch, T.; Wurzbacher, J. A. Direct Air Capture Device. **2019**, US Patent 10232305.

(11) Eisenberger, P. System and Method for Carbon Dioxide Capture and Sequestration. **2013**, US Patent 8500855.

(12) Sun, N.; Tang, Z.; Wei, W.; Snape, C. E.; Sun, Y. Solid Adsorbents for Low-Temperature CO2 Capture with Low-Energy Penalties Leading to More Effective Integrated Solutions for Power Generation and Industrial Processes. *Front. Energy Res.* **2015**, *3*, 1–16. https://doi.org/10.3389/fenrg.2015.00009.

(13) Shen, X.; Du, H.; Mullins, R. H.; Kommalapati, R. R. Polyethylenimine Applications in

Carbon Dioxide Capture and Separation: From Theoretical Study to Experimental Work. *Energy Technol.* **2017**, *5* (6), 822–833. https://doi.org/10.1002/ente.201600694.
(14) Jahandar Lashaki, M.; Khiavi, S.; Sayari, A. Stability of Amine-Functionalized CO2 Adsorbents: A Multifaceted Puzzle. *Chem. Soc. Rev.* **2019**, *48*, 3320–3405. https://doi.org/10.1039/C8CS00877A.
(15) Qi, G.; Wang, Y.; Estevez, L.; Duan, X.; Anako, N.; Park, A. H. A.; Li, W.; Jones, C. W.; Giannelis, E. P. High Efficiency Nanocomposite Sorbents for CO2 Capture Based on Amine-Functionalized Mesoporous Capsules. *Energy Environ. Sci.* **2011**, *4* (2), 444–452. https://doi.org/10.1039/c0ee00213e.
(16) Wang, M.; Yao, L.; Wang, J.; Zhang, Z.; Qiao, W.; Long, D.; Ling, L. Adsorption and Regeneration Study of Polyethylenimine-Impregnated Millimeter-Sized Mesoporous Carbon Spheres for Post-Combustion CO2 Capture. *Appl. Energy* **2016**, *168*, 282–290. https://doi.org/10.1016/j.apenergy.2016.01.085.
(17) Chen, Z.; Deng, S.; Wei, H.; Wang, B.; Huang, J.; Yu, G. Polyethylenimine-Impregnated Resin for High CO2 Adsorption: An Efficient Adsorbent for CO2 Capture from Simulated Flue Gas and Ambient Air. *ACS Appl. Mater. Interfaces* **2013**, *5* (15), 6937–6945. https://doi.org/10.1021/am400661b.
(18) Zhang, L.; Zhan, N.; Jin, Q.; Liu, H.; Hu, J. Impregnation of Polyethylenimine in Mesoporous Multilamellar Silica Vesicles for CO2 Capture: A Kinetic Study. *Ind. Eng. Chem. Res.* **2016**, *55* (20), 5885–5891. https://doi.org/10.1021/acs.iecr.5b04760.
(19) Zhou, L.; Fan, J.; Cui, G.; Shang, X.; Tang, Q.; Wang, J.; Fan, M. Highly Efficient and Reversible CO2 Adsorption by Amine-Grafted Platelet SBA-15 with Expanded Pore Diameters and Short Mesochannels. *Green Chem.* **2014**, *16* (8), 4009–4016. https://doi.org/10.1039/c4gc00832d.
(20) Franchi, R. S.; Harlick, P. J. E.; Sayari, A. Applications of Pore-Expanded Mesoporous Silica. 2. Development of a High-Capacity, Water-Tolerant Adsorbent for CO2. *Ind. Eng. Chem. Res.* **2005**, *44* (21), 8007–8013. https://doi.org/10.1021/ie0504194.
(21) Drage, T. C.; Arenillas, A.; Smith, K. M.; Snape, C. E. Thermal Stability of Polyethylenimine Based Carbon Dioxide Adsorbents and Its Influence on Selection of Regeneration Strategies. *Microporous Mesoporous Mater.* **2008**, *116* (1–3), 504–512. https://doi.org/10.1016/j.micromeso.2008.05.009.
(22) Vieira, R. B.; Pastore, H. O. Polyethylenimine-Magadiite Layered Silicate Sorbent for CO2 Capture. *Environ. Sci. Technol.* **2014**, *48* (4), 2472–2480. https://doi.org/10.1021/es404501e.
(23) Fan, Y.; Rezaei, F.; Yang, X. Mixed Alkanolamine-Polyethylenimine Functionalized Silica for CO 2 Capture. *Energy Technol.* **2019**, *7* (2), 253–262. https://doi.org/10.1002/ente.201800481.
(24) Yue, M. B.; Sun, L. B.; Cao, Y.; Wang, Z. J.; Wang, Y.; Yu, Q.; Zhu, J. H. Promoting the CO2 Adsorption in the Amine-Containing SBA-15 by Hydroxyl Group. *Microporous Mesoporous Mater.* **2008**, *114* (1–3), 74–81. https://doi.org/10.1016/j.micromeso.2007.12.016.
(25) Lawson, S.; Griffin, C.; Rapp, K.; Rownaghi, A. A.; Rezaei, F. Amine-Functionalized MIL-101 Monoliths for CO2 Removal from Enclosed Environments. *Energy and Fuels* **2019**, *33* (3), 2399–2407. https://doi.org/10.1021/acs.energyfuels.8b04508.

(26) Jeon, S.; Jung, H.; Jo, D. H.; Kim, S. H. Development of Crosslinked PEI Solid Adsorbents for CO2 Capture. *Energy Procedia* **2017**, *114* (November 2016), 2287–2293. https://doi.org/10.1016/j.egypro.2017.03.1373.
(27) Zhang, H.; Goeppert, A.; Czaun, M.; Prakash, G. K. S.; Olah, G. A. CO2 Capture on Easily Regenerable Hybrid Adsorbents Based on Polyamines and Mesocellular Silica Foam. Effect of Pore Volume of the Support and Polyamine Molecular Weight. *RSC Adv.* **2014**, *4* (37), 19403–19417. https://doi.org/10.1039/c4ra02145b.
(28) Ahmadalinezhad, A.; Sayari, A. Oxidative Degradation of Silica-Supported Polyethylenimine for CO2 Adsorption: Insights into the Nature of Deactivated Species. *Phys. Chem. Chem. Phys.* **2014**, *16* (4), 1529–1535. https://doi.org/10.1039/c3cp53928h.
(29) Heydari-Gorji, A.; Sayari, A. Thermal, Oxidative, and CO2-Induced Degradation of Supported Polyethylenimine Adsorbents. *Ind. Eng. Chem. Res.* **2012**, *51* (19), 6887–6894. https://doi.org/10.1021/ie3003446.
(30) Tsuda, T.; Fujiwara, T. Polyethyleneimine and Macrocyclic Polyamine Silica Gels Acting as Carbon Dioxide Absorbents. *J. Chem. Soc. Chem. Commun.* **1992**, 1659–1661. https://doi.org/10.7868/s0032180x16080128.
(31) Kassab, H.; Maksoud, M.; Aguado, S.; Pera-Titus, M.; Albela, B.; Bonneviot, L. Polyethylenimine Covalently Grafted on Mesostructured Porous Silica for CO2 Capture. *RSC Adv.* **2012**, *2* (6), 2508–2516. https://doi.org/10.1039/c2ra01007k.
(32) Zhou, Z.; Balijepalli, S. K.; Nguyen-Sorenson, A. H. T.; Anderson, C. M.; Park, J. L.; Stowers, K. J. Steam-Stable Covalently Bonded Polyethylenimine Modified Multiwall Carbon Nanotubes for Carbon Dioxide Capture. *Energy and Fuels* **2018**, *32* (11), 11701–11709. https://doi.org/10.1021/acs.energyfuels.8b02864.
(33) Mane, S.; Gao, Z. Y.; Li, Y. X.; Liu, X. Q.; Sun, L. B. Rational Fabrication of Polyethylenimine-Linked Microbeads for Selective CO2 Capture. *Ind. Eng. Chem. Res.* **2018**, *57* (1), 250–258. https://doi.org/10.1021/acs.iecr.7b04212.
(34) Liu, F. Q.; Li, W.; Zhao, J.; Li, W. H.; Chen, D. M.; Sun, L. S.; Wang, L.; Li, R. X. Covalent Grafting of Polyethyleneimine on Hydroxylated Three-Dimensional Graphene for Superior CO 2 Capture. *J. Mater. Chem. A* **2015**, *3* (23), 12252–12258. https://doi.org/10.1039/c5ta01536g.
(35) Wu, Q.; Chen, S.; Liu, H. Effect of Surface Chemistry of Polyethyleneimine-Grafted Polypropylene Fiber on Its CO2 Adsorption. *RSC Adv.* **2014**, *4* (52), 27176–27183. https://doi.org/10.1039/c4ra01232a.
(36) Zhu, J.; Wu, L.; Bu, Z.; Jie, S.; Li, B. G. Polyethylenimine-Grafted HKUST-Type MOF/PolyHIPE Porous Composites (PEI@PGD-H) as Highly Efficient CO2 Adsorbents. *Ind. Eng. Chem. Res.* **2019**, *58* (10), 4257–4266. https://doi.org/10.1021/acs.iecr.9b00213.
(37) Kishor, R.; Ghoshal, A. K. Polyethylenimine Functionalized As-Synthesized KIT-6 Adsorbent for Highly CO2/N2 Selective Separation. *Energy and Fuels* **2016**, *30* (11), 9635–9644. https://doi.org/10.1021/acs.energyfuels.6b02082.
(38) Zhai, Y.; Chuang, S. S. C. Enhancing Degradation Resistance of Polyethylenimine for CO2 Capture with Cross-Linked Poly(Vinyl Alcohol). *Ind. Eng. Chem. Res.* **2017**, *56* (46), 13766–13775. https://doi.org/10.1021/acs.iecr.7b03636.
(39) Sakwa-Novak, M. A.; Tan, S.; Jones, C. W. Role of Additives in Composite PEI/Oxide CO2 Adsorbents: Enhancement in the Amine Efficiency of Supported PEI by PEG in CO2

Capture from Simulated Ambient Air. *ACS Appl. Mater. Interfaces* **2015**, *7* (44), 24748–24759. https://doi.org/10.1021/acsami.5b07545.

(40) Choi, W.; Min, K.; Kim, C.; Ko, Y. S.; Jeon, J. W.; Seo, H.; Park, Y. K.; Choi, M. Epoxide-Functionalization of Polyethyleneimine for Synthesis of Stable Carbon Dioxide Adsorbent in Temperature Swing Adsorption. *Nat. Commun.* **2016**, *7*, 1–8. https://doi.org/10.1038/ncomms12640.

(41) Min, K.; Choi, W.; Kim, C.; Choi, M. Oxidation-Stable Amine-Containing Adsorbents for Carbon Dioxide Capture. *Nat. Commun.* **2018**, *9* (1), 726. https://doi.org/10.1038/s41467-018-03123-0.

(42) Kruk, M.; Jaroniec, M.; Antochshuk, V.; Sayari, A. Mesoporous Silicate-Surfactant Composites with Hydrophobic Surfaces and Tailored Pore Sizes. *J. Phys. Chem. B* **2002**, *106* (39), 10096–10101. https://doi.org/10.1021/jp026252z.

(43) Sayari, A. Unprecedented Expansion of the Pore Size and Volume of Periodic Mesoporous Silica. *Angew. Chemie - Int. Ed.* **2000**, *39* (16), 2920–2922. https://doi.org/10.1002/1521-3773(20000818)39:16<2920::AID-ANIE2920>3.0.CO;2-3.

(44) Harlick, P. J. E.; Sayari, A. Applications of Pore-Expanded Mesoporous Silica. 5. Triamine Grafted Material with Exceptional CO2 Dynamic and Equilibrium Adsorption Performance. *Ind. Eng. Chem. Res.* **2007**, *46* (2), 446–458. https://doi.org/10.1021/ie060774+.

(45) Kolle, J. M.; Sayari, A. Substrate Dependence on the Fixation of CO2 to Cyclic Carbonates over Reusable Porous Hybrid Solids. *J. CO2 Util.* **2018**, *26* (April), 564–574. https://doi.org/10.1016/j.jcou.2018.06.013.

(46) Ravikovitcha, P. I.; Hallera, G. L.; Neimark, A. V. Density Functional Theory Model for Calculating Pore Size Distributions: Pore Structure of Nanoporous Catalysts. *Adv. Colloid Interface Sci.* **1998**, *76–77*, 203–226.

(47) Ziaei-Azad, H.; Kolle, J. M.; Al-Yasser, N.; Sayari, A. One-Pot Synthesis of Large-Pore AlMCM-41 Aluminosilicates with High Stability and Adjustable Acidity. *Microporous Mesoporous Mater.* **2018**, *262* (November 2017), 166–174. https://doi.org/10.1016/j.micromeso.2017.11.036.

(48) Jahandar Lashaki, M.; Sayari, A. CO2 Capture Using Triamine-Grafted SBA-15: The Impact of the Support Pore Structure. *Chem. Eng. J.* **2018**, *334* (October 2017), 1260–1269. https://doi.org/10.1016/j.cej.2017.10.103.

(49) Keller, J.; Staudt, R. Gas Adsorption Equilibria - Experimental Methods and Adsorption Isotherms. In *Separation and Purification Methods*; 2005; pp 359–363. https://doi.org/10.1007/b102056.

(50) Pinto, M. L.; Mafra, L.; Guil, J. M.; Pires, J.; Rocha, J. Adsorption and Activation of CO2 by Amine-Modified Nanoporous Materials Studied by Solid-State NMR and 13CO2 Adsorption. *Chem. Mater.* **2011**, *23* (6), 1387–1395. https://doi.org/10.1021/cm1029563.

(51) Li, W.; Choi, S.; Drese, J. H.; Hornbostel, M.; Krishnan, G.; Eisenberger, P. M.; Jones, C. W. Steam-Stripping for Regeneration of Supported Amine-Based CO2 Adsorbents. *ChemSusChem* **2010**, *3* (8), 899–903. https://doi.org/10.1002/cssc.201000131.

Appendix A4: Supplementary Data for Chapter 4

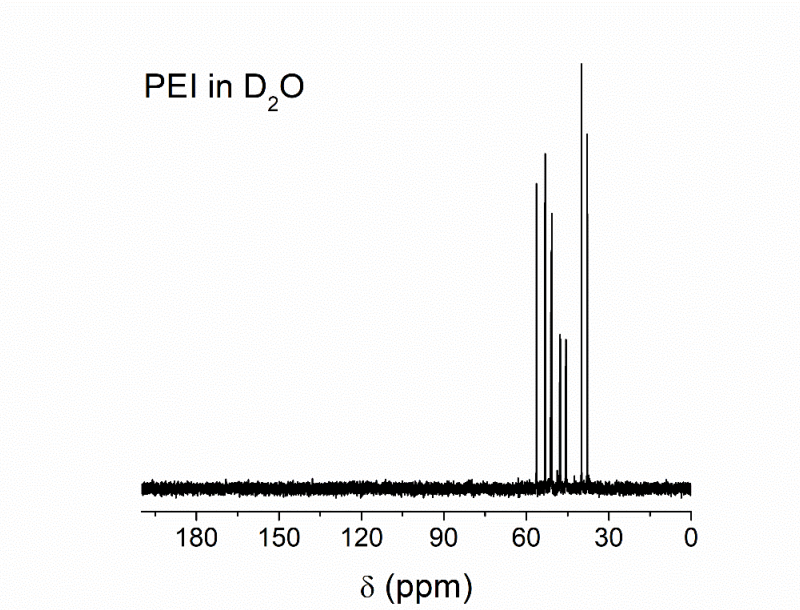

Figure A4- 1. ^{13}C NMR spectrum of PEI in D_2O

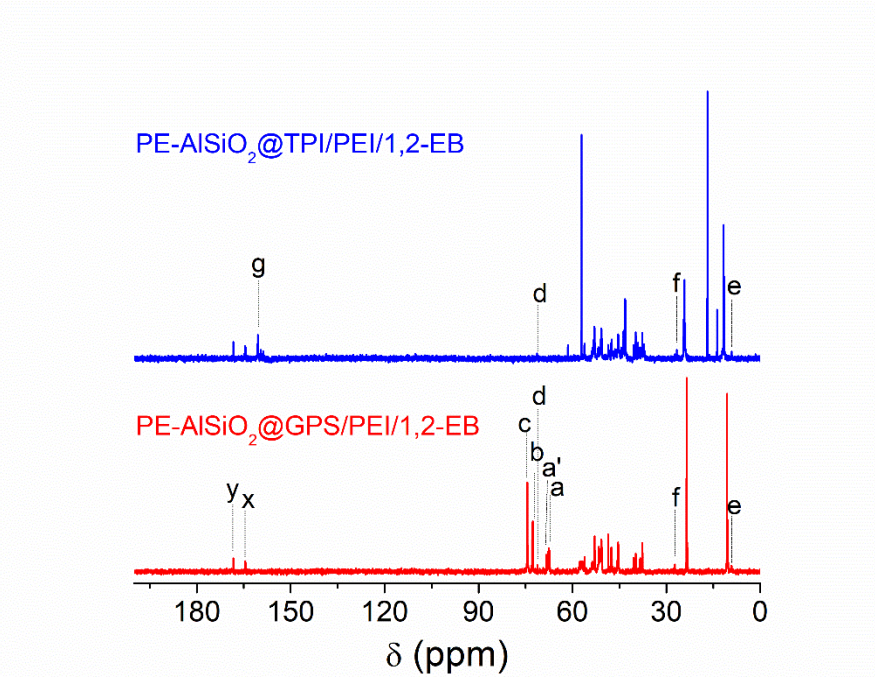

Figure A4- 2. ^{13}C NMR spectra of solid materials, with higher grafting agent-to-PEI ratio, dissolved in 10% NaOH (D_2O)

Table A4- 1. Changes in CO_2 capacity and organic content following leaching in EtOH

		CO_2 uptake (mmol/g)			**Organic content (wt%)**		
Entry	**Material**	**Fresh**	**EtOH-leached**	**% difference**	**Fresh**	**EtOH-leached**	**% difference**
1	M1 - 68	2.76	0.48	83	47.18	23.63	50
2	M2	2.76	1.17	58	52.32	30.39	42
3	M3 - 59	2.89	1.34	54	47.31	32.07	32
4	M4	2.31	1.51	35	49.79	40.46	19
5	M5	2.28	1.39	39	49.82	38.78	22
6	M6	2.34	1.68	28	51.20	43.73	15
7	M7	2.46	1.83	26	51.58	45.59	12
8	M8	2.44	2.01	18	53.44	49.5	7
9	M9	2.19	1.56	29	49.15	45.24	8
10	M10	2.19	1.65	25	50.12	45.61	9
11	M11 - 62	2.75	1.15	59	51.64	36.47	29

Leaching test procedure: 0.5 g of material stirred in 50 mL EtOH for 2 h

Table A4- 2. Variation of CO_2 uptake following thermal oxidation degradation at 100 ^oC over time

Entry	**Material**	**Thermal oxidation duration**			
		0 h	**16 h**	**24 h**	**40 h**
1	M1	2.76	-	0.63	-
2	M2	2.76	2.21	0.97	0.23
3	M7	2.46	1.84	1.05	0.34
4	M8	2.44	2.19	1.97	1.13
5	M9	2.19	1.95	1.55	0.76
6	M10	2.19	2.09	1.82	0.98
7	M11	2.75	-	1.05	-

CHAPTER 5 UNDERSTANDING THE EFFECT OF WATER ON CO_2 ADSORPTION – A REVIEW

5.0. Overview

Water vapor is a ubiquitous component in flue gas and other CO_2-rich industrial gases. Accordingly, understanding the role played by water during humid CO_2 adsorption is of paramount importance to the development of efficient adsorbents and processes for CO_2 capture. This review attempts to provide a critical analysis on the effect of water over different types of adsorbents, including; carbon-based materials, zeolites, MOFs, amine-functionalized materials, clays, metal oxides and carbonates. For carbon-based materials, water seemed to be beneficial to CO_2 uptake only at high pressures, while the high affinity of many zeolites for water significantly decreased their CO_2 uptake with rising humidity. MOFs, on the other hand, may undergo structurally degradation in the presence of water vapor either by ligand displacement or hydrolysis, adding the need for water-stable MOFs for application in CO_2 adsorption under humid conditions. Nonetheless, for water-stable MOFs there exists a threshold of quantity of (pre-)adsorbed water below which CO_2 uptake is enhanced and above which a severe decrease in CO_2 uptake is observed due to pore blockage by pre-adsorbed water. Amine-containing adsorbents are an attractive class of materials and generally showed a beneficial effect of moisture owing to a maximum amine efficiency, i.e., CO_2/N ratio of 1 in the presence of moisture, compared to 0.5 for dry conditions. As for reactive adsorbents, e.g. metal oxides and carbonates, they showed a mixed effect under humid conditions. Any gain in CO_2 uptake in the presence of

moisture is usually associated with an energy penalty for water desorption during regeneration. Several approaches to material and process design were proposed to reduce this energy demand.

5.1. Introduction

Climate change and global warming are arguably the greatest challenges faced by mankind; most of which is linked to CO_2 emissions. [1] The development of efficient materials and industrial-scale processes for CO_2 capture is one of several strategies to mitigate CO_2 emissions and improve our chances for long-term human survival.[2–4] CO_2 adsorption using a variety of materials capable of reversibly removing CO_2 has been proposed as a more viable and sustainable approach with lower energy requirements compared to CO_2 absorption using aqueous amine.[5] Several types of adsorbents have been developed for CO_2 capture,[6,7] including metal-organic frameworks (MOFs),[8–10] coordination organic polymers (COPs),[11,12] zeolites,[13,14] clays,[15,16] carbons,[17–20] silica,[21,22] basic oxides[23,24] and amine-containing porous materials.[25–27]

Flue gas and many other CO_2-rich industrial gases may contain 6 to 18% water vapor (Table 5-1),[28] whereas biogas is typically water-saturated with 6-7% moisture.[29] Taking into account the high molar specific heat capacity and large dipole moment of water, it is therefore critically important to understand the different roles that water may play with respect to CO_2 adsorption, and their implications on the selection of materials and processes. Although there are some review articles on the effect of water vapor on CO_2 capture performance of MOFs[30,31] and membranes,[30] there is no comprehensive report on the effect of water vapor on CO_2 capture performance over a wide range of adsorbent types. Such a report would be highly informative since different types of adsorbents demonstrate completely different behaviors when CO_2 adsorption is conducted under humid conditions. The current review aims at filling this gap,

starting with discussion of analytical techniques to quantify CO_2 uptake under moist condition, to the effect of water on CO_2 adsorption over physisorbents, then over amine-containing adsorbents, and reactive materials. Specifically, the effects of water on structural stability of the adsorbent, CO_2 capacity, CO_2 kinetics and regenerability are discussed.

Table 5-1. Typical compositions of different flue gases[28]

Components	Pulverized coal	Waste incineration	Coal-fired IGCC	Natural gas-fired CC	Cement rotary kiln
O_2 (vol%)	6	7–14	12	14	7
N_2 (vol%)	76	Balance	66	76	59
CO_2 (vol%)	11	6–12	7	3	19
H_2O (vol%)	6	10–18	14	6	13
Ar (vol%)	1	1	1	1	1
SO_2 (ppm)	300–5000	200–1500	10–200	–	5–1200
NOx (ppm)	500–800	200–500	10–100	10–300	100–1500

5.2. Measuring CO_2 uptake in the presence of humidity

Different techniques, e.g. gravimetric analysis using TGA, dynamic column breakthrough experiments, and TPD-MS experiments, have been applied to measure the effect of humidity on CO_2 adsorption. To separate CO_2 uptake from water uptake using TGA experiments, humid nitrogen adsorption and humid CO_2 adsorption were conducted separately, with the difference in uptake attributed to CO_2.[32] Alternatively, pre-hydrating the adsorbent using a CO_2-free stream containing specific amount of RH, and conducting dry CO_2 adsorption was reported amid potential displacement of pre-adsorbed water during exposure to dry CO_2. The most applied method used to decouple the adsorption of water from the adsorption of CO_2 is saturating the adsorbent using a CO_2-free stream containing water vapor, and subsequently conducting

adsorption tests on the samples using identical humidified gaseous stream containing CO_2, with the mass gain attributed to CO_2 adsorption (Figure 5-1).[33] Nevertheless, Sayari group[34] found that TGA data significantly underestimated CO_2 uptake, even when the above-mentioned procedure is undertaken.

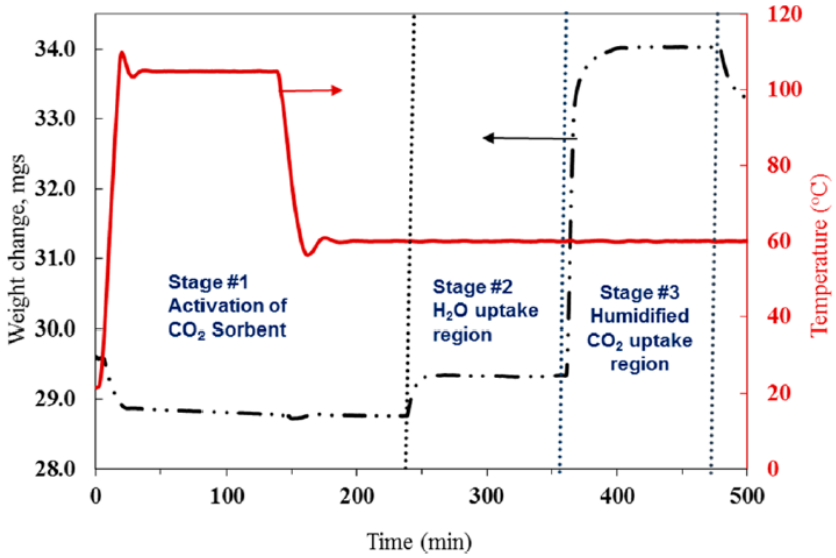

Figure 5-1. TGA experiments during humid CO_2 adsorption on PEI-impregnated CARiACT silica.[33]

Breakthrough experiments which rely on CO_2 and water vapor co-adsorb in a column containing adsorbent, while CO_2 concentration in the outlet flow is continuously measured using a variety of instruments such as GC-TCD, MS and gas analyzer, are generally more precise than their TGA counterparts. Nevertheless, the accuracy of breakthrough experiments also strongly depends on the monitoring instrument, especially for direct air capture (DAC).[35,36]

5.3. Physical adsorbents

5.3.1 Carbon-based materials

The large surface area and low cost of activated carbons (ACs), carbon nanotubes (CNTs) and graphene make them an attractive material for CO_2 adsorption. AC often have low affinity toward water vapor at low RH; however, at high RH levels, water uptake increases significantly, eventually forming three-dimensional water clusters, which make the study of competitive adsorption of water and CO_2 complicated.[37,38] Most studies on carbonaceous materials under sub-atmospheric pressures reported a negative impact of humidity on CO_2 uptake as a result of competitive adsorption of water,[39,40] while a few studies found that water had no effect on CO2 uptake[41,42] A number of theoretical investigation on the effect on brown coal[43], AC[44], neutral and charged CNT,[45] and N-doped AC[46] on the competitive adsorption of water and CO_2 were reported. At high pressure however, several studies showed the beneficial effect of water on CO_2 adsorption over carbon adsorbents; coconut shells carbon[47], bamboo carbon[48] and activated carbon BY-1[49]. Such enhancement in CO2 uptake was ascribed to mechanisms other than adsorption, including dissolution, and bicarbonate or hydrate formation.

5.3.2. Zeolites

Zeolites, notably ion-exchanged zeolites have been reported as efficient CO_2 adsorbents, because of the strong interactions between the extra framework cations and CO_2 molecules.[50,51]. Nonetheless, strong electrostatic interactions between extra-framework cations and water molecules result in significantly higher affinity of zeolites toward water (through electrostatic forces) compared to CO_2, leading to less favorable CO_2[52,53]

5.3.3. Metal Organic Frameworks

Metal organic frameworks (MOFs) have shown great potential for a wide range of applications, including carbon capture.[54–56] Water-stability of MOFs is an important factor surrounding their use for carbon capture from humid gas streams, with the degradation of MOFs in the presence of water vapor thought to occurs through two mechanisms, namely ligand displacement and hydrolysis.[57,58] MOFs containing high-valence metal cations (e.g. Fe^{3+} and Zr^{4+})[59,60], bi-metallic atoms,[61] hydrophobic groups[62], basic ligands[63,64] and ligands with special structures[65–67] exhibit strong metal-ligand bonding and/or shield the metal atom from water, were reported to improve their stability towards water. Nonetheless, structural collapse of adsorbent upon water exposure is not the only reason for dramatic loss in CO_2 uptake of MOFs. The effect of water vapor or pre-adsorbed water on CO_2 capture performance of different MOFs is influence by the quantity of water adsorbed by the MOF. For some MOFs, there exist a threshold of quantity of pre-adsorbed water below which CO_2 uptake is enhanced (due to the confinement effect), and above which a severe decrease in CO_2 uptake is observed due pore blockage by pre-adsorbed water.[68,69] Moreover, several properties of the MOF-based adsorbent, including the nature of metal centers,[70,71] ligand type,[31,72]and framework structure,[73,74] were tailored in an attempt to improve CO_2 uptake under humid conditions. Furthermore, several groups reported on the beneficial effect of amine-functionalization of MOFs on wet CO_2 capture owing to the selective binding between amine groups and CO_2 molecules via chemical interactions.[75,76] For instance, Long group[77] showed that diamine tethering on CuBTTri increased CO_2 uptake at 0.15 bar and 25 °C by 350 %, i.e. from 0.69 to 2.38 mmol/g. In addition, coating MOFs with amines was also found to improve their water stability and CO_2 uptake under moist

conditions.[78,79] The presence of water was also reported to have an adverse[80,81] and in some rare cases no effect[82] on CO_2 uptake.

The above experimental findings are complimented by theoretical studies on the effect of water of CO_2 uptake of MOFs, highlighting; the maximum quantity of pre-adsorbed water required for enhanced CO_2 uptake,[83] and the effect of charged MOF framework.[84] Furthermore, Llewellyn group[85] conducted a comprehensive screening study on the effect of pre-adsorbed water on CO_2 uptake over 45 MOFs, using 100 % CO_2. As shown in Table 5-2, the materials were categorized into five groups based on trends of CO_2 uptake as measured by TGA versus preadsorbed water. As expected, the CO_2 uptake of MOFs is affected by trends in their water uptake, as well as the strength of water interaction with the material surface as expressed by Henry law constants (K_H).[85]

Table 5-2. Summary of trends in water uptake of different MOFs

Groups	Trend in water uptake	Example of MOFs
Group I	hydrophobic MOFs: CO_2 uptake not affected by pre-adsorbed water.	ZIFs, ScBDCs, MIL-121s, MIL-69(Al), MIL-103(La)
Group II	CO_2 uptake decreased linearly with increasing pre-adsorbed water, indicating that CO_2 and water share the same adsorption sites	MIL-102(Cr), CPO-27(Ni)
Group III	decreasing CO_2 adsorption capacity as the amount of pre-adsorbed water increased, albeit with different slopes	MIL-100(Cr), MIL-100(Cr)-Me, MIL-101(Cr), MIL-130(Al), MIL-68(Ga)
Group IV	decreasing CO_2 uptake with increasing amount of pre-adsorbed water, combined with a plateau region for low water contents.	MIL-53(Cr), MIL-53(Al)
Group V	a maximum water uptake at particular water loadings	MIL-110(Al), MIL-163(Zr), HKUST-1, UiO-66(Zr)s (UiO-66(Zr), UiO-66(Zr)-CF3, UiO-66(Zr)-2CF3, UiO-66(Zr)-Me, UiO-66(Zr)-2Me

5.4. Amine-containing Adsorbents

Amine-containing adsorbents (ACAs), prepared by impregnation on porous support or grafting of aminosilane on surface hydroxyl groups of supports, are attractive materials for CO_2 capture owing to achievable high adsorption site density, reversible CO_2-amine interaction, and practical regeneration energy demands.[86] In the absence of moisture, CO_2 adsorption on ACAs with primary or secondary amine occurs primarily via carbamate formation, while in the presence of moisture, the formation of bicarbonate and carbonate are obtained to different extends depending on the type of amine, i.e., 1°, 2° and 3°, on the adsorbent.[25] Coincidentally, in the presence of humidity, the maximum amine efficiency, i.e., CO_2/N ratio, is 1 compared to 0.5 for dry conditions, which generally implies more CO_2 uptake under wet conditions.[87]

5.4.1. Amine-Impregnated Adsorbents

Several studies were devoted to the role played by water during CO_2 (≥ 2% CO_2 in feed gas) uptake on a wide range of amine-impregnated materials including; PEI/MCM-41,[88] TEPA/KIT-6,[89] PEI/hierarchical silica monolith,[90] PEI/mesoporous silica foams,[91] PEI/carbon,[92] PEI/clays,[93] PEI/single-walled CNT,[94] hyperbranched polyamine/SiO_2,[95] 5-diazo-bicyclo[4.3.0]non-5-ene/AC,[96] and PEI/C_{60}.[97] While the presence of water, within specified humidity limits, led to an enhanced in CO_2 uptake for these materials, other amine-impregnated adsorbents showed no effect on CO_2 uptake at low (6.7% RH)[98] and high (>70% RH)[77] humidity level. In the same vein, higher CO_2 uptake were reported for amine-impregnated adsorbents for CO_2 capture from air (DAC), i.e., poly(allyamine)/SiO_2,[99] PEI/mesoporous carbon,[100] PEI/styrene-divinylbenzene, lewatit and PEI/metal carbonates,[101] PEI/nanofibrillated cellulose.[36] Nonetheless, some studies found no effect no effect of moisture (TEPA/CARiACT silica[102]) and a negative effect of moisture on CO_2 uptake (PEI/fumed silica[103] and PEI/polymer resins[104]).

As a general observation for amine-impregnated materials, the presence of adsorbents with high amine loading can negatively affect CO_2 adsorption especially at high RHs.[36] For some materials, pre-adsorption of water as opposed to co-adsorbed of water and CO_2 may be beneficial as conducting adsorption on a dry adsorbent hinders water build-up, which is required for efficient formation of bicarbonate. Moreover, water inside the pores facilitate the loosening of the polymer network, thereby facilitating the diffusion of CO_2 molecules to the active sites[99,105]

5.4.2. Amine-Grafted Adsorbents

Compared to amine-impregnated materials, amine-grafting adsorbents (AGAs) or covalently immobilized amines are less volatile and thermally stable. Different AGAs have equally

been studies for CO_2 adsorption, with reported enhancement in CO_2 uptake in the presence of water, including; propylamine(monoamine)/MCM-48,[106] diamine/SBA-15,[107] and triamine/SBA-15,[108,109] monoamine/hexagonal mesoporous silica (HMS) [110] and polyamines/SiO_2.[111] In comparison to amine-impregnated adsorbents, significantly less AGAs were studied for DAC, although less dramatic increase in CO2 update were obtained. Some of such adsorbent included; monoamine/SBA-15,[112] diamine/nanofiber cellulose,[105] and triamine/PE-MCM-41.[113] In a series of breakthrough contributions involving in-depth investigation of CO_2 adsorption-desorption cycling under dry and humid conditions, Sayari group, discovered the key role of humidity in stabilizing any supported amine against CO_2-induced deactivation. Such deactivation, which occurred under dry conditions, proceeded via the formation of stable urea linkages.[114] Although tertiary amines do not react with CO_2 under dry condition, yet in the presence of moisture, they contribute to CO_2 adsorption via bicarbonate formation.[115,116] Theoretical studies by Cho *et al.*[117] outlined the key role of silanol groups, acting as assisting species, in facilitating proton transfer reaction in amine groups during CO_2 adsorption over amine-grafted silica.

5.4.2.2. Amine-functionalized zeolites and others

Given the microporous nature of zeolites, the rational of combining zeolites and amines for the purpose of CO_2 adsorption is questionable. Nonetheless, different groups have studied amine-functionalized zeolites for CO_2 capture, including; monoethanolamine (MEA)-impregnated 13X zeolite, [118] TEPA-modified Y-zeolite and APTES-impregnated beta zeolite.[119] For these adsorbents, enhancement in CO_2 uptake under humid conditions attained a maximum as a specific moisture content, beyond which CO_2 uptake decrease with further increase in water content. In addition to zeolites, nitrogen-rich porous polymers[120,121] and quaternized amines

attached to a polymer resin with hydroxide or carbonate groups as mobile counterions,[122] with mixed outcomes of CO_2 uptake under humid conditions.

5.4.3. Regeneration of amine-containing adsorbents

CO_2 adsorption technology based on amine-containing adsorbents is centered on the reversible reaction between CO_2 and amine. The total energy required to regenerate (Q_{reg}) an adsorbent is a sum of heat of CO_2 desorption (Q_{des}), sensible heat (Q_{sen}) required to increase temperature of sorbent to regeneration temperature and latent heat of vaporization of water (Q_{vap})[123] – eqn 5.1

$$Q_{reg} = Q_{des} + Q_{sen} + Q_{vap} \qquad (5.1)$$

Different regeneration approaches including pressure swing adsorption (PSA), vacuum swing adsorption (VSA), temperature swing adsorption (TSA), have been used separately or in combination.[124,125] For ACAs, the gain in CO_2 uptake in the presence of moisture is associated with energy penalty for water desorption during regeneration, quantified by the desorption temperature. The need for high desorption temperatures is related to the high specific heat capacity of water and its slow desorption rate.[126–128] Two main approaches, i.e., material[124,128–131] and process[126,132] designs have been proposed to curb the energy demand for the regeneration of ACA.

5.5. Reactive Adsorbents

5.5.1. Alkali and Alkaline Earth Metal-Based Adsorbents

Due to the basic nature of some metal oxides, hydroxides and carbonates they are reactive towards acidic CO_2, notably at high temperatures with high CO_2 uptake and selectivity over water.[133] Alkali metal carbonates react with CO_2 under humid conditions to form different

salts (e.g. bicarbonate, $Na_5H_3(CO_3)_4$, Wegscheider's salt, sesquicarbonate, etc.) depending on the CO_2 concentration, adsorption temperature and humidity;[134,135] while pre-hydration was found to be beneficial during regeneration.[136] Jayakumar *et al.*[137] showed for the co-adsorption of water vapor and CO_2, parallel reactions involving K_2CO_3 and pre-hydration active species (K_2CO_3•($1.5H_2O$)) led to the formation of $KHCO_3$. Contrary to alkali metal-based adsorbents, alkali earth metal-derived adsorbents can react with CO_2 in the absence of water, with CO_2 uptake and kinetics reportedly enhanced[138–140] and decreased[141] under humid conditions.

5.5.2. Hydrotalcite Adsorbents

In general, the presence of water exhibits a beneficial effect on CO_2 uptake of Hydrotalcite materials (also known as layered double hydroxides (LDH)), notably at high temperature,[142] while the calcination temperature during adsorbent preparation was reported to affect CO_2 uptake.[143] Using a potassium-promoted hydrotalcite based adsorbent, Coenen *et al.*[144] established four adsorption sites (A, B, C and D) with different affinities toward CO_2 and water (Figure 5-2). Sites A and B were assigned to water and CO_2 adsorption, respectively, and can be regenerated under flowing nitrogen, while site C, which can be either occupied by water or CO_2, can be regenerated only by water vapor and not N_2 flushing. Site D can adsorb CO_2 only during exposure to both CO_2 and water, and can be regenerated completely using water, or partly using nitrogen.

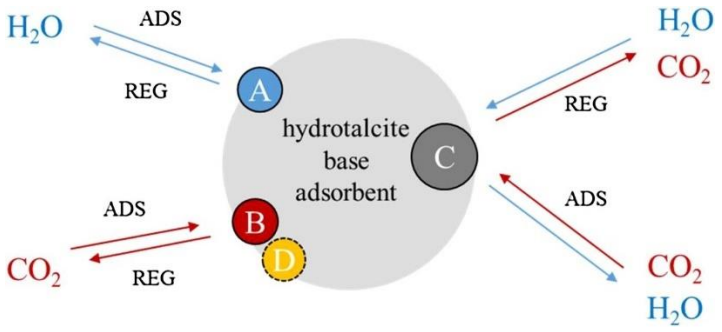

Figure 5-2. The different adsorption sites for CO_2 and water on a hydrotalcite-based adsorbent.[145] Copyright (2018) Creative Commons

5.5.3. Metal oxides (excluding Group I and II metals)

In the absence of moisture, metals with surface defect sites, lattice oxygen or surface hydroxyl groups, e.g. Fe, react with CO_2 to form bicarbonates ($Fe–OCO_2H$), while $Fe–CO_3^-$ + H_3O^+ was formed under humid conditions. For some metals (Cu and Zn) CO_2 was adsorbed in the form of solvated carbonate through the intermediacy of carbonic acid at high RH.[146]

Conclusion

This review attempts to provide an understanding on the effect of water across a wide range of materials (carbon-base materials, zeolites, MOFs, amine-functionalized materials, clays, metal oxides and carbonates) during CO_2 uptake under humid conditions. For each material, test conditions and material design parameters which enhanced or diminished CO_2 uptake in the presence of water was discussed. Moreover, the energy penalty associated with the regeneration of CO_2-saturated wet adsorbents was presented.

References

(1) Tans, P. NASA global climate change - carbon dioxide https://climate.nasa.gov/vital-signs/carbon-dioxide/ (accessed Apr 1, 2019).

(2) Lecomte, F.; Broutin, P.; Lebas, E. *CO2 Capture: Technologies to Reduce Greenhouse Gas Emissions*; Editions Technips, 2010.
(3) Papadopoulos, A. I.; Seferlis, P. *Process Systems and Materials for CO2 Capture*; Papadopoulos, A. I., Seferlis, P., Eds.; Wiley, 2017.
(4) D'Alessandro, D. M.; Smit, B.; Long, J. R. Carbon Dioxide Capture: Prospects for New Materials. *Angew. Chemie - Int. Ed.* **2010**, *49* (35), 6058–6082. https://doi.org/10.1002/anie.201000431.
(5) Sjostrom, S.; Krutka, H. Evaluation of Solid Sorbents as a Retrofit Technology for CO2 Capture. *Fuel* **2010**, *89* (6), 1298–1306. https://doi.org/10.1016/j.fuel.2009.11.019.
(6) Lu, A. H.; Hao, G. P. Porous Materials for Carbon Dioxide Capture. *Annu. Reports Prog. Chem. - Sect. A* **2013**, *109*, 484–503. https://doi.org/10.1039/c3ic90003g.
(7) Nie, L.; Mu, Y.; Jin, J.; Chen, J.; Mi, J. Recent Developments and Consideration Issues in Solid Adsorbents for CO2 Capture from Flue Gas. *Chinese J. Chem. Eng.* **2018**, *26* (11), 2303–2317. https://doi.org/10.1016/j.cjche.2018.07.012.
(8) Liu, J.; Tian, J.; Thallapally, P. K.; McGrail, B. P. Selective CO2 Capture from Flue Gas Using Metal-Organic Frameworks - A Fixed Bed Study. *J. Phys. Chem. C* **2012**, *116* (17), 9575–9581. https://doi.org/10.1021/jp300961j.
(9) Trickett, C. A.; Helal, A.; Al-Maythalony, B. A.; Yamani, Z. H.; Cordova, K. E.; Yaghi, O. M. The Chemistry of Metal–Organic Frameworks for CO2 Capture, Regeneration and Conversion. *Nat. Rev. Mater.* **2017**, *2* (17045), 1–16.
(10) Shalini, S.; Nandi, S.; Justin, A.; Maity, R.; Vaidhyanathan, R. Potential of Ultramicroporous Metal-Organic Frameworks in CO2 Clean-Up. *Chem. Commun.* **2018**, *54* (96), 13472–13490. https://doi.org/10.1039/c8cc03233e.
(11) Patel, H. A.; Je, S. H.; Park, J.; Chen, D. P.; Jung, Y.; Yavuz, C. T.; Coskun, A. Unprecedented High-Temperature CO2 Selectivity in N2-Phobic Nanoporous Covalent Organic Polymers. *Nat. Commun.* **2013**, *4* (1), 1357–1358. https://doi.org/10.1038/ncomms2359.
(12) Choi, H. S.; Suh, M. P. Highly Selective CO2 Capture in Flexible 3D Coordination Polymer Networks. *Angew. Chemie - Int. Ed.* **2009**, *48* (37), 6865–6869. https://doi.org/10.1002/anie.200902836.
(13) Liu, Q.; Pham, T.; Porosoff, M. D.; Lobo, R. F. ZK-5: A CO2-Selective Zeolite with High Working Capacity at Ambient Temperature and Pressure. *ChemSusChem* **2012**, *5* (11), 2237–2242. https://doi.org/10.1002/cssc.201200339.
(14) Hudson, M. R.; Queen, W. L.; Mason, J. A.; Fickel, D. W.; Lobo, R. F.; Brown, C. M. Unconventional, Highly Selective CO2 Adsorption in Zeolite SSZ-13. *J. Am. Chem. Soc.* **2012**, *134* (4), 1970–1973. https://doi.org/10.1021/ja210580b.
(15) Bhatta, L. K. G.; Subramanyam, S.; Chengala, M. D.; Bhatta, U. M.; Venkatesh, K. Enhancement in CO2 Adsorption on Hydrotalcite-Based Material by Novel Carbon Support Combined with K2CO3 Impregnation. *Ind. Eng. Chem. Res.* **2015**, *54* (43), 10876–10884. https://doi.org/10.1021/acs.iecr.5b02020.
(16) Elkhalifah, A. E. I.; Maitra, S.; Bustam, M. A.; Murugesan, T. Effects of Exchanged Ammonium Cations on Structure Characteristics and CO2 Adsorption Capacities of Bentonite Clay. *Appl. Clay Sci.* **2013**, *83–84*, 391–398. https://doi.org/10.1016/j.clay.2013.07.016.
(17) Shen, W.; Fan, W. Nitrogen-Containing Porous Carbons: Synthesis and Application. *J.*

Mater. Chem. A **2013**, *1* (4), 999–1013. https://doi.org/10.1039/c2ta00028h.
(18) Li, P. Z.; Zhao, Y. Nitrogen-Rich Porous Adsorbents for CO2 Capture and Storage. *Chem. - An Asian J.* **2013**, *8* (8), 1680–1691. https://doi.org/10.1002/asia.201300121.
(19) Sethia, G.; Sayari, A. Nitrogen-Doped Carbons: Remarkably Stable Materials for CO2 Capture. *Energy and Fuels* **2014**, *28* (4), 2727–2731. https://doi.org/10.1021/ef500283e.
(20) Creamer, A. E.; Gao, B. Carbon-Based Adsorbents for Postcombustion CO2 Capture: A Critical Review. *Environ. Sci. Technol.* **2016**, *50* (14), 7276–7289. https://doi.org/10.1021/acs.est.6b00627.
(21) Belmabkhout, Y.; Sayari, A. Adsorption of CO2 from Dry Gases on MCM-41 Silica at Ambient Temperature and High Pressure. 2: Adsorption of CO2/N2, CO2/CH4 and CO2/H2 Binary Mixtures. *Chem. Eng. Sci.* **2009**, *64* (17), 3729–3735. https://doi.org/10.1016/j.ces.2009.05.039.
(22) Belmabkhout, Y.; Serna-Guerrero, R.; Sayari, A. Adsorption of CO2 from Dry Gases on MCM-41 Silica at Ambient Temperature and High Pressure. 1: Pure CO2 Adsorption. *Chem. Eng. Sci.* **2009**, *64* (17), 3721–3728. https://doi.org/10.1016/j.ces.2009.03.017.
(23) Radfarnia, H. R.; Sayari, A. A Highly Efficient CaO-Based CO2 Sorbent Prepared by a Citrate-Assisted Sol-Gel Technique. *Chem. Eng. J.* **2015**, *262*, 913–920. https://doi.org/10.1016/j.cej.2014.09.074.
(24) Kierzkowska, A. M.; Pacciani, R.; Müller, C. R. CaO-Based CO2 Sorbents: From Fundamentals to the Development of New, Highly Effective Materials. *ChemSusChem* **2013**, *6* (7), 1130–1148. https://doi.org/10.1002/cssc.201300178.
(25) Sayari, A.; Belmabkhout, Y.; Serna-Guerrero, R. Flue Gas Treatment via CO2 Adsorption. *Chem. Eng. J.* **2011**, *171* (3), 760–774. https://doi.org/10.1016/j.cej.2011.02.007.
(26) Choi, S.; Drese, J. H.; Jones, C. W. Adsorbent Materials for Carbon Dioxide Capture from Large Anthropogenic Point Sources. *ChemSusChem* **2009**, *2* (9), 796–854. https://doi.org/10.1002/cssc.200900036.
(27) Zhao, X.; Cui, Q.; Wang, B.; Yan, X.; Singh, S.; Zhang, F.; Gao, X.; Li, Y. Recent Progress of Amine Modified Sorbents for Capturing CO 2 from Flue Gas. *Chinese J. Chem. Eng.* **2018**, *26* (11), 2292–2302. https://doi.org/10.1016/j.cjche.2018.04.009.
(28) Zevenhoven, R.; Kilpinen, P. *Control of Pollutants in Flue Gases and Fuel Gases. Chapter 2: Flue Gases and Fuel Gases*; Espoo : Helsinki University of Technology: Helsinki, 2001.
(29) Biogas Composition https://www.biogas-renewable-energy.info/biogas_composition.html.
(30) Wang, J.; Wang, S.; Xin, Q.; Li, Y. Perspectives on Water-Facilitated CO2 Capture Materials. *J. Mater. Chem. A* **2017**, *5* (15), 6794–6816. https://doi.org/10.1039/c7ta01297g.
(31) González-Zamora, E.; Ibarra, I. A. CO2 Capture Under Humid Conditions in Metal–Organic Frameworks. *Mater. Chem. Front.* **2017**, *1* (8), 1471–1484. https://doi.org/10.1039/C6QM00301J.
(32) Peralta, R. A.; Alcántar-Vázquez, B.; Sánchez-Serratos, M.; González-Zamora, E.; Ibarra, I. A. Carbon Dioxide Capture in the Presence of Water Vapour in InOF-1. *Inorg. Chem. Front.* **2015**, *2* (10), 898–903. https://doi.org/10.1039/c5qi00077g.
(33) Monazam, E. R.; Breault, R. W.; Fauth, D. J.; Shadle, L. J.; Bayham, S. Insights into the Adsorption of Carbon Dioxide in the Presence of Water Vapor Utilizing a Low Molecular

Weight Polyethylenimine-Impregnated CARiACT Silica Sorbent. *Ind. Eng. Chem. Res.* **2017**, *56* (32), 9054–9064. https://doi.org/10.1021/acs.iecr.7b01271.
(34) Serna-Guerrero, R.; Da'na, E.; Sayari, A. New Insights into the Interactions of CO2 with Amine-Functionalized Silica. *Ind. Eng. Chem. Res.* **2008**, *47* (23), 9406–9412. https://doi.org/10.1021/ie801186g.
(35) Belmabkhout, Y.; Serna-Guerrero, R.; Sayari, A. Adsorption of CO2-Containing Gas Mixtures over Amine-Bearing Pore-Expanded MCM-41 Silica: Application for Gas Purification. *Ind. Eng. Chem. Res.* **2010**, *49*, 359–365. https://doi.org/10.1021/ie900837t.
(36) Sehaqui, H.; Gálvez, M. E.; Becatinni, V.; Cheng Ng, Y.; Steinfeld, A.; Zimmermann, T.; Tingaut, P. Fast and Reversible Direct CO2 Capture From Air onto All-Polymer Nanofibrillated Cellulose-Polyethylenimine Foams. *Environ. Sci. Technol.* **2015**, *49* (5), 3167–3174. https://doi.org/10.1021/es504396v.
(37) Xu, D.; Zhang, J.; Li, G.; Xiao, P.; Webley, P.; Zhai, Y. Effect of Water Vapor from Power Station Flue Gas on CO2 Capture by Vacuum Swing Adsorption with Activated Carbon. *J. Fuel Chem. Technol.* **2011**, *39* (3), 169–174. https://doi.org/10.1016/S1872-5813(11)60016-9.
(38) Müller, E. A.; Rull, L. F.; Vega, L. F.; Gubbins, K. E. Adsorption of Water on Activated Carbons: A Molecular Simulation Study. *J. Phys. Chem.* **1996**, *100* (4), 1189–1196. https://doi.org/10.1021/jp952233w.
(39) Durán, I.; Rubiera, F.; Pevida, C. Separation of CO2 in a Solid Waste Management Incineration Facility Using Activated Carbon Derived from Pine Sawdust. *Energies* **2017**, *10* (6), 827. https://doi.org/10.3390/en10060827.
(40) Younas, M.; Leong, L. K.; Mohamed, A. R.; Sethupathi, S. CO2 Adsorption by Modified Palm Shell Activated Carbon (PSAC) Via Chemical and Physical Activation and Metal Impregnation. *Chem. Eng. Commun.* **2016**, *203* (11), 1455–1463. https://doi.org/10.1080/00986445.2016.1201660.
(41) Chiang, Y. C.; Chen, Y. J.; Wu, C. Y. Effect of Relative Humidity on Adsorption Breakthrough of CO2 on Activated Carbon Fibers. *Materials (Basel).* **2017**, *10* (11), 1296. https://doi.org/10.3390/ma10111296.
(42) Plaza, M. G.; Durán, I.; Querejeta, N.; Rubiera, F.; Pevida, C. Experimental and Simulation Study of Adsorption in Postcombustion Conditions Using a Microporous Biochar. 2. H2O, CO2, and N2 Adsorption. *Ind. Eng. Chem. Res.* **2016**, *55* (24), 6854–6865. https://doi.org/10.1021/acs.iecr.6b01720.
(43) Zhou, W.; Wang, H.; Zhang, Z.; Chen, H.; Liu, X. Molecular Simulation of CO2/CH4/H2O Competitive Adsorption and Diffusion in Brown Coal. *RSC Adv.* **2019**, *9* (6), 3004–3011. https://doi.org/10.1039/c8ra10243k.
(44) You, Y. Y.; Liu, X. J. Modeling of CO 2 Adsorption and Recovery from Wet Flue Gas by Using Activated Carbon. *Chem. Eng. J.* **2019**, *369* (January), 672–685. https://doi.org/10.1016/j.cej.2019.03.118.
(45) Liu, L.; Nicholson, D.; Bhatia, S. K. Exceptionally High Pperformance of Charged Carbon Nanotube Arrays for CO2 Separation from Flue Gas. *Carbon N. Y.* **2017**, *125*, 245–257. https://doi.org/10.1016/j.carbon.2017.09.050.
(46) Psarras, P.; He, J.; Wilcox, J. Effect of Water on the CO2 Adsorption Capacity of Amine-Functionalized Carbon Sorbents. *Ind. Eng. Chem. Res.* **2017**, *56* (21), 6317–6325.

https://doi.org/10.1021/acs.iecr.6b05064.
(47) Sun, Y.; Wang, Y.; Zhang, Y.; Zhou, Y.; Zhou, L. CO2 Sorption in Activated Carbon in the Presence of Water. *Chem. Phys. Lett.* **2007**, *437* (1–3), 14–16. https://doi.org/10.1016/j.cplett.2007.02.008.
(48) Wang, Y.; Zhou, Y.; Liu, C.; Zhou, L. Comparative Studies of CO2 and CH4 Sorption on Activated Carbon in Presence of Water. *Colloids Surfaces A Physicochem. Eng. Asp.* **2008**, *322* (1–3), 14–18. https://doi.org/10.1016/j.colsurfa.2008.02.014.
(49) Jalilov, A. S.; Li, Y.; Kittrell, C.; Tour, J. M. Increased CO2 Selectivity of Asphalt-Derived Porous Carbon through Introduction of Water into Pore Space. *Nat. Energy* **2017**, *2* (12), 932–938. https://doi.org/10.1038/s41560-017-0030-y.
(50) Cavenati, S.; Grande, C. A.; Rodrigues, A. E. Adsorption Equilibrium of Methane, Carbon Dioxide, and Nitrogen on Zeolite 13X at High Pressures. *J. Chem. Eng. Data* **2004**, *49* (4), 1095–1101. https://doi.org/10.1021/je0498917.
(51) Triebe, R. W.; Tezel, F. H. Adsorption of Nitrogen, Carbon Dioxide and Nitric Oxide on Molecular Sieves. *Gas Sep. Purif.* **1995**, *9* (4), 223–230.
(52) Maurin, G.; Llewellyn, P. L.; Bell, R. G. Adsorption Mechanism of Carbon Dioxide in Faujasites: Grand Canonical Monte Carlo Simulations and Microcalorimetry Measurements. *J. Phys. Chem. B* **2005**, *109* (33), 16084–16091. https://doi.org/10.1021/jp052716s.
(53) Kim, J. H.; Lee, C. H.; Kim, W. S.; Lee, J. S.; Kim, J. T.; Suh, J. K.; Lee, J. M. Adsorption Equilibria of Water Vapor on Alumina, Zeolite 13X, and a Zeolite X/Activated Carbon Composite. *J. Chem. Eng. Data* **2003**, *48* (1), 137–141. https://doi.org/10.1021/je0201267.
(54) Sabouni, R.; Kazemian, H.; Rohani, S. Carbon Dioxide Capturing Technologies: A Review Focusing on Metal Organic Framework Materials (MOFs). *Environ. Sci. Pollut. Res.* **2014**, *21* (8), 5427–5449. https://doi.org/10.1007/s11356-013-2406-2.
(55) Sumida, K.; Rogow, D. L.; Mason, J. A.; McDonald, T. M.; Bloch, E. D.; Herm, Z. R.; Bae, T.-H.; Long, J. R. Carbon Dioxide Capture in Metal–Organic Frameworks. *Chem. Rev.* **2012**, *112* (2), 724–781. https://doi.org/10.1021/cr2003272.
(56) Xiang, S.; He, Y.; Zhang, Z.; Wu, H.; Zhou, W.; Krishna, R.; Chen, B. Microporous Metal-Organic Framework with Potential for Carbon Dioxide Capture at Ambient Conditions. *Nat. Commun.* **2012**, *3*, 954–959. https://doi.org/10.1038/ncomms1956.
(57) Canivet, J.; Fateeva, A.; Guo, Y.; Coasne, B.; Farrusseng, D. Water Adsorption in MOFs: Fundamentals and Applications. *Chem. Soc. Rev.* **2014**, *43* (16), 5594–5617. https://doi.org/10.1039/c4cs00078a.
(58) Li, P.; Chen, J.; Zhang, J.; Wang, X. Water Stability and Competition Effects toward CO2 Adsorption on Metal Organic Frameworks. *Sep. Purif. Rev.* **2015**, *44* (1), 19–27. https://doi.org/10.1080/15422119.2014.884507.
(59) Cavka, J. H.; Jakobsen, S.; Olsbye, U.; Guillou, N.; Lamberti, C.; Bordiga, S.; Lillerud, K. P. A New Zirconium Inorganic Building Brick Forming Metal Organic Frameworks with Exceptional Stability. *J. Am. Chem. Soc* **2008**, *6* (130), 13850–13851.
(60) Feng, D.; Gu, Z. Y.; Li, J. R.; Jiang, H. L.; Wei, Z.; Zhou, H. C. Zirconium-Metalloporphyrin PCN-222: Mesoporous Metal-Organic Frameworks with Ultrahigh Stability as Biomimetic Catalysts. *Angew. Chemie - Int. Ed.* **2012**, *51* (41), 10307–10310.

https://doi.org/10.1002/anie.201204475.
(61) Jiao, Y.; Morelock, C. R.; Burtch, N. C.; Mounfield, W. P.; Hungerford, J. T.; Walton, K. S. Tuning the Kinetic Water Stability and Adsorption Interactions of Mg-MOF-74 by Partial Substitution with Co or Ni. *Ind. Eng. Chem. Res.* **2015**, *54* (49), 12408–12414. https://doi.org/10.1021/acs.iecr.5b03843.
(62) Wu, T.; Shen, L.; Luebbers, M.; Hu, C.; Chen, Q.; Ni, Z.; Masel, R. I. Enhancing the Stability of Metal-Organic Frameworks in Humid Air by Incorporating Water Repellent Functional Groups. *Chem. Commun.* **2010**, *46* (33), 6120–6122. https://doi.org/10.1039/c0cc01170c.
(63) Choi, H. J.; Dincă, M.; Dailly, A.; Long, J. R. Hydrogen Storage in Water-Stable Metal-Organic Frameworks Incorporating 1,3- and 1,4-Benzenedipyrazolate. *Energy Environ. Sci.* **2010**, *3* (1), 117–123. https://doi.org/10.1039/b917512a.
(64) Nguyen, N. T. T.; Furukawa, H.; Gándara, F.; Nguyen, H. T.; Cordova, K. E.; Yaghi, O. M. Selective Capture of Carbon Dioxide under Humid Conditions by Hydrophobic Chabazite-Type Zeolitic Imidazolate Frameworks. *Angew. Chemie - Int. Ed.* **2014**, *53* (40), 10645–10648. https://doi.org/10.1002/anie.201403980.
(65) Jasuja, H.; Walton, K. S. Effect of Catenation and Basicity of Pillared Ligands on the Water Stability of MOFs. *Dalt. Trans.* **2013**, *42* (43), 15421–15426. https://doi.org/10.1039/c3dt51819a.
(66) Gupta, V.; Mandal, S. K. A Robust and Water-Stable Two-Fold Interpenetrated Metal-Organic Framework Containing Both Rigid Tetrapodal Carboxylate and Rigid Bifunctional Nitrogen Linkers Exhibiting Selective CO 2 Capture. *Dalt. Trans.* **2019**, *48* (2), 415–425. https://doi.org/10.1039/c8dt03844a.
(67) Tang, Y.; Kourtellaris, A.; Tasiopoulos, A. J.; Teat, S. J.; Dubbeldam, D.; Rothenberg, G.; Tanase, S. Selective CO2 Adsorption in Water-Stable Alkaline-Earth Based Metal-Organic Frameworks. *Inorg. Chem. Front.* **2018**, *5* (3), 541–549. https://doi.org/10.1039/c7qi00734e.
(68) Yu, J.; Ma, Y.; Balbuena, P. B. Evaluation of the Impact of H2O, O2 , and SO2 on Postcombustion CO2 Capture in Metal-Organic Frameworks. *Langmuir* **2012**, *28* (21), 8064–8071. https://doi.org/10.1021/la3009514.
(69) Yazaydın, A. Ö.; Benin, A. I.; Faheem, S. A.; Jakubczak, P.; Low, J. J.; Willis, R. R.; Snurr, R. Q. Enhanced CO2 Adsorption in Metal-Organic Frameworks via Occupation of Open-Metal Sites by Coordinated Water Molecules. *Chem. Mater.* **2009**, *21* (8), 1425–1430. https://doi.org/10.1021/cm900049x.
(70) Liu, J.; Benin, A. I.; Furtado, A. M. B.; Jakubczak, P.; Willis, R. R.; Levan, M. D. Stability Effects on CO2 Adsorption for the DOBDC Series of Metal-Organic Frameworks. *Langmuir* **2011**, *27* (18), 11451–11456. https://doi.org/10.1021/la201774x.
(71) Kizzie, A. C.; Wong-Foy, A. G.; Matzger, A. J. Effect of Humidity on the Performance of Microporous Coordination Polymers as Adsorbents for CO2 Capture. *Langmuir* **2011**, *27* (10), 6368–6373. https://doi.org/10.1021/la200547k.
(72) Bhatt, P. M.; Belmabkhout, Y.; Cadiau, A.; Adil, K.; Shekhah, O.; Shkurenko, A.; Barbour, L. J.; Eddaoudi, M. A Fine-Tuned Fluorinated MOF Addresses the Needs for Trace CO2 Removal and Air Capture Using Physisorption. *J. Am. Chem. Soc.* **2016**, *138* (29), 9301–9307. https://doi.org/10.1021/jacs.6b05345.
(73) Llewellyn, P. L.; Bourrelly, S.; Serre, C.; Filinchuk, Y.; Férey, G. How Hydration Drastically

Improves Adsorption Selectivity for CO2 over CH4 in the Flexible Chromium Terephthalate MIL-53. *Angew. Chemie - Int. Ed.* **2006**, *45* (46), 7751–7754. https://doi.org/10.1002/anie.200602278.

(74) Millange, F.; Guillou, N.; Walton, R. I.; Grenèche, J. M.; Margiolaki, I.; Férey, G. Effect of the Nature of the Metal on the Breathing Steps in MOFs with Dynamic Frameworks. *Chem. Commun.* **2008**, No. 39, 4732–4734. https://doi.org/10.1039/b809419e.

(75) McDonald, T. M.; Mason, J. A.; Kong, X.; Bloch, E. D.; Gygi, D.; Dani, A.; Crocellà, V.; Giordanino, F.; Odoh, S. O.; Drisdell, W. S.; et al. Cooperative Insertion of CO2 in Diamine-Appended Metal-Organic Frameworks. *Nature* **2015**, *519* (7543), 303–308. https://doi.org/10.1038/nature14327.

(76) Montoro, C.; García, E.; Calero, S.; Pérez-Fernández, M. A.; López, A. L.; Barea, E.; Navarro, J. A. R. Functionalisation of MOF Open Metal Sites with Pendant Amines for CO2 Capture. *J. Mater. Chem.* **2012**, *22* (20), 10155–10158. https://doi.org/10.1039/c2jm16770k.

(77) McDonald, T. M.; D'Alessandro, D. M.; Krishna, R.; Long, J. R. Enhanced Carbon Dioxide Capture upon Incorporation of N,N'-Dimethylethylenediamine in the Metal–Organic Framework CuBTTri. *Chem. Sci.* **2011**, *2* (10), 2022–2028. https://doi.org/10.1039/c1sc00354b.

(78) Kang, M.; Kim, J. E.; Kang, D. W.; Lee, H. Y.; Moon, D.; Hong, C. S. A Diamine-Grafted Metal-Organic Framework with Outstanding CO2 Capture Properties and a Facile Coating Approach for Imparting Exceptional Moisture Stability. *J. Mater. Chem. A* **2019**, *7* (14), 8177–8183. https://doi.org/10.1039/c8ta07965j.

(79) Peng, L.; Yang, S.; Sun, D. T.; Asgari, M.; Queen, W. L. MOF/Polymer Composite Synthesized Using a Double Solvent Method Offers Enhanced Water and CO2 Adsorption Properties. *Chem. Commun.* **2018**, *54* (75), 10602–10605. https://doi.org/10.1039/c8cc05428b.

(80) Zarate, A.; Peralta, R. A.; Bayliss, P. A.; Howie, R.; Sanchez-Serratos, M.; Carmona-Monroy, P.; Solis-Ibarra, D.; Gonzalez-Zamora, E.; Ibarra, I. A. CO2 Capture under Humid Conditions in NH2-MIL- 53(Al): The Influence of the Amine Functional Group. *RSC Adv.* **2016**, *6*, 9978–9983. https://doi.org/10.1039/C5RA26517G.

(81) Yu, J.; Balbuena, P. B. How Impurities Affect CO2 Capture in Metal-Organic Frameworks Modified with Different Functional Groups. *ACS Sustain. Chem. Eng.* **2015**, *3* (1), 117–124. https://doi.org/10.1021/sc500607y.

(82) Moghadam, P. Z.; Ivy, J. F.; Arvapally, R. K.; Dos Santos, A. M.; Pearson, J. C.; Zhang, L.; Tylianakis, E.; Ghosh, P.; Oswald, I. W. H.; Kaipa, U.; et al. Adsorption and Molecular Siting of CO2, Water, and Other Gases in the Superhydrophobic, Flexible Pores of FMOF-1 from Experiment and Smulation. *Chem. Sci.* **2017**, *8* (5), 3989–4000. https://doi.org/10.1039/c7sc00278e.

(83) Soubeyrand-Lenoir, E.; Vagner, C.; Yoon, J. W.; Bazin, P.; Ragon, F.; Hwang, Y. K.; Serre, C.; Chang, J. S.; Llewellyn, P. L. How Water Fosters a Remarkable 5-Fold Increase in Low-Pressure CO2 Uptake Within Mesoporous MIL-100(Fe). *J. Am. Chem. Soc.* **2012**, *134* (24), 10174–10181. https://doi.org/10.1021/ja302787x.

(84) Kumar, A.; Madden, D. G.; Lusi, M.; Chen, K. J.; Daniels, E. A.; Curtin, T.; Perry, J. J.; Zaworotko, M. J. Direct Air Capture of CO2 by Physisorbent Materials. *Angew. Chemie -*

Int. Ed. **2015**, *54* (48), 14372–14377. https://doi.org/10.1002/anie.201506952.
(85) Chanut, N.; Bourrelly, S.; Kuchta, B.; Serre, C.; Chang, J. S.; Wright, P. A.; Llewellyn, P. L. Screening the Effect of Water Vapour on Gas Adsorption Performance: Application to CO2 Capture from Flue Gas in Metal–Organic Frameworks. *ChemSusChem* **2017**, *10* (7), 1543–1553. https://doi.org/10.1002/cssc.201601816.
(86) Zhao, W.; Veneman, R.; Chen, D.; Li, Z.; Cai, N.; Brilmana, D. W. F. Post-Combustion CO2 Capture Demonstration Using Supported Amine Sorbents: Design and Evaluation of 200 KWth Pilot. In *Energy Procedia*; 2014; Vol. 63, pp 2374–2383. https://doi.org/10.1016/j.egypro.2014.11.259.
(87) Li, K.; Kress, J. D.; Mebane, D. S. The Mechanism of CO2 Adsorption under Dry and Humid Conditions in Mesoporous Silica-Supported Amine Sorbents. *J. Phys. Chem. C* **2016**, *120* (41), 23683–23691. https://doi.org/10.1021/acs.jpcc.6b08808.
(88) Xu, X.; Song, C.; Andresen, J. M.; Miller, B. G.; Scaroni, A. W. Novel Polyethylenimine-Modified Mesoporous Molecular Sieve of MCM-41 Type as High-Capacity Adsorbent for CO2 Capture. *Energy and Fuels* **2002**, *16* (6), 1463–1469. https://doi.org/10.1021/ef020058u.
(89) Liu, Y.; Ye, Q.; Shen, M.; Shi, J.; Chen, J.; Pan, H.; Shi, Y. Carbon Dioxide Capture by Functionalized Solid Amine Sorbents with Simulated Flue Gas Conditions. *Environ. Sci. Technol.* **2011**, *45* (13), 5710–5716. https://doi.org/10.1021/es200619j.
(90) Chen, C.; Yang, S. T.; Ahn, W. S.; Ryoo, R. Amine-Impregnated Silica Monolith with a Hierarchical Pore Structure: Enhancement of CO2 Capture Capacity. *Chem. Commun.* **2009**, No. 24, 3627–3629.
(91) Subagyono, D. J. N.; Marshall, M.; Knowles, G. P.; Chaffee, A. L. CO2 Adsorption by Amine Modified Siliceous Mesostructured Cellular Foam (MCF) in Humidified Gas. *Microporous Mesoporous Mater.* **2014**, *186*, 84–93. https://doi.org/10.1016/j.micromeso.2013.11.032.
(92) Wang, J.; Chen, H.; Zhou, H.; Liu, X.; Qiao, W.; Long, D.; Ling, L. Carbon Dioxide Capture Using Polyethylenimine-Loaded Mesoporous Carbons. *J. Environ. Sci. (China)* **2013**, *25* (1), 124–132. https://doi.org/10.1016/S1001-0742(12)60011-4.
(93) Gómez-Pozuelo, G.; Sanz-Pérez, E. S.; Arencibia, A.; Pizarro, P.; Sanz, R.; Serrano, D. P. CO2 Adsorption on Amine-Functionalized Clays. *Microporous Mesoporous Mater.* **2019**, *282* (December 2018), 38–47. https://doi.org/10.1016/j.micromeso.2019.03.012.
(94) Andreoli, E.; Cullum, L.; Barron, A. R. Carbon Dioxide Absorption by Polyethylenimine-Functionalized Nanocarbons: A Kinetic Study. *Ind. Eng. Chem. Res.* **2015**, *54* (3), 878–889. https://doi.org/10.1021/ie504277s.
(95) Kim, H. J.; Chaikittisilp, W.; Jang, K. S.; Didas, S. A.; Johnson, J. R.; Koros, W. J.; Nair, S.; Jones, C. W. Aziridine-Functionalized Mesoporous Silica Membranes on Polymeric Hollow Fibers: Synthesis and Single-Component CO2 and N2 Permeation Properties. *Ind. Eng. Chem. Res.* **2015**, *54* (16), 4407–4413. https://doi.org/10.1021/ie503781u.
(96) Alesi, W. R.; Gray, M.; Kitchin, J. R. CO2 Adsorption on Supported Molecular Amidine Systems on Activated Carbon. *ChemSusChem* **2010**, *3* (8), 948–956. https://doi.org/10.1002/cssc.201000056.
(97) Koutsianos, A.; Barron, A. R.; Andreoli, E. CO2 Capture Partner Molecules in Highly Loaded PEI Sorbents. *J. Phys. Chem. C* **2017**, *121* (39), 21772–21781.

https://doi.org/10.1021/acs.jpcc.7b07541.
(98) Liu, S. H.; Wu, C. H.; Lee, H. K.; Liu, S. Bin. Highly Stable Amine-Modified Mesoporous Silica Materials for Efficient CO2 Capture. *Top. Catal.* **2010**, *53* (3–4), 210–217. https://doi.org/10.1007/s11244-009-9413-z.
(99) Zerze, H.; Tipirneni, A.; McHugh, A. J. Reusable Poly(Allylamine)-Based Solid Materials for Carbon Dioxide Capture under Continuous Flow of Ambient Air. *Sep. Sci. Technol.* **2017**, *52* (16), 2513–2522. https://doi.org/10.1080/01496395.2017.1345943.
(100) Wang, J.; Huang, H.; Wang, M.; Yao, L.; Qiao, W.; Long, D.; Ling, L. Direct Capture of Low-Concentration CO2 on Mesoporous Carbon-Supported Solid Amine Adsorbents at Ambient Temperature. *Ind. Eng. Chem. Res.* **2015**, *54* (19), 5319–5327. https://doi.org/10.1021/acs.iecr.5b01060.
(101) Smal, I. M.; Yu, Q.; Veneman, R.; Fränzel-Luiten, B.; Brilman, D. W. F. TG-FTIR Measurement of CO2-H2O Co-Adsorption for CO2 Air Capture Sorbent Screening. *Energy Procedia* **2014**, *63*, 6834–6841. https://doi.org/10.1016/j.egypro.2014.11.717.
(102) Brilman, D. W. F.; Veneman, R. Capturing Atmospheric CO2 Using Supported Amine Sorbents. *Energy Procedia* **2013**, *37*, 6070–6078. https://doi.org/10.1016/j.egypro.2013.06.536.
(103) Goeppert, A.; Czaun, M.; May, R. B.; Prakash, G. K. S.; Olah, G. A.; Narayanan, S. R. Carbon Dioxide Capture from the Air Using a Polyamine Based Regenerable Solid Adsorbent. *J. Am. Chem. Soc.* **2011**, *133* (50), 20164–20167. https://doi.org/10.1021/ja2100005.
(104) Wang, J.; Wang, M.; Li, W.; Qiao, W.; Long, D.; Ling, L. Application of Polyethylenimine-Impregnated Solid Adsorbents for Direct Capture of Low-Concentration CO2. *Am. Inst. Chem. Eng.* **2014**, *60* (972–980). https://doi.org/10.1002/aic.
(105) Gebald, C.; Wurzbacher, J. A.; Borgschulte, A.; Zimmermann, T.; Steinfeld, A. Single-Component and Binary CO2 and H2O Adsorption of Amine-Functionalized Cellulose. *Environ. Sci. Technol.* **2014**, *48* (4), 2497–2504. https://doi.org/10.1021/es404430g.
(106) Huang, H. Y.; Yang, R. T.; Chinn, D.; Munson, C. L. Amine-Grafted MCM-48 and Silica Xerogel as Superior Sorbents for Acidic Gas Removal from Natural Gas. *Ind. Eng. Chem. Res.* **2003**, *42* (12), 2427–2433. https://doi.org/10.1021/ie020440u.
(107) Zheng, F.; Tran, D. N.; Busche, B. J.; Fryxell, G. E.; Addleman, R. S.; Zemanian, T. S.; Aardahl, C. L. Ethylenediamine-Modified SBA-15 as Regenerable CO2 Sorbent. *Ind. Eng. Chem. Res.* **2005**, *44* (9), 3099–3105. https://doi.org/10.1021/ie049488t.
(108) Norihito, H.; Katsunori, Y.; Tatsuaki, Y. Adsorption of Carbon Dioxide on Amine Modified SBA-15 in the Presence of Water Vapor. *Chem. Lett.* **2004**, *33* (510–511).
(109) Hiyoshi, N.; Yogo, K.; Yashima, T. Adsorption Characteristics of Carbon Dioxide on Organically Functionalized SBA-15. *Microporous Mesoporous Mater.* **2005**, *84* (1–3), 357–365. https://doi.org/10.1016/j.micromeso.2005.06.010.
(110) Knowles, G. P.; Graham, J. V.; Delaney, S. W.; Chaffee, A. L. Aminopropyl-Functionalized Mesoporous Silicas as CO2 Adsorbents. *Fuel Process. Technol.* **2005**, *86* (14–15), 1435–1448. https://doi.org/10.1016/j.fuproc.2005.01.014.
(111) Hicks, J. C.; Drese, J. H.; Fauth, D. J.; Gray, M. L.; Qi, G.; Jones, C. W. Designing Adsorbents for CO2 Capture from Flue Gas-Hyperbranched Aminosilicas Capable of Capturing CO2 Reversibly. *J. Am. Chem. Soc.* **2008**, *130* (10), 2902–2903.

https://doi.org/10.1021/ja077795v.
(112) Stuckert, N. R.; Yang, R. T. CO2 Capture from the Atmosphere and Simultaneous Concentration Using Zeolites and Amine-Grafted SBA-15. *Environ. Sci. Technol.* **2011**, *45* (23), 10257–10264. https://doi.org/10.1021/es202647a.
(113) Belmabkhout, Y.; Serna-Guerrero, R.; Sayari, A. Amine-Bearing Mesoporous Silica for CO2 Removal from Dry and Humid Air. *Chem. Eng. Sci.* **2010**, *65* (11), 3695–3698. https://doi.org/10.1016/j.ces.2010.02.044.
(114) Sayari, A.; Belmabkhout, Y. Stabilization of Amine-Containing CO2 Adsorbents: Dramatic Effect of Water Vapor. *J. Am. Chem. Soc.* **2010**, *132* (18), 6312–6314. https://doi.org/10.1021/ja1013773.
(115) Lee, J. J.; Chen, C. H.; Shimon, D.; Hayes, S. E.; Sievers, C.; Jones, C. W. Effect of Humidity on the CO2 Adsorption of Tertiary Amine Grafted SBA-15. *J. Phys. Chem. C* **2017**, *121* (42), 23480–23487. https://doi.org/10.1021/acs.jpcc.7b07930.
(116) Chen, C. H.; Shimon, D.; Lee, J. J.; Mentink-Vigier, F.; Hung, I.; Sievers, C.; Jones, C. W.; Hayes, S. E. The “Missing” Bicarbonate in CO 2 Chemisorption Reactions on Solid Amine Sorbents. *J. Am. Chem. Soc.* **2018**, *140* (28), 8648–8651. https://doi.org/10.1021/jacs.8b04520.
(117) Cho, M.; Park, J.; Yavuz, C. T.; Jung, Y. A Catalytic Role of Surface Silanol Groups in CO2 Capture on the Amine-Anchored Silica Support. *Phys. Chem. Chem. Phys.* **2018**, *20* (17), 12149–12156. https://doi.org/10.1039/c7cp07973g.
(118) Jadhav, P. D.; Chatti, R. V.; Biniwale, R. B.; Labhsetwar, N. K.; Devotta, S.; Rayalu, S. S. Monoethanol Amine Modified Zeolite 13X for CO2 Adsorption at Different Temperatures. *Energy and Fuels* **2007**, *21* (6), 3555–3559. https://doi.org/10.1021/ef070038y.
(119) Madden, D.; Curtin, T. Carbon Dioxide Capture with Amino-Functionalised Zeolite-β: A Temperature Programmed Desorption Study under Dry and Humid Conditions. *Microporous Mesoporous Mater.* **2016**, *228*, 310–317. https://doi.org/10.1016/j.micromeso.2016.03.041.
(120) Zhang, B.; Yan, J.; Li, G.; Wang, Z. Cost-Effective Preparation of Microporous Polymers from Formamide Derivatives and Adsorption of CO2 under Dry and Humid Conditions. *Polym. Chem.* **2019**, *10* (24), 3371–3379. https://doi.org/10.1039/c9py00465c.
(121) Song, J.; Liu, J.; Zhao, W.; Chen, Y.; Xiao, H.; Shi, X.; Liu, Y.; Chen, X. Quaternized Chitosan/PVA Aerogels for Reversible CO2 Capture from Ambient Air. *Ind. Eng. Chem. Res.* **2018**, *57* (14), 4941–4948. https://doi.org/10.1021/acs.iecr.8b00064.
(122) Wang, T.; Lackner, K. S.; Wright, A. Moisture Swing Sorbent for Carbon Dioxide Capture from Ambient Air. *Environ. Sci. Technol.* **2011**, *45* (15), 6670–6675. https://doi.org/10.1021/es201180v.
(123) Quang, D. V.; Dindi, A.; Rayer, A. V; Hadri, N. El; Abdulkadir, A.; Abu-Zahra; R.M., M. Effect of Moisture on the Heat Capacity and the Regeneration Heat Required for CO2 Capture Process Using PEI Impregnated Mesoporous Precipitated Silica. *Greenh. Gases Sci. Technol.* **2014**, *1*, 1–11. https://doi.org/10.1002/ghg.
(124) Yamada, H.; Fujiki, J.; Chowdhury, F. A.; Yogo, K. Effect of Isopropyl-Substituent Introduction into Tetraethylenepentamine-Based Solid Sorbents for CO2 Capture. *Fuel* **2018**, *214* (November 2017), 14–19. https://doi.org/10.1016/j.fuel.2017.10.108.
(125) Mulgundmath, V.; Tezel, F. H. Optimisation of Carbon Dioxide Recovery from Flue Gas in

a TPSA System. *Adsorption* **2010**, *16* (6), 587–598. https://doi.org/10.1007/s10450-010-9255-9.
(126) Veneman, R.; Frigka, N.; Zhao, W.; Li, Z.; Kersten, S.; Brilman, W. Adsorption of H2O and CO2 on Supported Amine Sorbents. *Int. J. Greenh. Gas Control* **2015**, *41*, 268–275. https://doi.org/10.1016/j.ijggc.2015.07.014.
(127) Min, K.; Choi, W.; Kim, C.; Choi, M. Rational Design of the Polymeric Amines in Solid Adsorbents for Postcombustion Carbon Dioxide Capture. *ACS Appl. Mater. Interfaces* **2018**, *10* (28), 23825–23833. https://doi.org/10.1021/acsami.8b05988.
(128) Yamada, H.; Chowdhury, F. A.; Fujiki, J.; Yogo, K. Enhancement Mechanism of the CO2 Adsorption-Desorption Efficiency of Silica-Supported Tetraethylenepentamine by Chemical Modification of Amino Groups. *ACS Sustain. Chem. Eng.* **2019**, *7* (10), 9574–9581. https://doi.org/10.1021/acssuschemeng.9b01064.
(129) Lackner, K. S. Capture of Carbon Dioxide from Ambient Air. *Eur. Phys. J. Spec. Top.* **2009**, *176* (1), 93–106. https://doi.org/10.1140/epjst/e2009-01150-3.
(130) He, H.; Tang, H.; Chen, X.; Hou, X.; Zhou, X.; Chen, H.; Wu, S.; Wang, S. Structure Design of Low-Temperature Regenerative Hyperbranched Polyamine Adsorbent for CO 2 Capture. *Langmuir* **2018**, *34* (47), 14169–14179. https://doi.org/10.1021/acs.langmuir.8b02493.
(131) Choi, W.; Min, K.; Kim, C.; Ko, Y. S.; Jeon, J. W.; Seo, H.; Park, Y. K.; Choi, M. Epoxide-Functionalization of Polyethyleneimine for Synthesis of Stable Carbon Dioxide Adsorbent in Temperature Swing Adsorption. *Nat. Commun.* **2016**, *7*, 1–8. https://doi.org/10.1038/ncomms12640.
(132) Lara, Y.; Romeo, L. M. Amine-Impregnated Alumina Solid Sorbents for CO2 Capture. Lessons Learned. *Energy Procedia* **2017**, *114* (November 2016), 2372–2379. https://doi.org/10.1016/j.egypro.2017.03.1383.
(133) Lee, K. B.; Beaver, M. G.; Caram, H. S.; Sircar, S. Reversible Chemisorbents for Carbon Dioxide and Their Potential Applications. *Ind. Eng. Chem. Res.* **2008**, *47* (21), 8048–8062. https://doi.org/10.1021/ie800795y.
(134) Liang, Y.; Harrison, D. P.; Gupta, R. P.; Green, D. A.; McMichael, W. J. Carbon Dioxide Capture Using Dry Sodium-Based Sorbents. *Energy and Fuels* **2004**, *18* (2), 569–575. https://doi.org/10.1021/ef030158f.
(135) Hayashi, H.; Taniuchi, J.; Furuyashiki, N.; Sugiyama, S.; Hirano, S.; Shigemoto, N.; Nonaka, T. Efficient Recovery of Carbon Dioxide from Flue Gases of Coal-Fired Power Plants by Cyclic Fixed-Bed Operations over K2CO3-on-Carbon. *Ind. Eng. Chem. Res.* **2002**, *37* (1), 185–191. https://doi.org/10.1021/ie9704455.
(136) Seo, Y.; Jo, S. H.; Ryu, C. K.; Yi, C. K. Effects of Water Vapor Pretreatment Time and Reaction Temperature on CO2 Capture Characteristics of a Sodium-Based Solid Sorbent in a Bubbling Fluidized-Bed Reactor. *Chemosphere* **2007**, *69* (5), 712–718. https://doi.org/10.1016/j.chemosphere.2007.05.036.
(137) Jayakumar, A.; Gomez, A.; Mahinpey, N. Post-Combustion CO2 Capture Using Solid K2CO3: Discovering the Carbonation Reaction Mechanism. *Appl. Energy* **2016**, *179*, 531–543. https://doi.org/10.1016/j.apenergy.2016.06.149.
(138) Fagerlund, J.; Highfield, J.; Zevenhoven, R. Kinetics Studies on Wet and Dry Gas-Solid Carbonation of MgO and Mg(OH)2 for CO2 Sequestration. *RSC Adv.* **2012**, *2* (27), 10380–

10393. https://doi.org/10.1039/c2ra21428h.
(139) Xie, Y.; Zhang, Z.; Jiang, T.; He, J.; Han, B.; Wu, T.; Ding, K. CO2 Cycloaddition Reactions Catalyzed by an Ionic Liquid Grafted onto a Highly Cross-Linked Polymer Matrix. *Angew. Chemie - Int. Ed.* **2007**, *46* (38), 7255–7258. https://doi.org/10.1002/anie.200701467.
(140) Azmi, N.; Yusup, S.; Sabil, K. M. Effect of Water onto Porous CaO for CO2 Adsorption: Experimental and Extended Isotherm Model. *J. Clean. Prod.* **2017**, *168*, 973–982. https://doi.org/10.1016/j.jclepro.2017.08.225.
(141) Ding, Y. D.; Song, G.; Liao, Q.; Zhu, X.; Chen, R. Bench Scale Study of CO2 Adsorption Performance of MgO in the Presence of Water Vapor. *Energy* **2016**, *112*, 101–110. https://doi.org/10.1016/j.energy.2016.06.064.
(142) Ding, Y.; Alpay, E. Equilibria and Kinetics of CO2 Adsorption on Hydrotalcite Adsorbent. *Chem. Eng. Sci.* **2000**, *55* (17), 3461–3474. https://doi.org/10.1016/S0009-2509(99)00596-5.
(143) Ram Reddy, M. K.; Xu, Z. P.; Lu, G. Q.; Da Costa, J. C. D. Layered Double Hydroxides for CO2 Capture: Structure Evolution and Regeneration. *Ind. Eng. Chem. Res.* **2006**, *45* (22), 7504–7509. https://doi.org/10.1021/ie060757k.
(144) Coenen, K.; Gallucci, F.; Pio, G.; Cobden, P.; van Dijk, E.; Hensen, E.; van Sint Annaland, M. On the Influence of Steam on the CO2 Chemisorption Capacity of a Hydrotalcite-Based Adsorbent for SEWGS Applications. *Chem. Eng. J.* **2017**, *314*, 554–569. https://doi.org/10.1016/j.cej.2016.12.013.
(145) Coenen, K.; Gallucci, F.; Hensen, E.; Van Sint Annaland, M. CO2 and H2O Chemisorption Mechanism on Different Potassium-Promoted Sorbents for SEWGS Processes. *J. CO2 Util.* **2018**, *25* (March), 180–193. https://doi.org/10.1016/j.jcou.2018.04.002.
(146) Gankanda, A.; Cwiertny, D. M.; Grassian, V. H. Role of Atmospheric CO2 and H2O Adsorption on ZnO and CuO Nanoparticle Aging: Formation of New Surface Phases and the Impact on Nanoparticle Dissolution. *J. Phys. Chem. C* **2016**, *120* (34), 19195–19203. https://doi.org/10.1021/acs.jpcc.6b05931.

PART TWO

CHAPTER 6 MESOPOROUS ORGANOSILICAS FOR CO_2 FIXATION TO CYCLIC CARBONATES: REACTION INSIGHT AND MATERIAL DEVELOPMENT

6.0. Introduction to CO_2 utilization

With advances in CO_2 capture and storage technologies,[1] the demand for CO_2 is projected to increase steadily over the years (Figure 6-1), thereby creating opportunities for CO_2 reuse and ultimately contributing to greenhouse gas mitigation. Currently, besides the commercial production of urea, other large-scale applications of CO_2 involve direct use of the gas (non-conversion pathways), e.g. enhanced oil recovery, food and beverage production (Figure 6-1).[2] New opportunities to use carbon dioxide (CO_2) as a raw material for the production of different products (conversion pathways) are capturing the attention of governments, industry and the investors interested in mitigating climate change and supporting a circular economy, with targeted products including; fuels, chemicals and building materials (Figure 6-2).

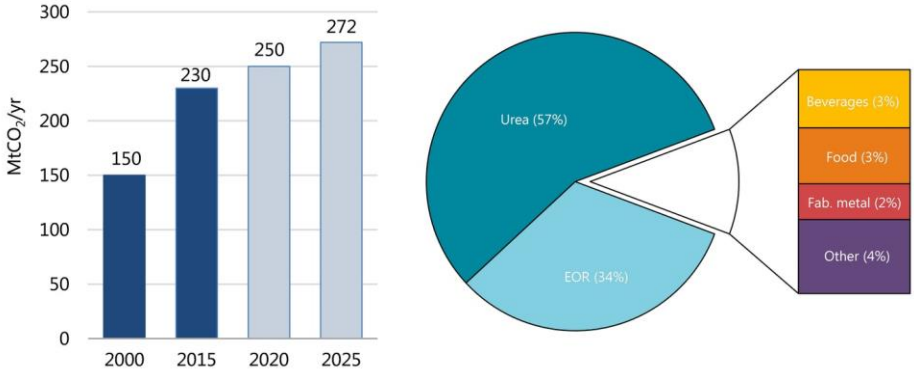

Figure 6-1. Growth in global demand of CO_2 over the years (left); breakdown of demand in 2015 (right).[3] Copyright (2019) International Energy Agency.

Governments and private investors in Canada (NRG COSIA Carbon XPrize)[4], Japan[5], United Kingdom[6], United States of America,[7] Germany[8] and other European countries,[9,10] and China[11,12] are providing significant research, development and demonstration (RD&D) support for CO_2 use. The market for CO_2 fixation is expected to remain relatively small in the short term, while in the long term, CO_2 conversion could play a key role in a net-zero CO_2 emission economy. For this to come into effect, applications for CO_2 reuse need to be scalable, use low-to-no carbon energy, replace fossil fuel-derived products, and generate products with longer life-cycle emissions (e.g. polymers). While fuel (e.g. methane, methanol, gasoline and aviation fuels) provide potentially high CO_2 use by volume, CO_2-derived construction materials[13] (e.g. fillers, cement and concrete) have the greatest potential to deliver climate benefits as they can retain CO_2 for many years. Moreover, employing energy from carbon-free renewable sources in CO_2-to-chemicals/fuel conversion processes, i.e. CO_2-neutral chemicals production, will reduce CO_2 emission significantly, while offering economic opportunities.[14,15]

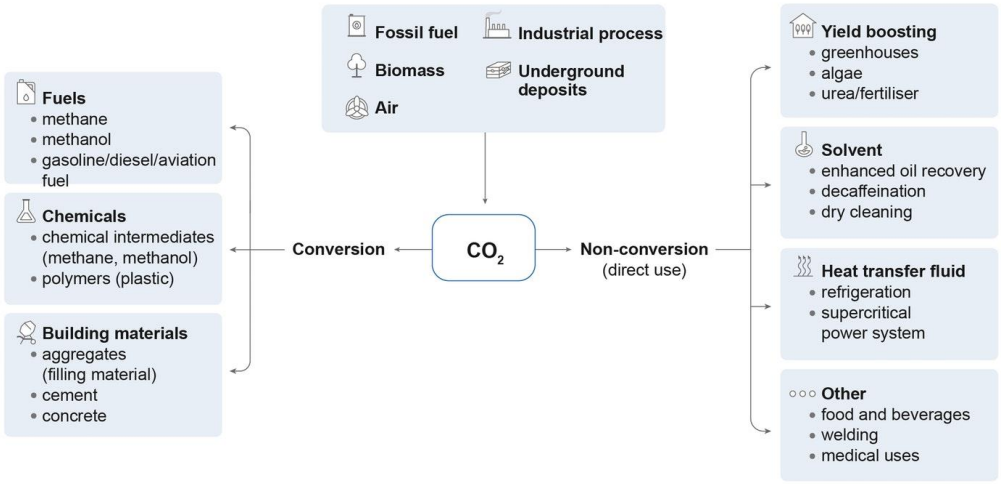

Figure 6-2. Pathways for CO_2 utilization.[16] Copyright (2020) International Energy Agency.

Due to relatively low energy requirement and high market value, polymer processing with CO_2 can compete with established processes. Reports claim that if CO_2 is cheaper than fossil fuel-derived monomer, CO_2-based polymers can be made at up to 30% lower costs than their fossil counterparts. Moreover, climate benefit of CO_2-derived polymers is echoed by the fact that some CO_2-derived polymer can contain up to 50% by mass CO_2.[6,17] Although relatively small compared to the production of CO_2-derived polymers, CO_2 fixation to fuels and fine chemicals through catalytic[18–21], photo-catalytic/photochemical,[22–24] electro-catalytic/electrochemical,[25–27] enzymatic/biochemical[28,29] and plasma[30,31] processes represent an important contribution towards the production of sustainable energy carriers and carbon derived products. Using captured CO_2 as a carbon source for the production of a chemicals and fuels is very attractive because CO_2 is readily available, non-toxic and offers several conversion pathways (Figure 6-3).

Nonetheless, because of its high thermodynamic stability, chemical fixation of CO_2 is very challenging.[32] Other technical challenges to CO_2 reuse has to do with the need for CO_2 reuse facilities to be near the sources of captured CO_2 (cost of transport), and for these technologies to be deployed on a commercial-scale quickly. [33] Moreover, the fact that economic and climate

benefits of many CO_2 reuse technologies are not fully quantified is a significant market challenge.[34,35] Accordingly, in-depth and systematic strategies are needed for the design of sustainable CO_2 utilization processes that guarantee profitability.[36] The ambiguity surrounding the potential economic benefits of CO_2 conversion is a major hurdle as to why established technologies based on fossil fuel-derived feed materials are reluctant to invest into CO_2 reuse. Furthermore, regulations on CO_2 emissions need to be stringent enough to accelerate the creation of a commodity market for CO_2. A simple approach could be to incorporate a label for all CO_2-derived products, with associated benefits compared to its traditional counterpart.

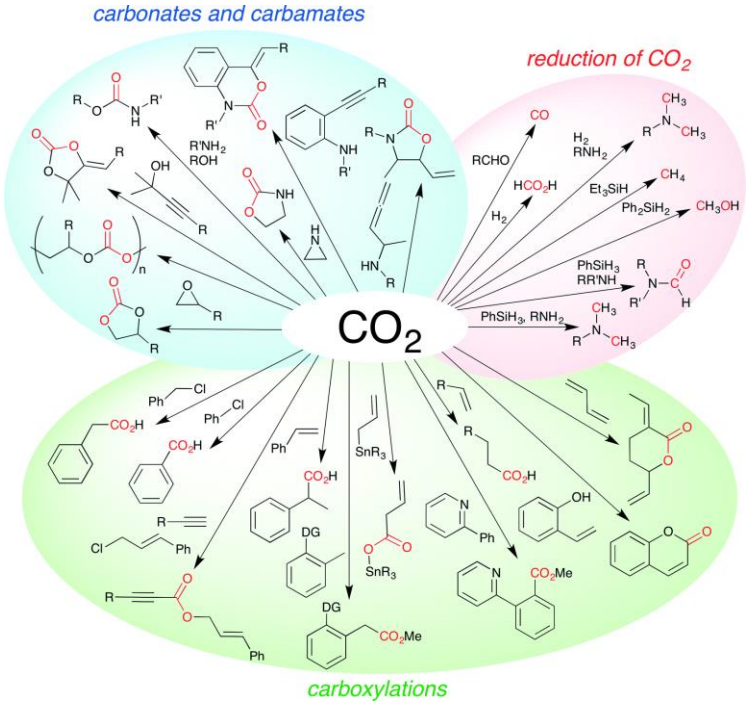

Figure 6-3. Examples of chemical fixation of CO_2.[37] Copyright (2014) Royal Society of Chemistry.

Despite these challenges, several breakthrough findings on CO_2 utilization have been patented.[38] Moreover, a good number of companies in their early stages of development across the globe have taken a lead in emulating nature in an attempt to close the carbon dioxide cycle

via conversion (Table 6-1); an extensive list of companies can be found in ref.[39] One extensively studied reaction is that between CO_2 and epoxides, which can be controlled to form either cyclic carbonates (CCs) or polycarbonates[40]. Industrial production of cyclic carbonates involves mainly the transesterification of diols with highly toxic phosgene in an energy-intensive process[41] CCs are used in the chemical industry as precursors for the synthesis of polycarbonates, resins, biomaterials, electrolytes, aprotic polar solvents, and as intermediates in fine chemical production such as dialkyl carbonates, glycols, carbamates and pyrimidines.[42] Polycarbonate production from CO_2 is currently being commercialized in the UK, Japan, Germany, USA and South Korea.[43]

Table 6-1. Selected companies worldwide converting CO_2 to fuels and chemicals

Target products	**Companies (location)**
fuels and plastics	ThyssenKrupp, Sunfire, Novomer and Covestro A.G.(**Germany**)
polyols	Econic Technologies[44] (**United Kingdom**)
bioplastic	Newlight Technologies[45] (**United States of America**)
Methanol	George Olah facility of Carbon Recycling International[46] (**Iceland**)
diesel or gasoline	Carbon Engineering[47] (**Canada**).
polycarbonates	Asahi Kasei Chemicals and Chi Mei Corp[48] (**Japan**)
Cyclic carbonates	Huntsman Corporation[49] (**United States of America**)

Using CO_2 as a C1-building block, a number of pathways have been reported for the production of CCs (Figure 6-4), with CO_2 addition to epoxide being the most studied.[43,50,51] Although the synthesis of CCs from epoxides and CO_2 has been a low scale commercial process since the 1950s,[52] current commercial CCs synthesis proceeds via phosgenation reactions due to its high efficiency and the lack of an economically sustainable alternative. If the cost of CO_2 and

energy demand of the reaction (CO_2 pressure and temperature) can be reduced, CCs synthesis using CO_2 can compete economically with the phosgenation route, such that other companies may follow the path of Huntsman Corporation[49] in the reuse of CO_2 in the synthesis of CCs. One approach to reducing this energy demand lies on employing catalysts that is highly active at mild reaction conditions. In this regard, different homogeneous catalysts (e.g. ionic liquids[53] and metal complexes[54]), immobilized catalysts including supported ionic liquids[53,55] , MOFs-derived,[56] and traditional heterogeneous catalysts[57] were reported to be active towards CO_2 cycloaddition. Of these catalysts, quaternary ammonium salts are amongst the most active.[50,52,58–64]

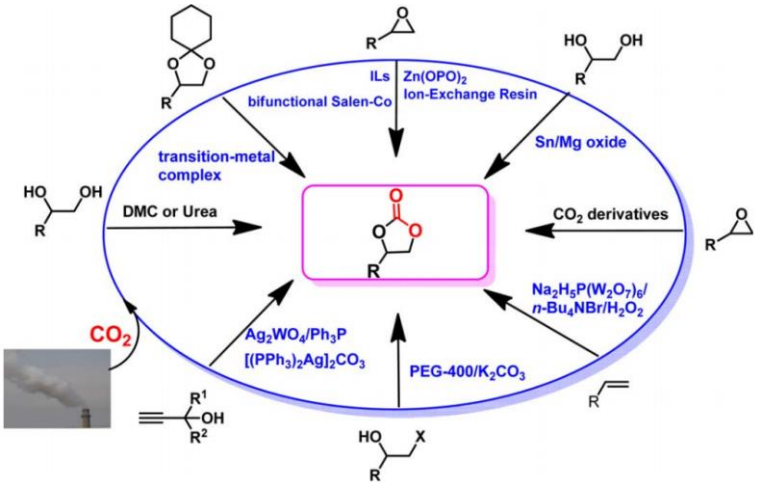

Figure 6-4. Chemical pathways for cyclic carbonate synthesis using CO_2.[62] Copyright (2016) John Wiley & Sons.

This section of the thesis is devoted to two studies in line with CC synthesis from CO_2 and epoxides using supported ammonium halides as catalyst. An analysis of different reports on the reusability of supported ammonium salts (ionic liquids) revealed high and steady yield over multiple cycles with propylene oxide and 1,2-epoxybutane as substrates. However, a decrease in yield was observed when similar catalysts were used with styrene oxide. In the first study (**Chapter 7**), a thoroughly investigated substrate dependence on the recyclability of this type of

catalyst is presented. In **chapter 8**, novel porous immobilized quaternary ammonium salts based on three classes of porous materials, i.e. disordered, ordered and periodic mesoporous organosilicas, are presented. The catalytic activity of these organosilicas was then compared, with the most active employed in reusability studies.

References

(1) Centre for Climate and Energy Solutions. Technology solutions: Carbon Capture https://www.c2es.org/content/carbon-capture/ (accessed Dec 23, 2019).

(2) IHS Markit. Chemical Economics Handbook – Carbon Dioxide https://ihsmarkit.com/products/carbon-dioxide-chemical-economics-handbook.html (accessed Dec 22, 2019).

(3) International Energy Agency. Putting CO2 to Use: Creating value from emissions https://www.iea.org/topics/carbon-capture-and-storage/policiesandinvestment/ (accessed Dec 21, 2019).

(4) COSIA. NRG COSIA Carbon XPRIZE https://carbon-xprize.cosia.ca/xprize-about (accessed Dec 22, 2019).

(5) Greenhouse Gas Inventory Office of Japan. National Greenhouse Gas Inventory Report of JAPAN https://www.env.go.jp/earth/ondanka/ghg-mrv/unfccc/material/NIR-JPN-2017_E.pdf (accessed Dec 23, 2019).

(6) Alberici, S.; Noothout, P.; Mir, G. U. R.; Stork, M.; Wiersma, F. *Assessing the Potential of CO2 Utilisation in the UK*; 2017.

(7) U.S. Department of Energy. No TitleU.S. Department of Energy Announces $110M for Carbon Capture, Utilization, and Storage https://www.energy.gov/articles/us-department-energy-announces-110m-carbon-capture-utilization-and-storage (accessed Dec 23, 2019).

(8) Mennicken, L.; Janz, A.; Roth, S. The German R&D Program for CO2 Utilization—Innovations for a Green Economy. *Environ. Sci. Pollut. Res.* **2016**, *23* (11), 11386–11392. https://doi.org/10.1007/s11356-016-6641-1.

(9) European Commission. Commission activities to enable CO2 transformation and utilisation https://setis.ec.europa.eu/publications/setis-magazine/carbon-capture-utilisation-and-storage/commission-activities-enable-co2 (accessed Dec 22, 2019).

(10) SETIS. Carbon Capture Utilisation and Storage https://setis.ec.europa.eu/system/files/setis-maga (accessed Dec 22, 2019).

(11) Fan, J. L.; Zhang, X.; Zhang, J.; Peng, S. Efficiency Evaluation of CO2 Utilization Technologies in China: A Super-Efficiency DEA Analysis Based on Expert Survey. *J. CO2 Util.* **2015**, *11* (2015), 54–62. https://doi.org/10.1016/j.jcou.2015.01.004.

(12) Lin, J.; Khanna, N.; Liu, X.; Teng, F.; Wang, X. China's Non-CO2 Greenhouse Gas Emissions: Future Trajectories and Mitigation Options and Potential. *Sci. Rep.* **2019**, *9* (1), 1–10. https://doi.org/10.1038/s41598-019-52653-0.

(13) Carbon Upcycling Technologies. Products https://www.carbonupcycling.com/products (accessed Dec 21, 2019).
(14) Chen, Q.; Lv, M.; Tang, Z.; Wang, H.; Wei, W.; Sun, Y. Opportunities of Integrated Systems with CO2 Utilization Technologies for Green Fuel & Chemicals Production in a Carbon-Constrained Society. *J. CO2 Util.* **2016**, *14*, 1–9. https://doi.org/10.1016/j.jcou.2016.01.004.
(15) Dutta, A.; Farooq, S.; Karimi, I. A.; Khan, S. A. Assessing the Potential of CO2 Utilization with an Integrated Framework for Producing Power and Chemicals. *J. CO2 Util.* **2017**, *19*, 49–57. https://doi.org/10.1016/j.jcou.2017.03.005.
(16) International Energy Agency. Putting CO2 to Use: Creating value from emissions. https://www.iea.org/reports/putting-co2-to-use (accessed April 20, 2020)
(17) Saudi Aramco. Converge® polyol technology https://www.saudiaramco.com/en/creating-value/products/converge# (accessed Dec 22, 2019).
(18) Aresta, M.; Dibenedetto, A.; Quaranta, E. State of the Art and Perspectives in Catalytic Processes for CO2 Conversion into Chemicals and Fuels : The Distinctive Contribution of Chemical Catalysis and Biotechnology. *J. Catal.* **2016**, *343*, 2–45. https://doi.org/10.1016/j.jcat.2016.04.003.
(19) Song, Q. W.; Zhou, Z. H.; He, L. N. Efficient, Selective and Sustainable Catalysis of Carbon Dioxide. *Green Chem.* **2017**, *19* (16), 3707–3728. https://doi.org/10.1039/c7gc00199a.
(20) Martens, J. A.; Bogaerts, A.; De Kimpe, N.; Jacobs, P. A.; Marin, G. B.; Rabaey, K.; Saeys, M.; Verhelst, S. The Chemical Route to a Carbon Dioxide Neutral World. *ChemSusChem* **2017**, *10* (6), 1039–1055. https://doi.org/10.1002/cssc.201601051.
(21) Dibenedetto, A.; Angelini, A.; Stufano, P. Use of Carbon Dioxide as Feedstock for Chemicals and Fuels: Homogeneous and Heterogeneous Catalysis. *J. Chem. Technol. Biotechnol.* **2014**, *89* (3), 334–353. https://doi.org/10.1002/jctb.4229.
(22) Tu, W.; Zhou, Y.; Zou, Z. Photocatalytic Conversion of CO2 into Renewable Hydrocarbon Fuels: State-of-the-Art Accomplishment, Challenges, and Prospects. *Adv. Mater.* **2014**, *26* (27), 4607–4626. https://doi.org/10.1002/adma.201400087.
(23) Das, S.; Bobbink, F. D.; Laurenczy, G.; Dyson, P. J. Metal-Free Catalyst for the Chemoselective Methylation of Amines Using Carbon Dioxide as a Carbon Source. *Angew. Chemie - Int. Ed.* **2014**, *53* (47), 12876–12879. https://doi.org/10.1002/anie.201407689.
(24) Ran, J.; Jaroniec, M.; Qiao, S. Z. Cocatalysts in Semiconductor-Based Photocatalytic CO2 Reduction: Achievements, Challenges, and Opportunities. *Adv. Mater.* **2018**, *30* (7), 1–31. https://doi.org/10.1002/adma.201704649.
(25) Zhang, W.; Hu, Y.; Ma, L.; Zhu, G.; Wang, Y.; Xue, X.; Chen, R.; Yang, S.; Jin, Z. Progress and Perspective of Electrocatalytic CO2 Reduction for Renewable Carbonaceous Fuels and Chemicals. *Adv. Sci.* **2018**, *5* (1). https://doi.org/10.1002/advs.201700275.
(26) Pander, J. E.; Ren, D.; Huang, Y.; Loo, N. W. X.; Hong, S. H. L.; Yeo, B. S. Understanding the Heterogeneous Electrocatalytic Reduction of Carbon Dioxide on Oxide-Derived Catalysts. *ChemElectroChem* **2018**, *5* (2), 219–237. https://doi.org/10.1002/celc.201701100.
(27) Khezri, B.; Fisher, A. C.; Pumera, M. CO2 Reduction: The Quest for Electrocatalytic Materials. *J. Mater. Chem. A* **2017**, *5* (18), 8230–8246. https://doi.org/10.1039/c6ta09875d.

(28) Shi, J.; Jiang, Y.; Jiang, Z.; Wang, X.; Wang, X.; Zhang, S.; Han, P.; Yang, C. Enzymatic Conversion of Carbon Dioxide. *Chem. Soc. Rev.* **2015**, *44* (17), 5981–6000. https://doi.org/10.1039/c5cs00182j.
(29) Simakov, D. S. A. Biological Conversion of CO2. In *Renewable Synthetic Fuels and Chemicals from Carbon Dioxide*; Springer: Cham, 2017.
(30) Ashford, B.; Tu, X. Non-Thermal Plasma Technology for the Conversion of CO2. *Curr. Opin. Green Sustain. Chem.* **2017**, *3*, 45–49. https://doi.org/10.1016/j.cogsc.2016.12.001.
(31) Yu, S.; Wilson, A. J.; Kumari, G.; Zhang, X.; Jain, P. K. Opportunities and Challenges of Solar-Energy-Driven Carbon Dioxide to Fuel Conversion with Plasmonic Catalysts. *ACS Energy Lett.* **2017**, *2* (9), 2058–2070. https://doi.org/10.1021/acsenergylett.7b00640.
(32) Müller, K.; Mokrushina, L.; Arlt, W. Thermodynamic Constraints for the Utilization of CO2. *Chemie-Ingenieur-Technik* **2014**, *86* (4), 497–503. https://doi.org/10.1002/cite.201300152.
(33) Pérez-Fortes, M.; Bocin-Dumitriu, A.; Tzimas, E. CO2 Utilization Pathways: Techno-Economic Assessment and Market Opportunities. In *Energy Procedia*; 2014; Vol. 63, pp 7968–7975. https://doi.org/10.1016/j.egypro.2014.11.834.
(34) Zimmermann, A. W.; Schomäcker, R. Assessing Early-Stage CO2 Utilization Technologies—Comparing Apples and Oranges? *Energy Technol.* **2017**, *5* (6), 850–860. https://doi.org/10.1002/ente.201600805.
(35) Zimmermann, A.; Kant, M. The Business Side of Innovative CO2 Utilisation http://enco2re.climate-kic.org/wp-content/uploads/2016/01/The-business-side-of-innovative-CO2-utilisation.pdf (accessed Dec 23, 2019).
(36) Roh, K.; Frauzem, R.; Nguyen, T. B. H.; Gani, R.; Lee, J. H. A Methodology for the Sustainable Design and Implementation Strategy of CO2 Utilization Processes. *Comput. Chem. Eng.* **2016**, *91*, 407–421. https://doi.org/10.1016/j.compchemeng.2016.01.019.
(37) Maeda, C.; Miyazaki, Y.; Ema, T. Recent Progress in Catalytic Conversions of Carbon Dioxide. *Catal. Sci. Technol.* **2014**, *4*, 1482–1497. https://doi.org/10.1039/c3cy00993a.
(38) Norhasyima, R. S.; Mahlia, T. M. I. Advances in CO2 Utilization Technology: A Patent Landscape Review. *J. CO2 Util.* **2018**, *26*, 323–335. https://doi.org/10.1016/j.jcou.2018.05.022.
(39) Renture Radar https://www.ventureradar.com/keyword/CO2 conversion# (accessed Dec 22, 2019).
(40) Ariga, T.; Takata, T.; Endo, T. Cationic Ring-Opening Polymerization of Cyclic Carbonates with Alkyl Halides To Yield Polycarbonate without the Ether Unit by Suppression of Elimination of Carbon Dioxide. *Macromolecules* **1997**, *30* (4), 737–744. https://doi.org/10.1021/ma9607325.
(41) Shaikh, A. A. G.; Sivaram, S. Organic Carbonates. *Chem. Rev.* **1996**, *96* (3), 951–976. https://doi.org/10.1021/cr950067i.
(42) Yadav, N.; Seidi, F.; Crespy, D.; D'Elia, V. Polymers Based on Cyclic Carbonates as Trait d'Union Between Polymer Chemistry and Sustainable CO 2 Utilization. *ChemSusChem* **2019**, *12* (4), 724–754. https://doi.org/10.1002/cssc.201802770.
(43) Kamphuis, A. J.; Picchioni, F.; Pescarmona, P. P. CO2-Fixation into Cyclic and Polymeric Carbonates: Principles and Applications. *Green Chemistry*. Royal Society of Chemistry 2019, pp 406–448. https://doi.org/10.1039/c8gc03086c.

(44) Econic technologies. Product Potentials https://econic-technologies.com/economic-potential/ (accessed Dec 21, 2019).
(45) Newlight Technologies Inc. Discover https://www.newlight.com/discover (accessed Dec 21, 2019).
(46) Carbon Recycling International. Technology and Services https://www.carbonrecycling.is/technology-and-services (accessed Dec 21, 2019).
(47) Carbon Engineering Ltd. Technology https://carbonengineering.com/our-technology/ (accessed Dec 21, 2019).
(48) Asahi Kasei Chemicals and Chi Mei Corp https://www.asahi-kasei.co.jp/advance/en/business/plastics/plastics_polycarbo.html (accessed Dec 22, 2019).
(49) Huntsman Corporation https://www.huntsman.com/performance_products/a/Products/Carbonates (accessed Dec 22, 2019).
(50) Martín, C.; Fiorani, G.; Kleij, A. W. Recent Advances in the Catalytic Preparation of Cyclic Organic Carbonates. *ACS Catal.* **2015**, *5* (2), 1353–1370. https://doi.org/10.1021/cs5018997.
(51) Büttner, H.; Longwitz, L.; Steinbauer, J.; Wulf, C.; Werner, T. Recent Developments in the Synthesis of Cyclic Carbonates from Epoxides and CO2. *Top. Curr. Chem.* **2017**, *375* (3), 50. https://doi.org/10.1007/s41061-017-0136-5.
(52) Peppel, W. J. Preparation and Properties of the Alkylene Carbonates. *Ind. Eng. Chem.* **1958**, *50* (5), 767–770. https://doi.org/10.1021/ie50581a030.
(53) Cokoja, M.; Wilhelm, M. E.; Anthofer, M. H.; Herrmann, W. A.; Kühn, F. E. Synthesis of Cyclic Carbonates from Epoxides and Carbon Dioxide by Using Organocatalysts. *ChemSusChem* **2015**, *8* (15), 2436–2454. https://doi.org/10.1002/cssc.201500161.
(54) Comerford, J. W.; Ingram, I. D. V.; North, M.; Wu, X. Sustainable Metal-Based Catalysts for the Synthesis of Cyclic Carbonates Containing Five-Membered Rings. *Green Chem.* **2015**, *17* (4), 1966–1987. https://doi.org/10.1039/C4GC01719F.
(55) Calabrese, C.; Giacalone, F.; Aprile, C. Hybrid Catalysts for CO 2 Conversion into Cyclic Carbonates. *Catalysts* **2019**, *9* (4), 1–30. https://doi.org/10.3390/catal9040325.
(56) Huh, S. Direct Catalytic Conversion of CO2 to Cyclic Organic Carbonates under Mild Reaction Conditions by Metal—Organic Frameworks. *Catalysts* **2019**, *9* (1). https://doi.org/10.3390/catal9010034.
(57) North, M. Synthesis of Cyclic Carbonates from Carbon Dioxide and Epoxides. In *New and Future Developments in Catalysis - Activation of Carbon Dioxide*; Elsevier B.V., 2013; pp 379–413. https://doi.org/10.1016/B978-0-444-53882-6.00014-0.
(58) Chaugule, A. A.; Tamboli, A. H.; Kim, H. Ionic Liquid as a Catalyst for Utilization of Carbon Dioxide to Production of Linear and Cyclic Carbonate. *Fuel* **2017**, *200*, 316–332. https://doi.org/10.1016/j.fuel.2017.03.077.
(59) Darensbourg, D. J.; Holtcamp, M. W. Catalysts for the Reactions of Epoxides and Carbon Dioxide. *Coord. Chem. Rev.* **1996**, *153*, 155–174. https://doi.org/10.1016/0010-8545(95)01232-X.
(60) Bobbink, F. D.; Dyson, P. J. Synthesis of Carbonates and Related Compounds Incorporating CO2 Using Ionic Liquid-Type Catalysts: State-of-the-Art and Beyond. *J.*

Catal. **2016**, *343*, 52–61. https://doi.org/10.1016/j.jcat.2016.02.033.
(61) Fiorani, G.; Guo, W.; Kleij, A. W. Sustainable Conversion of Carbon Dioxide: The Advent of Organocatalysis. *Green Chem.* **2015**, *17* (3), 1375–1389. https://doi.org/10.1039/c4gc01959h.
(62) Lang, X. D.; He, L. N. Green Catalytic Process for Cyclic Carbonate Synthesis from Carbon Dioxide under Mild Conditions. Chem. Rec. 2016, 1337–1352. https://doi.org/10.1002/tcr.201500293.
(63) Saptal, V. B.; Bhanage, B. M. Current Advances in Heterogeneous Catalysts for the Synthesis of Cyclic Carbonates from Carbon Dioxide. *Curr. Opin. Green Sustain. Chem.* **2017**, *3*, 1–10. https://doi.org/10.1016/j.cogsc.2016.10.006.
(64) Monfared, A.; Mohammadi, R.; Hosseinian, A.; Sarhandi, S.; Kheirollahi Nezhad, P. D. Cycloaddition of Atmospheric CO 2 to Epoxides under Solvent-Free Conditions: A Straightforward Route to Carbonates by Green Chemistry Metrics. *RSC Adv.* **2019**, *9* (7), 3884–3899. https://doi.org/10.1039/c8ra10233c.

CHAPTER 7 SUBSTRATE DEPENDENCE ON THE FIXATION OF CO2 TO CYCLIC CARBONATES OVER REUSABLE POROUS HYBRID SOLIDS

7.0. Overview

An analysis of reports on the reusability of immobilized ionic liquids for the synthesis of CC showed that for some substrates no decrease in yield over multiple cyles occurred, while with other substrates, a drop in yield was observed from one reaction cycle to the next. To gain insight into this discrepancy, *N,N,N*-tributyl-*N*-propylammonium iodide-functionalized mesoporous silicas (SBA-15 and a silica gel) were prepared, and their reusability in the solvent-free synthesis of cyclic carbonates (CCs) from epoxides and CO_2 investigated by analyzing reaction quantification, TGA, textural property and ^{13}C MAS NMR data. The reusability of the catalysts was found to be dependent on the nature of the support and the substrate. In the presence of 1,2-epoxybutane (1,2-EB) as substrate, the SBA-15-based catalyst (PHS-1) exhibited a constant catalytic activity for five reaction cycles (yield > 96.0%) under mild conditions (1.0 MPa CO_2, 100 ^oC and 4 h). Conversely, in the presence of styrene oxide, a gradual decrease in yield was observed. Based on textural properties and ^{13}C CP-MAS NMR measurements, such decline was attributed to the adsorption of reaction product (styrene carbonate - SC) onto the catalyst surface. Using a chromatographic silica gel as support and an improved catalyst recovery step gave rise to a highly efficient, robust and fully reusable catalyst (PHS-2) for the synthesis of CCs. Notably, PHS-2 led to a 33 - 50% decrease in reaction time, and maintained an excellent and

steady catalytic activity over 5 cycles in the synthesis of SC (yield > 96% and selectivity > 97%). The amount of trapped solid SC product on PHS-2 surface was also significantly reduced.

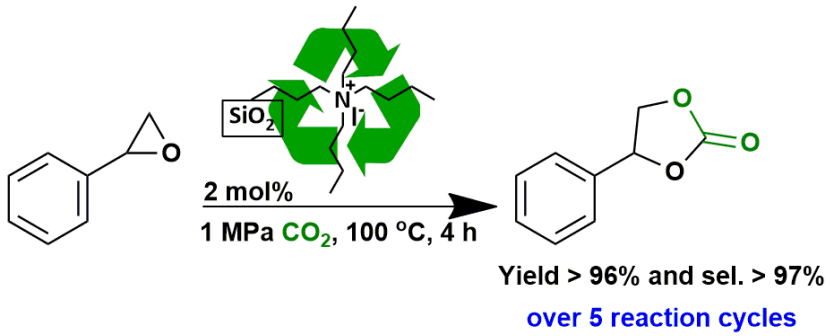

7.1. Introduction

There is strong evidence linking our long-standing energy dependence on fossil fuels (oil, coal and natural gas) and the associated greenhouse gas (GHG) emissions, particularly CO_2, due to their deleterious impact on the world climate.[1,2] In order to abate anthropogenic GHG emissions, arguably one of the most critical challenges of our time, a number of international treaties on climate change have been ratified, such as the 2015 Paris Agreement (COPS21) and others.[3] The main goal of these treaties is to curb GHG emissions, with a major focus on CO_2. Four broadly defined options are proposed to cut down CO_2 emissions; (i) reduction in energy consumption by improving the efficiency of existing processes and buildings, (ii) substitution of fossil fuels with renewable energy sources, (iii) CO_2 capture and sequestration (CCS), and (iv) utilization of CO_2, including its conversion to useful chemicals.[4]

CCS technologies have made great progress in recent years.[5–8] Nonetheless, carbon capture and utilization is gaining increased popularity.[9–14] Although relatively small, CO_2 utilization through chemical, biological or photo- and electro-chemical activations

represents a long term contributor to GHG mitigation. Using CO_2 as a carbon source for the production of useful chemicals is very attractive because CO_2 is readily available, cheap and non-toxic. Nonetheless, because of its high stability, only a handful of chemicals such as urea, methanol and carbonates are produced using CO_2, with only urea on a large commercial scale.[15] A more recent example is the successful commercialization of CO_2-derived polyols.[16] Often, high temperatures and pressures are required in CO_2 functionalization reactions.[17] Nevertheless, the development of efficient catalytic processes for the fixation of CO_2 into valuable organic chemicals under mild conditions has received considerable attention.[9–14] While catalysts can play a significant role in reducing the activation energy of such reactions, highly reactive co-reactants are amongst the best options to considerably reduce this energy barrier. One such CO_2 functionalization reactions is the cycloaddition of CO_2 and epoxides into cyclic carbonates (CCs) as shown in Scheme 7-1. CCs are valuable organic chemicals, with many applications such as aprotic polar solvents, active pharmaceutical ingredients (APIs), and starting materials in the production of fine chemicals and polymers.[17,18]

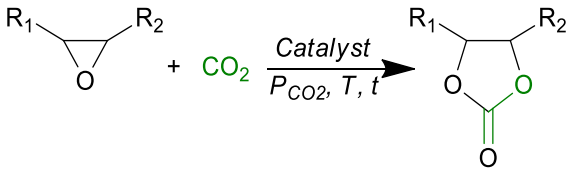

Scheme 7-1. Synthesis of cyclic carbonate from epoxide and CO_2

A variety of homogeneous (e.g. ionic liquids), immobilized (e.g. supported ionic liquids) and traditional heterogeneous (e.g. metal oxides) catalysts, have been reported

to be active towards this cycloaddition reaction. Progress in this area has been summarized in a number of reviews.[9,13–16] With the catalyst dissolved in the reaction medium and all active sites readily accessible, homogeneous catalysts offer improved selectivity, increased activity, and enhanced mass transfer, consistent with lower reaction temperature and pressure. Heterogeneous catalysts often suffer from mass and heat transfer limitations. Consequently, they are generally less active than homogeneous catalysts, and often require higher temperature and pressure, which may lead to reduced selectivity. However, they offer several advantages such as stability of active species, easy catalyst separation/recovery/reuse, and simplified reactor/process design.[19] Another option is to use hybrid solid catalysts, with the expectation to combine the unique properties of homogeneous catalysts and the technical advantages of heterogeneous catalysts.[20]

Metal-free supported or immobilized ammonium salts, i.e. ionic liquids, are a group of hybrid solid catalysts, with reported good to excellent performance towards CO_2-epoxide cycloaddition reactions.[21–23] This class of catalysts combines the high activity of quaternary ammonium salts with the easy-to-handle attributes of solid catalysts.[24] It is generally accepted that the mode of action of these hybrid catalysts involves a synergistic effect between an easy-leaving nucleophilic species such as a halide, and an electrophilic alkylammonium ion. The former activates the ring-opening of the epoxide, while the latter stabilizes the transition state, leading to an easier and faster insertion of CO_2 in the rate-limiting step of the reaction[25] Porous materials such as mesoporous silica used as supports[21,22,26] are expected to accommodate large numbers of active sites with enhanced

accessibility and productivity. Recently, Werner and co-workers[27] reported an immobilized phosphonium bromide with surprisingly fourfold higher activity compared to its homogeneous counterpart. They attributed this enhancement to the availability of multiple functional groups in close proximity in the immobilized catalyst. This finding not only highlights the advantages of immobilized organocatalysts, but also offers the opportunity to develop more active hybrid catalysts than their homogeneous counterparts.

For economic viability, it is important to achieve efficient methodologies for catalyst reuse without affecting its performance. Most reusability studies of immobilized catalysts used propylene oxide (PO)[23,28] and 1,2-epoxybutane (1,2-EB)[25] as substrates; which are easy to activate. It is not surprising that in almost all cases, high yields were obtained upon catalyst cycling. However, in the presence of styrene oxide (SO), a significant decrease in the yield was observed upon catalyst reuse.[29,30] This drop was attributed to steric hindrance and active site or pore blockage by the reaction product. However, no evidence was provided to support these claims. Hence, there is need to understand the substrate-deactivation relationship upon recycling, to be able to mitigate any shortcoming.

Tetrabutylammonium bromide in dimethyl carbonate[31] or supported on silica[32] was reported to be a reusable catalyst in the synthesis of CCs. However, the need for a solvent and the tedious recovery of the former catalyst, or the use of supercritical conditions (8 MPa CO_2, 150 ^oC) with the likelihood of leaching of ionic liquid in the latter catalyst, makes both systems unattractive. Interestingly, there is indication that

alkylammonium salts containing bulkier and more nucleophilic halide such as tetrabutylammonium iodide lead to moderate yields under solvent-free and mild conditions.[25,33] However, no heterogenized butylammonium iodide has been used for the synthesis of CCs. Inspired by the recent finding that a supported phosphonium salt was more active than its homogeneous counterpart[27], we immobilized a tributylpropylammonium iodide on two porous silicas, expecting that OH-groups of the supports will enhance the catalytic activity by activating epoxides via hydrogen bonding.

In this chapter, it is demonstrated that such hybrid materials are effective catalysts for the solvent-free synthesis of CCs under mild reaction conditions using terminal and internal epoxides. Moreover, immobilized tributylpropylammonium iodide was found to be more active than its homogeneous analog. To investigate the relationship between the reusability of immobilized catalysts and the nature of the substrate, a systematic study of the catalytic and textural properties of fresh and spent catalysts was carried out.

7.2. Experimental

N-butylaminopropyltrimethoxysilane (98%) was purchased from Gelest. Chromatography grade silica gel mesh 230-400 (hereafter referred to as SiL), triblock copolymer P123 (average M_n ~ 5,800), tetraethyl orthosilicate - TEOS (98%), tetrabutylammonium iodide (99%), 1-iodobutane (99%), styrene oxide (97%), 1,2-epoxybutane (99%), epichlorohydrin (99%), cyclohexene oxide (98%), diethyl ether (99.8%), and dichloromethane (98) were purchased from Sigma Aldrich. Ethyl acetate (99.9%) hydrochloric acid (37%) and anhydrous toluene (99.9 %) were obtained from Fisher. Chloroform-D was obtained from Cambridge Isotope Laboratories. All chemicals

were used as obtained with no further purification. Carbon dioxide (99.998%) was obtained from Linde AG.

7.2.1. Preparation of materials

7.2.1.1. SBA-15 synthesis

SBA-15 was synthesized based on an established procedure.[34] Typically, in a 200 mL Teflon-lined container, 4.0 g of triblock copolymer P123 was dissolved in a mixture of 30 g distilled water and 120 g of 2M HCl solution. Thereafter, 8.5 g of TEOS was added under vigorous stirring. To obtain rod-like particles, stirring was stopped after 5 min.[34] The resultant mixture was kept under static conditions at 40 ^{o}C for 20 h. Finally, it was transferred into an autoclave and heated at 100 ^{o}C under static condition for 24 h. The solid products were collected by filtration, washed with distilled water, dried at ambient temperature and calcined in flowing N_2 at 550 ^{o}C by raising the temperature at 1 ^{o}C/min. The gas was then switched to air at 550 ^{o}C and kept for 5 h.

7.2.1.2. Grafting of aminosilane

The silica supports were dried at 120 ^{o}C for 4 h to remove the residual moisture. An amount of silica (1 and 2 g for SBA-15 and SiL, respectively) was dispersed in 40 mL of toluene at room temperature for 60 min, followed by addition of 3 mL of *N*-butylaminopropyltrimethoxysilane. The resultant mixture was refluxed at 85 ^{o}C for 20 h in an oil bath. The grafted materials were then filtered, washed with toluene, ethyl acetate and finally pentane. The powder was dried under vacuum at 60 ^{o}C for 2 h. The obtained

solids are hereafter referred to as SBA-15@amine and SiL@amine, depending on their respective supports.

7.2.1.3 Quaternization of amine grafted silica

An amount of amine functionalized support (1 and 2 g for SBA-15@amine and SiL@amine respectively) was stirred in 20 mL of toluene at room temperature for 60 min, followed by addition of 3 mL of 1-iodobutane. The mixture was then heated at 70 ^{o}C in an oil bath and refluxed for 40 h. The obtained solids were filtered off, washed with ethyl acetate and dried under vacuum (90 ^{o}C for 3 h) to yield yellow powder materials of immobilized tributylpropylammonium iodide (tBPAI). These obtained porous hybrid materials, labelled PHS-1 (SBA-15@tBPAI) and PHS-2 (SiL@tBPAI), were kept in a desiccator containing $CaCl_2$. Because of its hygroscopic nature, tetrabutylammonium iodide was also dried under vacuum at 90 ^{o}C for 3 h and stored in the same desiccator. The preparation of the PHSs is illustrated in Scheme 7-2.

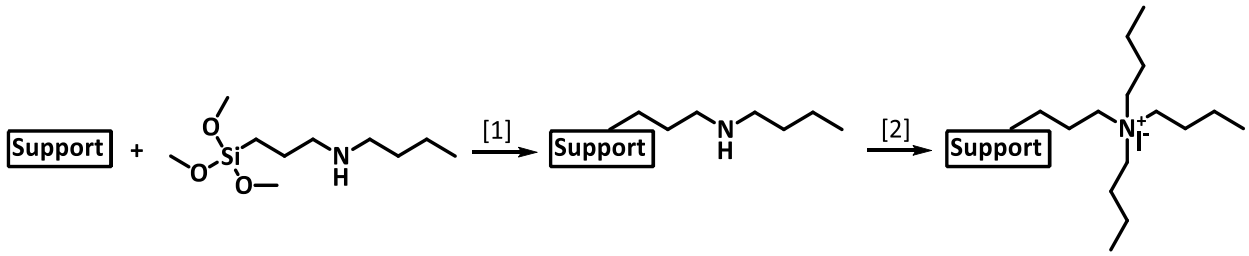

[1] 1 g (or 2 g) SBA-15 (or silica gel), 3 mL SIB1932.2, 40 mL toluene, 85 ^{o}C under reflux, 20 h
[2] 1 g (or 2 g) SBA-15@amine (SiL@amine), 20 mL toluene, 3 mL 1-iodobutane, 70 ^{o}C, reflux, 40 h

Scheme 7-2. Preparation of porous hybrid solid (PHS) catalysts

7.2.2. Characterization of materials

7.2.2.1 Textural properties and organic content

The specific surface area, pore volume and mean pore diameter of the supports, amine-grafted materials and PHSs were determined by nitrogen adsorption measurements at −196 °C on a Micromeritics 2020 instrument, using a previously reported method.[35,36] Samples were degassed for 4 h at 100 °C prior to analysis. Specific surface areas were calculated using the BET method at relative pressures of 0.06 to 0.2. The total pore volume (Vp) was recorded at p/p0 = 0.99 to exclude possible interparticle pores. The average pore size (Dp) was determined using the density functional theory.

The organic or nitrogen content (N-content) of amine-grafted and PHS materials were determined using thermogravimetric analysis (TGA) on a TA Q500 instrument. The sample was heated to 800 °C (at 10 °C min^{-1}) under flowing nitrogen, then air at 800 °C for 10 min. The organic content was calculated based on the weight loss beyond 200 °C [36].

7.2.2.2. FT-IR spectroscopy

In situ FT-IR measurements were carried out on a Nicolet 6700 spectrometer equipped with a mercury cadmium telluride (MCT) detector, using ambient air as background. Self-supported translucent wafers of about 5 mg and 1 cm diameter were placed inside a stainless-steel IR cell equipped with CaF_2 windows. All samples were thermally pre-treated in N_2 at 120 °C for 90 min to remove any adsorbed species. Then, the cell was allowed to cool down to room temperature, and a spectrum was recorded

through 128 scans under nitrogen. All FT-IR experiments were run in triplicate to ensure the reproducibility of the results, and average wavenumbers are reported herein.

7.2.2.3 Solid state and solution NMR analysis

Solid-state NMR (^{13}C and ^{15}N) spectra were recorded with a Bruker AVANCE III 200 NMR spectrometer with the following settings:

13C CPMAS and 13C CPMAS with dipolar dephasing: Chemical shifts with respect to the carbonyl carbon of glycine at 176.5 ppm (TMS at 0 ppm), MAS rotor size = 7 mm, magic angle spinning speed = 4500 Hz, cross polarization with high power decoupling, proton 90 degree pulse = 3.75 microseconds, contact time = 2 milliseconds, acquisition time = 25.4 milliseconds, recycle time = 2 seconds, 1024 points collected, spectral width = 20161.291 Hz, data zero filled to 4K points, 40 Hz of exponential line broadening applied, number of scans collected: 3000 – 17000 and dipolar dephasing time used (when applied) = 40 microseconds.

15N CPMAS: Chemical shift with respect to NH_4Cl at -341.2 ppm (neat nitromethane at 0 ppm), MAS rotor size = 7 mm (stretch rotor), magic angle spinning speed = 3000 Hz. cross polarization with high power decoupling, proton 90-degree pulse = 3.30 microseconds, contact time = 5 milliseconds, acquisition time = 45.9 milliseconds, recycle time = 2 seconds. 1024 points collected, spectral width = 11160.714 Hz. Data zero filled to 8K points, 10 Hz of exponential line broadening applied and number of scans collected: 123888

For solution NMR analysis, ^{13}C and ^{1}H NMR spectra of liquid samples were obtained using a Bruker AV 400 spectrometer. Chemical shifts are reported in ppm relative to the deuterated solvent, chloroform-D.

Where separation was needed to isolate the cyclic carbonate prior to NMR analysis, silica gel (grain size 400 – 230 mesh from Sigma Aldrich) flash chromatography was used with a 3:1 ethylacetate:ether mixture as solvent.

7.2.3. Cycloaddition reaction and analysis of reaction mixture

A 100 mL high-pressure autoclave equipped with a magnetic stirrer was charged with 2 mL of a model epoxide (corresponding to 22.7 and 17 mmol of 1,2-EB and SO respectively) and 2 mol% of catalyst (PHS or NBu_4I) with respect to the epoxide. This volume of substrate was chosen to ensure proper mixing, which is critical in triphasic reactions. The reactor was pressurized with CO_2 to 1.0 MPa and heated to 100 ^{o}C under vigorous stirring. At the end of the reaction, the reactor was cooled with an ice bath to ≤ 15 ^{o}C and CO_2 was released slowly. When NBu_4I was used as catalyst, the reaction mixture was directly collected using diethyl ether, whereas in the presence of solid catalysts, the reaction mixture was suspended in diethyl ether and filtered to recover the catalyst. The solid catalyst was then washed with diethyl ether or acetone (5 x 20 mL) and dried in a vacuum oven at 90 ^{o}C for 2 h. N-content measurements were carried out on all spent solid catalysts by TGA, while only selected spent catalysts were subjected to N_2-adsorption and ^{13}C solid state NMR measurements.

After removal of all volatiles using a rotavap, a solvent-free reaction mixture was obtained. With SO as substrate, the reaction mixture was a liquid, a slurry or a solid

depending on the conversion of SO. For all other substrates, the reaction mixture was a liquid. 0.1 g of slurry or solid reaction product was dissolved in 0.4 mL of toluene and 50 µL of dodecane (internal standard) was added. To 100 µL of liquid reaction mixture, 50 µL of dodecane was added. 0.4 µL of this mixture were injected into a Varian CP-3800 GC equipped with a HP-1 capillary column (15 m length, 0.25 mm inner diameter and 0.25 µm film thicknesses) and a flame ionization detector (FID); with helium as carrier gas. The temperature program used for the analysis was as follows: initial oven temperature 80 ^{o}C (1.5 min); ramp at 30°C/min and held at 250 ^{o}C (3 min); injector port temperature: 250 ^{o}C; detector

7.3. Results and discussion

7.3.1. Catalyst characterization

As shown in Figure 7-1, the nitrogen adsorption–desorption isotherms for the functionalized materials as well as the silica supports were of Type IV with H1 hysteresis loop characteristic of mesoporous solids[37] The corresponding textural properties are presented in Table 7-1.

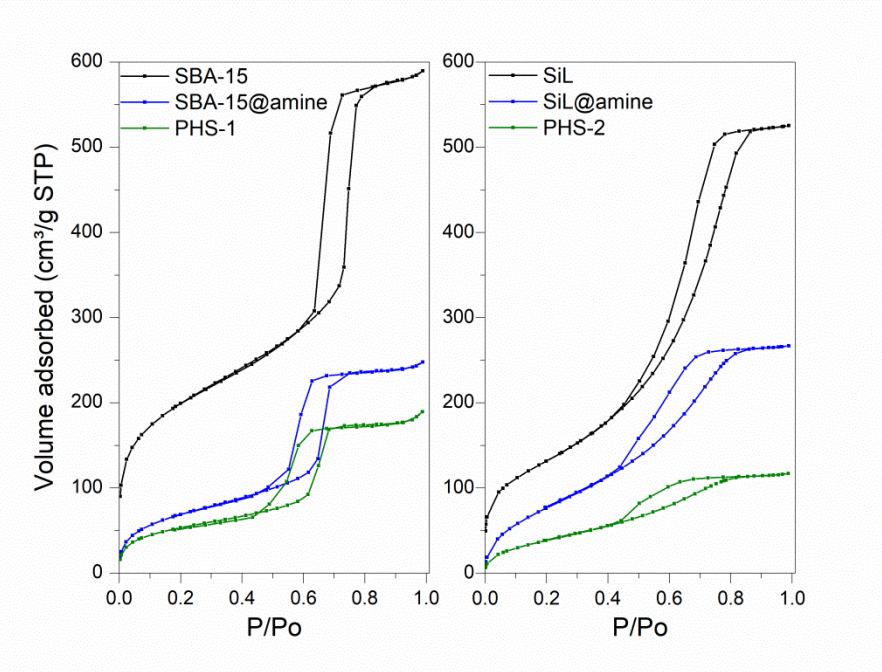

Figure 7-1. Nitrogen adsorption–desorption isotherms of pristine and functionalized supports

Table 7-1. Textural properties and N-content of solid materials

Material	Specific S_A (m^2/g)	Vp (mL/g)	Dp (nm)	N-content (mmol/g)
SBA-15	716	0.90	6.82	
SBA-15@amine	459	0.71	6.50	1.49
PHS-1	228	0.42	6.22	1.05
SiL	478	0.83	6.19	
SiL@amine	308	0.41	4.65	1.25
PHS-2	151	0.18	4.31	0.86

All grafted-materials had lower BET surface areas and pore volumes than their pure silica counterparts. Moreover, the nitrogen capillary condensation in functionalized materials occurred at lower relative pressure, indicating a decrease in the average pore size. These

findings provide strong evidence that immobilization of the organic moieties took place on the internal surface.

The organic contents of grafted silicas as determined by TGA are also shown in Figure 7-2. The higher N-content for SBA-15@amine compared to SiL@amine, and for PHS-1 compared to PHS-2 (Table 7-1), is likely to be associated with the higher surface area of the SBA-15 silica support. The observed decrease in N-content following amine quaternization confirmed the incorporation of additional organic moieties. Considering the N-content per gram of silica for both the amine grafted and quaternized solids to be the same, the yield of the quaternization reactions was evaluated to be 85 % for both PHSs.

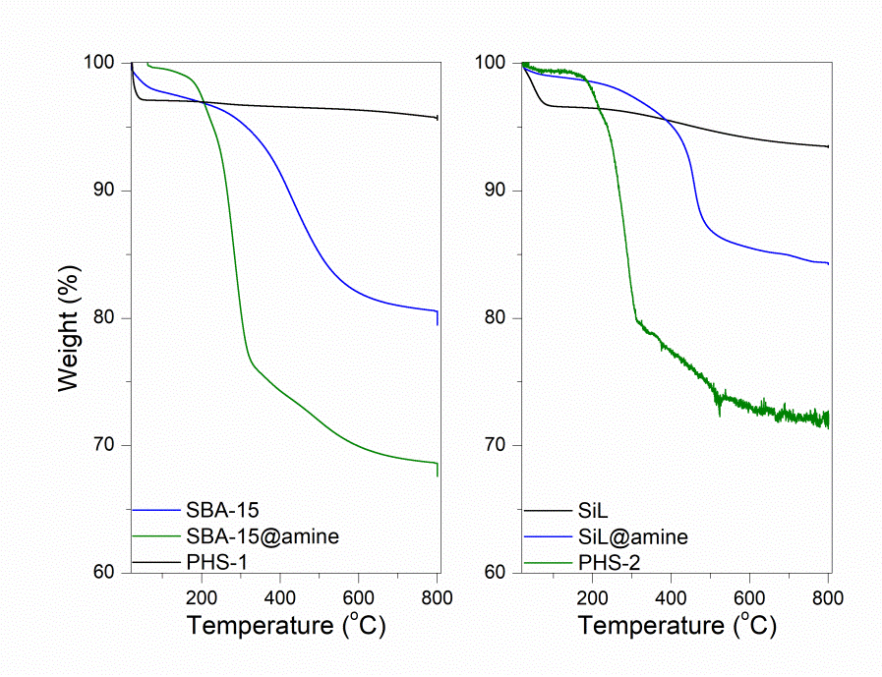

Figure 7-2. TGA profiles of pristine and functionalized supports

FT-IR spectra depicted in Figure 7-3, show broad bands centered at 3350 and 1630 cm^{-1}, associated with the silanol (SiO–H) groups in both supports. Owing to their higher

organic loading, all SBA-15 based materials showed stronger bands compared to SiL-based materials. Bands around 2939, 2850, 1850 (on SBA-15@amine only) and 1450 cm^{-1} were assigned to the $–CH_2–$ units of the grafted tributylpropylamine.[22]

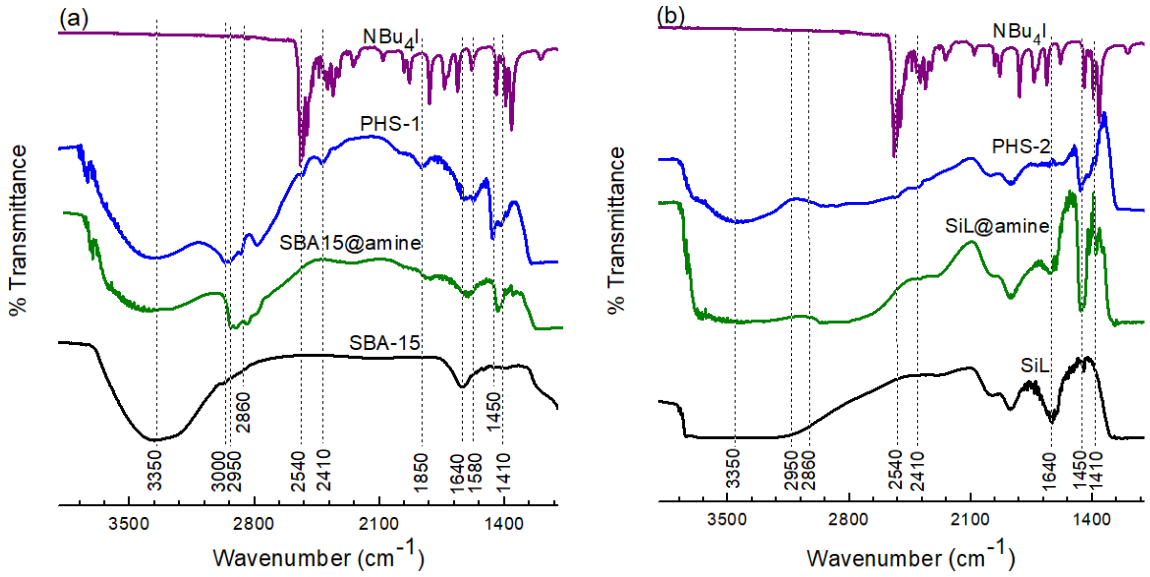

Figure 7-3. FT-IR spectra of supports, amine-grafted supports and immobilized catalysts of (a) SBA-15 and (b) SiL based materials; and NBu_4I

Weak bands observed at 3000 and 1580 cm^{-1} were assigned to N-H stretching and deformation, respectively.[38] Finally, the band at 1410 cm^{-1} was ascribed to C–N stretching. The identification of these functional groups ($-CH_2-$, N-H and C-N) confirmed the presence of alkyl amine groups on the supports.[38] Comparing the spectra of amine-functionalized materials and that of PHSs, new bands were observed at 2540 and 2410 cm^{-1}. These bands, which were identified in the spectrum of NBu_4I, were assigned to C-N vibrations of the $C\text{-}N^+$ bond.[30] For both PHSs, the broad signal centered at 3300 cm^{-1} suggests that both functionalized catalysts contained unreacted silanol groups, which are expected to

enhance the catalytic activity through hydrogen bonding with the epoxide. This effect was more pronounced for PHS-2, suggesting it contained more unreacted silanol groups.

NBu_4I and the functionalized catalysts were further characterized by solid-state ^{13}C and ^{15}N CP-MAS NMR studies. For ^{13}C CP-MAS, peaks around 64, 28, 23 and 16 ppm were assigned to the four carbon nuclei of the butyl groups as illustrated in Figure 7-4a. Functionalized catalysts showed no distinctive peaks corresponding to the propyl group, most likely because of a combination of the low intensity of the propyl $–CH_2–$ signals and their overlap with the corresponding $–CH_2–$peaks (b, c and d) of the butyl groups.

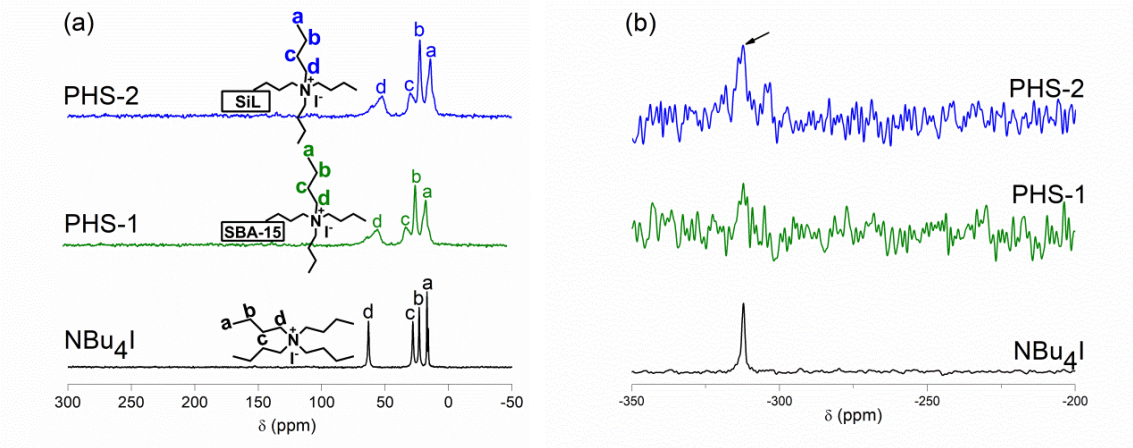

Figure 7-4. a) ^{13}C CP-MAS NMR and (b) ^{15}N CP-MAS NMR of NBu_4I and immobilized catalysts.

The ^{15}N MAS NMR spectra of NBu_4I showed a single peak at around -312 ppm, which corresponds to the lone N-atom (Figure 7-4b). A similar peak, although of significantly lower intensity, was observed in the presence of immobilized catalysts. The low signal-to-noise ratio was attributed to the combined effect of the low natural abundance of ^{15}N (0.37 %) and N-content of the samples (0.86 – 1.05 mmol/g). Combination of NMR and FT-IR data clearly indicates the chemical identity of immobilized moieties, thereby confirming the structure of the PHSs (Scheme 7-1).

7.3.2. Catalytic activity

7.3.2.1. NBu_4I vs. tributylpropylammonium iodide immobilized on SBA-15 (PHS-1)

The activity of NBu_4I and immobilized PHS-1 catalyst was evaluated using two model reactions (Scheme 7-3); the solvent-free cycloaddition of CO_2 and 1,2-epoxybutane (1,2-EB) to 1,2-butylene carbonate (1,2-BC), and styrene oxide (SO) to styrene carbonate (SC). 1,2-BC was obtained as a clear oily liquid, while SC was white crystals. These reactions were chosen due to the less reactive nature of SO compared to 1,2-EB, enabling a meaningful comparison of catalytic performance. PHS-1 was used instead of PHS-2 because of its higher N-content.

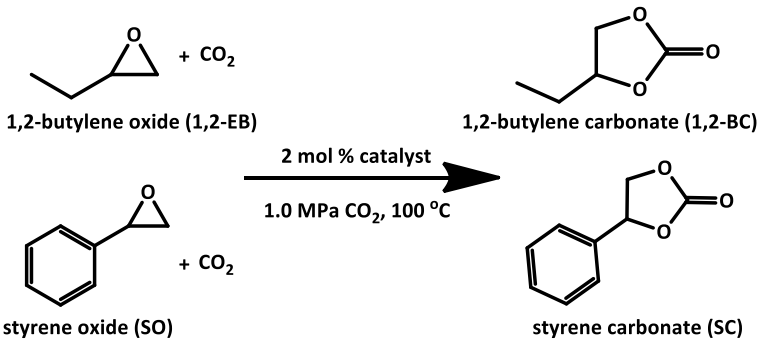

Scheme 7-3. Model reactions for the cycloaddition of CO_2 and epoxides to CCs.

The effect of time on both reactions is presented in Table 7-2. Surprisingly, the immobilized PHS-1 catalyst showed significantly higher activity compared to homogeneous NBu_4I in both reactions (Table 7-2: entries 1 vs. 4, 2 vs. 5 and 3 vs. 6). The slightly lower selectivity towards 1,2-BC compared to SC was due to the higher reactivity of 1,2-EB compared to SO. The β-carbon atom of the former is more reactive than that of the latter. This favour the reaction of 1,2-BC with available water molecules to form 1,2

butanediol as a by-product. This diol was reported as the main side product along with minor amounts of the carbonyl isomers of the epoxide.[32]

Table 7-2 A comparison of the catalytic performance of NBu_4I and PHS-1 for cycloaddition of CO_2 and 1,2-epoxybutane into 1,2-butylene carbonate (1,2-BC) or styrene oxide into styrene carbonate (SC)

			1,2-BC		**SC**	
Entry	Catalyst	Time (h)	Yield (%)	Sel. (%)	Yield (%)	Sel. (%)
1		2	25.2	95.5	27.3	96.0
2	NBu_4I	4	70.5	92.1	60.4	94.1
3		6	80.5	90.8	70.1	91.7
4		2	70.4	97.1	60.6	98.1
5	PHS-1	4	96.2	96.8	81.7	96.9
6		6	90.5	91.5	98.0	98.5

Reaction conditions: 2 mol % NBu_4I or PHS-1, 100 ^oC, 1 MPa CO_2, solvent-free

In addition to the diol product, poly(carbonates) have also been reported as side products.[39] Purging the reactor twice with 0.5 MPa CO_2 did not lead to any significant changes in yield and selectivity. This observation prompted us to look into the effect of added water on the synthesis of 1,2-BC. As shown in Table A7-1 (Appendix), addition of water had no effect on the yield and selectivity of 1,2-BC. Although addition of water has been reported to improve both the yield and selectivity of CCs[40] this was not observed under the current reaction conditions. The main by-products for this reaction were 1,2-butandiol and poly(butylene carbonate). The former is formed by hydrolysis of the epoxide, while the latter is formed either from the ring opening polymerization of 1,2-EB and CO_2 or 1,2-BC. Literature data indicate that such polymerization reactions may be catalyzed by zinc-containing ionic liquids.[41–44] Nonetheless, it seems that these reactions proceed to a small extent in the absence of an appropriate catalyst. The yield of 1,2-

butanediol and poly(butylene carbonate) were observed to increase and decrease respectively with the amount of water, suggesting that the presence of water favours the formation of 1,2-butanediol over poly(butylene carbonate). Judging from the observed trend, it can be inferred that once poly(butylene carbonate) is produced, it partially undergoes hydrolysis into 1,2-butanediol, leading to an increase in the amount of the latter with water.

The observed decrease in selectivity with reaction time was attributed to further formation of these side products. For both NBu_4I and PHS-1, the optimum reaction time was 4 and 6 h for 1,2-EB and SO, respectively. Hence, the reaction conditions used for reusability studies on PHS-1 were 1.0 MPa CO_2, 100 ^oC and 4 h (for 1,2-EB) and 6 h (for SO). Similar optimum reaction conditions, were reported with *N,N,N*-tris(hydroxyethyl)propylammonium iodide supported on non-porous silica.[25] Alkylammonium salt containing hydroxyalkyl or carboxyalkyl groups are well known to activate epoxides through hydrogen-bonding.[45] However, long alkyl chains, notably butyl, have been reported to be equally active due to a stronger nucleophilicity of the halide. This enhancement in nucleophilicity originates from the weakened electrostatic interaction between the halide and the butyl ammonium center.[46]

The observed high activity of the immobilized catalyst compared to its homogeneous counterpart may be attributed to three reasons. Firstly, activation of the epoxides by unreacted silanol groups on the support (SBA-15) is enhanced through hydrogen bonding. Such an interaction increases the strain on the epoxide ring system, leading to a lower energy barrier to open the oxygen bridge.[45] In line with this statement,

catalysts containing functional groups that are capable of forming hydrogen bonds with epoxides were reported to be highly active towards the cycloaddition of epoxides and CO_2.[47–49] Secondly, the -Si-O-Si-C- linkages at the interface of the silica surface and the immobilized organic moieties is known to improve the thermal stability (or resistance to thermally induced deactivation processes) of immobilized catalysts.[50] Thirdly, the fraction of un-quaternized secondary amino groups on PHS-1 could be involved in CO_2 capture, creating and maintaining a CO_2 pool close to the active sites and substrate. Consistent with the current findings, similar activity enhancement was reported following the immobilization of molecular catalysts.[27,51,52] Toshiyasu and co-workers[51] reported a 300-fold increase in rate constant of propylene and CO_2 cycloaddition reaction over silica supported phosphonium salts compared to their homogeneous counterparts. In addition to activation of the epoxide by silanol groups, the authors attributed this improvement to a decrease in the frequency factor of the molecular catalysts once immobilized. The lower frequency factor indicates that the immobilized species collide more readily with the substrate molecules rather than with each other.

Under mild conditions, alkyl ammonium iodides achieve less than 75 % yield in CCs.[53] To achieve higher yields, they are often used as co-catalysts in the synthesis of CCs, alongside other species able to activate epoxides through hydrogen bonding, e.g. 3-hydroxypyridine and tetra-n-butylammonium iodide[54], tetrabutylammonium bromide in dimethylcarbonate[31], tetrabutylammonium bromide and (ethylenediaminetetraacetic acid) EDTA,[48] and tetrabutylammonium iodide and tannic acid.[55] We believe the lower activity of tetrabutylammonium iodide compared to the PHSs is due to its inability to

activate the epoxides. Such activation is possible of the PHSs due to the availability of silanol groups.

7.3.2.2. Reusability of PHS-1 Catalyst

The main purpose of this study was to develop a substrate-independent reusable solid catalyst under the optimized reaction conditions. Following reactions, spent PHS-1 was recovered by filtration (up to 95% by weight), washed with Et_2O (5 x 20 mL) and dried under vacuum at 90 ^oC for 2 h. Prior to each reaction cycle, the N-content of the catalyst was determined by TGA and the weight adjusted accordingly to meet the required 2 mol% catalyst loading with respect to the substrate (22.7 and 17 mmol for 1,2-EB and SO, respectively). Moreover, nitrogen adsorption-desorption measurements were carried out on the spent catalysts from cycles 1 and 5. Results on the reusability of PHS-1 in the synthesis of 1,2-BC are shown in Figure 7-5.

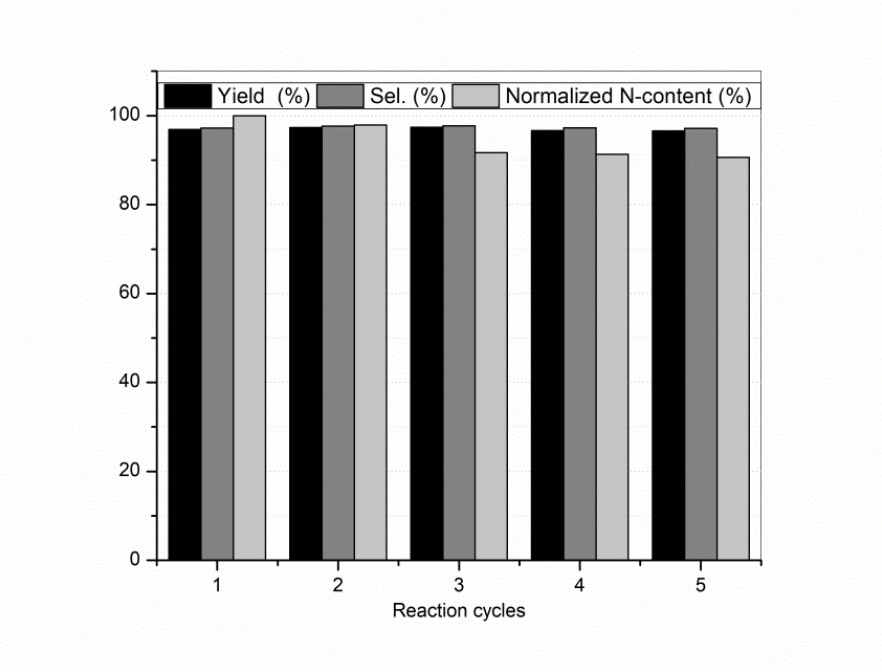

Figure 7-5. Reusability studies of immobilized PHS-1 catalyst. Reaction conditions: 22.7 mmol 1,2-EB, 2 mol% PHS-1, 100 ^{o}C, 1 MPa CO_2 and 4 h.

Cycle 1 represents the run using the fresh catalyst, while cycle 2 stands for the first reused catalyst and so on. As seen, this catalyst could be reused at least 5 times without any noticeable loss of activity. Excellent conversions (≥ 99%) and yields (≥ 96%) were obtained, which demonstrate the effectiveness of PHS-1 towards this reaction

Nevertheless, the normalized N-content showed a gradual decrease with reuse, particularly during the first three cycles. Although proper washing was ensured during the catalyst preparation steps, some *N*-butylaminopropyltrimethoxysilane molecules could have been physically adsorbed on the amine grafted material, a fraction eventually ending up quaternized and stayed on the catalyst surface. These deposited ammonium species may leach, particularly during the first two reuses. Another reason behind the early loss of nitrogen is the leaching of immobilized active sites; possibly via dealkylation of the

ammonium groups, which may involve a loss in butyl group(s) or the complete leaching of ammonium ion units. Different pathways for these deactivation processes of supported ionic liquids were reported by Villuendas and co-workers [56] After the third cycle, further loss in activity was negligible. This can be ascribed to the presence of strongly bonded alkylammonium iodide species on the supports; which were relatively stable towards dealkylation/leaching processes.

We then investigated the reusability of PHS-1 in the presence of a more challenging substrate, SO. With the exception of the reaction time, i.e. 6 versus 4 h, the recycling experiments were carried out as with 1,2-EB. As shown in Figure 7-6, very good to excellent yields and selectivity (≥ 96%) were obtained for up to 3 cycles. However, a decrease in yield (90 and 83% in the 4^{th} and 5^{th} cycles, respectively) was observed thereafter, although the selectivity remained constant. This decline in catalytic activity may be due to catalyst deactivation and/or physical phenomena such as pore and/or active site blockage by the reaction product.

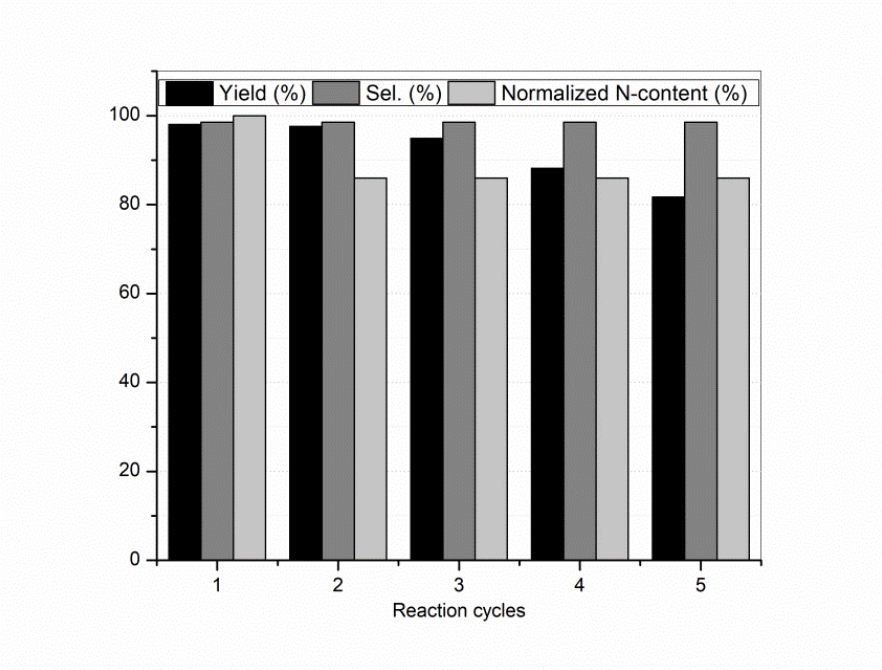

Figure 7-6. Reusability studies of immobilized catalyst PHS-1. Reaction conditions: 17 mmol SO, 2 mol% PHS-1, 100 °C, 1 MPa CO_2 and 6 h.

Although diffusion constraints due to the steric requirements of immobilized bulky species such as *N*-substituted azaphosphatrane on SBA-15 was found to decrease the catalytic activity[57], tributylpropylammonium iodide is presumably not bulky enough for diffusion limitations to be a factor in catalyst deactivation. Previous studies also reported poor reusability of immobilized catalysts in the synthesis of SC, with the observed behavior attributed to the leaching of active sites.[22,58] However, we found that the N-content decreased by 15% after the first reaction cycle and remained unchanged thereafter. As already mentioned, the early loss of nitrogen may be due to the leaching of adsorbed alkylammonium iodide species. However, the observed decrease in the yield of SC at a constant N-content (from cycle 2-5) was unusual. To shed light on this issue, we looked at changes in the textural properties of the fresh and selected spent PHS-1

catalysts. If the leaching of active species via dealkylation processes are responsible for the decrease in the N-content, then changes in the textural properties of the spent catalysts, with a systematic trend, should be expected. The textural properties of the fresh and spent PHS-1 from cycles 1 and 5 are shown in Table 7-3.

Table 7-3 Textural properties of fresh and spent PHS-1 from the model reactions in Scheme 3

Entry	Catalyst	BET (m^2/g)	V_p (mL/g)	D_p (nm)	N-content (mmol/g)
		1,2-EB + CO_2 = 1,2-BC			
1	Fresh PHS-1	228	0.42	6.22	1.05
2	After cycle 1	228	0.42	6.30	1.02
3	After cycle 5	299	0.52	6.55	0.95
		SO + CO_2 = SC			
4	Fresh PHS-1	228	0.43	6.22	1.05
5	After cycle 1	227	0.41	6.03	0.90
6	After cycle 5	204	0.39	5.86	0.90

For both model reactions, the textural properties and N-content of the fresh catalyst and that from cycle 1 were similar (Table 7-3: entries 1 vs. 2 and 4 vs. 5). The leaching of adsorbed species is not expected to lead to a noticeable change in the surface area of the immobilized catalyst. For the synthesis of 1,2-BC, the spent catalyst from cycle 5 showed an increase in surface area, pore volume and pore diameter compared to that after cycle 1 (Table 7-3: entries 2 and 3). These increases are likely due to the loss of organic moieties from the support, mainly as a result of dealkylation processes. If quaternization of amine grafted silica led to a decrease in all three textural properties (Table 7-1), then dealkylation should have the opposite effect. The observed increase in all three textural properties is in agreement with this expectation. In line with this, trends in TGA and N_2 adsorption data

are consistent with the observed decrease in the N-content of spent PHS-1 catalysts with reaction cycles being due to the loss of immobilized organic moieties. Using Energy Dispersive X-Ray Analysis (EDX) elemental mapping, similar losses of nitrogen and bromine in immobilized phosphonium salt were found to take place during recycling in the synthesis of cyclic carbonates.[27] Hence, a combination of textural properties and TGA data, provides a useful tool to gain insights into the deactivation of immobilised organocatalysts by dealkylation processes.

Considering the reusability of PHS-1 in the synthesis of SC, negligible decreases were observed in surface area and pore volume after cycle 1, while a more noticeable decrease in pore diameter and N-content was recorded (Table 7-3: entries 4 and 5). The latter pair of observations seems to indicate the simultaneous occurrence of two phenomena: deposition of SC crystals on the surface of the spent catalyst (leading to a decrease in pore diameter), and the loss of organic moieties (leading to lower N-content). The longer reaction time for the synthesis of SC, compared to 1,2-BC, might have contributed to the more severe drop in N-content after cycle 1 (Table 7-3: entries 2 and 5). Additionally, an opposite trend in textural properties was observed, as the surface area, pore volume and mean pore diameter decreased when comparing the spent PHS-1 of cycles 2 and 5 (Table 7-3: entries 5 and 6). Keeping in mind the viscous nature of the reaction mixture and the porous nature of PHS-1, solid SC product could be trapped in the pores and/or block the active sites of the catalyst cycle-after-cycle. Occurrence of deposited SC in spent catalysts was confirmed by ^{13}C CP-MAS NMR data. As shown in Fig. 7-7, the ^{13}C NMR peaks between 10 and 60 ppm observed in fresh PHS-1 (Figure 7-7) were

attributed to the C-atoms of immobilized tributylpropylammonium iodide, whereas the spent catalysts exhibited additional peaks at around 60, 65, and overlapped peaks centered at 130, 144 and 220 ppm.

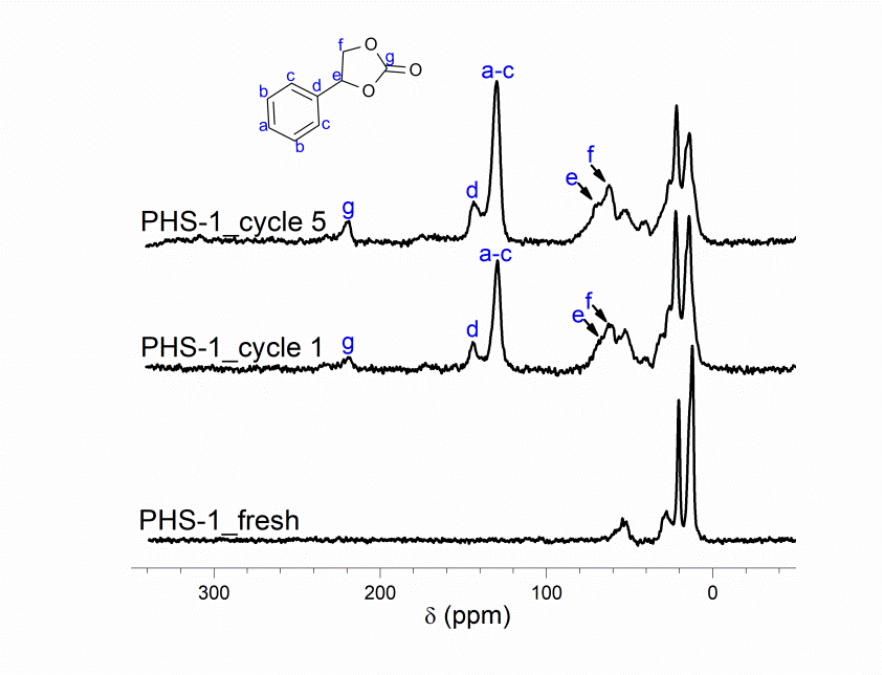

Figure 7-7. ^{13}C CP-MAS NMR spectra of fresh and spent catalysts PHS-1

All these peaks are consistent with the occurrence of SC (Fig. 7-7). The relative amount of adsorbed SC was found to be higher after the 5th cycle, suggesting that the SC deposition accumulated upon catalyst recycling. These observations indicate that even the extensive washing of recovered catalyst (with 5 x 20 mL of diethyl ether) was not sufficient to remove all the SC product. Washing the recovered catalysts with more polar solvents might eliminate or at least further reduce the accumulation of SC. Nevertheless, this was not investigated as we were not satisfied with the long reaction time (6 h) needed in the synthesis of SC using PHS-1.

Based on the current findings and related literature, the observed decrease in SC yield with reaction cycles coupled with a constant N-content after cycle 1 (Figure 7-6) strongly indicates that the weight gain due to SC deposition and the weight loss due to dealkylation were comparable, leading to a constant and overestimated N-content as determined by TGA. Consequently, the actual catalyst loading of spent catalysts was likely lower than 2 mol% (for cycles 2 to 5). This could partly account for the declining catalytic performance with reuse. Moreover, deposited SC species could block both the active sites and pores of the immobilized catalyst, further causing a drop in catalyst performance.

Ideally, catalytic cycloaddition of CO_2 and epoxides takes place under mild conditions, including low temperature and CO_2 pressure as well as short reaction time. Although PHS-1 catalyst demonstrated very good to excellent activity towards the model cycloaddition reactions, long reaction times and reusability issues with SO called for improvement of the material and the catalyst recovery step. Despite its higher N-content (compared to PHS-2), the low apparent density of SBA-15 means a high volume of PHS-1 is required, creating a viscous reaction mixture, leading to longer reaction times to achieve high conversion.

7.3.2.3. PHS-2 catalyst: Reusability studies

In an attempt to reduce the impact of heavy deposits on the recyclability of the catalysts, a more extensive washing procedure was adopted, using SO as substrate in the presence of more active PHS-2 catalyst. Each spent catalyst was further stirred in acetone for 30 min at room temperature, filtered and washed with more acetone. The recovered catalyst was then dried at 90 ^{o}C for 2 h under vacuum. Because of its higher polarity

compared to diethyl ether, acetone is expected to better dissolve and wash off adsorbed SC crystals.

Interestingly, PHS-2 showed significant improvement in catalytic performance compared to PHS-1. Notably, the optimum reaction time was found to be 4 h, compared to 6 h for PHS-1. Moreover, as shown in Figure 7-8, no noticeable changes in the product yield were observed over five reaction cycles.

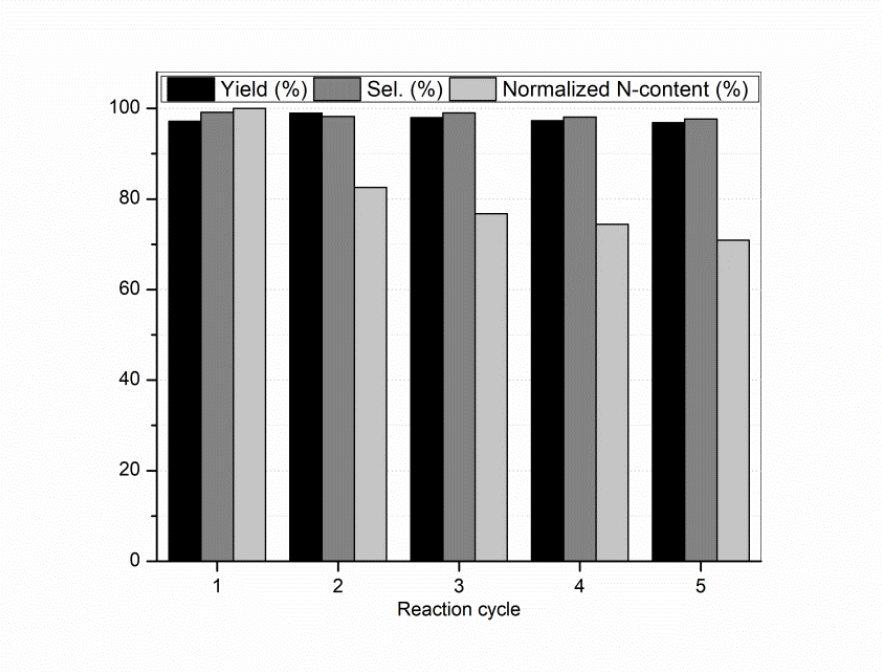

Figure 7-8. Recycling studies of immobilized PHS-2 catalyst. Reaction conditions: 17 mmol SO, 2 mol% PHS-2, 100 °C, 1 MPa CO_2 and 4 h.

This remarkable outcome was attributed to a two-fold higher apparent density of the support (SiL, 40 – 60 µm in size), compared to SBA-15 (about 1 µm in size [34]). This brought about a major improvement in mixing, mass and heat transfer processes. Also, the presence of more un-functionalized silanol groups on PHS-2 compared to PHS-1, might have enhanced the activation of SO. Finally, as explained later, the improved catalyst recovery step had a positive

impact on the catalyst reusability. Similar to PHS-1, the N-content of PHS-2 showed a noticeable decrease in cycle 1, which was attributed mainly to the leaching of adsorbed active sites. The drop in the N-content was significantly less pronounced from cycles 3 to 5; an indication of a more stable catalyst, which underwent minimal deactivation. Comparison of the textural properties of fresh and spent PHS-2 after cycles 1 and 5 (Figure 7-9) showed an increase in surface area and pore volume with reuse. This finding is consistent with deactivation of PHS-2 via dealkylation processes. Although a 38% increase in surface area and a 30% drop in N-content were observed after 5 reaction cycles, no attempt was made to correlate these two findings. Moreover, the mean pore diameter of PHS-2 was observed to slightly increase (1.3 %) after cycle 1 and decrease after cycle 5. If dealkylation proceeds with negligible deposition of SC, pore diameter is expected to increase; which is consistent with our findings. The recorded decrease in pore diameter after cycle 5 was attributed to minimal dealkylation accompanied by a significant deposition of SC.

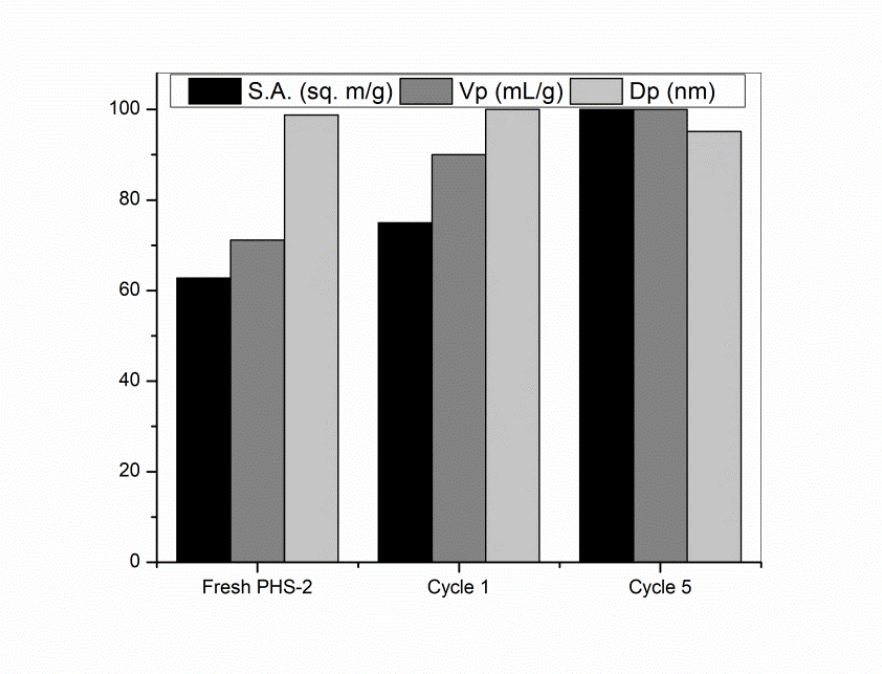

Figure 7-9. Normalized textural properties of fresh and spent PHS-2 catalyst after cycles 1 and 5

^{13}C NMR spectra for PHS-2 before reaction and after the first cycle were identical (Fig. 7-10), whereas, after cycle 5, spent PHS-2 showed all the signals associated with SC as identified in Figure 7-7. This finding indicates that even after extensive washing, heavy products may still accumulate on the catalyst surface, albeit at a lower rate. Based on these results, one can argue that the observed accumulation of SC on PHS-1 with reuse could be significantly reduced by the two-step extensive catalyst washing procedure used on spent PHS-2, thereby improving its reusability.

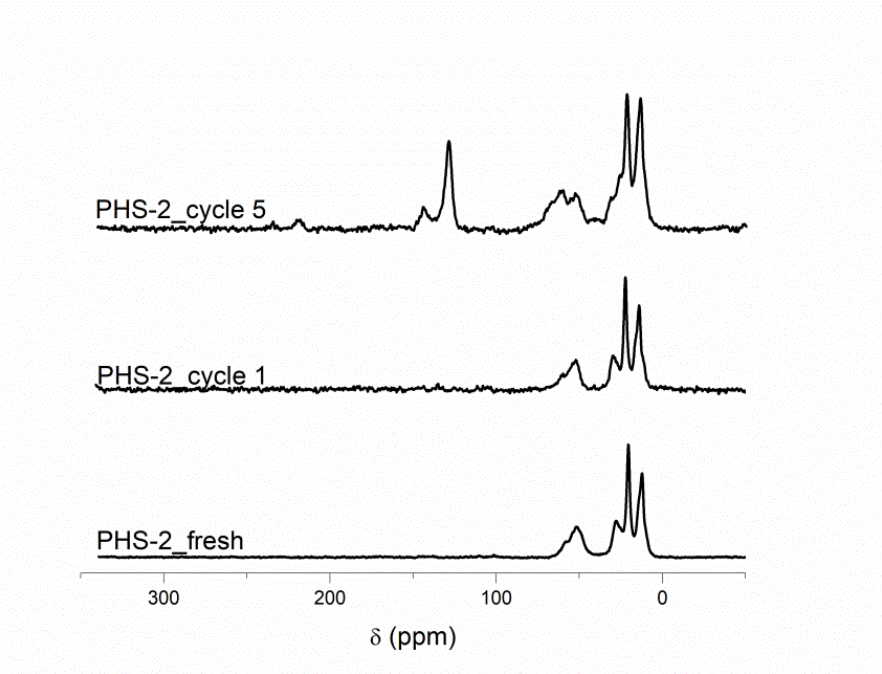

Figure. 7-10. ^{13}C CP-MAS NMR spectra of fresh and spent PHS-2 catalyst after cycles 1 and 5

To the best of our knowledge, this is the first time that a systematic study using N-content, textural properties and ^{13}C NMR measurements to correlate the surface and textural properties of an immobilized catalyst to its recyclability performance in the synthesis of CCs has been reported.

A survey of literature data was carried out to compare the performance of other silica and polystyrene-supported ammonium and phosphonium salts (Table 7-4, entries 1-13) to PHS-2 (Table 7-4, entry 14). Although lower CO_2 pressures were used in entries 1-3, the reaction temperature and duration were significantly higher than the current optimum conditions. Whilst entries 4-9 dealt with solid catalysts operated at moderate pressures similar to the current study, comparable performances to PHS-2 were obtained only at significantly higher catalyst loading (entry 6-7), temperature (entry 8) and duration

(entry 9). The operating conditions of entries 4 and 5 were similar to ours, but the obtained yields were lower.

Table 7-4 Immobilized ionic liquids on silica and polystyrene for the synthesis of SC from SO and CO_2

Entry	immobilized catalyst	Cat. (mol%)	P_{CO2} (MPa)	T (°C)	t (h)	Yield (%)	Ref
1	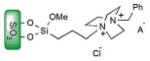	2.77	0.4	120	24	92	22
2	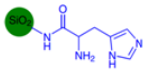	1.93	0.5	130	10	99	58
3	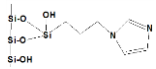	0.25	0.6	130	10	77	18
4	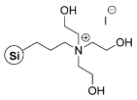	2.00	1.0	90	6	85	25
5	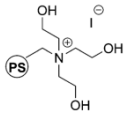	2.0	1.0	90	4	93	25
6		8.0	1.0	65	18	98	45
7	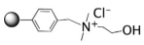	6.50	1.0	85	6	99	59
8	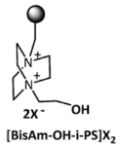	3.37	1.2	130	2.5	94	60
9	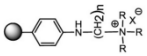	0.6	1.2	120	12	97	49
10	PDDA-Br-$ZnBr_2$-2/SiO_2	0.45	2.5	100	12	93	61
11	MCM-41-Imi/Br	0.13	3.0	100	4	98	30
12	*n*-Bu_4NBr/SiO_2	1.70	8.0	150	8	97	32
13*	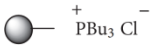		5.0	150	10	96	62
14	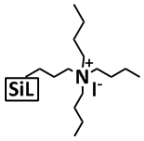	2.00	1.0	100	4	98	This work

* 0.08 g of catalyst per 3 mL of substrate

Even though very good to excellent yields were obtained in entries 10-13, the CO_2 pressure employed was 2.5 to 8 times higher than in the current study. A similar high yield of SC was reported over an insoluble ion exchange resin functionalized with $-N^+(CH_3)_3Cl^-$ species, albeit under supercritical CO_2 (8 MPa, 100 ^oC, 12 h).[63] These results highlight the importance of the iodide ion as a superior leaving group, critical towards achieving high yield under mild conditions. Clearly, metal-free PHS-2 showed a superior performance compared to literature data as it offers the best compromise between CO_2 pressure, reaction temperature, reaction time and catalytic performance.

Finally, we investigated the scope of PHS-2 using two more substrates, namely epichlorohydrin (EPH) and cyclohexene oxide (CHO), to synthesize 4-(Chloromethyl)-1,3-dioxolan-2-one and hexahydrobenzo[*d*][1,3]dioxol-2-one, respectively. Although less reactive than 1,2-EB, the former epoxide is relatively easy to activate, whereas the latter, an internal epoxide, is even more difficult to activate than SO. For both substrates, optimum reaction conditions were used, and the effect of time was studied. Both EPH and 1,2-EB required just 2 h to attain maximum conversion (Table 7-5, entries 1 and 3). A decrease in yield and selectivity was observed after 4 h (Table 7-5, entries 2 and 4).

Table 7-5 Yield and selectivity of various epoxides with CO_2 using PHS-2

Entry	Epoxide	Cyclic carbonate	time (h)	Yield (%)	Sel. (%)
1	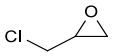	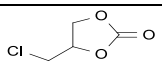	2	92.2	94.7
2			4	85.4	89.0
3		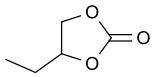	2	95.1	98.1
4			4	90.2	91.5
5		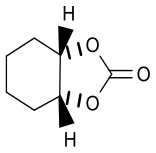	4	3.1	90.3
6*			24	22.5	62.3

Reaction conditions: 2 mol % PHS-2, 100 °C, 1 MPa, solvent-free. *CHC was exclusively formed as the *cis* isomer, as identified by ^{1}H and ^{13}C NMR, and FT-IR analysis.[64]

In contrast, after 2 h, CHO led to a mere 3.1% cyclohexene carbonate (CHC) (

Table 7-5, entry 5). However, when the reaction time was extended to 24 h, the reaction yield was 7 times higher (Table 7-5, entry 6). Many research groups reported low yields in the synthesis of CHC, which was attributed to steric hindrance.[45,49,58] Although 93% CHC yield was reported by Xie *et al.,*[28] this was achieved under harsh conditions (6 MPa CO_2, 110 °C, and 72 h). Based on the current findings, it is clear that PHS-2 is a versatile catalyst for the efficient synthesis of CCs from external epoxides under mild conditions.

Conclusion

Two tributylpropylammonium iodide immobilized on mesoporous silicas (PHS-1 and PHS-2) were prepared and tested in the conversion of CO_2 with two model epoxides (1,2-

EB and SO) to produce CCs. These materials were found to be effective and easily reusable hybrid catalysts for this cycloaddition reaction, under mild conditions (2 mol% catalyst loading, 1.0 MPa CO_2, 100 ^oC, ≤ 6 h reaction time). The desired CCs were obtained in excellent yields and high selectivity (both > 95%). The synergistic effect between the support, notably its silanol groups, and immobilized organic moieties resulted in superior catalytic activity compared to the homogeneous NBu_4I salt. Moreover, we found that for reusability studies with SO as substrate, the apparent densities of the supports and catalyst recovery steps were critical parameters affecting the activity of the catalyst. Compared with similar solid catalysts reported in the literature, our PHS-2 catalyst was significantly more active, selective, and stable for the cycloaddition of CO_2 and SO to styrene oxide.

References

(1) Matthews, H. D.; Gillett, N. P.; Stott, P. a; Zickfeld, K. The Proportionality of Global Warming to Cumulative Carbon Emissions. *Nature* **2009**, *459* (7248), 829–832. https://doi.org/10.1038/nature08047.

(2) World Meteorological Organization. *WMO Statement on the State of the Global Climate in 2016*; 2017.

(3) United Nations. Towards a climate agreement http://www.un.org/climatechange/towards-a-climate- (accessed Mar 3, 2018).

(4) Razali, N. A. M.; Lee, K. T.; Bhatia, S.; Mohamed, A. R. Heterogeneous Catalysts for Production of Chemicals Using Carbon Dioxide as Raw Material: A Review. *Renew. Sustain. Energy Rev.* **2012**, *16* (7), 4951–4964. https://doi.org/10.1016/j.rser.2012.04.012.

(5) Song, C.; Liu, Q.; Ji, N.; Deng, S.; Zhao, J.; Li, Y.; Song, Y.; Li, H. Alternative Pathways for Efficient CO2 Capture by Hybrid Processes—A Review. *Renew. Sustain. Energy Rev.* **2018**, *82*, *Part 1* (2018), 215–231. https://doi.org/https://doi.org/10.1016/j.rser.2017.09.040.

(6) Aminu, M. D.; Nabavi, S. A.; Rochelle, C. A.; Manovic, V. A Review of Developments in Carbon Dioxide Storage. *Appl. Energy* **2017**, *208* (September), 1389–1419. https://doi.org/https://doi.org/10.1016/j.apenergy.2017.09.015.

(7) Koytsoumpa, E. I.; Bergins, C.; Kakaras, E. The CO2 Economy: Review of CO2 Capture and Reuse Technologies. *J. Supercrit. Fluids* **2017**, *132*, 3–16.

https://doi.org/10.1016/j.supflu.2017.07.029.
(8) Consoli, C. P.; Wildgust, N. Current Status of Global Storage Resources. *Energy Procedia* **2017**, *114* (November 2016), 4623–4628. https://doi.org/10.1016/j.egypro.2017.03.1866.
(9) Song, Q.-W.; Zhou, Z.-H.; He, L.-N. Efficient, Selective and Sustainable Catalysis of Carbon Dioxide. *Green Chem.* **2017**, *19* (16), 3707–3728. https://doi.org/10.1039/C7GC00199A.
(10) Zimmermann, A. W.; Schomäcker, R. Assessing Early-Stage CO2 Utilization Technologies—Comparing Apples and Oranges? *Energy Technol.* **2017**, *5* (6), 850–860. https://doi.org/10.1002/ente.201600805.
(11) Lin, H.; Biddinger, E. J. Challenges and Opportunities for Carbon Dioxide Utilization. *Energy Technol.* **2017**, *5* (6), 771–772. https://doi.org/10.1002/ente.201700336.
(12) Al-Mamoori, A.; Krishnamurthy, A.; Rownaghi, A. A.; Rezaei, F. Carbon Capture and Utilization Update. *Energy Technol.* **2017**, *5* (6), 1–4. https://doi.org/10.1002/ente.201600747.
(13) Aresta, M.; Dibenedetto, A.; Quaranta, E. State of the Art and Perspectives in Catalytic Processes for CO2 Conversion into Chemicals and Fuels : The Distinctive Contribution of Chemical Catalysis and Biotechnology. *J. Catal.* **2016**, *343*, 2–45. https://doi.org/10.1016/j.jcat.2016.04.003.
(14) Klankermayer, J.; Wesselbaum, S.; Beydoun, K. Selective Catalytic Synthesis Using the Combination of Carbon Dioxide and Hydrogen : Catalytic Chess at the Interface of Energy and Chemistry Angewandte Reviews. *Angew. Chemie - Int. Ed.* **2016**, 2–50. https://doi.org/10.1002/anie.201507458.
(15) Sakakura, T.; Choi, J.; Yasuda, H. Transformation of Carbon Dioxide. *Chem. Rev.* **2007**, *107*, 2365−2387.
(16) Mennicken, L.; Janz, A.; Roth, S. The German R&D Program for CO2 Utilization—Innovations for a Green Economy. *Environ. Sci. Pollut. Res.* **2016**, *23* (11), 11386–11392. https://doi.org/10.1007/s11356-016-6641-1.
(17) Zhao, Y.; Yu, B.; Yang, Z.; Zhang, H.; Hao, L.; Gao, X.; Liu, Z. A Protic Ionic Liquid Catalyzes CO2 Conversion at Atmospheric Pressure and Room Temperature: Synthesis of Quinazoline-2,4(1H,3H)-Diones. *Angew. Chemie - Int. Ed.* **2014**, *53* (23), 5922–5925. https://doi.org/10.1002/anie.201400521.
(18) Sankar, M.; Ajithkumar, T. G.; Sankar, G.; Manikandan, P. Supported Imidazole as Heterogeneous Catalyst for the Synthesis of Cyclic Carbonates from Epoxides and CO2. *Catal. Commun.* **2015**, *59*, 201–205. https://doi.org/10.1016/j.catcom.2014.10.026.
(19) Dibenedetto, A.; Angelini, A.; Stufano, P. Use of Carbon Dioxide as Feedstock for Chemicals and Fuels: Homogeneous and Heterogeneous Catalysis. *J. Chem. Technol. Biotechnol.* **2014**, *89* (3), 334–353. https://doi.org/10.1002/jctb.4229.
(20) Valkenberg, M. H.; deCastro, C.; Hölderich, W. F. Immobilisation of Ionic Liquids on Solid Supports. *Green Chem.* **2002**, *4* (2), 88–93. https://doi.org/10.1039/b107946h.
(21) Udayakumar, S.; Lee, M. K.; Shim, H. L.; Park, S. W.; Park, D. W. Imidazolium Derivatives Functionalized MCM-41 for Catalytic Conversion of Carbon Dioxide to Cyclic Carbonate. *Catal. Commun.* **2009**, *10* (5), 659–664. https://doi.org/10.1016/j.catcom.2008.11.017.
(22) Hajipour, A. R.; Heidari, Y.; Kozehgary, G. Silica Grafted Ammonium Salts Based on DABCO as Heterogeneous Catalysts for Cyclic Carbonate Synthesis from Carbon Dioxide

and Epoxides. *RSC Adv.* **2015**, *5* (29), 22373–22379. https://doi.org/10.1039/C4RA16083E.
(23) Sun, J.; Cheng, W.; Fan, W.; Wang, Y.; Meng, Z.; Zhang, S. Reusable and Efficient Polymer-Supported Task-Specific Ionic Liquid Catalyst for Cycloaddition of Epoxide with CO2. *Catal. Today* **2009**, *148* (3–4), 361–367. https://doi.org/10.1016/j.cattod.2009.07.070.
(24) Collis, A. E. C.; Horváth, I. T. Heterogenization of Homogeneous Catalytic Systems. *Catal. Sci. Technol.* **2011**, *1*, 912–919. https://doi.org/10.1039/c1cy00174d.
(25) Kohrt, C.; Werner, T. Recyclable Bifunctional Polystyrene and Silica Gel-Supported Organocatalyst for the Coupling of CO2 with Epoxides. *ChemSusChem* **2015**, *8* (12), 2031–2034. https://doi.org/10.1002/cssc.201500128.
(26) Adam, F.; Appaturi, J. N.; Ng, E. P. Halide Aided Synergistic Ring Opening Mechanism of Epoxides and Their Cycloaddition to CO2 Using MCM-41-Imidazolium Bromide Catalyst. *J. Mol. Catal. A Chem.* **2014**, *386*, 42–48. https://doi.org/10.1016/j.molcata.2014.02.008.
(27) Steinbauer, J.; Longwitz, L.; Frank, M.; Epping, J.; Kragl, U.; Werner, T. Immobilized Bifunctional Phosphonium Salts as Recyclable Organocatalysts in the Cycloaddition of CO2 and Epoxides. *Green Chem.* **2017**, *19*, 4435–4445. https://doi.org/10.1039/C7GC01782K.
(28) Xie, Y.; Zhang, Z.; Jiang, T.; He, J.; Han, B.; Wu, T.; Ding, K. CO2 Cycloaddition Reactions Catalyzed by an Ionic Liquid Grafted onto a Highly Cross-Linked Polymer Matrix. *Angew. Chemie - Int. Ed.* **2007**, *46* (38), 7255–7258. https://doi.org/10.1002/anie.200701467.
(29) Jadhav, A. H.; Thorat, G. M.; Lee, K.; Lim, A. C.; Kang, H.; Seo, J. G. Effect of Anion Type of Imidazolium Based Polymer Supported Ionic Liquids on the Solvent Free Synthesis of Cycloaddition of CO2 into Epoxide. *Catal. Today* **2016**, *265*, 56–67. https://doi.org/10.1016/j.cattod.2015.09.048.
(30) Appaturi, J. N.; Adam, F. A Facile and Efficient Synthesis of Styrene Carbonate via Cycloaddition of CO2 to Styrene Oxide over Ordered Mesoporous MCM-41-Imi/Br Catalyst. *Appl. Catal. B Environ.* **2013**, *136–137*, 150–159. https://doi.org/10.1016/j.apcatb.2013.01.049.
(31) Kumar, S.; Jain, S. L.; Sain, B. Significant Rate Acceleration in Carbonate Synthesis from Carbon Dioxide and Oxiranes Using Dimethyl Carbonate as a Recyclable Medium. *Tetrahedron Lett.* **2011**, *52* (51), 6957–6959. https://doi.org/10.1016/j.tetlet.2011.10.082.
(32) Wang, J.-Q.; Kong, D.-L.; Chen, J.-Y.; Cai, F.; He, L.-N. Synthesis of Cyclic Carbonates from Epoxides and Carbon Dioxide over Silica-Supported Quaternary Ammonium Salts under Supercritical Conditions. *J. Mol. Catal. A Chem.* **2006**, *249* (1–2), 143–148. https://doi.org/10.1016/j.molcata.2006.01.008.
(33) Kumatabara, Y.; Okada, M.; Shirakawa, S. Triethylamine Hydroiodide as a Simple Yet Effective Bifunctional Catalyst for CO2 Fixation Reactions with Epoxides under Mild Conditions. *ACS Sustain. Chem. Eng.* **2017**, *5* (8), 7295–7301. https://doi.org/10.1021/acssuschemeng.7b01535.
(34) Sayari, A.; Han, B. H.; Yang, Y. Simple Synthesis Route to Monodispersed SBA-15 Silica Rods. *J. Am. Chem. Soc.* **2004**, *126* (44), 14348–14349. https://doi.org/10.1021/ja0478734.
(35) Jahandar Lashaki, M.; Ziaei-Azad, H.; Sayari, A. Insights into the Hydrothermal Stability of

Triamine-Functionalized SBA-15 Silica for CO2 Adsorption. *ChemSusChem* **2017**, *5*, 4037–4045. https://doi.org/10.1002/cssc.201701439.
(36) Sayari, A.; Belmabkhout, Y.; Da'na, E. CO2 Deactivation of Supported Amines: Does the Nature of Amine Matter? *Langmuir* **2012**, *28* (9), 4241–4247. https://doi.org/10.1021/la204667v.
(37) Keller, J. U.; Staudt, R. Chapter 8: Adsorption Isotherms. In *Gas adsorption equilibria: Experimental methods and adsorption isotherms.*; Springer US, 2005; pp 359–413. https://doi.org/10.1007/0-387-23598-1_8.
(38) Huang, J.; Yin, J.; Chai, W.; Liang, C.; Shen, J.; Zhang, F. Multifunctional Mesoporous Silica Supported Palladium Nanoparticles as Efficient and Reusable Catalyst for Water-Medium Ullmann Reaction. *New J. Chem.* **2012**, *36* (6), 1378. https://doi.org/10.1039/c2nj21073h.
(39) Hoon, S. K.; Jai, J. K.; Hyeck, N. K.; Moon, J. C.; Byung, G. L.; Ho, G. J. Well-Defined Highly Active Heterogeneous Catalyst System for the Coupling Reactions of Carbon Dioxide and Epoxides. *J. Catal.* **2002**, *205* (1), 226–229. https://doi.org/10.1006/jcat.2001.3444.
(40) Sun, J.; Ren, J.; Zhang, S.; Cheng, W. Water as an Efficient Medium for the Synthesis of Cyclic Carbonate. *Tetrahedron Lett.* **2009**, *50* (4), 423–426. https://doi.org/10.1016/j.tetlet.2008.11.034.
(41) Kadokawa, J. I.; Iwasaki, Y.; Tagaya, H. Ring-Opening Polymerization of Ethylene Carbonate Catalyzed with Ionic Liquids: Imidazolium Chloroaluminate and Chlorostannate Melts. *Macromol. Rapid Commun.* **2002**, *23* (13), 757–760. https://doi.org/10.1002/1521-3927(20020901)23:13<757::AID-MARC757>3.0.CO;2-0.
(42) Paul, S.; Zhu, Y.; Romain, C.; Brooks, R.; Saini, P. K.; Williams, C. K. Ring-Opening Copolymerization (ROCOP): Synthesis and Properties of Polyesters and Polycarbonates. *Chem. Commun.* **2015**, *51* (30), 6459–6479. https://doi.org/10.1039/C4CC10113H.
(43) Darensbourg, D. J.; Lewis, S. J.; Rodgers, J. L.; Yarbrough, J. C. Carbon Dioxide/Epoxide Coupling Reactions Utilizing Lewis Base Adducts of Zinc Halides as Catalysts. Cyclic Carbonate versus Polycarbonate Production. *Inorg. Chem.* **2003**, *42* (2), 581–589. https://doi.org/10.1021/ic0259641.
(44) Kapiti, G.; Keul, H.; Möller, M. Organocatalytic Polymerization of Ethylene Carbonate. *Mater. Today Commun.* **2015**, *5*, 1–9. https://doi.org/10.1016/j.mtcomm.2015.09.002.
(45) Whiteoak, C. J.; Henseler, A. H.; Ayats, C.; Kleij, A. W.; Pericàs, M. A. Conversion of Oxiranes and CO2 to Organic Cyclic Carbonates Using a Recyclable, Bifunctional Polystyrene-Supported Organocatalyst. *Green Chem.* **2014**, *16* (3), 1552. https://doi.org/10.1039/c3gc41919c.
(46) Büttner, H.; Lau, K.; Spannenberg, A.; Werner, T. Bifunctional One-Component Catalysts for the Addition of Carbon Dioxide to Epoxides. *ChemCatChem* **2015**, *7* (3), 459–467. https://doi.org/10.1002/cctc.201402816.
(47) Werner, T.; Büttner, H. Phosphorus-Based Bifunctional Organocatalysts for the Addition of Carbon Dioxide and Epoxides. *ChemSusChem* **2014**, *7* (12), 3268–3271. https://doi.org/10.1002/cssc.201402477.
(48) Liu, X. F.; Song, Q. W.; Zhang, S.; He, L. N. Hydrogen Bonding-Inspired Organocatalysts for CO2 Fixation with Epoxides to Cyclic Carbonates. *Catal. Today* **2016**, *263*, 69–74. https://doi.org/10.1016/j.cattod.2015.08.062.
(49) Lee, S. Do; Kim, B. M.; Kim, D. W.; Kim, M. Il; Roshan, K. R.; Kim, M. K.; Won, Y. S.; Park, D.

W. Synthesis of Cyclic Carbonate from Carbon Dioxide and Epoxides with Polystyrene-Supported Quaternized Ammonium Salt Catalysts. *Appl. Catal. A Gen.* **2014**, *486*, 69–76. https://doi.org/10.1016/j.apcata.2014.08.029.

(50) Zhao, X. S.; Bao, X. Y.; Guo, W.; Lee, F. Y. Immobilizing Catalysts on Porous Materials. *Mater. Today* **2006**, *9* (3), 32–39. https://doi.org/10.1016/S1369-7021(06)71388-8.

(51) Takahashi, T.; Watahiki, T.; Kitazume, S.; Yasuda, H.; Sakakura, T. Synergistic Hybrid Catalyst for Cyclic Carbonate Synthesis: Remarkable Acceleration Caused by Immobilization of Homogeneous Catalyst on Silica. *Chem. Commun.* **2006**, No. 15, 1664. https://doi.org/10.1039/b517140g.

(52) Sakai, T.; Tsutsumi, Y.; Ema, T. Highly Active and Robust Organic–Inorganic Hybrid Catalyst for the Synthesis of Cyclic Carbonates from Carbon Dioxide and Epoxides. *Green Chem.* **2008**, *10* (3), 337. https://doi.org/10.1039/b718321f.

(53) He, Q.; O'Brien, J. W.; Kitselman, K. A.; Tompkins, L. E.; Curtis, G. C. T.; Kerton, F. M. Synthesis of Cyclic Carbonates from CO2 and Epoxides Using Ionic Liquids and Related Catalysts Including Choline Chloride–Metal Halide Mixtures. *Catal. Sci. Technol.* **2014**, *4* (6), 1513–1528. https://doi.org/10.1039/C3CY00998J.

(54) Wang, X.; Wang, L.; Zhao, Y.; Kodama, K.; Hirose, T. Efficient and Practical Organocatalytic System for the Synthesis of Cyclic Carbonates from Carbon Dioxide and Epoxides: 3-Hydroxypyridine/Tetra-n-Butylammonium Iodide. *Tetrahedron* **2017**, *73* (8), 1190–1195. https://doi.org/10.1016/j.tet.2017.01.018.

(55) Sopeña, S.; Fiorani, G.; Martín, C.; Kleij, A. W. Highly Efficient Organocatalyzed Conversion of Oxiranes and CO2 into Organic Carbonates. *ChemSusChem* **2015**, *8* (19), 3179. https://doi.org/10.1002/cssc.201501195.

(56) North, M.; Villuendas, P. Influence of Support and Linker Parameters on the Activity of Silica-Supported Catalysts for Cyclic Carbonate Synthesis. *ChemCatChem* **2012**, *4* (6), 789–794. https://doi.org/10.1002/cctc.201200117.

(57) Chatelet, B.; Joucla, L.; Dutasta, J.-P.; Martinez, A.; Dufaud, V. Immobilization of a N-Substituted Azaphosphatrane in Nanopores of SBA-15 Silica for the Production of Cyclic Carbonates. *J. Mater. Chem. A* **2014**, *2* (34), 14164. https://doi.org/10.1039/C4TA01500B.

(58) Hajipour, A. R.; Heidari, Y.; Kozehgary, G. Silica-Grafted Basic Amino Acids as Environmentally Benign Catalysts for the Solventless Synthesis of Cyclic Carbonates from Epoxides and CO2 under Metal-Free and Halide-Free Conditions. *Synlett* **2016**, *27* (6), 929–933. https://doi.org/10.1055/s-0035-1561309.

(59) Amaral, A. J. R.; Coelho, J. F. J.; Serra, A. C. Synthesis of Bifunctional Cyclic Carbonates from CO2 Catalysed by Choline-Based Systems. *Tetrahedron Lett.* **2013**, *54* (40), 5518–5522. https://doi.org/10.1016/j.tetlet.2013.07.152.

(60) Deng, Q.; He, G.; Pan, Y.; Ruan, X.; Zheng, W.; Yan, X. Bis-Ammonium Immobilized Polystyrenes with Co-Catalyzing Functional End Groups as Efficient and Reusable Heterogeneous Catalysts for Synthesis of Cyclic Carbonate from CO2 and Epoxides. *RSC Adv.* **2016**, *6* (3), 2217–2224. https://doi.org/10.1039/C5RA23808K.

(61) Song, B.; Guo, L.; Zhang, R.; Zhao, X.; Gan, H.; Chen, C.; Chen, J.; Zhu, W.; Hou, Z. The Polymeric Quaternary Ammonium Salt Supported on Silica Gel as Catalyst for the Efficient Synthesis of Cyclic Carbonate. *J. CO2 Util.* **2014**, *6*, 62–68.

https://doi.org/10.1016/j.jcou.2014.03.005.
(62) Xiong, Y.; Bai, F.; Cui, Z.; Guo, N.; Wang, R. Cycloaddition Reaction of Carbon Dioxide to Epoxides Catalyzed by Polymer-Supported Quaternary Phosphonium Salts. *J. Chem.* **2013**, *2013*. https://doi.org/10.1155/2013/261378.
(63) Du, Y.; Cai, F.; Kong, D.-L.; He, L.-N. Organic Solvent-Free Process for the Synthesis of Propylene Carbonate from Supercritical Carbon Dioxide and Propylene Oxide Catalyzed by Insoluble Ion Exchange Resins. *Green Chem.* **2005**, *7* (7), 518. https://doi.org/10.1039/b500074b.
(64) Miao, C.-X.; Wang, J.-Q.; Wu, Y.; Du, Y.; He, L.-N. Bifunctional Metal-Salen Complexes as Efficient Catalysts for the Fixation of CO2 with Epoxides under Solvent-Free Conditions. *ChemSusChem* **2008**, *1* (3), 236–241. https://doi.org/10.1002/cssc.200700133.

CHAPTER 8 NOVEL POROUS ORGANOCATALYSTS FOR CYCLOADDITION OF CO_2 AND EPOXIDES

8.0. Overview

While immobilized ammonium salts prepared by grafting aminosilane onto porous silica (referred to as disordered mesoporous organosilicas - DMO) have been extensively studied for the synthesis of cyclic carbonates from CO_2 and epoxide, similar catalysts prepared directly by one-step co-condensation of an aminosilane/alkoxy-ammonium salt (referred to as ordered mesoporous organosilica - OMO) with TEOS, or polycondensation of organic bridged-silsesquioxane (referred to as periodic mesoporous organosilicas PMO) have received less attention. In this study, these three classes of organosilicas (DMO, OMOs and PMOs) containing immobilized multi-hydroxyl bis-(quaternary ammonium) iodide salts were prepared and tested in the cycloaddition of CO_2 and epoxides. Owing to its higher surface area, pore volume and optimum nucleophilicity of the iodide ion, OMO-2 with two hydroxyl groups was found to be the most active catalyst. For substrates that are easy to activate such as propylene oxide, 1,2-epoxybutane and epichlorohydrin, excellent yields and selectivity were obtained under mild reaction conditions (0.5 MPa CO2, 50 ^{o}C and 10 – 15 h). Moreover, OMO-2 showed very good catalytic properties (yield ≥ 93% and selectivity ≥ 98%), and excellent chemical and textural stability in the synthesis of 1,2-butylene carbonate over 5 cycles.

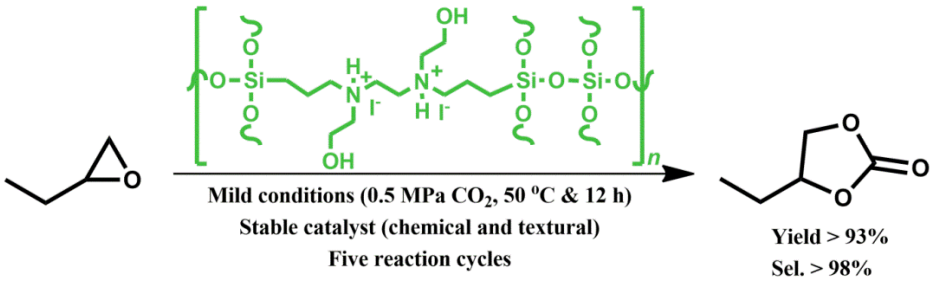

8.1. Introduction

Among greenhouse gases (GHGs), carbon dioxide (CO_2) is the main anthropogenic contributor to global warming and climate change.[1,2] Carbon capture is recognized as one of the most promising strategies to mitigate the adverse effects of CO_2 emissions.[3,4] Previously viewed largely as an industrial waste product, CO_2 is increasingly being valued as a cheap, readily available and non-toxic C1 source for the synthesis of chemicals and fuels.[5,6] Accordingly, CO_2 utilization is gaining popularity as a complementing tool to CO_2 capture and sequestration towards GHG mitigation. However, the inherent thermodynamic stability of CO_2 makes its less reactive with several molecules. As such, high CO_2 pressure and reaction temperature are generally required for its transformation. Nonetheless, combining CO_2 with highly reactive substrates such as epoxides and aziridines, in the presence of suitable catalysts, provides a pathway to overcome this energy barrier. The catalytic conversion of CO_2 and epoxides to cyclic carbonates (CCs) is one of many reactions using CO_2 as a reactant. Application of CCs as aprotic polar solvents, active pharmaceutical ingredients, and monomers in the production of fine chemicals makes them an important group of organic materials in the chemical industry. In the generalized mechanism for the synthesis of CCs, regioselective CO_2 insertion is achieved by a combination of epoxide activation by Y through oxygen atom coordination and ring-opening by a nucleophile, X^- (Scheme 8-1).

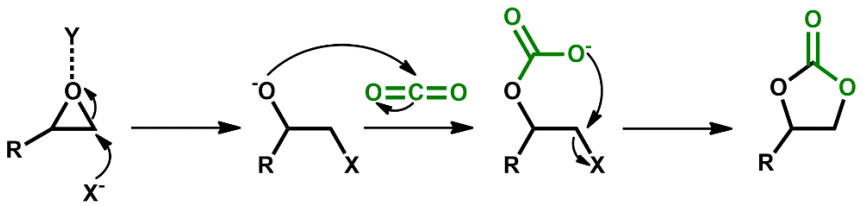

Scheme 8-1. Synthesis of cyclic carbonate from epoxide and CO_2

A variety of homogeneous catalysts such as ionic liquids[7] and metal complexes[8], immobilized catalysts including supported ionic liquids[7], and traditional heterogeneous catalysts[9] were reported to be active towards CO_2 cycloaddition. On their own, the last group of catalysts showed low reactivity, and as such received less attention compared to free and immobilized homogeneous catalysts. The latter may consist of a single catalytic component, or a combination of a catalyst and a co-catalyst.[8] Examples of one-component catalysts include tributylpropylammonium iodide immobilized on silica[10], quaternary ammonium[11] and phosphonium[12] salts. Two-component catalysts include benzyl bromide/DMF[13], tetrabutylammonium salt/ EDTA[14], and polymer-supported quaternary onium salts/aqueous solutions of metal salts.[15] These catalysts are not highly popular as they increase the complexity of the process, leading to tedious catalyst separation/recovery and product purification steps. Accordingly, to achieve simplified and cost-effective chemical processes, one-component catalysts are preferred.

One-component catalysts can be mono- or bifunctional in nature. Mono-functional catalysts such as alkyl quaternary ammonium[16] or phosphonium[17] halides play a single role, which consists of opening the epoxide ring, leading to the insertion of CO_2. These extensively investigated catalysts were found to exhibit good to excellent yields in the cycloaddition of CO_2 and epoxides.[18,19] Moreover, one-component bifuntional homogeneous or immobilized catalysts may contain specific functional groups, such as –COOH, $–NH_2$ and –OH or metals (e.g. Zn, Co and Al). Bifunctionality implies that the catalytic material plays two roles in the course of the reaction, namely; *(1)* activation of the epoxide by the functional groups,[20] rendering it more susceptible to undergo cycloaddition – Y in Scheme 1, and *(2)* opening of the epoxide ring by the halide ion[21],

similar to the mono-functional catalysts, X^- in Scheme 1. The above functional groups activate the epoxides via hydrogen bonding, while epoxide activation by metal occurs through the formation of metal alkoxides via Lewis acid interactions.[22,23] Examples of metal-free one-component bifunctional catalysts include free and supported hydroxylalkyl ammonium salts[11] or phosphonium[17] salts. Regardless of the design, type or functionality of the catalyst, the ring opening of all epoxides requires a nucleophile. The iodide ion was reported as one of the most efficient owing to its exceptional leaving group ability, stemming from its bulky nature and lower electronegativity.

In terms of sustainable and low-cost processes, highly active metal-free one-component bifunctional catalysts with stable active sites and easy reusability are attractive. Many such catalysts, covalently anchored onto a variety of solid materials were reported in the literature.[24] In some cases, these hybrid solids demonstrate similar or even better activities compared to their homogeneous counterparts.[17,25] Porous inorganic solids such as mesoporous SBA-15 silica [26,27] were used as supports for one-component porous hybrid solid (PHS) catalysts for the synthesis of cyclic carbonates. Compared to organic supports such as polystyrene, they offer better thermal and mechanical stability, enhanced chemical interaction between the support and the active organic species and high loading of active sites, thereby enhancing production. Moreover, mesoporous inorganic supports alleviate molecular traffic within the pore system, which could enhance both the rate and selectivity of the reaction.

The main preparation method for PHS entails post-synthesis surface functionalization of a silica; typically through grafting of an aminosilane or phosphine-silane, followed by quaternization to afford an immobilized quaternary ammonium or phosphonium salt - Scheme

8-2a. Often, such organosilicas consist of a disordered distribution of the organic moieties; hence these solids may be referred to as disordered mesoporous organosilicas (DMO). Alternatively, the co-condensation of a silica network former (e.g. TEOS or TMOS) and an organosilica precursor (organotrialkoxysilanes, bridged- or poly-silsesquioxanes) over a structure directing agent is a one-pot synthesis method to obtain ordered mesoporous organosilicas (OMOs) - Scheme 8-2b. Furthermore, a distinctive group of mesoporous organocatalysts, with a unique homogeneous distribution and high loading of covalently linked organic functionalities within the silica framework are periodic mesoporous organosilicas (PMOs). These materials are derived from the hydrolytic sol–gel polycondensation of organic bridged-silsesquioxanes ($R[Si(OR')_3]_n$; $n \geq 2$) in the presence of surfactant templates without addition of silica precursors - Scheme 8-2c.

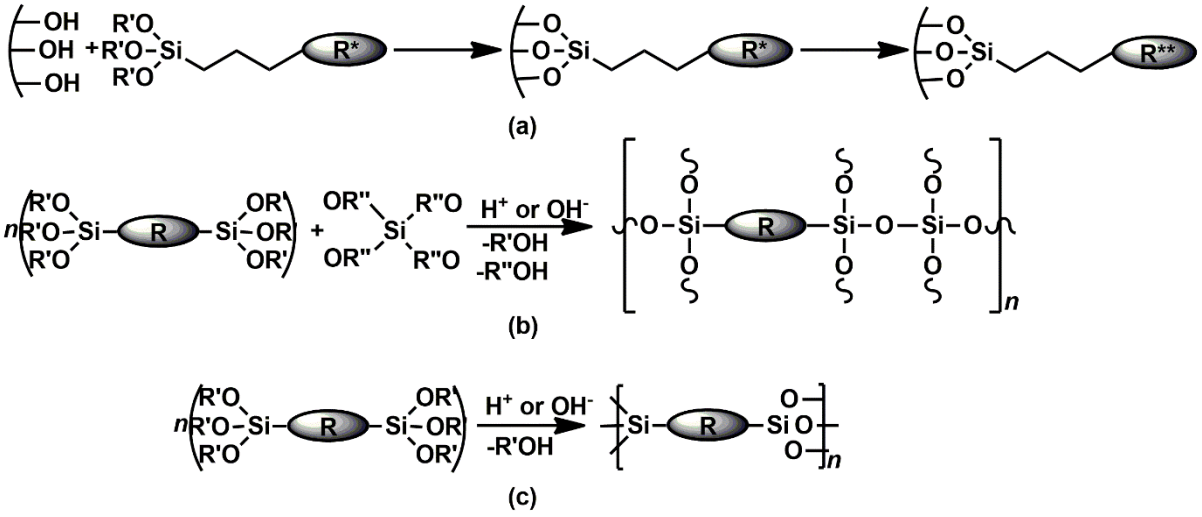

Scheme 8-2. Synthesis of (a) DMO via surface grafting and quaternization (b) OMO via the co-condensation route (c) periodic mesoporous organosilicas – PMO

Significant progress in the synthesis of CCs from CO_2 and epoxides over mesoporous organocatalysts derived by the grafting of aminosilane followed by quaternization (Scheme 8-2a) has been reported in a number of reviews.[7,28] Although OMOs containing ammonium halides[29,30],

and PMOs containing melamine[31] and urea[32] moieties were reported as active catalysts in the synthesis of CCs, OMOs and PMOs received noticeably less attention compared to DMOs. Considering the higher surface area of OMOs compared to DMOs, and the significantly higher organic content achievable with PMOs, organocatalysts with greater surface area and active sites can be obtained from OMOs and PMOs respectively. If such active sites can be readily accessed, a significant enhancement in catalytic performance (i.e. higher reaction rates, selectivity and yield) can be expected. In addition, higher active site density is expected to enhance catalytic activity. In this sense, homogeneous[33] and heterogeneous[34] organocatalysts containing two active sites per molecule were found to be more effective than those containing only one. Although immobilized catalysts with multiple active sites and OH groups may be beneficial, too many of these sites may be detrimental to the activity of the catalyst. In this chapter, we present four groups of novel immobilized multi-hydroxyl bis-(quaternary ammonium) salts prepared via three routes: *(1)* grafting of a bridged-SQ on silicas, followed by quaternization, *(2)* co-condensation of *(i)* bridged-SQ and *(ii)* poly-SQ with TEOS, and *(3)* PMOs derived from *(i)* bridge-SQ and *(ii)* poly-SQ. Furthermore, their activity in the synthesis of CCs from CO_2 and epoxides under mild reaction conditions was discussed. The reusability of the most active catalyst was also investigated to better understand the catalyst performance (yield and selectivity), chemical stability (resistance to leaching) and structural stability (textural properties) with reuse.

8.2. Experimental

Materials

N,N'-bis(2-hydroxyethyl)-*N,N*'-bis(trimethoxysilylpropyl)ethylenediamine - BHBPD (66-68% in methanol) was purchased from Gelest. Chromatography grade silica gel mesh 230-400

(hereafter referred to as SiL), 2-iodoethanol (99%), ammonium iodide (99.5%), P123 (average M_n ~ 5,800), tetraethyl orthosilicate - TEOS (98%), 3-chloropropyltrimethoxysilane - 3CPTS (97%), styrene oxide (97%), propylene oxide - PO (99%), 1,2-epoxybutane - 1,2-EB (99%), epichlorohydrin (99%), cyclohexene oxide - CHO (98%), 3-glycidoxypropyltrimethoxysilane (GPS), triethylamine - TEA (99%) and KCl (99%) were purchased from Sigma Aldrich. Ethyl acetate (99.9%), diethyl ether -Et_2O (99.8%), ethanol (99%), methanol (99%), hydrochloric acid (37%) and toluene (99 %) were obtained from Fisher. P-10 and Q-10 mesoporous silica supports were donated by Fuji Silysia Chemical Ltd. Chloroform-D was obtained from Cambridge Isotope Laboratories. All chemicals were used as obtained with no further purification. Carbon dioxide (99.998%) was obtained from Linde AG.

8.2.1. Preparation of Mesoporous Organosilica Materials

8.2.1.1. Method A: preparation of DMOs via grafting and quaternization of amine

Three commercial grade silicas (Q-10, P-10 and SiL) and SBA-15 silica were used as supports. SBA-15 was prepared using an established procedure.[35] Grafting was carried out in toluene in the presence of water. Our group previously demonstrated that addition of water improves both the quality and loading of grafted amine on MCM-41.[36] Based on literature reports,[37] it is possible to estimate the amount of water required to obtain a fully hydroxylated silica surface. This can be achieved by considering the maximum number of surface silanol groups to be 5 x 1018 Siu per m^2, and by introducing twice as many water molecules/m^2.[38] Accordingly, for a typical silica with a surface area of 300 m^2/g, the volume of water to be added is approximately 0.1 mL/g.

A typical procedure for grafting was as follows; 1 g of thermally pretreated (at 130 ^{o}C for 4 h) silica was dispersed in 30 mL of toluene at room temperature, followed by addition of an appropriate volume of water; 0.1 mL for Q-10 and P-10, 0.15 mL for SiL, and 0.3 mL for SBA-15. The temperature of the mixture was raised to 85 ^{o}C and further stirred for 30 min. Finally, 2 mL of BHBPD was added and the resultant mixture was refluxed at 85 ^{o}C for 16 h in an oil bath. The grafted materials were then filtered, washed with toluene, methanol, then Et_2O, and dried under vacuum at 60 ^{o}C for 4 h. The obtained solids are hereafter referred to as S@amine, where S indicates the support. The amine-grafted solids were then quaternized as follows: 1 g of material was dispersed in 15 mL of toluene, followed by addition of 2 mL of 2-iodoethanol under a nitrogen atmosphere. The reaction mixture was kept under reflux at 70 ^{o}C for 3 days. The obtained solids were filtered off, washed with toluene, methanol, then Et_2O, and dried at 70 ^{o}C under vacuum for 4 h to yield pale yellow powder materials of immobilized diammonium iodide salt. The obtained solids are hereafter referred to as DMO-Q10, DMO-P10, DMO-SiL and DMO-SBA15 after the corresponding S@amine. The synthesis of amine-grafted materials and their quaternized counterparts is represented in Scheme 8-3, with Q-10 as silica support.

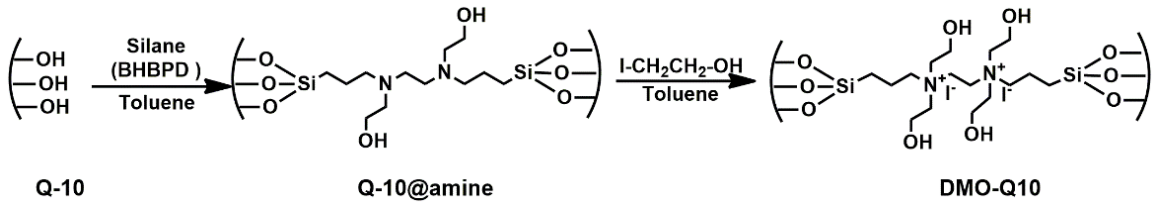

Scheme 8-3. Synthesis of Q-10@amine and DMO-Q10 via grafting and quaternization

8.2.1.2. Method B: Preparation of OMOs via co-condensation of BHBPD or poly-SQ salt and TEOS:

The synthesis of all porous organosilicas by hydrolysis and condensation with a silica precursor was performed in the presence of a neutral surfactant (P123) under acidic conditions. In a typical procedure, 2.0 g of triblock copolymer P123 and 2 g of KCl were dissolved in a mixture of 30 g distilled water and 60 g of 2M HCl solution in a 250 mL teflon-liner at 40 ^{o}C. Notice that the use of KCl was shown to enhance ordering of mesoporous organosilicas.[39] To this solution, 4.3 g of TEOS was added and the mixture stirred for 1 h to ensure the pre-hydrolysis of TEOS. Thereafter, 2 mL (2.83 mmol) of BHBPD, corresponding to a nominal amine loading of 2.0 mmol per gram of silica, was slowly added under stirring. The resultant mixture was further stirred at 40 ^{o}C for 20 h. Finally, the mixture was transferred into an autoclave and heated at 100 ^{o}C under static condition for 2 days. The solid products were collected by filtration, washed with water, and dried at ambient conditions. The surfactant was removed by refluxing in 100 mL of a 98:2 v/v % ratio of ethanol: conc. HCl mixture at 60 ^{o}C for 6 h. The powder material was collected by filtration, washed with ethanol, and dried at ambient conditions. A similar preparation, but without BHBPD, was carried out for SBA-15 silica, herein referred to as SBA-15*. To make sure all P123 has been removed, 1 g of the solid ethanol-extracted material was subjected to additional soxhlet extraction with 100 mL of methanol at 70 ^{o}C for 16 h. The obtained solid was dried overnight in ambient condition, then at 60 ^{o}C under vacuum for 4 h.

An off-white powder material, hereafter referred to as OMO-1, was obtained from the co-condensation of TEOS and BHBPD. Because of the acidic conditions, OMO-1 was actually in the form of a quaternary ammonium chloride salt. OMO-1 was subjected to; *(1)* ion-exchange

with ammonium iodide to obtain the corresponding ammonium iodide salt – OMO-2 and *(2)* dequaternization, regenerate the amine – OMO-3. To obtain a QAS with additional –OH groups, OMO-3 was quaternized with 2-iodoethanol to afford OMO-4. The structures of OMO-(1-4) are represented in Scheme 8-4.

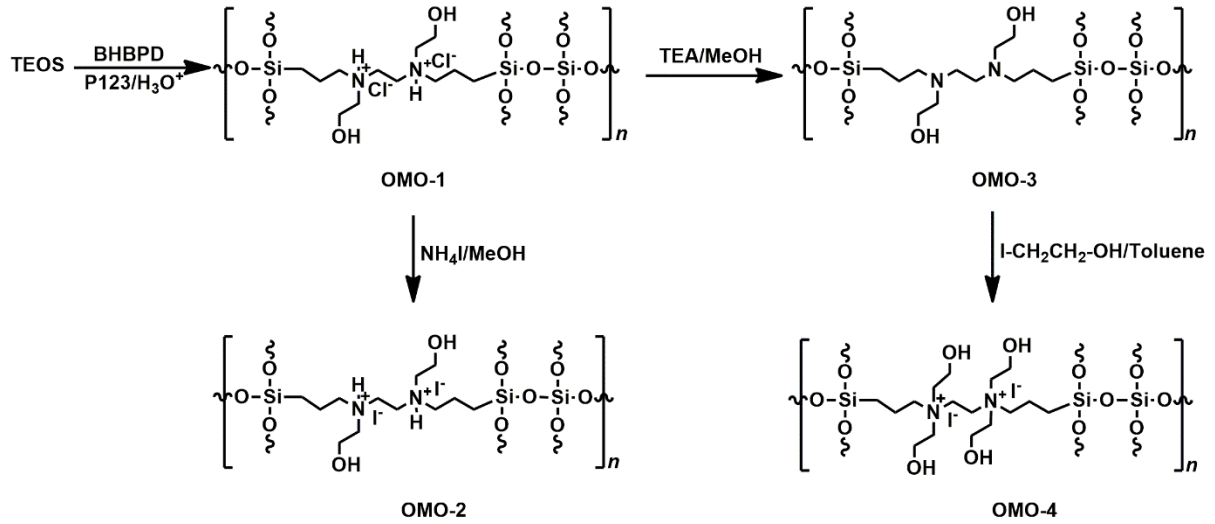

Scheme 8-4. Synthesis of OMO-1 to OMO-4 via co-condensation followed by ion-exchange or quaternization

Ion-exchange was carried out as follows; 1 g of OMO-1 was dissolved in 30 mL of methanol followed by addition of 1 mL of ammonium iodide under a nitrogen atmosphere. The mixture was refluxed at 65 ^{o}C for 16 h. The resultant solid was recovered by filtration, washed with methanol, then Et_2O and dried under vacuum at 70 ^{o}C for 4 h to afford a yellow powder (OMO-2). To regenerate the amine from OMO-1, 1 g of material was dispersed in 50 mL of ethanol, followed by the addition of 1 mL of triethylamine. After reflux at 60 ^{o}C for 2 h, the solid was recovered by hot-filtration and washed with boiling ethanol, then dried at 60 ^{o}C under vacuum for 4 h to afford an off-white powder material - OMO-3. OMO-3 was quaternized as described in method A to afford a yellow powder - OMO-4.

The preparation of OMOs from BHBPD-derived salt involves two steps; the synthesis of the salt, hereafter referred to as poly-SQ salt, followed by its co-condensation with TEOS. The poly-SQ salt was synthesized as follows; to a 25 mL two-neck round bottom flask containing 10 mL of toluene, 2 mL (2.83 mmol) of BHBPD was added. Under a nitrogen atmosphere, 2.0 equivalent of 3-chloropropyltrimethoxysilane was added. The reaction flask was sealed under nitrogen and refluxed at 85 ^{o}C for 24 h. Toluene and unreacted reagents were removed under reduced pressure at 90 ^{o}C to afford a brownish-yellow liquid. The procedure for the co-condensation of the poly-SQ salt and TEOS was similar to that of BHBPD and TEOS (OMO-1). An amount of poly-SQ salt was added to a pre-hydrolyzed TEOS solution with a nominal amine loading of 2.0 mmol per gram of silica. The template was extracted as described for OMO-1 to afford a light grey solid denoted OMO-5. Ion-exchange of OMO-5 with ammonium iodide (as described for OMO-1) produced a yellow solid, OMO-6 (Scheme 8-5).

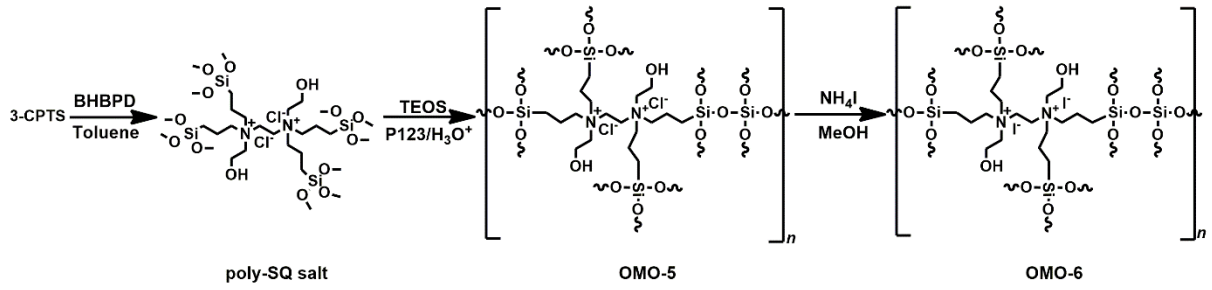

Scheme 8-5. Synthesis of poly-SQ salt and OMO-5 and OMO-6 via co-condensation followed by ion-exchange

8.2.1.3. Method C: Synthesis of PMOs via condensation of BHBPD and poly-SQ salt:

To an aqueous solution of P123, prepared as described in method B, 2 mL of BHBPD or 2.8 mL of poly-SQ salt was added slowly under stirring. The resultant mixture was further stirred at 40 ^{o}C for 20 h, and the mixture was transferred into an autoclave and heated at 100 ^{o}C under static condition for 2 days. The solid products were collected by filtration, washed with water, and dried at ambient conditions. Surfactant extraction, ion-exchange, dequaternization and quaternization were carried out on the resultant solid as described for OMO-1. All PMOs are represented in Scheme 8-6. PMO-1 and PMO-3 were obtained as off-white solids; PMO-5 was light-grey; and PMO-2, PMO-4 and PMO-6 were yellow powder materials.

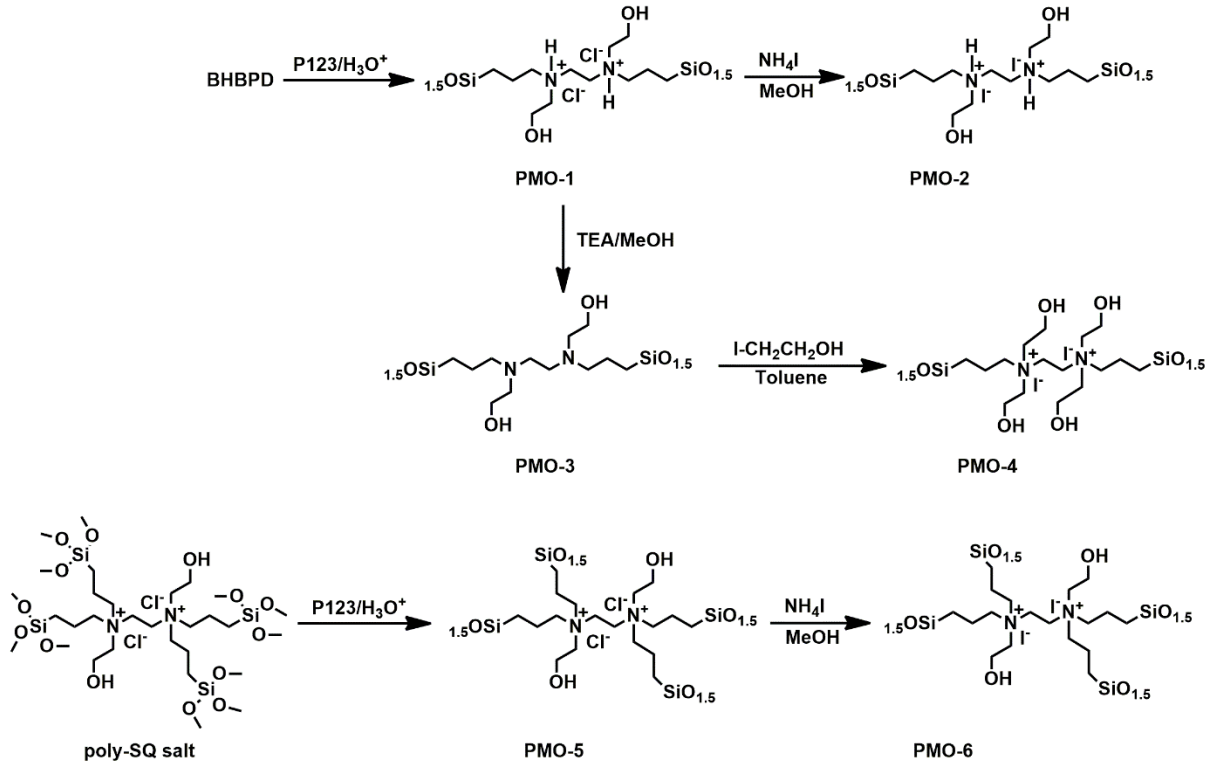

Scheme 8-6. Synthesis of PMOs via condensation of *(top)* BHBPD, and *(bottom)* poly-SQ salt

8.2.2. Characterization of materials

8.2.2.1. Textural properties and organic content

The specific surface area, pore volume and mean pore diameter of all materials were determined by nitrogen adsorption-desorption measurements at −196 °C on a Micromeritics 2020 instrument, as reported earlier.[10] Samples were degassed under nitrogen for 4 h at 120 ^{o}C prior to analysis. Specific surface areas were calculated using the BET method at relative pressures of 0.06 to 0.2. The total pore volume (Vp) was recorded at p/p0 = 0.99 to exclude possible interparticle pores. The average pore size (Dp) was determined using the density functional theory.

The organic or nitrogen content (N-content) of all organosilicas was determined using thermogravimetric analysis (TGA) on a TA Q500 instrument. Sample were heated to 120 ^{o}C at 10 ^{o}C min^{-1} under flowing nitrogen and held for 30 min, to ensure the removal of physisorbed species (e.g. water and solvents). Then the temperature was raised to 800 °C under flowing nitrogen, then air at 800 ^{o}C for 10 min. The organic content was calculated based on the weight loss beyond 200 ^{o}C.

8.2.2.2. IR spectroscopy

To identity the incorporated organic species, ATR-IR measurements were recorded on a Nicolet 6700 spectrometer equipped with a liquid N_2-cooled MTC-A (mercury–tellurium–cadmium) detector and a Fisher Scientific horizontal ATR unit with a ZnSe crystal. For this, a few mg of powder sample was homogeneously spread onto the surface of the ATR crystal, and the IR spectra were recorded from 600 to 4000 cm^{-1} at a resolution of 2 cm^{-1} using 128 scans. For each

scanning, the spectrum was collected by subtracting air (background) spectrum from the original spectrum. All ATR-FTIR experiments were run in triplicate to ensure the reproducibility of the results, and average wavenumbers are reported herein.

8.2.2.3. ^{13}C and ^{29}Si solid state and solution NMR

Solid-state NMR spectra were collected at room temperature using an AVANCE III 200 MHz spectrometer equipped with a MAS probe. The spectra were recorded using cross polarization with high power decoupling, with samples spinning at 4.5 kHz. The number of scans was in the range of 6000 – 8000. The contact time and recycling delays were set at 10 ms and 2 s for ^{13}C NMR respectively. For ^{29}Si NMR, the contact time and recycling delays were set at 2 ms and 1.5 s.

For solution NMR measurements, ^{13}C and ^{1}H NMR spectra were obtained using a Bruker AV 400 MHz spectrometer. Chemical shifts are reported in ppm relative to deuterated chloroform.

Where separation was needed to isolate the cyclic carbonate prior to NMR analysis, silica gel flash chromatography was used with a 3:1 ethylacetate:ether mixture as solvent.

8.2.3. Cycloaddition reaction

Catalytic activity was evaluated using the model reaction in Scheme 8-7. The reaction conditions were chosen such that the reaction was significantly away from total conversion; enabling a meaningful comparison of catalytic activity and stability. In a typical procedure, a 100 mL high pressure autoclave equipped with a magnetic stirrer was charged with 2 mL (17 mmol) of styrene epoxide (SO) and 2 mol% of catalyst (DMO, OMO or PMO). The reactor was directly pressurized with CO_2 to 0.5 MPa and heated to 50 ^{o}C under stirring for 5 h.

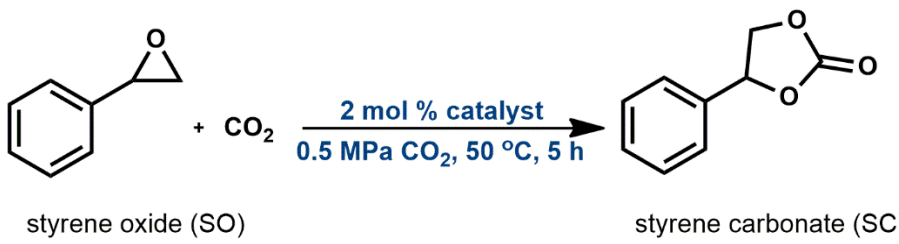

Scheme 8-7. Model cycloaddition reaction

At the end of the reaction, the reactor was cooled with an ice bath to ≤ 15 °C and CO_2 was released slowly. Then, 50 µL of dodecane (internal standard for GC analysis) was added to the reaction mixture, which was then suspended in diethyl ether and filtered off to recover the catalyst. After removal of all volatiles using a rotavap, a solvent-free reaction mixture was obtained. The spent catalyst was further stirred in acetone for 30 min, filtered off and dried in a vacuum oven at 70 °C for 2 h. TG analysis and nitrogen adsorption–desorption measurements were carried out on all spent catalysts to determine variations in N-content and textural properties.

Analysis of reaction mixture: About 0.2 µL of the solvent-free reaction mixture was injected into a Varian CP-3800 GC equipped with Agilent J&W VF-1ms capillary column (15 m length, 0.25 mm inner diameter and 0.25 µm film thickness) and a flame ionization detector (FID); with helium as carrier gas. The temperature program used for analysis was as follows: initial oven temperature 80 °C (1.5 min); ramp at 30 °C/min and held at 250 °C (3 min); injector port temperature: 200 °C; detector temperature: 250 °C. For solid reaction mixtures, 0.1 g of the mixture was dissolved in 0.2 mL of toluene, and 0.2 µL of this solution was injected into the GC.

^{13}C and ^{1}H NMR spectra of liquid samples were obtained using a Bruker AV 400 MHz spectrometer with tetramethylsilane as the internal standard. Chemical shifts are reported in ppm relative to deuterated chloroform.

8.3. Results and discussion

8.3.1. Characterization of mesoporous organosilicas

As shown in Figure 8-1 (and Figure A8- 1 – supplementary data for chapter 8), the nitrogen adsorption–desorption isotherms for the support and organosilica materials were of Type IV with H1 hysteresis loop, characteristic of solids with mesopores. The corresponding textural properties and organic content are presented in Table 8-1. The TGA profiles of these materials may be found in Figure 8-2. Compared to their pure silica, all organosilica materials derived by grafting, i.e. DMOs, had lower BET surface areas and pore volumes (Table 8-1, entries 1-8) – an indication of immobilization of organic species within the internal surface. The SBA-15 support obtained by template extraction in EtOH/HCl solution had a higher surface area and pore volume compared to that derived by calcination (Table 8-1, entry 5 vs. 9). Although thermal calcination in air can completely remove the organic template, it may however cause significant framework shrinkage stemming from further silica condensation. On the other hand, template removal by solvent extraction minimizes framework shrinkage, leading to higher surface area, pore volume and number of silanols compared to its calcined counterpart.[40,41]

The capillary condensation of all DMOs and OMOs was observed to be less sharp compared to their corresponding supports and SBA-15*, respectively; an indication of decreased pore size. This provided further evidence that immobilization of the organic moieties took place on the internal surface of the supports. Compared to DMOs and OMOs, all PMOs had significantly

lower surface areas, while their pore volumes were also lower than the corresponding OMOs (Table 8-1, entries 10 vs. 13, 11 vs. 14 and 12 vs. 15).

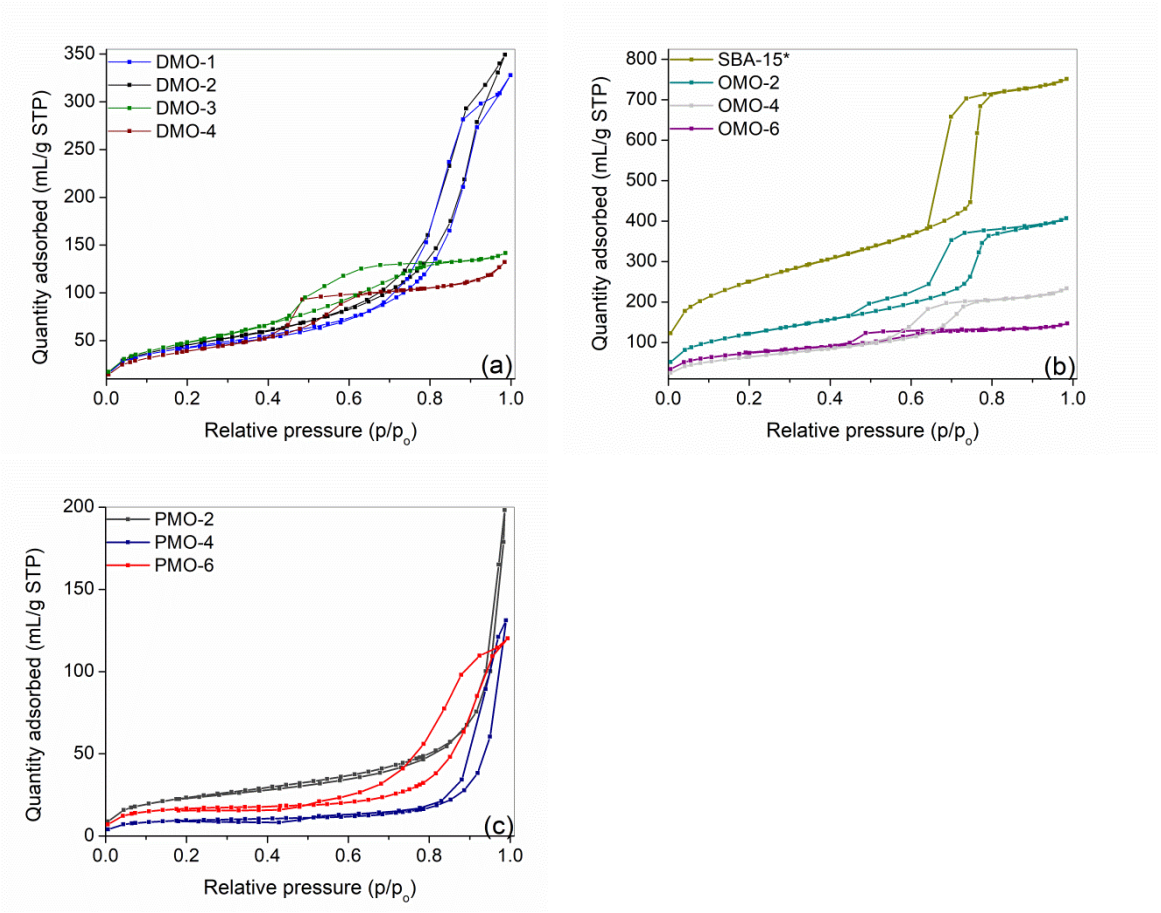

Figure 8-1. Nitrogen adsorption–desorption isotherms of pristine and functionalized supports

Table 8-1. Textural properties of solid materials

Entry	Material	Specific S.A. (m^2/g)	Vp (mL/g)	Dp (nm)	N-content (mmol/g)
1	Q-10	316	1.34	18.2	-
2	DMO-Q10	160	0.48	11.9	1.26
3	P-10	327	1.53	21.2	-
4	DMO-P10	170	0.54	12.0	1.22
5	SiL	478	0.83	9.2	-
6	DMO-SiL	182	0.22	4.6	1.37
7	SBA-15	763	1.07	7.2	-
8	DMO-SBA15	146	0.21	5.1	1.41
9	SBA-15*	913	1.23	6.18	-
10	OMO-2	449	0.66	6.0	1.22
11	OMO-4	241	0.37	5.8	1.29
12	OMO-6	270	0.22	4.1	1.22
13	PMO-2	86	0.31	15.7	2.38
14	PMO-4	34	0.20	30	2.37
15	PMO-6	60	0.18	16.7	2.11

Moreover, PMOs showed a broad pore size distribution (Figure A8- 2). This finding may be attributed to the higher organic content of PMOs, which adversely affects their textural properties.

Similar organic contents were measured for all amine functionalized supports and DMOs (Figure 8-2a). The calculated organic content of Q-10@amine, P-10@amine, SiL@amine and SBA-15@amine were 1.59, 1.70, 1.64 and 1.80 mmol/g respectively – accounting for a grafting efficiency between 80 and 90 %. This finding illustrates that despite the smaller surface areas of P-10 and Q-10 silicas compared to SiL and SBA-15, their larger pore volume and pore diameter enabled them to accommodate as much BHBPDs as SiL and SBA-15.

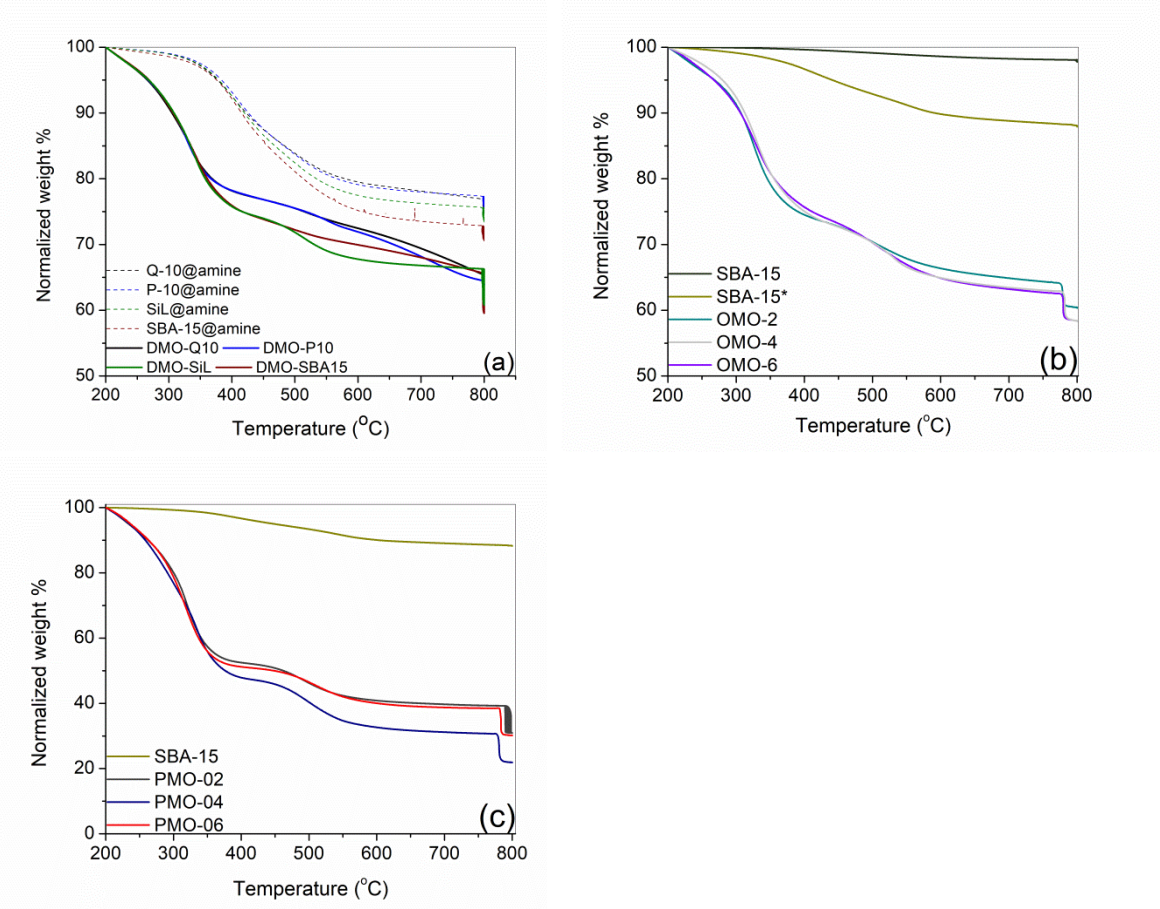

Figure 8-2. TGA profile of (a) amine-functionalized supports and DMOs, (b) OMOs and (c) PMOs

The N-content per gram of silica support for both S@amine solids and DMOs being the same, the yield of the quaternization reactions was evaluated to be between 92 and 97 %. This finding confirms the structure of DMOs, i.e. as immobilized symmetrical diammonium salts. The weight lost below 200 °C of SBA-15 was < 2% compared to ca. 10% for SBA-15* (Figure 8-2b), suggesting the presence of some P123 surfactant (*vide infra*). It is known that template removal via solvent extraction does not completely remove the surfactant[42]. Hence, the N-content of all OMOs and PMOs was obtained taking into account the presence of about 8 wt% of surfactant. Relatively

higher organic content, up to 80 wt%, was obtained for PMOs compared to DMOs and OMOs (Figure 8-2c).

The ^{13}C NMR of amine@Q-10 and DMO-Q10 showed peaks around 10, 17, 51, 56, 58 and 62 ppm, which were assigned to the five carbon nuclei of BHBPD as illustrated in Figure 8-3a. As-synthesized SBA-15 exhibited resonances attributed to $–CH_2–CH–$ (76 and 74 ppm) and $–CH_3$ (18 ppm) groups of the PPO, and $–CH_2–$ (71 ppm) of the PEO block of P123.[43] Following template removal by solvent extraction, ^{13}C NMR of the resultant material, SBA-15*, showed very low intensity signals between 71 and 75 ppm, and the complete disappearance of the signal at 18 ppm. Moreover, signals at 16, 50 and 59 ppm were assigned to trapped methanol and ethanol molecules used during template removal (the ^{13}C MAS NMR spectra of as-SBA-15 and SBA-15* are compared in Figure A8- 3). Hence, the 8 wt% organic content of SBA-15*, as determined by TGA was assigned to the presence of small amount of template. As with DMOs, five carbon nuclei could be identified in the ^{13}C NMR of all OMOs (Figure 8-3b) and PMOs (Figure 8-3c).

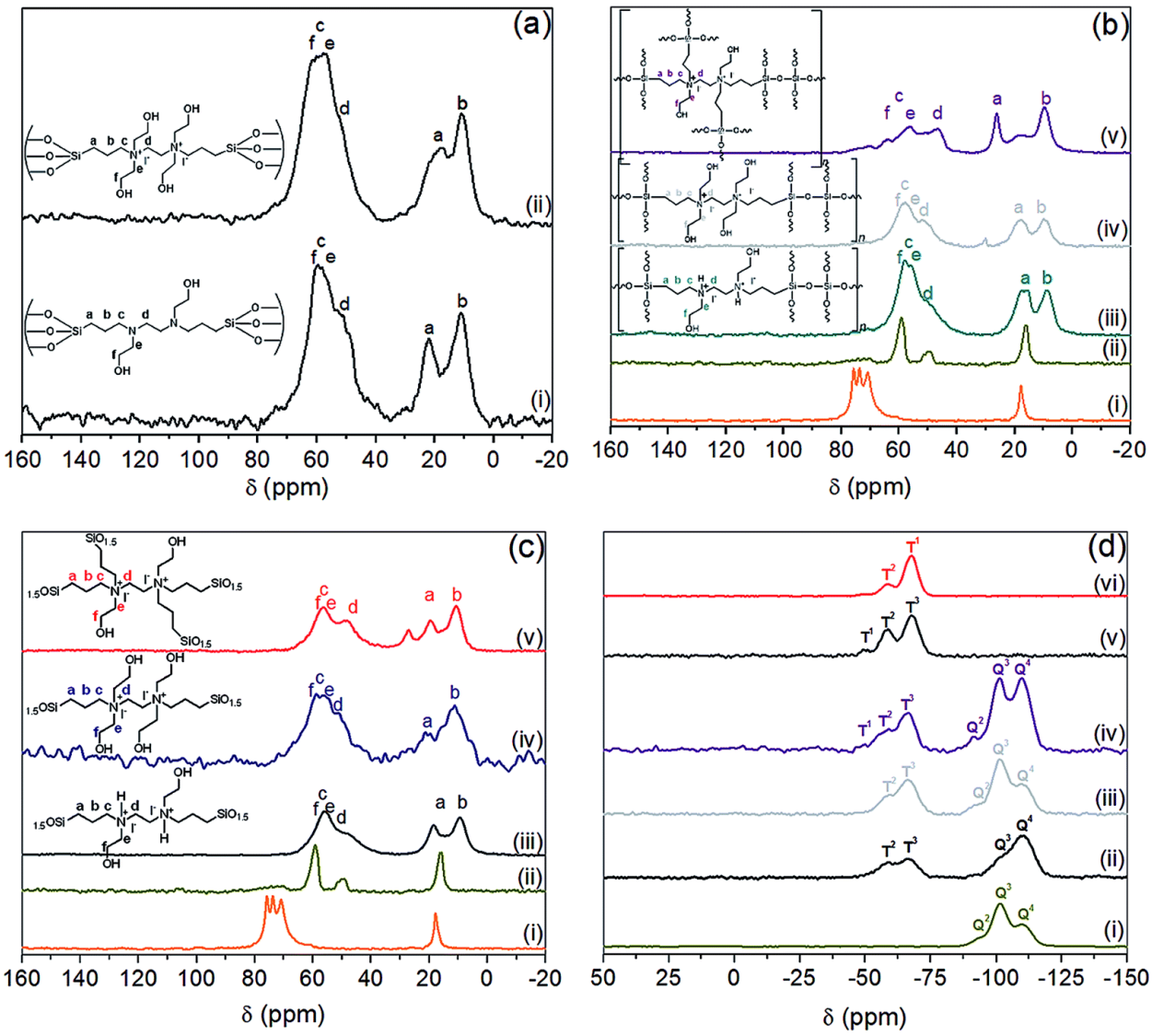

Figure 8-3. ^{13}C CP-MAS NMR spectra of (a) i – Q10@amine, ii – DMO-Q10: (b) i – as-synthesized SBA-15, ii – SBA-15*, iii – OMO-2, iv – OMO-4, v – OMO-6: (c) i – as-synthesized SBA-15, ii – SBA-15*, iii – PMO-2, iv – PMO-4, v – PMO-5 and (d) ^{29}Si MAS NMR of; i – SBA-15*, ii – OMO -2, iii – OMO-4, iv – OMO-6, v – PMO-2, vi – PMO-6

The ^{29}Si CP MAS NMR spectra showed only Q^n species for SBA-15*, Q^n and T^n for DMOs and PMOs, and only T^n for PMOs (Figure 8-3d). The characteristic resonances in the range of -89 to -118 ppm were ascribed to Q^n units, with the peaks at about -97, -102.1 and -110.9 ppm corresponding to Q^2 [$Si(HO)_2(OSi)_2$], Q^3 [$Si(HO)(OSi)_3$] and Q^4[$Si(OSi)_4$] species, respectively (Figure 8-3d(i)). All

DMOs, OMOs and PMOs showed two intense signals at ca. −58 and −66 ppm, attributed to Si-species covalently bonded to carbon atoms, namely T^2 [C-*Si*(OH)$(OSi)_2$] and T^3 [C-*Si*$(OSi)_3$] respectively (Figure 8-3d(i) – (iv)).[44] These signals arise from immobilization of BHBPD onto the silica surface and framework of silica for DMOs and OMOs/PMOs, respectively. Furthermore, for some OMOs and PMOs, a weak shoulder at ca. 50 ppm, attributed to T^1 [C-*Si*$(OH)_2$(OSi)] species was also observed. The presence of T^1 and T^2-signals is an indication that the condensation process was not complete for these materials. Hence, the calculated nitrogen content based on TGA results, which assumes 100 % condensation, may be slightly overestimated.

All materials showed IR absorption bands (Figure 8-4 and Figure A8- 4 - supplementary data for chapter 8) at approximately 640, 800 and 1080 cm^{-1}, which were attributed to Si-O-Si bonds of the silicate network. The broad band centered at ca. 3320 or 3440 cm^{-1} was assigned to the O–H stretching vibrations of silanol groups, hydroxyl groups of BHBPD and/or adsorbed water. A band at 1650 cm^{-1} confirmed the presence of adsorbed water, whose physisorption was enhanced by the ionic nature of the -N-I bond. Furthermore, the spectra of all organosilica materials showed $–CH_2–$ stretching vibrations of the propyl chain characterized by weak absorbance at ca. 3030 and 2980 cm^{-1}, $–CH_2–$ bending at 1550 cm^{-1} and C-N stretching at 1450 cm^{-1}.[45] These findings are consistent with the presence of BHBPD on the silica supports. The absence of a band at 960 cm^{-1} suggests that the amount of uncondensed Si-OH groups was minimal; which is in agreement with ^{29}Si MAS NMR data. It is worth noting that bands at slightly different wavenumbers were observed for PMOs and OMOs/DMOs, suggesting differences in the chemical environment between these two groups of materials.

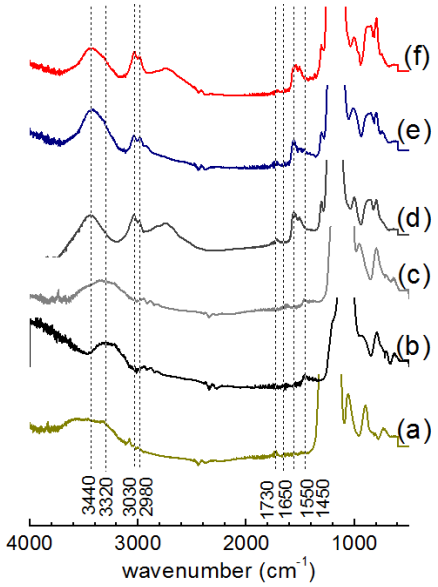

Figure 8-4. IR adsorption spectra of (a) SBA-15, (b) DMO-1, (c) OMO-4, (d) PMO-2, (e) PMO-4 and (f) PMO-6

8.3.2. Catalytic activity

8.3.2.1. Comparative analysis

The catalytic activity of iodide-containing organosilicas was evaluated using the cycloaddition of CO_2 and styrene oxide (SO) to styrene carbonate (SC) under neat conditions. Because of its low activity, SO provides a more meaningful comparison than a highly active epoxide such as 1,2-epoxybutane (1,2-EB). It is worth mentioning that even trace amount of water may lead to the formation of corresponding diol as side product, alongside minor amounts of the carbonyl isomers of the epoxide. The effect of temperature, time and CO_2 pressure on the selectivity and yield and is presented in Table 8-2, entries 1-11. At 100 ^{o}C, 4 h and 1 MPa CO_2, yields and selectivity ≥ 97 % were obtained (Table 8-2, entry 1) with DMO-SiL as catalysts. In an earlier study, we reported similar findings in the presence of N,N,N-tributyl-N-propylammonium iodide-functionalized mesoporous silicas.[10] These results are in agreement with other reports

where immobilized ammonium[46] and phosphonium[17] salts were used. To obtain yields significantly below 100 %, the following mild conditions were; 50 ^{o}C, 5 h and 0.5 MPa CO_2. As seen in Table 8-2, entries 2 – 11, conversion was found to be < 50 % for all catalysts.

Table 8-2. A comparison of the catalytic performance of different organosilica materials

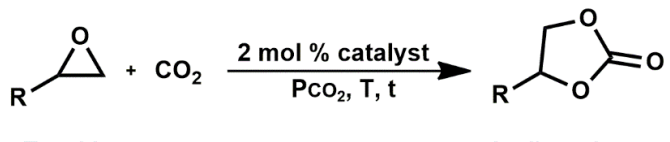

Entry	Catalyst		Reaction condition			Quantification		Spent cat.
	Type	N-content (mmol/g)	T (^{o}C)	t (h)	P_{CO_2} (MPa)	Yield (%)	Sel. (%)	Retained N-content (%)
1	DMO-SIL	1.41	100	4	1.0	96.8	98.5	96.4
2	DMO-Q10	1.22	50	5	0.5	26.2	94.0	96.5
3	DMO-P10	1.26	50	5	0.5	31.8	98.6	93.5
4	DMO-SiL	1.41	50	5	0.5	31.6	98.5	96.8
5	DMO-SBA15	1.37	50	5	0.5	24.3	98.0	94.9
6	OMO-2	1.24	50	5	0.5	44.9	96.1	95.2
7	OMO-4	1.29	50	5	0.5	38.3	97.8	97.6
8	OMO-6	1.22	50	5	0.5	25.8	97.0	95.7
9	PMO-2	2.38	50	5	0.5	23.9	98.5	95.7
10	PMO-4	2.37	50	5	0.5	21.2	98.9	97.1
11	PMO-6	2.11	50	5	0.5	20.0	98.2	93.8
12	OMO-2	1.24	50	15	0.5	76.9	98.5	96.1

Reaction conditions; 2 mol% catalysts based on N-content, 17 mmol styrene oxide (SO)

Amongst the DMOs, the highest yield was obtained with DMO-P10 and DMO-SiL (Table 8-2, entries 3 and 4). This may be attributed to smaller particle size of the silicas supports P-10 (40 µm) and SiL (40 – 60 µm) compared to Q-10 (75 – 150 µm) and SBA-15 (< 150 µm).[47]

With respect to OMOs, a 45 % yield of SC was obtained with OMO-2 (Table 8-2, entry 6). However, OMO-4 consisting of four CO_2-activating hydroxyl groups, exhibited lower activity (Table 8-2, entry 7), suggesting that increasing the number of hydroxyl groups from two to four was not beneficial to OMOs. A similar finding by Cheng *et al,*[48] was attributed to an enhancement in hydrogen bond formation between the halide and additional OH groups, leading to decreased nucleophilicity or epoxide ring-opening ability of the iodide ion. Alternatively, the observed decrease in activity could originate from increased diffusion-constraints with additional ethylhydroxyl groups, such that any benefit in CO_2 activation due to extra hydroxyl groups was suppressed by slow reaction kinetics. This finding suggests that similar to homogeneous systems[49], there is an optimal number of hydroxyl groups required for efficient activation of epoxides. A combination of diffusion-constrain and a high ratio of hydroxyl groups to organics may be at the origin of the low yield obtained with OMO-6 (Table 8-2, entry 8). Interestingly, OMO-4 with four hydroxyl groups, showed superior catalytic activity to all DMOs. This finding was attributed to the larger surface area and moderate pore volume of the latter, leading to enhanced accessibility to active sites and improved mass transport. PMOs were found to be the least active class of organosilicas, with PMO-2 the most active of all PMOs - 24 % yield (Table 8-2, entry 9). The inferior catalytic performance of PMOs was attributed to their low surface area, pore volume and disordered pore structure. Accordingly, OMO-2, the most active catalyst, was used to optimize the reaction conditions and material reusability.

8.3.2.2. Optimization of reaction time

Using SO as substrate, an increase in yield (44.9 to 76.9%) was observed when the reaction time was raised from 5 to 15 h (Table 8-2, entry 6 vs. 12). Compared to 1,2-EB for instance, SO is significantly more difficult to activate, and expected to take significantly longer reaction times under mild conditions to attain high yields. However, prolonged reaction times may lead to the formation of side products, ultimately reducing product yield and selectivity. Hence, optimization of reaction time was carried out with 1,2-EB. As seen in Figure 8-5, the yield of 1,2-butylene carbonate (1,2-BC) was found to peak after 15 h (97.2 %), which is 25 % more than was obtained for SC under similar conditions (Table 8-2, entry 12). Moreover, no noticeable change in selectivity (≥ 97.5 %) was observed after 20 h. Nonetheless, a slight decrease in yield was recorded after 20 h, suggesting the onset of the formation of side products beyond 15 h. Hence, optimum reaction conditions for the synthesis of 1,2-BC using OMO-2 were; 2 mol% catalyst, 0.5 MPa CO_2, 50 ^oC and 15 h.

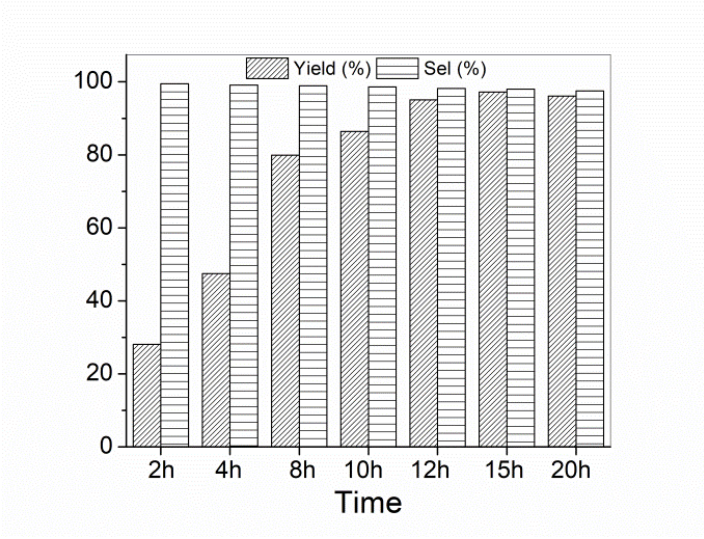

Figure 8-5. Optimization of reaction time. Reaction conditions; 2 mol% catalysts, 22.7 mmol 1,2-EB

8.3.2.3. Reusability studies

One of the most attractive attributes of heterogeneous catalysts is their reusability. In this regard, OMO-2 was subjected to recycling experiments with 1,2-EB as substrate. As shown in Table 8-3, no significant changes in product yield and selectivity were observed over five cycles. Although a 7 % decrease in organic content was observed compared to the fresh catalyst (Table 8-3, entry 1 vs. 2), the N-content of all spent catalysts was relatively constant, indicating the stable nature of OMO-2. This finding is consistent with the textural properties of fresh and spent catalysts being comparable.

Table 8-3. Reusability of OMO-2 in the synthesis of 1,2-butylene carbonate

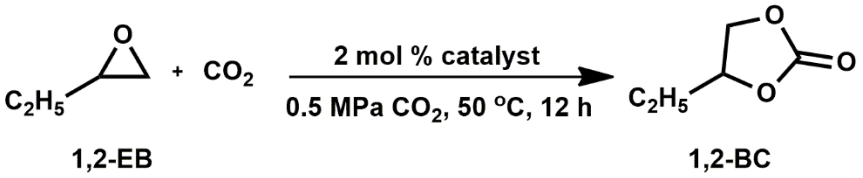

1,2-EB 1,2-BC

Entry	Reaction	N-content (mmol/g)	Yield (%)	Sel. (%)	BET SA[a] (m^2/g)	Vp[b] (mL/g)	Dp[c] (nm)
1	Run 1[d]	1.22	96.4	98.2	449	0.66	6.0
2	Run 2[e]	1.14	94.7	98.4	469	0.72	5.9
3	Run 3	1.11	95.1	98.5	453	0.68	5.9
4	Run 4	1.13	93.2	97.8	446	0.69	6.0
5	Run 5	1.12	94.3	98.0	456	0.61	6.2

[a]BET surface area, [b]pore volume, [c]pore diameter, [d]fresh catalyst, [e]first reuse

8.3.2.4. Scope of substrates

The scope of OMO-2 was investigated using four additional substrates, namely propylene oxide (PO), epichlorohydrin (ECH), cyclohexene oxide (CHO) and 3-glycidyloxypropyltrimethoxysilane (GPS) to synthesize propylene carbonate (PC), 4-(chloromethyl)-1,3-dioxolan-2-one (4-CDO) and hexahydrobenzo[*d*][1,3]dioxol-2-one (HDO) and

4-((3-(trimethoxysilyl)propoxy)methyl)-1,3-dioxolan-2-one (4-PDO), respectively. An excellent yield (98.2 %) of PC was obtained after 10 h under mild reaction conditions (Table 8-4, entry 1). Doubling the reaction temperature and pressure led to a very good yield (96%) after just 3 h (Table 8-4, entry 2). The observed marginal decreases in yield and selectively were attributed to the formation of side products, which are facilitated at higher temperatures.

Similar high yields were obtained in the synthesis of 1,2-BC and 4-(chloromethyl)-1,3-dioxolan-2-one under mild reaction conditions (Table 8-4, entries 3 and 5). As with the synthesis of PC, similar high yields of 1,2-BC and 4-CDO were obtained at 4 h, but at higher temperature and pressure (Table 8-4, entries 4 and 6). It is worth noting the high yield and selectively of these cyclic carbonates under the current mild reactions condition using a metal-free catalyst. Compared to other immobilized organocatalaysts, namely; ammonium salts on nanocrystalline zeolites[50], imidazole-based ionic liquid (IL) on graphene oxide[51] and covalent organic frameworks[52], triphosphonate cavitand on SBA-15[53], phosphonium-based polymeric IL[54], phosphonium salt on polystyrene[55], OMO-2 was significantly more active.

As noted earlier, under the current mild reaction conditions, the yield of SC was limited to 77% (Table 8-4, entry 7). However, 97% yield was obtained by doubling the reaction temperature and pressure, while limiting the reaction to 4 h (Table 8-4, entry 8). Furthermore, reacting CHO and GPS under the current mild reaction conditions led to very low yields (Table 8-4, entries 9 and 11). Nonetheless, significantly higher yields were obtained at higher temperature and pressure (Table 8-4, entries 10 and 12). This is not surprising as these three epoxides are much more difficult to activate (due to steric hindrance) than the first three in Table 8-4.

Table 8-4. Yield and selectivity of various epoxides with CO_2 using OMO-2

Entry	Epoxide	Cyclic carbonate	P_{CO_2} (MPa)	T (°C)	t (h)	Yield (%)	Sel. (%)
1		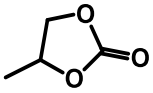	0.5	50	10	98.2	99.1
2			1.0	100	3	96.0	97.2
3	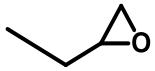	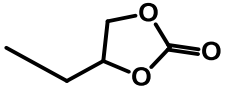	0.5	50	15	96.4	98.2
4			1.0	100	4	95.5	97.4
5	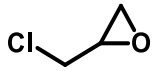	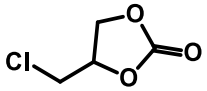	0.5	50	15	95.3	97.5
6			1.0	100	4	94.8	97.0
7	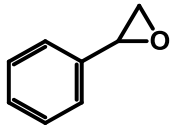	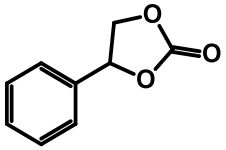	0.5	50	15	76.9	98.5
8			1.0	100	4	97.5	98.6
9	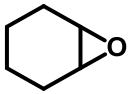	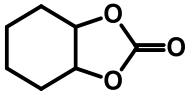	0.5	50	15	3.3	96.7
10			1.0	100	15	70.0	85.2
11	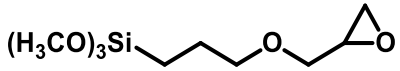	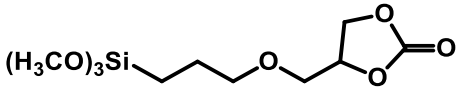	0.5	50	15	10.2	96.4
12			1.0	100	24	85.1	95.3

Conclusion

A series of novel DMOs, OMOs and PMOs were prepared, characterized and screened against the cycloaddition reaction of CO_2 and epoxides. Results showed that OMOs were the most active class of all materials. Furthermore, OMO-2, containing two hydroxyl groups per immobilized molecule was found to be the most active material. For substrates which are easy to activate such as PO, 1,2-EB and ECH, excellent yield and selectivity were obtained under mild reaction conditions (0.5 MPa CO_2, 50 ^oC and 10 – 15 h). However, higher CO_2 pressure and temperature were required with substrates which are more difficult to activate, e.g. SO, CHO and GPS. Furthermore, OMO-2 proved to be both chemically and structurally stable after five cycles of 1,2-EB synthesis.

References

(1) Ritchie, H.; Roser, M. CO2 and other Greenhouse Gas Emissions https://ourworldindata.org/co2-and-other-greenhouse-gas-emissions (accessed Nov 26, 2018).

(2) IPCC. *Global Warming of 1.5°C. An IPCC Special Report: Summary for Policymakers*; Masson-Delmotte, V., Zhai, P., Pörtner, H. O., Roberts, D., J. Skea, P. R., Shukla, Pirani, A., Moufouma-Okia, W., Péan, C., Pidcock, R., et al., Eds.; Geneva, 2018.

(3) Koytsoumpa, E. I.; Bergins, C.; Kakaras, E. The CO2 Economy: Review of CO2 Capture and Reuse Technologies. *J. Supercrit. Fluids* **2018**, *132* (July 2017), 3–16. https://doi.org/10.1016/j.supflu.2017.07.029.

(4) Luis Míguez, J.; Porteiro, J.; Pérez-Orozco, R.; Patiño, D.; Rodríguez, S. Evolution of CO2 Capture Technology between 2007 and 2017 through the Study of Patent Activity. *Appl. Energy* **2018**, *211*, 1282–1296. https://doi.org/10.1016/j.apenergy.2017.11.107.

(5) Song, C.; Liu, Q.; Ji, N.; Deng, S.; Zhao, J.; Li, Y.; Song, Y.; Li, H. Alternative Pathways for Efficient CO2 Capture by Hybrid Processes—A Review. *Renew. Sustain. Energy Rev.* **2018**, *82*, *Part 1* (2018), 215–231. https://doi.org/https://doi.org/10.1016/j.rser.2017.09.040.

(6) Aresta, M.; Dibenedetto, A.; Quaranta, E. State of the Art and Perspectives in Catalytic Processes for CO2 Conversion into Chemicals and Fuels : The Distinctive Contribution of Chemical Catalysis and Biotechnology. *J. Catal.* **2016**, *343*, 2–45. https://doi.org/10.1016/j.jcat.2016.04.003.

(7) Cokoja, M.; Wilhelm, M. E.; Anthofer, M. H.; Herrmann, W. A.; Kühn, F. E. Synthesis of Cyclic Carbonates from Epoxides and Carbon Dioxide by Using Organocatalysts.

ChemSusChem **2015**, *8* (15), 2436–2454. https://doi.org/10.1002/cssc.201500161.
(8) Comerford, J. W.; Ingram, I. D. V.; North, M.; Wu, X. Sustainable Metal-Based Catalysts for the Synthesis of Cyclic Carbonates Containing Five-Membered Rings. *Green Chem.* **2015**, *17* (4), 1966–1987. https://doi.org/10.1039/C4GC01719F.
(9) North, M. Synthesis of Cyclic Carbonates from Carbon Dioxide and Epoxides. In *New and Future Developments in Catalysis - Activation of Carbon Dioxide*; Elsevier B.V., 2013; pp 379–413. https://doi.org/10.1016/B978-0-444-53882-6.00014-0.
(10) Kolle, J. M.; Sayari, A. Substrate Dependence on the Fixation of CO2 to Cyclic Carbonates over Reusable Porous Hybrid Solids. *J. CO2 Util.* **2018**, *26* (April), 564–574. https://doi.org/10.1016/j.jcou.2018.06.013.
(11) Büttner, H.; Lau, K.; Spannenberg, A.; Werner, T. Bifunctional One-Component Catalysts for the Addition of Carbon Dioxide to Epoxides. *ChemCatChem* **2015**, *7* (3), 459–467. https://doi.org/10.1002/cctc.201402816.
(12) Büttner, H.; Steinbauer, J.; Werner, T. Synthesis of Cyclic Carbonates from Epoxides and Carbon Dioxide by Using Bifunctional One-Component Phosphorus-Based Organocatalysts. *ChemSusChem* **2015**, *8* (16), 2655–2669. https://doi.org/10.1002/cssc.201500612.
(13) Wang, L.; Lin, L.; Zhang, G.; Kodama, K.; Yasutake, M.; Hirose, T. Synthesis of Cyclic Carbonates from CO2 and Epoxides Catalyzed by Low Loadings of Benzyl Bromide/DMF at Ambient Pressure. *Chem. Commun. (Camb).* **2014**, *50* (94), 14813–14816. https://doi.org/10.1039/c4cc06791f.
(14) Liu, X. F.; Song, Q. W.; Zhang, S.; He, L. N. Hydrogen Bonding-Inspired Organocatalysts for CO2 Fixation with Epoxides to Cyclic Carbonates. *Catal. Today* **2016**, *263*, 69–74. https://doi.org/10.1016/j.cattod.2015.08.062.
(15) Siewniak, A.; Jasiak, K.; Baj, S. An Efficient Method for the Synthesis of Cyclic Carbonates from CO2 and Epoxides Using an Effective Two-Component Catalyst System: Polymer-Supported Quaternary Onium Salts and Aqueous Solutions of Metal Salts. *Appl. Catal. A Gen.* **2014**, *482*, 266–274. https://doi.org/10.1016/j.apcata.2014.05.033.
(16) Kumatabara, Y.; Okada, M.; Shirakawa, S. Triethylamine Hydroiodide as a Simple Yet Effective Bifunctional Catalyst for CO2 Fixation Reactions with Epoxides under Mild Conditions. *ACS Sustain. Chem. Eng.* **2017**, *5* (8), 7295–7301. https://doi.org/10.1021/acssuschemeng.7b01535.
(17) Steinbauer, J.; Longwitz, L.; Frank, M.; Epping, J.; Kragl, U.; Werner, T. Immobilized Bifunctional Phosphonium Salts as Recyclable Organocatalysts in the Cycloaddition of CO2 and Epoxides. *Green Chem.* **2017**, *19*, 4435–4445. https://doi.org/10.1039/C7GC01782K.
(18) North, M.; Pasquale, R.; Young, C. Synthesis of Cyclic Carbonates from Epoxides and CO2. *Green Chem.* **2010**, *12* (9), 1514. https://doi.org/10.1039/c0gc00065e.
(19) Fiorani, G.; Guo, W.; Kleij, A. W. Sustainable Conversion of Carbon Dioxide: The Advent of Organocatalysis. *Green Chem.* **2015**, *17* (3), 1375–1389. https://doi.org/10.1039/C4GC01959H.
(20) Bobbink, F. D.; Dyson, P. J. Synthesis of Carbonates and Related Compounds Incorporating CO2 Using Ionic Liquid-Type Catalysts: State-of-the-Art and Beyond. *J. Catal.* **2016**, *343*, 52–61. https://doi.org/10.1016/j.jcat.2016.02.033.

(21) Lee, J. K.; Kim, Y. J.; Choi, Y. S.; Lee, H.; Lee, J. S.; Hong, J.; Jeong, E. K.; Kim, H. S.; Cheong, M. Zn-Containing Ionic Liquids Bearing Dialkylphosphate Ligands for the Coupling Reactions of Epoxides and CO 2. *Appl. Catal. B Environ.* **2012**, *111–112*, 621–627. https://doi.org/10.1016/j.apcatb.2011.11.015.
(22) Martín, C.; Fiorani, G.; Kleij, A. W. Recent Advances in the Catalytic Preparation of Cyclic Organic Carbonates. *ACS Catal.* **2015**, *5* (2), 1353–1370. https://doi.org/10.1021/cs5018997.
(23) Ren, Y.; Jiang, O.; Zeng, H.; Mao, Q.; Jiang, H. Lewis Acid–Base Bifunctional Aluminum–Salen Catalysts: Synthesis of Cyclic Carbonates from Carbon Dioxide and Epoxides. *RSC Adv.* **2016**, *6* (4), 3243–3249. https://doi.org/10.1039/C5RA24596F.
(24) Kamphuis, A. J.; Picchioni, F.; Pescarmona, P. P. CO2-Fixation into Cyclic and Polymeric Carbonates: Principles and Applications. *Green Chem.* **2019**, *21* (3), 406–448. https://doi.org/10.1039/c8gc03086c.
(25) Sakai, T.; Tsutsumi, Y.; Ema, T. Highly Active and Robust Organic–Inorganic Hybrid Catalyst for the Synthesis of Cyclic Carbonates from Carbon Dioxide and Epoxides. *Green Chem.* **2008**, *10* (3), 337. https://doi.org/10.1039/b718321f.
(26) Adam, F.; Appaturi, J. N.; Ng, E. P. Halide Aided Synergistic Ring Opening Mechanism of Epoxides and Their Cycloaddition to CO2 Using MCM-41-Imidazolium Bromide Catalyst. *J. Mol. Catal. A Chem.* **2014**, *386*, 42–48. https://doi.org/10.1016/j.molcata.2014.02.008.
(27) Chatelet, B.; Joucla, L.; Dutasta, J.-P.; Martinez, A.; Dufaud, V. Immobilization of a N-Substituted Azaphosphatrane in Nanopores of SBA-15 Silica for the Production of Cyclic Carbonates. *J. Mater. Chem. A* **2014**, *2* (34), 14164. https://doi.org/10.1039/C4TA01500B.
(28) Lang, X. D.; He, L. N. Green Catalytic Process for Cyclic Carbonate Synthesis from Carbon Dioxide under Mild Conditions. *Chem. Rec.* **2016**, 1337–1352. https://doi.org/10.1002/tcr.201500293.
(29) Udayakumar, S.; Raman, V.; Shim, H. L.; Park, D. W. Cycloaddition of Carbon Dioxide for Commercially-Imperative Cyclic Carbonates Using Ionic Liquid-Functionalized Porous Amorphous Silica. *Appl. Catal. A Gen.* **2009**, *368* (1–2), 97–104. https://doi.org/10.1016/j.apcata.2009.08.015.
(30) Udayakumar, S.; Park, S. W.; Park, D. W.; Choi, B. S. Immobilization of Ionic Liquid on Hybrid MCM-41 System for the Chemical Fixation of Carbon Dioxide on Cyclic Carbonate. *Catal. Commun.* **2008**, *9* (7), 1563–1570. https://doi.org/10.1016/j.catcom.2008.01.001.
(31) Prasetyanto, E. A.; Ansari, M. B.; Min, B. H.; Park, S. E. Melamine Tri-Silsesquioxane Bridged Periodic Mesoporous Organosilica as an Efficient Metal-Free Catalyst for CO2activation. *Catal. Today* **2010**, *158* (3–4), 252–257. https://doi.org/10.1016/j.cattod.2010.03.081.
(32) Liu, M.; Lu, X.; Shi, L.; Wang, F.; Sun, J. Periodic Mesoporous Organosilica with a Basic Urea-Derived Framework for Enhanced Carbon Dioxide Capture and Conversion Under Mild Conditions. *ChemSusChem* **2017**, *10* (6), 1110–1119. https://doi.org/10.1002/cssc.201600973.
(33) Peng, J.; Wang, S.; Yang, H. J.; Ban, B.; Wei, Z.; Wang, L.; Lei, B. Highly Efficient Fixation of Carbon Dioxide to Cyclic Carbonates with New Multi-Hydroxyl Bis-(Quaternary Ammonium) Ionic Liquids as Metal-Free Catalysts under Mild Conditions. *Fuel* **2018**, *224*

(March), 481–488. https://doi.org/10.1016/j.fuel.2018.03.119.
(34) Zhang, X.; Geng, W.; Yue, C.; Wu, W.; Xiao, L. Multilayered Supported Ionic Liquids Bearing a Carboxyl Group: Highly Efficient Catalysts for Chemical Fixation of Carbon Dioxide. *J. Environ. Chem. Eng.* **2016**, *4* (2), 2565–2572. https://doi.org/10.1016/j.jece.2016.05.001.
(35) Zhu, J.; Kailasam, K.; Xie, X.; Schomaecker, R.; Thomas, A. High-Surface-Area SBA-15 with Enhanced Mesopore Connectivity by the Addition of Poly(Vinyl Alcohol). *Chem. Mater.* **2011**, *23* (8), 2062–2067. https://doi.org/10.1021/cm1028639.
(36) Serna-guerrero, R.; Da, E.; Sayari, A. New Insights into the Interactions of CO2 with Amine-Functionalized Silica. *Ind. Eng. Chem. Res.* **2008**, *47*, 9406–9412. https://doi.org/10.1021/ie801186g.
(37) Lindlar, B.; Lüchinger, M.; Röthlisberger, A.; Haouas, M.; Pirngruber, G.; Kogelbauer, A.; Prins, R. Chemical Modification of High-Quality Large-Pore M41S Materials. *J. Mater. Chem.* **2002**, *12* (3), 528–533. https://doi.org/10.1039/b109205g.
(38) Feng, X.; Fryxell, G. E.; Wang, L. Q.; Kim, A. Y.; Liu, J.; Kemner, K. M. Functionalized Monolayers on Ordered Mesoporous Supports. *Science (80-.).* **1997**, *276* (5314), 923–926. https://doi.org/10.1126/science.276.5314.923.
(39) Da'na, E.; Sayari, A. Adsorption of Copper on Amine-Functionalized SBA-15 Prepared by Co-Condensation: Equilibrium Properties. *Chem. Eng. J.* **2011**, *166* (1), 445–453. https://doi.org/10.1016/j.cej.2010.11.016.
(40) Barczak, M. Template Removal from Mesoporous Silicas Using Different Methods as a Tool for Adjusting Their Properties. *New J. Chem.* **2018**, *42* (6), 4182–4191. https://doi.org/10.1039/c7nj04642a.
(41) Knöfel, C.; Lutecki, M.; Martin, C.; Mertens, M.; Hornebecq, V.; Llewellyn, P. L. Green Solvent Extraction of a Triblock Copolymer from Mesoporous Silica: Application to the Adsorption of Carbon Dioxide under Static and Dynamic Conditions. *Microporous Mesoporous Mater.* **2010**, *128* (1–3), 26–33. https://doi.org/10.1016/j.micromeso.2009.07.021.
(42) Mishler, R. E.; Biradar, A. V.; Duncan, C. T.; Schiff, E. A.; Asefa, T. Solvent-Washable Polymer Templated Synthesis of Mesoporous Materials and Solid-Acid Nanocatalysts in One-Pot. *Chem. Commun.* **2009**, No. 41, 6201–6203. https://doi.org/10.1039/b913035g.
(43) Oc, H. H.; Yoon, K. B. Solid-State NMR Study on the Structure and Dynamics of Triblock Copolymer P123 Remaining in SBA-15 after Solvent Washing. *Bull. Korean Chem. Soc.* **2008**, *29* (5), 911–912. https://doi.org/10.5012/bkcs.2008.29.5.911.
(44) Li, C.; Yang, J.; Shi, X.; Liu, J.; Yang, Q. Synthesis of SBA-15 Type Mesoporous Organosilicas with Diethylenebenzene in the Framework and Post-Synthetic Framework Modification. *Microporous Mesoporous Mater.* **2007**, *98* (1–3), 220–226. https://doi.org/10.1016/j.micromeso.2006.09.013.
(45) Srikanth, C. S.; Chuang, S. S. C. Spectroscopic Investigation into Oxidative Degradation of Silica-Supported Amine Sorbents for CO2 Capture. *ChemSusChem* **2012**, *5* (8), 1435–1442. https://doi.org/10.1002/cssc.201100662.
(46) Kohrt, C.; Werner, T. Recyclable Bifunctional Polystyrene and Silica Gel-Supported Organocatalyst for the Coupling of CO2 with Epoxides. *ChemSusChem* **2015**, *8* (12), 2031–2034. https://doi.org/10.1002/cssc.201500128.

(47) North, M.; Villuendas, P. Influence of Support and Linker Parameters on the Activity of Silica-Supported Catalysts for Cyclic Carbonate Synthesis. *ChemCatChem* **2012**, *4* (6), 789–794. https://doi.org/10.1002/cctc.201200117.
(48) Cheng, W.; Xiao, B.; Sun, J.; Dong, K.; Zhang, P.; Zhang, S.; Ng, F. T. T. Effect of Hydrogen Bond of Hydroxyl-Functionalized Ammonium Ionic Liquids on Cycloaddition of CO2. *Tetrahedron Lett.* **2015**, *56* (11), 1416–1419. https://doi.org/10.1016/j.tetlet.2015.01.174.
(49) Sun, J.; Han, L.; Cheng, W.; Wang, J.; Zhang, X.; Zhang, S. Efficient Acid-Base Bifunctional Catalysts for the Fixation of CO 2 with Epoxides under Metal- and Solvent-Free Conditions. *ChemSusChem* **2011**, *4* (4), 502–507. https://doi.org/10.1002/cssc.201000305.
(50) Sarmah, B.; Srivastava, R. Activation and Utilization of CO2 Using Ionic Liquid or Amine-Functionalized Basic Nanocrystalline Zeolites for the Synthesis of Cyclic Carbonates and Quinazoline-2,4(1H,3H)-Dione. *Ind. Eng. Chem. Res.* **2017**, *56* (29), 8202–8215. https://doi.org/10.1021/acs.iecr.7b01406.
(51) Zhu, J.; Wang, S.; Gu, Y.; Xue, B.; Li, Y. A New and Efficient Method of Graphene Oxide Immobilized with Ionic Liquids: Promoted Catalytic Activity for CO2 Cycloaddition. *Mater. Chem. Phys.* **2018**, *208*, 68–76. https://doi.org/10.1016/j.matchemphys.2018.01.031.
(52) Qiu, J.; Zhao, Y.; Li, Z.; Wang, H.; Shi, Y.; Wang, J. J. Imidazolium Salts Functionalized Covalent Organic Frameworks for Highly Efficient Catalysis of CO2 Conversion. *ChemSusChem* **2019**, *12* (11), 2421–2427. https://doi.org/10.1002/cssc.201900570.
(53) Mirabaud, A.; Martinez, A.; Bayard, F.; Dutasta, J. P.; Dufaud, V. A New Heterogeneous Host-Guest Catalytic System as an Eco-Friendly Approach for the Synthesis of Cyclic Carbonates from CO2 and Epoxides. *New J. Chem.* **2018**, *42* (20), 16863–16874. https://doi.org/10.1039/c8nj03065k.
(54) Liu, Y.; Cheng, W.; Zhang, Y.; Sun, J.; Zhang, S. Controllable Preparation of Phosphonium-Based Polymeric Ionic Liquids as Highly Selective Nanocatalysts for the Chemical Conversion of CO2 with Epoxides. *Green Chem.* **2017**, *19* (9), 2184–2193. https://doi.org/10.1039/c7gc00444c.
(55) Yan, X.; Fu, R.; Liu, F.; Pan, Y.; Ding, X.; He, G. Novel Electron-Rich and Sterically Hindered Phosphonium as a Highly Efficient and Recyclable Heterogeneous Catalyst for CO2 Cycloaddition. *Ind. Eng. Chem. Res.* **2018**, *57* (9), 3195–3203. https://doi.org/10.1021/acs.iecr.7b05419.

Appendix

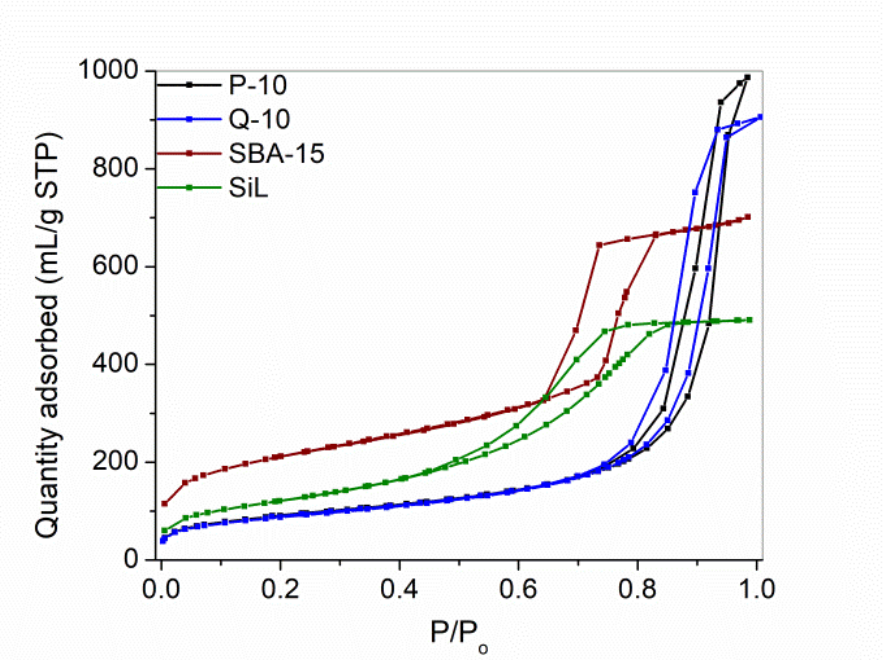

Figure A8- 1. Nitrogen adsorption–desorption isotherms of pristine supports

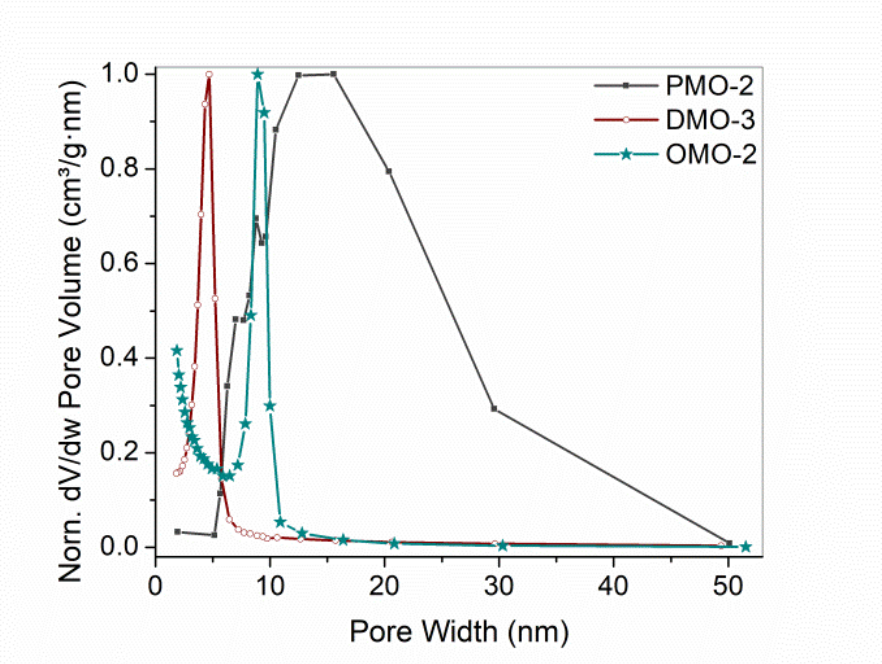

Figure A8- 2. Pore size distribution for representative organosilicas

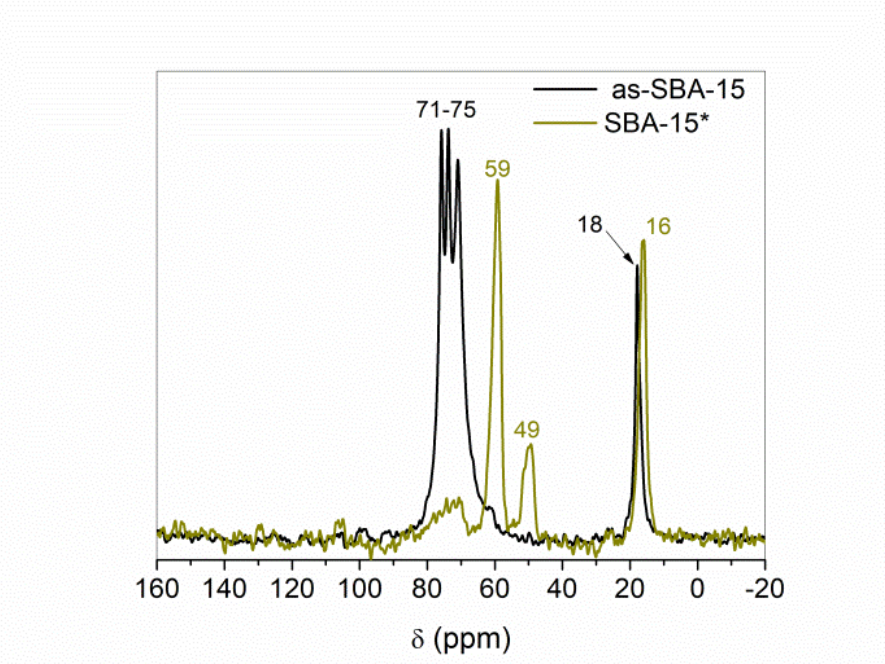

Figure A8- 3. ^{13}C CP-MAS NMR spectra of SBA-15; (black) as-synthesized, as-SBA-15 and (dark yellow) solvent-extracted (SBA-15*)

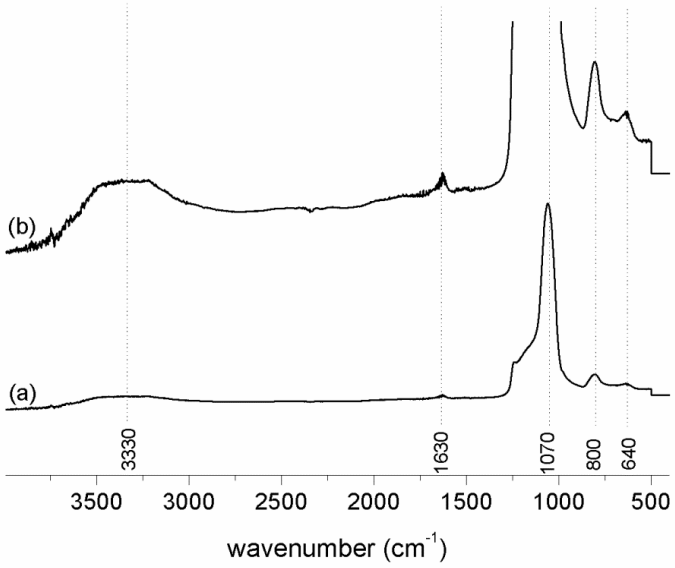

Figure A8- 4. ATR-IR spectrum of silica support (similar spectra were obtained for all support materials). Spectrum (b) is the enlarged spectrum of (a)

CHAPTER 9 CONCLUSION AND RECOMMENDATION FOR FUTURE WORK

9.0. Conclusion

Hydrocarbons will for years continue to serve as a major energy source while the world transitions to a lower-carbon energy economy. While the long-term goal is to substitute fossil fuel with renewable energy, pathways to a net-zero emissions including technologies to remove and permanently store CO_2 (i.e. including carbon capture, utilization and storage -CCUS), are the main short- to medium-term targets. Accordingly, research, development and demonstration in the areas of CO_2 capture and utilization have made significant advances in recent years, with a number of large-scale CO_2 capture and reuse plants in operation around the world. Nonetheless, fundamental questions regarding CO_2-amine interaction during CO_2 adsorption/absorption remain unanswered. Moreover, for supported polyethylenimine, an adsorbent with high CO_2 capacity prepared mainly by impregnation, to be efficiently used at higher temperatures and in the presence of moisture, its oxidation stability and leaching resistance need to be improved. Of the many chemical pathways available for CO_2 reuse, the reaction of CO_2 and epoxides to yield cyclic carbonates has received a lot of attention owing to their application as biodegradable solvents, monomers in the synthesis of polycarbonates, solvents in lithium-ion batteries, active pharmaceutical ingredients, etc. The main findings of this thesis are summarized in Table 9-1.

Table 9-1. Summary of the main findings

Chapter	Aspects investigated	Main finding(s)
Three	CO_2-amine interaction during CO_2 absorption/adsorption.	The nucleophilic attack of CO_2 by amine requires the catalytic assistance of a Brønsted base (another amine, water or other species) through a 6-centered mechanism to achieve proton transfer/exchange. An important consequence of this concerted mechanism is that the N and H atoms added to the C=O double bond do not originate from a single amine group. The widely reported zwitterion, $R\text{-}NH_2^+\text{-}COO^-$ was deemed highly unlikely, because not only the associated 4-centered mechanism has a high energy barrier, but it is not consistent with the orbital symmetry requirements for chemical reactions
	Source of ammonium bicarbonate/carbonate during CO_2 uptake under moist conditions.	formation of ammonium bicarbonate/carbonate does not take place through the widely accepted hydration of carbamate/carbamic acid. Instead, water acts as a nucleophile that attacks CO_2 with catalytic assistance by amine groups, and carbamate/carbamic acid decomposes back to amine and CO_2.
Four	Covalent immobilization of polyethylenimine on PE-$AlSiO_2$ (PEI@PE-$AlSiO_2$)	In the presence of Et_3N or NaOH as catalyst, 3-glycidoxypropyltrimethoxysilane (GPS) or 3-triethoxysilylpropyl isocyanate (TPI) were successfully used as grafting agents to prepare PEI@PE-$AlSiO_2$. These materials showed enhanced thermal stability and resistance to leaching (in EtOH) compared to their impregnated counterparts.
	Oxidation stability of PEI@PE-$AlSiO_2$	PEI@PE-$ALSiO_2$ materials showed superior oxidation stability (100 ^oC in air) compared to their impregnated counterparts. Further modification of PEI with 1,2-epoxybutane led to addition enhancement in oxidation stability.
Seven	In the synthesis of cyclic carbonates using supported ammonium salts, some epoxides show no decrease in yield over multiple cycles, while with others, a drop in yield was observed from one reaction cycle to another.	*N,N,N*-tributyl-*N*-propylammonium iodide-functionalized mesoporous silicas proved to be an effect catalyst in the solvent-free synthesis of cyclic carbonates (CCs) from epoxides and CO_2. Compared to 1,2-butylene carbonate, the yield of styrene carbonate was found to decrease with catalyst reuse, which was attributed to the adsorption of solid reaction product on the catalyst surface. Using a

Chapter	Aspects investigated	Main finding(s)
		chromatographic silica gel as support and an improved catalyst recovery step, gave rise to a highly efficient, robust and fully reusable catalyst for the synthesis of styrene carbonate.
Eight	How different supported ammonium salts based on different mesoporous structures; disordered and periodic mesoporous organosilicas, compare in the synthesis of cyclic carbonates.	Owing to its higher surface area, pore volume and optimum nucleophilicity of the iodide ion, ordered mesoporous organosilica with two hydroxyl groups was found to be the most active catalyst. Moreover, OMO-2 showed very good catalytic properties (yield ≥ 93% and selectivity ≥ 98%), and excellent chemical and textural stability in the synthesis of 1,2-butylene carbonate over 5 cycles.

9.1. Publications

The work reported in this thesis led to the publication of four articles in peer-reviewed journals, including;

1. H. Ziaei-Azad, J.M. Kolle, N. Al-Yasser, A. Sayari, One-pot synthesis of large-pore AlMCM-41 aluminosilicates with high stability and adjustable acidity, Microporous Mesoporous Mater. 262 (**2018**) 166–174. doi:10.1016/j.micromeso.2017.11.036.
2. J.M. Kolle, A. Sayari, Substrate dependence on the fixation of CO2 to cyclic carbonates over reusable porous hybrid solids, J. CO2 Util. 26 (**2018**) 564–574. doi:10.1016/j.jcou.2018.06.013 – **Chapter 7 of thesis.**
3. J.M. Kolle, A. Sayari, Novel porous organocatalysts for cycloaddition of CO2 and epoxides, RSC Adv. 9 (**2019**) 24527–24538. doi:10.1039/c9ra05466a - **Chapter 8 of thesis**
4. J.M. Kolle, A. Sayari, Covalently Immobilized Polyethylenimine for CO2 Adsorption, Ind. Eng. Chem. Res. 25 Nov (2**019**) Just accepted. doi:10.1021/acs.iecr.9b04669 - **Chapter 4 of thesis.**
5. Said, R. B.; Kolle, J.M.; Essalah, K.; Tangour, B.; and Sayari, A. CO2 – Amine Reaction Mechanisms: A Unified Approach. Submitted to J. Mater. Chem. A. Currently under review - **Chapter 3 of thesis.**

In addition, a comprehensive review on the "Understanding the role of water during CO_2 adsortion" will be submitted soon – **Chapter 5 of thesis**.

9.2. Recommendation for future work

This study presents an insight into fundamental issues on CO_2-amine interactions, CO_2 fixation to cyclic carbonates, as well as materials development. Based on the reported findings, this study may be improved if the following suggestions, to improve both the materials and CO_2 adsorption and/or reuse processes, are implemented:

- The use of chemicals such as antioxidants to improve oxidation stability of amine-based adsorbent, notably PEI-impregnated materials in the presence of oxygen.
- At the end of the reaction between CO_2 and epoxide, unreacted CO_2 is released into the atmosphere. It will be beneficial if this CO_2 could be collected and reused in subsequent CO2-epoxide reactions, or other reactions utilizing CO_2 as a substrate.
- Supported ammonium salts used as catalysts in the synthesis of cyclic carbonates from CO_2 and epoxides appear to undergo loss of the active site with reuse. A reaction condition under which such loss can be reduced to an unnoticeable level over multiple cycles will be highly beneficial. Alternatively, it will be useful to investigate the possibility of restoring the activity of the catalyst once the loss of active site becomes evident.